FLUIDISED BED GASIFICATION OF HIGH-ASH SOUTH AFRICAN COALS: AN EXPERIMENTAL AND MODELLING STUDY

by

André Daniël Engelbrecht
BSc. (Chem. Eng.) (UKZN)
M. Eng (Chem. Eng.) (NWU)

Thesis submitted in fulfilment of the requirements for the degree **Philosophiae Doctor in Chemical** Engineering in the School of Chemical and Minerals Engineering of the North-West University, Potchefstroom Campus, South Africa.

Supervisor:	Professor R.C. Everson (North-West University)
Co-supervisor:	Professor H.W.J.P. Neomagus (North-West University)
Assistant-supervisors:	Professor M.L. de Souza-Santos (University of Campinas)
	Dr A. Luckos (Sasol Technology)

September 2014
Potchefstroom

DECLARATION

This thesis is submitted in fulfilment of the requirements for the degree **Philosophiae Doctor in Engineering** at the School of Chemical and Minerals Engineering of the North-West University.

I, André Daniël Engelbrecht, hereby declare that:

1) The thesis with the title: FLUIDISED BED GASIFICATION OF HIGH-ASH SOUTH AFRICAN COALS: AN EXPERIMENTAL AND MODELLING STUDY is my own work and has not been submitted to any other university either in whole or in part.
2) The commissioning and operation of the fluidised bed gasifier pilot plant at the Council for Scientific and Industrial Research was my own work.
3) Development of the MATLAB® fluidised bed coal gasifier rate model was my own work.

Signed at Potchefstroom on this ……. day of September 2014

……..

A.D. Engelbrecht

ACKNOWLEDGEMENTS

The author wishes to sincerely thank the following people and organisations for their support during this project.

- Professors Ray Everson and Hein Neomagus at the School of Chemical and Minerals Engineering in Potchefstroom for their guidance and advice throughout the duration of this project.
- Dr Adam Luckos at Sasol Technology and Professor Marcio de Souza Santos at the University of Campinas, Brazil, for their guidance and advice on fluidised bed technology and process modelling.
- Mr Ashton Swartbooi, Dr Bilainu Oboirien and Mr Alphuis Bokaba for their assistance with the operation of the bench-scale and pilot-scale fluidised bed reactors at the Council for Scientific and Industrial Research (CSIR).
- Mr Hennie Coetzee (PhD student) at the North-West University for his assistance with the char-steam thermogravimetric analyser experiments.
- Mr Emanuel Makungo at the Department of Chemical Engineering at the University of Pretoria and Dr Graig Long at Material Science and Manufacturing at the CSIR for assistance with the use of MATLAB® and programming of the fluidised bed gasifier rate model.
- Colleagues at the CSIR for the useful discussions we had on the subject of coal and fluidised beds.
- The CSIR for providing financial support throughout the duration of this project.
- This work is based on the research supported by the South African Chairs Initiative of the Department of Science and Technology and the National Research Foundation of South Africa (SARChI Chair in Coal Research - Chair No. 86880, UID85643, UID85632).
- New Vaal and Grootegeluk collieries for the collection and preparation of coal samples that were used for the bench-scale experiments and pilot-scale fluidised bed gasification tests.
- Beverlie Davies from Stylus for editing the thesis.
- Family and friends for their encouragement.

DISCLAIMER

Any opinion, finding or conclusion or recommendation expressed in this thesis is that of the author and the National Research Foundation of South Africa does not accept any liability in this regard.

ABSTRACT

South Africa has large coal reserves and produces approximately 74% of its primary energy from coal. Coal gasification using moving bed gasifiers is one of the most important coal utilisation technologies, consuming ± 17.5% of locally produced coal.

This study was motivated by the need to investigate alternative coal gasification technologies for the utilisation of fine, high-ash and caking coals for future Integrated Gasification Combined Cycle (IGCC) and coal to liquids (CTL) plants. These coals are estimated to form a large percentage of the remaining coal reserves in South Africa and could be difficult to utilise efficiently in moving bed gasifiers.

Fluidised bed gasification was identified as a technology that could potentially utilise these coals. Coals from the New Vaal and Grootegeluk collieries were selected as being suitable for this investigation. The coals were subjected to detailed characterisation, bench-scale and pilot-scale fluidised bed gasification tests.

The results of the pilot-scale atmospheric bubbling fluidised bed gasification tests show that stable gasification is possible at temperatures between 880 °C and 980 °C. The maximum fixed carbon conversion achievable in the pilot plant is, however, limited to ± 88% due to the low reactivity of the coals tested and to thermal fragmentation and attrition of the coal in the gasifier. It was found that oxygen enrichment of the gasification air from 21% to 36% by means of oxygen addition produces a significant increase in the calorific value of the gas (3.0 MJ/Nm^3 to 5.5 MJ/Nm^3). This observation has not previously been reported at pilot-plant scale.

A mathematical model for a bubbling fluidised bed coal gasifier was developed based on sub-models for fluidised bed hydrodynamics, coal devolatilisation, chemical reactions, transfer processes and fines generation. A coal devolatilisation sub-model to predict the products of coal devolatilisation in a fluidised bed gasifier was developed and incorporated into the model. Parameters associated with the rates of the gasification reactions and the devoltilisation process were obtained by means of bench-scale tests. The heat loss parameter (Q) in the model was estimated by means of a heat loss calculation.

The results from the pilot-scale gasification tests were used to evaluate the predictive capability of the model. It was found that for temperature, fixed carbon conversion and calorific value of the gas the difference between measured and predicted values was less than 10%. Recommendations are made for further refinement of the model to improve its predictive capability and range of application.

The model was used to study the effect of major operating variables on gasifier performance. It was found that increasing the reactant gas (air, oxygen and steam) temperature from 250 °C to 550 °C increases the calorific value of the gas by ± 9.3% and the gasification efficiency by ± 6.0%. Increasing the fluidised bed height has a positive effect on fixed carbon conversion; however, at higher bed heights the benefit of increasing the bed height is less due to the inhibiting effects of H_2 and CO on the rates of char gasification.

Keywords: High-ash coal, gasification, fluidised bed, reaction kinetics, modelling.

OPSOMMING

Suid-Afrika besit volop steenkoolreserwes en produseer ongeveer 75% van sy primêre energie uit steenkool. Steenkoolvergassing deur middel van bewegende bedvergassers is een van die belangrikste steenkoolbenuttingstegnologieë en benut bykans 17.5% van die steenkool wat plaaslik geproduseer word.

Hierdie studie is gemotiveer deur die behoefte om alternatiewe steenkoolvergassingstegnologieë te ondersoek vir die benutting van fyn, asryke en koeksteenkole vir gebruik in toekomstige geïntegreerde vergassingsstelsels en vloiebare brandstof uit steenkool-aanlegte. Dit word beraam dat hierdie tiepe steenkool ‘n groot persentasie van die oorblywende steenkoolreserwes van Suid-Afrika verteenwoordig en dat effektiewe benutting van dié steenkool in bewegende vastebedvergassers ‘n moeilike taak sal wees.

Sweefbedvergassing is as ‘n tegnologie geidentifiseer wat potensieel vir die vergassing van fyn, asryke en koeksteenkole aangewend kan word. Steenkool afkomstig van New Vaal en Grootegeluk-myne is as geskik vir hierdie studie uitgeken. Gedetailleerde karakteriseringstoetse en sweefbedvergassingstoetse in ‘n proefaanleg is op hierdie steenkole uitgevoer.

Die resultate van die vergassingstoetse in die proefaanleg toon dat stabiele vergassing van die steenkool teen temperature tussen 880 °C en 980 °C moontlik is. Die maksimum omsetting van die vaste koolstofinhoud is egter tot ± 88% beperk as gevolg van die lae reaktiwiteit van die steenkool en termiese fragmentasie en verbrokkeling van die steenkool in die vergasser. Dit is bevind dat veryking van die vergassingslug van 21% tot 36%, deur middle van suurstof byvoeging, ’n buidende toename in die hittewaarde van die gas tot gevolg het (3.0 MJ/Nm^3 – 5.5 MJ/Nm^3). Hierdie waarneming is nog nie voorheen op n proefaanleg-skaal gemaak nie.

‘n Wiskundige model vir ‘n sweefbedvergasser is ontwikkel wat op sub-modelle vir sweefbedhidrodinamika, steenkoolontvlugting, chemiese reaksies, oordragprosesse en steenkoolverbrokkeling gebaseer is. ’n Steenkool ontvlugtings model om die produkte van steenkool ontvlugting te voorspel is ontwikkel en in die model ingesluit.

Parameters wat verbonde is aan die tempo van die vergassings reaksie en die steenkool ontvlugtingsproses word deur middel van bank-skaal toetse bepaal. Die hitteverlies parameter word geskat deur middel van n hitteverlies berekening.

Die resultate van die proefaanlegtoetse is gebruik om die model se voorspellende vermoë te evalueer. Vir temperatuur, vaste koolstofomsetting en hittewaarde van die gas is die veskil tusssen die voorspelde en gemete waardes minder as 10%. Aanbevelings is gemaak om die model verder te verfyn om sodoende die voorspellende vermoë en aanwendbaarheid te verbeter.

Die model is aangewend om die effek van belangrike inset-veranderlikes op die bedryf van die vergasser te ondersoek. Dit is gevind dat ’n toename in die temperatuur van die reaksiegas (lug, suurstof en stoom) van 250 °C tot 550 °C, die hittewaarde van die gas met ± 9.3% en die vergassings-effektiwiteit met ± 6.0% laat toeneem het. Alhoewel toename in die hoogte van die sweefbed ’n positiewe effek op die vaste steeenkool-omsetting het, is die effek laer by hoër bedhoogtes weens die inhiberende effek van CO en H_2 op die tempo van die vergassingsreaksies.

Sleutelwoorde: Asryke steenkool, sweefbedvergassing, reaksie kinetika, modellering.

LIST OF PUBLICATIONS

(Conference proceedings and accredited journals)

Engelbrecht, A.D., Everson, R.C., Neomagus, H.W.P.J. and North, B.C (2010). Fluidised bed gasification of selected South African coals. *The Journal of the South African Institute of Mining and Metallurgy* 110: 225-742.

Engelbrecht, A.D., North, B.C. and Oboirien, B.O. (2010). Making the most of South Africa's low-quality coal: Converting high-ash coal to fuel gas using bubbling fluidised bed gasifiers. Presented at the 3rd CSIR Biennial Conference, Science Real and Relevant. CSIR Conference Centre, Pretoria, South Africa, September 2010.

Engelbrecht, A.D., North, B.C., Oboirien, B.O. and Majozi, T. (2011). Fluidised bed gasification of South African coals – Experimental results and process integration. Presented at the 36th International Conference on Clean Coal and Fuel Systems: The Clearwater Clean Coal Conference. Shearton Sands Key, Clearwater, Florida, USA, June 2011.

Engelbrecht, A.D., North, B.C., Oboirien, B.O., Everson, R.C. and Neomagus, H.W.P.J. (2011). Fluidised bed gasification of high-ash South African coals: An experimental and modelling study. Presented at the Industrial Fluidisation South Africa 2011 Conference. Johannesburg, South Africa, November 2011.

Engelbrecht, A.D., North, B.C., Oboirien, B.O., Everson, R.C. and Neomagus, H.W.P.J. (2012). Fluidised bed gasification of high-ash South African coals: An experimental and modelling study. Presented at the 5th International Freiburg Conference on IGCC & XtL Technologies. Penta Hotel, Leipzig, Germany, May 2012.

Oboirien, B.O., Engelbrecht, A.D., North, B.C., Erasmus, R. and Falcon, R. (2011). Mineral-char interaction during the gasification of high-ash coals in a fluidised bed gasifier. *Energy and Fuels* 25: 5189-5199.

TABLE OF CONTENTS

LIST OF FIGURES

LIST OF TABLES

GLOSSARY OF SPECIALISED TERMINOLOGY

Char residence time

Average residence time of char particles in a gasifier based on the feedrate of dry devolatilised coal and the mass (inventory) of the fluidised bed.

Cold gas efficiency

Chemical energy content of the product gas relative to the chemical energy content of the coal, usually expressed as a percentage.

Dry gas calorific value

Gross chemical energy content of the gas on a water-free basis, usually expressed as MJ/Nm^3

Fixed carbon conversion

Fixed carbon in the coal converted to gas relative to the initial fixed carbon in the coal, usually expressed as a percentage.

Fluidisation velocity

Gas velocity in the fluidised bed based on the bed area of the gasifier

Gas composition

Concentration of species in the gas on a volume percentage basis

Gross heat content of the gas

Energy released during the combustion of a unit volume of gas, including the latent heat of evaporation of the water formed during combustion.

Oxygen-enriched air

Oxygen enrichment is the difference between the oxygen concentration (vol.%) in the enriched air and the oxygen concentration of air (21 vol.%).

Total carbon conversion

Carbon in the coal converted to gas relative to the initial total carbon in the coal, usually expressed as a percentage.

REFERENCES AND NOMECLATURE

References and nomenclature for each chapter have been listed separately at the end of each chapter. Nomenclature and references used in Appendices A to E has been included in the nomenclature and references of Chapters 1 to 5 respectively.

CHAPTER 1 GENERAL INTRODUCTION

This introductory chapter consists of six sections. Section 1.1 gives background information on the importance of coal in the South African economy, estimated future coal use and the need for new coal utilisation technologies. Commercial fluidised bed coal gasifiers and fluidised bed coal gasifier modelling are discussed in Sections 1.2 and 1.3. The motivation, objectives and scope of the investigation are given in Sections 1.4, 1.5 and 1.6.

1.1 Background information

1.1.1 The importance of coal in South Africa

To sustain economic growth in South Africa an increase in the primary energy supply of ± 2.5% per annum is required (Subramoney *et al*., 2009). The primary energy supply sources of South Africa and the world are given in Figures 1.1 and 1.2.

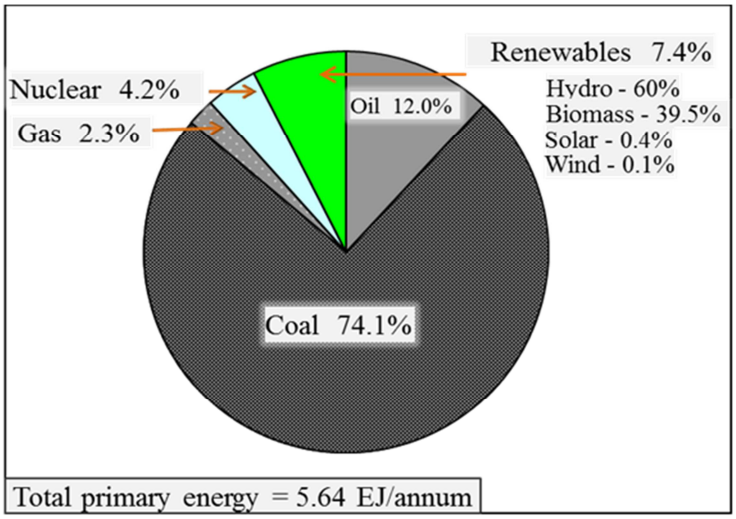

Figure 1.1: South African primary energy sources (Winkler, 2006)

Figure 1.1 shows that due to abundant reserves (34 billion tons), coal is the most important energy source in South Africa, supplying 74.1% of its primary energy. Figure 1.2 shows that due to higher gas and oil use by the rest of the world, coal contributes a significantly lower percentage (24%) to the world energy mix.

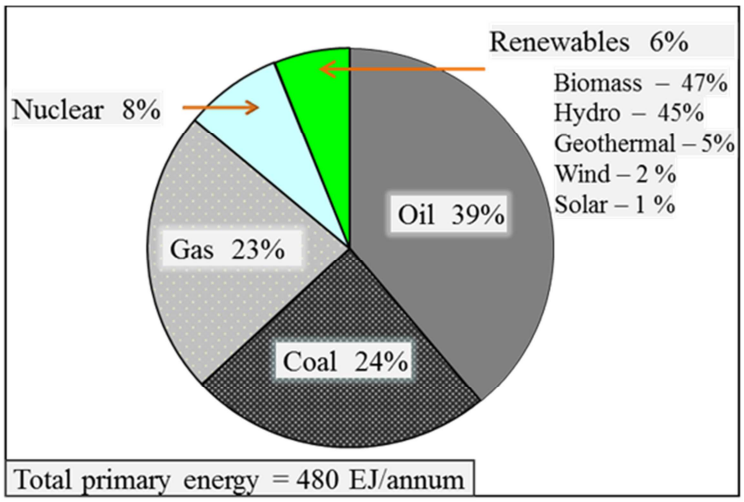

Figure 1.2: World primary energy sources (Winkler, 2006)

Figure 1.3 shows that the coal supply in South Africa consists of 287 Mt/a of run-of-mine production and 10 Mt/a that are reclaimed from stockpiles. Of the 297 Mt/a that is supplied, 40 Mt/a is utilised by Sasol for synfuel production, 110 Mt/a by Eskom for electricity production, 21 Mt/a by smaller industries for heat generation and metallurgical production, 69 Mt/a is exported, 55 Mt/a is discarded and 2 Mt/a is stockpiled. The technologies used for coal utilisation consist mainly of Sasol-Lurgi FBDB gasifiers, PF boilers, chaingrate boilers, fluidised beds, Corex and blast furnaces.

In the preliminary South African coal roadmap presentation by Hall (2011), three future coal use scenarios were presented in order to meet the increase in energy demand (2.5% per annum) in South Africa for the next 25 years. The three scenarios presented are:

Scenario A: Significant coal use

South Africa's extensive coal resources are further exploited. New coal combustion and gasification plants are commissioned in the Waterberg, Soutpansberg and Limpopo coalfields. Coal exports are sustained and increased post 2020. Renewable and nuclear power plants are limited due to capital constraints and delays.

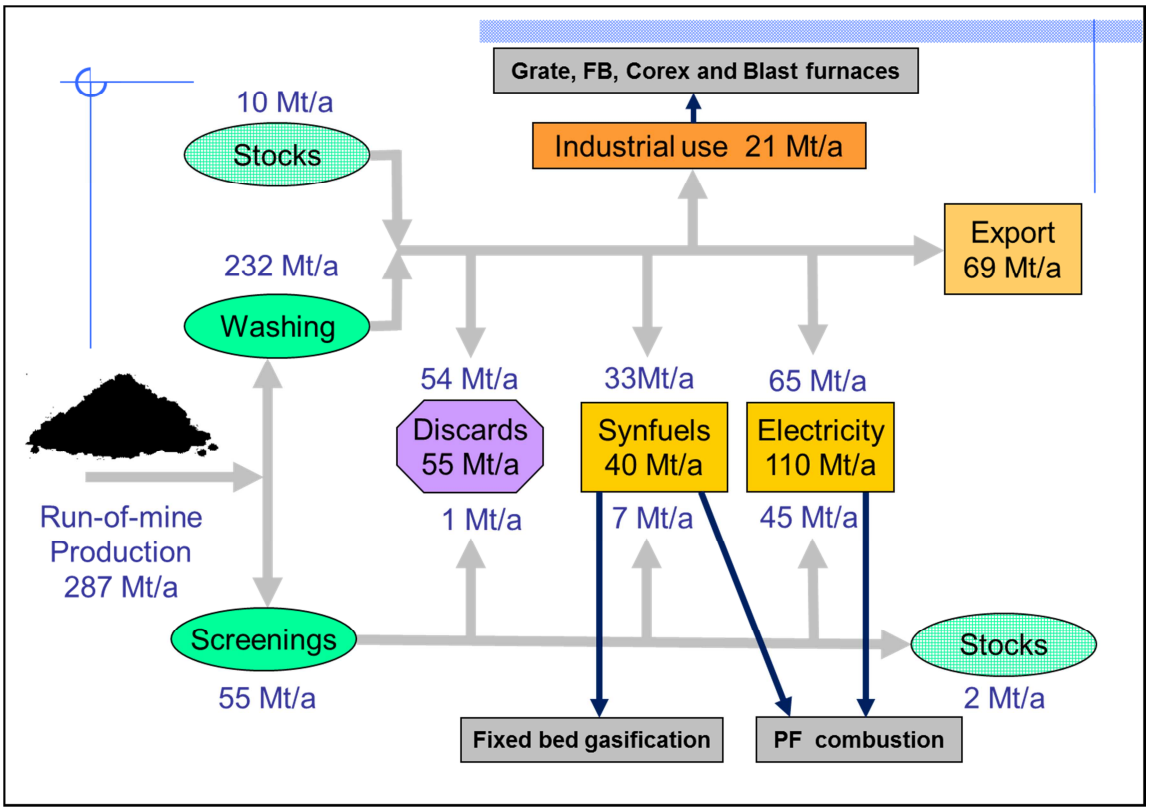

Figure 1.3: South African coal supply chain (Prévost and Msibi, 2005)

Scenario B: Moderate coal use

New coal combustion and gasification plants are planned for the Waterberg and other coalfields. Projects are, however, implemented at a lower rate due to requirements to achieve carbon emission reductions at these plants. After 2020 coal exports increase slowly, if at all. Renewable and nuclear industries experience growth.

Scenario C: Low coal use

Renewable and nuclear industries experience aggressive growth due to binding agreements on climate change. No new large coal plants are built after Medupi and Kusile power stations. The Waterberg coalfield is not developed beyond the current mines. Exports decline after 2015.

In the case of either scenario A or B being realised, significant new investment in coal combustion and gasification plant will be required. The estimated increase in the amount of coal consumed by gasification in 2036 above 2006 levels is 18 Mt/a, i.e. 48 Mt/a in total (Appendix A.1). The estimation is based on:

- The supply of primary energy increases at 2.5% per annum.
- The contribution of coal to the total energy mix decreases to 60% by 2036.
- Gasification utilises 17.5% of all coal utilised domestically to 2036.

Coal gasifiers are expected to be applied in future IGCC and CTL plants. The advantage of IGCC power plants based on coal gasification compared with conventional PF power plants that are based on coal combustion is that their water consumption and CO_2 emission rates per unit of energy generated are lower.

It is projected that, in future, more than 50% of South Africa's coal demand will be supplied from the Waterberg, Soutpansberg and Limpopo coal basins (Hartnady, 2010). Characterisation of these high-ash coals for efficient and clean utilisation by underground and surface gasification technologies is therefore important.

1.1.2 Coal gasification technologies

Technologies used for the gasification of coal are dominated by three basic configurations which are:

- Moving (or fixed) bed gasifiers.
- Fluidised bed gasifiers.
- Entrained flow gasifiers.

Although there are many variations within the three basic configurations, the principle of operations remains essentially the same. The three basic configurations are presented in Figure 1.4.

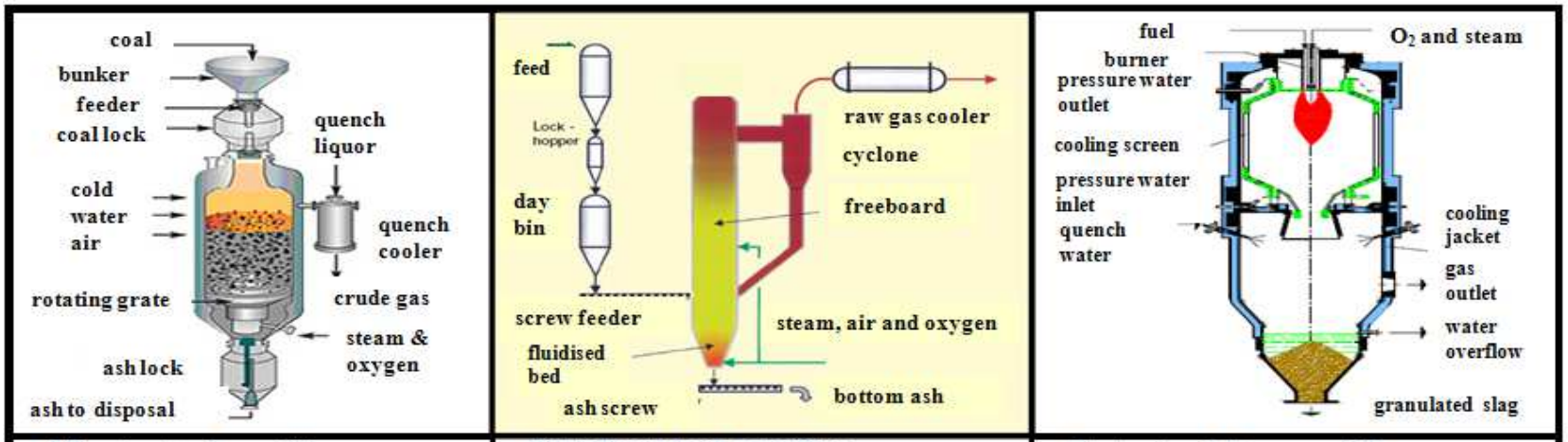

Moving bed gasifier

Advantages:
- High gasification efficiency
- Long coal residence time
- High-ash coals can be gasified
- Low O_2 consumption.

Disadvantages:
- Coal size 8 – 50 mm
- Produces tar and CH_4
- Rotating grate
- Caking coals - agglomeration.

Fluidised bed gasifier

Advantages:
- Coal size 0 - 5 mm
- High-ash coals can be gasified
- Low tar and CH_4 concentrations
- Extended refractory life

Disadvantages:
- Lower gasification efficiency
- Mixed flow reactor
- Bed agglomeration at high pressure
- High bed voidage limits gas output.

Entrained flow gasifier

Advantages:
- Very low tar and CH_4 concentrations
- Caking coals can be gasified
- High pressure operation possible
- Fine coal can be gasified.

Disadvantages:
- Reduced refractory life
- High sensible heat losses
- High oxygen consumption
- Low-ash coals required.

Figure 1.4: Basic gasifier configurations (Adapted from Morehead, 2006; Radtke, 2011)

1.1.2.1 Moving bed gasifiers

Sized lump coal (8–50 mm) is fed into the top of the gasifier. A bed of coal moves slowly down under gravity in plug flow and is gasified by reacting gases (air, oxygen and steam) moving upwards in a counter-current fashion. Three separate coal-processing zones are present in the gasifier: the devolatilisation zone, the gasification zone and the combustion zone. At the top of the gasifier, the coal is devolatilised by hot gases leaving the gasification zone.

In the gasification zone, char is gasified by hot CO_2 and H_2O leaving the combustion zone. In the high-temperature (1 350 °C) combustion zone, residual char is combusted by oxygen entering the bottom of the gasifier, resulting in a high fixed carbon conversion.

Due to the low temperature (500 °C) in the devolatilisation zone at the top of the gasifier, the gas produced by the gasifier contains high concentrations of CH_4, tars and oils. Coals that have a high free swelling index and a high caking index are difficult to process in moving bed gasifiers since swelling and caking of the coal results in agglomeration, which interferes with the free downward movement of the coal. Stirrers and rotating arms can be fitted to break up the agglomerates, but these components require extensive maintenance.

The oxygen consumption is low since the coal is pre-heated with the existing gas, and due to separation of the combustion and gasification zones, oxygen consumption by gas combustion is reduced to a minimum.

1.1.2.2 Bubbling fluidised bed gasifiers

In a fluidised bed gasifier, the reacting coal particles (0.5–5 mm) are suspended (fluidised) by the reactant gases (air, oxygen and steam) entering the bottom of the bed through a distributor plate. The coal particles are well mixed in the bed, resulting in an uniform temperature distribution in the bed. Fluidised bed gasifiers operate at temperatures (900–1 050 °C) that are well below the ash softening point of the coal to

avoid ash melting, agglomeration and subsequent defluidisation of the bed. Although the good mixing of gas and solids in a fluidised bed gasifier promotes good heat and mass transfer, it has its disadvantages. When ash is extracted from the bed in order to maintain a constant bed height, this will inevitably result in the removal of unreacted carbon particles, thereby reducing the fixed carbon conversion that can be achieved. Thermal fragmentation and attrition in the bed results in the entrainment of fine unconverted char particles from the gasifier with the exit gas, which also reduces the fixed carbon conversion. Fluidised bed gasifiers produce significantly lower concentrations of CH_4 and tar concentrations in the exit gas compared with moving bed gasifiers, since:

- The feed coal is devolatilised at a higher rate and at a higher temperature.
- The volatiles are released throughout the whole bed and react with oxygen in the lower part of the bed.

1.1.2.3 Entrained flow gasifiers

In an entrained flow gasifier, the coal and reacting gases flow co-currently through the gasifier. The coal is fine enough (< 100 µm) and the gas velocity high enough so that the coal particles are conveyed pneumatically (entrained) by the reacting gases to the exit of the gasifier. Due to the low residence time of coal particles, a high operating temperature is used (> 1 500 °C) to increase the fixed carbon conversion.

The operating temperature is usually above the ash melting point so that the molten ash is removed from the gasifier as a liquid slag. A fluxing agent such as limestone is often used to reduce the ash melting point of high-AFT coals, thereby reducing the oxygen consumption. The high operating temperature of entrained flow gasifiers results in very low concentrations of CH_4 and tars in the gas. The disadvantages of the high operating temperature of entrained flow gasifiers are:

- High sensible heat losses reduce the gasification efficiency.
- Attack of refractories and syngas coolers is accelerated.
- Oxygen consumption is high.

Entrained flow gasifiers are not specific to a particular coal and can gasify practically any type of coal. The use of coals with very high ash contents and high moisture contents, however, increases the oxygen consumption in order to maintain the high operating temperature.

1.1.3 Coal gasification in South Africa

The moving bed gasifier has been used extensively in South Africa since 1955. Sasol currently operates 84 moving bed gasifiers at its synfuel plants in Secunda, which gasify ± 30 Mt/a of high-ash, non-caking coal.

Six Kopers-Totzek entrained flow gasifiers were operated between 1975 and 1999 by African Explosives and Chemical Industries (AECI) at Modderfontein for ammonia production. The gasifiers gasified ± 1 Mt/a of bituminous coal and produced ± 100 000 Nm^3/h of syngas containing 60 vol.% CO.

Fluidised bed gasification has not been used commercially in South Africa. A few pilot-scale investigations and a demonstration-scale investigation have been carried out. Limited information on these investigations is however available in the public domain.

Although the moving bed gasifier has been successfully applied in South Africa for many years, in future new gasification technologies may be required for the utilisation of coal from the Waterberg, Soutpansberg and Limpopo coal basins. The coals from these basins are known to have caking properties (Pinheiro *et al.*, 1999), which could be problematic for their utilisation in moving bed gasifiers (Van Dyk *et al.*, 2005).

Although entrained flow gasifiers are able to gasify caking coals, the high ash content of coal from the Waterberg, Soutpansberg and Limpopo coal basins could be problematic when they are utilised in entrained flow gasifiers.

Although fluidised bed gasifiers are able to gasify high-ash South African coals, the low reactivity of these coals may result in lower gasification efficiencies for the reasons given in Section 1.1.2.2.

1.2 Commercial fluidised bed coal gasifiers

Three variations of the fluidised bed coal gasifier have been applied commercially.

1.2.1 The Winkler fluidised bed coal gasifier

The first Winkler gasifier started commercial operation in 1926, in Central Germany, producing fuel gas for gas engines that compressed ammonia synthesis gas and hydrogen for tar hydrogenation (Squires, 1983). The first Winkler gasifiers operated at atmospheric pressure and at temperatures of 850 °C to 950 °C, utilising lignite as fuel. The Rheinische Braunkohlenwerke in Germany developed the High-Temperature Winkler (HTW) process which can be operated at pressures up to 30 bar (Brungel *et al.*, 1989). The basic configuration of the HTW Winkler gasifier is given in Figure 1.4. A commercial HTW gasifier, with a feed capacity of 25 tons/h dry lignite, operated from 1989 to 1999 at Berrenrath near Cologne, West Germany. The gasifier operated at a pressure of 10 bar and produced 34 000 Nm^3/h synthesis gas for methanol production. The major disadvantage of the HTW gasifier is that only reactive non-caking coals can be used as feedstock. The use of unreactive caking coals in the HTW process results in low carbon conversions and de-fluidisation of the bed. Currently, there are no commercial HTW gasifiers in operation.

1.2.2 The U-GAS® fluidised bed agglomerating ash gasifier

The U-GAS® fluidised bed gasifier, which has the advantage that caking coals can be gasified, was developed by the Gas Technology Institute (GTI) in the USA. A schematic representation of the gasifier is given in Figure 1.5. The operating concept involves maintaining two distinct zones within the same vessel. The bottom ‘hot zone’ generated by a jet of steam, oxygen and coal is maintained at temperatures above the ash sintering temperature. At these temperatures the ash is sticky and agglomerates into particles that are low in carbon. The agglomerates grow in size until

they defluidise and drop out of the bed through the bottom classifying throat. The first commercial U-GAS® fluidised bed gasifier was commissioned during 2008 in Shandong province, China. High-ash discard coal is gasified, producing 28 000 Nm^3/h of syngas for methanol production. A second plant is scheduled for start-up in 2014 in Henan province, China, to produce 45 000 Nm^3/h of syngas for ammonia synthesis (Preston, 2012).

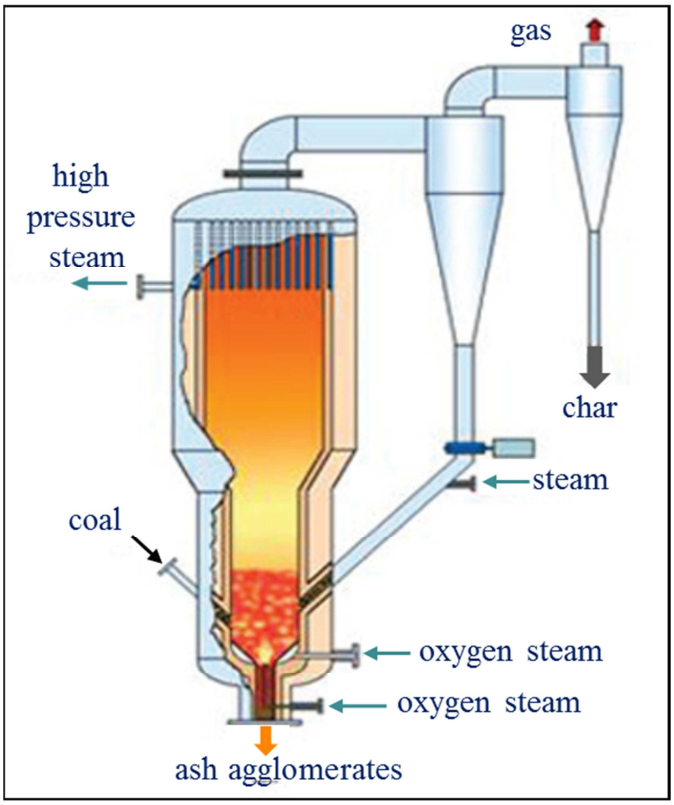

Figure 1.5: U-GAS® agglomerating ash gasifier (Preston, 2012)

1.2.3 The KBR - TRIG™ transport gasifier

The transport gasifier shown in Figure 1.6 is an advanced circulating fluidised bed gasifier designed to operate at higher pressures (2.8 MPa), gas velocities and solids circulation rates than conventional circulating fluidised bed gasifiers.

Finely ground coal (< 0.25 mm) and air are fed into the upper mixing zone where the coal is devolatilised and the oxygen in the air reacts with the char (devolatilised coal) to form CO and CO_2. Tar formed during devolatilisation is cracked in the riser due to

the high temperature (950–1 000 °C). Fine char particles leaving the riser are captured by a two-stage cyclone system which delivers the char to a standpipe from where it is recirculated to the riser by means of a J-valve. The recycled char reacts with oxygen and steam, which are injected into the lower mixing zone. To maintain a constant gasifier inventory (hold-up), ash is removed periodically from the lower region of the standpipe. The transport gasifier operates as a non-slagging gasifier, thereby increasing the refractory life (Pinkston and Morton, 2006).

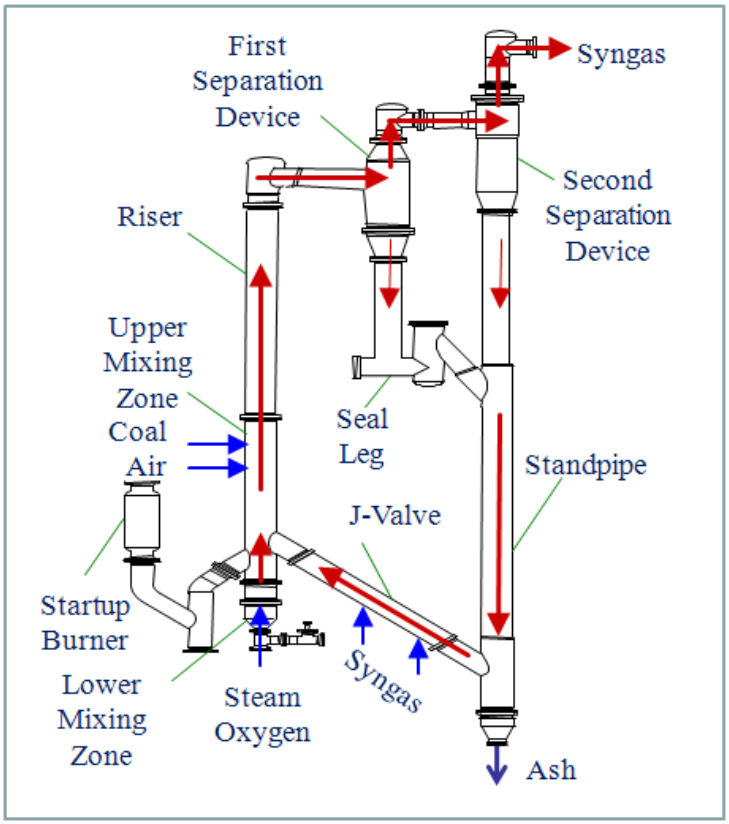

Figure 1.6: The KBR - TRIG™ transport gasifier (Pinkston and Morton, 2006)

Three plants that are scheduled to be commissioned within the next two years have selected KBR - TRIG™ technology for coal gasification.A 550 MW IGCC plant is scheduled for start-up during 2014 in Kemper County, Mississippi, USA. The plant will use two TRIG™ gasifiers for the gasification of lignite and the generation of fuel gas to be fired into two Siemens SGT6-5000F gas turbines. Three million tons per annum of CO_2 will be captured and sequestrated to saline aquifers.

In Dongguan province, China, a 120 MW IGCC plant is scheduled for start-up during 2014. The feed coal to the plant will be high-ash bituminous coal. A third plant is scheduled for start-up during 2015 in Inner Mongolia, China, to produce 35 000 Nm^3/h of syngas for ethylene glycol synthesis using high-ash lignite (Rush, 2011).

1.3 Mathematical modelling of fluidised bed coal gasifiers

Due to advances in computers and software, modelling has become one of the most important tools available to developers, designers and operators of fluidised bed coal gasifiers. The gasification of coal in a fluidised bed reactor is a complex process involving many sub-processes such as hydrodynamics, devolatilisation, chemical reactions, heat transfer and mass transfer, all of which occur simultaneously. Prediction of the effect of input variables such as the gasifier configuration, flow, composition and temperature of the reactants on the performance of the gasifier is therefore not straightforward. The human mind cannot interpret any single phenomenon or combination of phenomena in which more than three variables are involved. The use of graphical methods is also limited to a maximum of three input variables (de Souza-Santos, 2010). Mathematical models provide a systematic methodology based on combinations of fundamental and empirical equations and can therefore predict the effect of an unlimited number of input variables on the performance of a process (Grace and Abba, 2005).

The value of models to engineers and scientists are:

- During model development an in-depth understanding of and insight into the process and the various sub-models used in the model are obtained.

- Models can be used to identify factors that limit the performance of the process. Research efforts can therefore be focused in these areas in order to overcome these limitations.

- The performance of the gasifier can be explored outside the range of experimental data, thereby reducing the number of expensive pilot-scale tests that are required.

- The process can be analysed in areas where the measurement of conditions is difficult or impossible. In a fluidised bed gasifier this would be the temperature and gas composition of the bubble and emulsion phases in the bed.

- Models that have been calibrated using experimental data can be used for the design, optimisation, scale-up and adaptive control of fluidised bed coal gasifiers.

When modelling a complex system such as a fluidised bed coal gasifier, it is important to incorporate the appropriate degree of complexity relative to the application of the model. For example, if one is developing a model to predict the thermal performance of a gasifier in terms of fixed carbon conversion and calorific value of the gas, inclusion of reactions involving sulphur and nitrogen species to predict the emission of pollutants such as H_2S, COS, SO_2, NO, NO_2, N_2O and NH_3 would not be required.

1.4 Research motivation

The motivation for conducting an experimental and modelling study into the fluidised bed gasification of high-ash South African coals using oxygen-enriched air is:

- In future, new gasification technology may be required to gasify coals that cannot be effectively gasified by Sasol FBDB gasifiers. The generation of pilot-scale and bench-scale gasification data on coals that are expected to be utilised in these gasifiers (Waterberg coals) is therefore important.

- The ash content of South African coal for domestic use is expected to increase since lower-grade coal seams are being mined and high-ash waste coal is being generated due to the need to beneficiate coal for the export market.

- A pilot-scale fluidised bed coal gasifier is available at the CSIR in Pretoria, as well as extensive know-how regarding the set-up, commissioning and operation of pilot-scale fluidised beds.

- The decision to use oxygen-enriched air for gasification was motivated by the low gas calorific values that were obtained (Engelbrecht, 2008) during earlier pilot-scale fluidised bed gasification tests carried out on high-ash South African coals at the Council for Scientific and Industrial Research.

The motivation for developing a model for a bubbling fluidised bed coal gasifier is:

- An existing commercial fluidised bed coal gasifier simulation model was found to be unsuitable for simulating the gasification of high-ash unreactive South African coals in a fluidised bed at temperatures higher than 900 °C. Under these conditions the model produces stiff differential equations, which results in convergence problems and the generation of mass balance errors.

- An in-depth understanding of the chemical and physical processes that take place in a fluidised bed coal gasifier can be obtained during model development.

- The model can be used for process analysis, design, optimisation and scale-up.

- The model can be extended later to other processes such as:

    - Circulating fluidised bed gasifiers.
    - Chemical looping fluidised bed systems.
    - Dual fluidised bed gasifiers.

1.5 Objectives of the study

The overall objectives of this study are to:

- Conduct the following tests on two high-ash South African coals:
    - Characterisation tests using standard coal analytical techniques.
    - Thermogravimetric analyser tests to determine kinetic parameters for the char-steam and char-CO_2 gasification reactions.
    - Devolatilisation tests using a bench-scale fluidised bed reactor to determine evolution rates of volatile gases.
    - Pilot-scale fluidised bed gasification tests using oxygen-enriched air and steam as the gasification agents.

- Develop a fluidised bed coal gasifier model that is based on fluidised bed hydrodynamics, coal devolatilisation, rates of chemical reactions and rates of heat and mass transfer in the gasifier.
    - Carry out simulation runs using the model with kinetic parameters obtained from the thermogravimetric analyser and bench-scale tests on New Vaal and Grootegeluk coals.
    - Test the predictive capability of the model by comparing model predictions with the data from the pilot-scale fluidised bed gasifier.
    - Gain insight and understanding into the coal gasification process in a bubbling fluidised bed gasifier by studying the variation of the reaction rates, temperatures, gas concentrations and bed voidage as a function of bed height in the gasifier predicted by the model.
    - Study the effect of major operating variables on gasifier performance by using the fluidised bed coal gasifier model.

1.6 Scope of the investigation

1.6.1 Background and motivation

Chapter 1 gives an overview of coal as an energy source in South Africa and of coal gasification technology and gasifier modelling. It also gives the motivation for the project, followed by the objectives of the investigation.

1.6.2 Coal selection and characterisation

Chapter 2 contains information on the origin of the two coals selected and the criteria for their selection. The results of the detailed coal characterisation tests are given. The characterisation tests consisted of:

- Proximate, ultimate and calorific value analyses.
- Ash melting temperature and ash analysis.
- Petrographic analysis and rank.
- Structural and physical properties.
- Free swelling index and Roga index.
- Hardgrove grindability index.
- Particle size analysis.

1.6.3 Bench-scale gasification and devolatilisation experiments

Chapter 3 describes thermogravimetric analyser and bench-scale fluidised bed devolatilisation tests carried out on New Vaal and Grootegeluk coals. Thermogravimetric analyser tests were carried out to determine kinetic parameters for the Johnson char-steam and a first-order char-CO_2 rate equation which are included as sub-models in the fluidised bed coal gasifier model described in Chapter 5. FB coal devolatilisation tests were carried out using a 50 mm diameter fluidised bed reactor to determine parameters for a coal devolatilisation sub-model also included in the fluidised bed coal gasifier model.

1.6.4 Pilot-scale fluidised bed coal gasification tests

In Chapter 4 a detailed investigation is conducted into the gasification of coal in pilot-scale fluidised bed gasifiers. Included in Chapter 4 is a literature review of selected pilot-scale fluidised bed coal gasification studies that have been reported in the literature. Descriptions of the pilot-scale fluidised bed coal gasifier at the CSIR, the experimental programme and the results of gasification tests on two high-ash South African coals are given.

1.6.5 Fluidised bed coal gasifier modelling

In Chapter 5 a detailed investigation is conducted into the modelling of fluidised bed coal gasifiers. Included in Chapter 5 is a literature review of selected fluidised bed coal gasifier modelling studies that have been reported in the literature. The development of a fluidised bed coal gasifier rate model, its predictive capability and application are described.

1.6.6 Conclusions and recommendations

In Chapter 6 conclusions are drawn based on the results of this investigation. The contribution the investigation has made to the knowledge base of science and technology is stated. Finally, recommendations are made for future work on the gasification of high-ash South African coals.

1.7 Chapter 1 references

BRUNGEL, N., LAMBERTZ, J. AND THEIS, K.A. (1989). Stages of Development of the HTW Process Regarding its Suitability for Combined-cycle Plants. Rheinische Braunkohlenwerke AG report.

DE SOUZA-SANTOS, M.L. (2010). Solid fuels combustion and gasification – modeling, simulation and equipment operations, Chapter 1. Boca Raton, London, New York: Taylor and Francis Group, 1–17.

ENGELBRECHT, A.D. (2008). Characterization and fluidised bed gasification of selected high-ash South African coals. Master's dissertation, North-West University, South Africa.

GRACE, J.R. AND ABBA, I.A. (2005). Recent progress in the modelling of fluidised bed reactors. Proceedings of Industrial Fluidisation South Africa, Johannesburg, South Africa, 16 November 2005.

HALL, I. (2011). The SA coal industry: Present context and preliminary future scenarios. SANEA Lecture, Johannesburg, October 2011.

HARTNADY, C.J.H. (2010). South Africa's diminishing coal reserves. *The South African Journal of Science* 106: 1–5.

MOREHEAD, H. (2006). Siemens Global Gasification and Integrated Gasification Combined Cycle Update. Paper presented at the Gasification Technologies Conference, Washington, D.C., 2–4 October 2006.

PINHEIRO, H.J., PRETORIUS, C.C., BOSHOFF, H.P. AND BARKER, O.B. (1999). A techno-economic and historical review of the South African coal industry in the 19th and 20th centuries and analysis of coal product samples of South African collieries 1998-1999. Coal Bulletin 113. Issued by the South African Bureau of Standards (SABS) and the Department of Minerals and Energy (DME).

PINKSTON, T. AND MORTON, F. (2006). Orlando Gasification Project: Demonstration of a 285 MW coal-based transport gasifier. Paper presented at the 31st International Technical Conference on Coal Utilization and Fuel Systems, Sand Key Island, Florida, 21–25 May 2006.

PRESTON, W. (2012). Update on SES projects and progress. Paper presented at the Gasification Technologies Conference, Washington D.C., 29–31 October 2012.

PRÉVOST, X.M. AND MSIBI, M.D. (2005). In: DUVAL, J.A.G., *South African Minerals Industry 2005-2006*, Department of Minerals and Energy report, 42–50.

RADTKE, H. (2011). ThyssenKrupp Uhde's PRENFLO® and HTW™ Gasification Technologies. Global Update and Technology Projects. Paper presented at the Gasification Technologies Conference, San Francisco, CA, 9–12 October 2011.

RUSH, R. (2011). Overview of the Kemper County and TMEP IGCC Projects using Transport Integrated Gasification (TRIG^{TM}). Paper presented at the Gasification Technologies Conference, San Francisco, California, 9–12 October 2011.

SQUIRES, A.M. (1983). Three bold exploiters of coal gasification. In: HOWARD, J.R. (Ed), *Fluidized Beds – Combustion and Applications*, Chapter 8. London and New York: Applied Science, Winkler, Godel and Porta, 277–304.

SUBRAMONEY, J., VAN WYK, J., DITHUPE, M., MOLAPO, A., MAHLANGU, N. AND MORUMUDI, R. (2009). Digest of South African Energy Statistics – 2009. Directorate: Energy Information Management, Process Design and Publications.

VAN DYK, J.C., KEYSER, M.J. AND COERTZEN, B. (2005). Syngas production from South African coal resources using Sasol-Lurgi gasifiers. *International Journal of Coal Geology* 65: 243–253.

WINKLER, H. (2006). Energy policies for sustainable development in South Africa – Options for the future. Energy Research Centre, University of Cape Town, April 2006.

1.8 Chapter 1 and Appendix A nomenclature

Acronyms/Abbreviations

AECI	African Explosives and Chemical Industries
AFT	ash fusion temperature
CH_4	methane
CO_2	carbon dioxide
CSIR	Council for Scientific and Industrial Research
CTL	coal to liquids
EJ	Exajoule (10^{18} J)
FB	fluidised bed
FBDB	fixed bed dry bottom
GTI	Gas Technology Institute
H_2O	steam
HTW	high-temperature Winkler
IGCC	integrated gasification combined cycle
KBR	Kellogg Braun and Roots
Mt	million tons

Mt/a	million tons per annum
O_2	oxygen
PF	pulverised fuel
TGA	Thermogravimetric analyser
TRIG™	Transport Integrated Gasification
USA	United States of America

CHAPTER 2 COAL CHARACTERISATION

2.1 Introduction

This chapter describes aspects concerned with characterisation of the two coals selected for the bench-scale experimentation, pilot-scale fluidised bed gasification and fluidised bed gasifier modelling described in Chapters 3, 4 and 5. The formation process of coal and how it has resulted in the origin of different types of coal, is reviewed in Section 2.2. Section 2.3 gives the criteria used for coal selection and information on the origin of the coals. Section 2.4 gives a description and results of the various coal characterisation tests carried out on the two coals. The results are compared to the analysis of other South African coals that are utilised for power and synthetic fuel production. The coal characterisation results that are required as input to a fluidised bed coal gasifier model is given in Section 2.5. Finally, a summary of the coal characterisation tests is given in Section 2.6.

2.2 Literature review

The formation process of coals has resulted in the origin of many different types of coal that today affect their mining, processing and utilisation. Coal is known to have originated from dense forests that were covered with soil and water millions of years ago. The buried vegetation was subjected to increasing temperature and pressure as more soil layers were deposited over the course of time. The degree of metamorphism that the vegetation underwent resulted in the formation of coals with different ranks. Coals are usually classified as low-rank, medium-rank or high-rank depending on their degree of metamorphism and maturity as shown in Table 2.1 (Ergun, 1979). With increasing rank, the carbon content of coals increases while the moisture, hydrogen and oxygen contents decrease.

Coals of the same rank can have different properties such as mineral matter content and maceral composition depending on the conditions under which the coal was formed. These include:

- the prevailing climate.
- the nature of the underlying soil and rock.

- the physiography of the area surrounding the accumulated vegetation.
- the nature of the swamp water, that is, its pH level and its oxygen and mineral contents both in solution and in suspension.

The type of plants that were present when the swamp was formed also has an effect on coal properties (Horsfall, 1993).

Table 2.1: Rank classification system of coal

Coal rank		Approximate age (Myr)	Geological period of origin
Low-rank	Lignite	30 – 100	Tertiary and Cretaceous
	Sub-bituminous	80 – 250	Cretaceous, Jurassic and Triassic
Medium-rank	Bituminous	250 – 320	Permian and Carboniferous
High-rank	Semi-anthracite	300 – 360	Carboniferous
	Anthracite		Carboniferous

The majority of South African coal reserves (95%) are ranked as bituminous (Pinheiro *et al*., 1999). On the other hand, more than 50% of the coal reserves of North America and China are ranked as sub-bituminous and lignite.

During the Permian geological period South Africa, India and Australia formed the supercontinent of Gondwanaland in the southern hemisphere. Other major coal regions of the world such as North America, Europe, Russia and China formed the supercontinent of Laurasia in the northern hemisphere. It is thought that different climatic conditions and types of vegetation between the northern and southern hemispheres contributed to the differences in characteristic properties between typical northern hemisphere and southern hemisphere bituminous coals that are found today (Arnold, 2013).

Bituminous coals from South Africa, India and Australia generally have higher ash (mineral matter) contents and ash fusion temperatures than coals from North America and Europe. On the other hand, northern hemisphere bituminous coals have higher sulphur and volatiles matter contents than southern hemisphere bituminous coals (Hattingh, 2012).

The mineral matter in South African and Indian coals are often described as inherent and included, which means that the minerals are embedded in bands of vitrinite and inertinite (Falcon, 2013). When minerals are mixed with coal in this fashion it limits the extent to which coal can be beneficiated (de-ashed) economically. Fluidised bed combustors and gasifiers are therefore being investigated for the utilisation of high-ash South African coals that would otherwise not be suitable for pulverised fuel combustors and entrained flow gasifiers.

2.3 Coals selected for this study

The two coals chosen for the study are from the New Vaal and the Grootegeluk opencast coal mines. Geographical, technical and historical information on the selected coals is given in Table 2.2 and Figure 2.1 (Pinheiro *et al*., 1999).

Table 2.2: Information on the selected South African coals

Colliery	**New Vaal**	**Grootegeluk**
Location of mine	Free State province	Limpopo province
Coalfield	Vereeniging – Sasolburg	Waterberg
Production rate (Mt/a)[1]	15.2	15.0
Started production	1985	1985
Estimated lifetime (years)[1]	40–50	40–50
Coal preparation	Washing and screening	Washing
Receiving power station	Lethabo	Matimba
Power station rating (GWe)	3.6	3.6

[1] Mine production and estimated lifetime of the mine in 2005

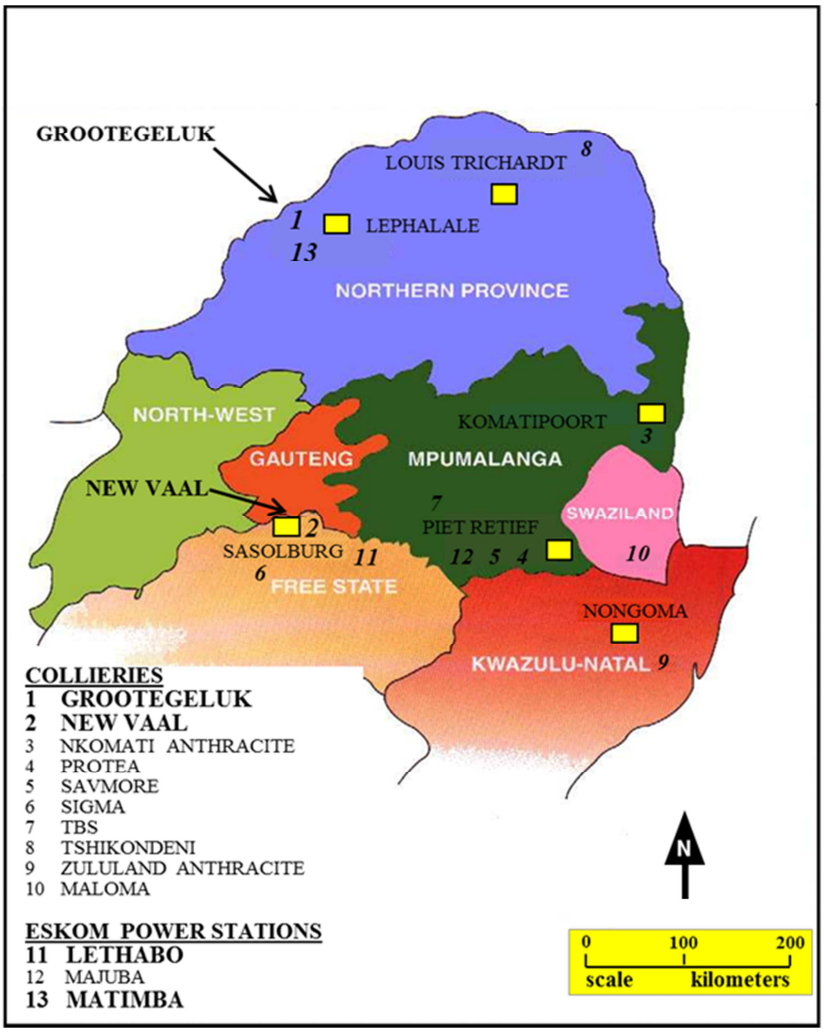

Figure 2.1: Location of selected coal mines and Eskom power stations (Adapted from Pinheiro *et al.*, 1999)

New Vaal and Grootegeluk coals were selected since they are potential feed coals to new coal gasification plants in the future. The criteria used for selection were:

- Extensive reserves of these coals are available.
- They have high ash contents.
- They have differing reactivities.

The SABS Coal Bulletin 113 (Pinheiro *et al.*, 1999) was used to obtain estimates of the coal reserves, the ash contents and the reactivities of coals produced by South African coal mines. It was therefore a useful aid in the final selection of the two coals for this study.

2.3.1 New Vaal coal

Figure 2.1 shows that the New Vaal coal colliery is located in the Vereeniging – Sasolburg coalfield and is a dedicated supplier of 15.2 Mt/a coal to the Lethabo power station. The colliery is situated 10 km south of Vereeniging on the Free State bank of the Vaal River.

At the New Vaal colliery, three seams are mined simultaneously using opencast strip mining techniques. The top seam (No. 3 seam), which is 9.7 m thick, is covered with 28.5 m of overburden (sand and shale). The middle seam (No. 2 seam) is 11.0 m below the top seam and has a thickness of 6.0 m. The bottom seam (No. 1 seam) is located a further 2 m below the middle seam and has a thickness of 4.9 m. Coal from the top seam has the lowest quality, and after beneficiation in two Drewboy washers, is blended with coal from the middle and bottom seams to yield a product with an ash content of ± 38% (Laybourne and Watts, 1990).

The blended sample that is supplied to the Lethabo power station is the coal that was used for this study. New Vaal coal is the coal with the highest ash content currently being utilised in an Eskom power station.

The reserves of the current New Vaal colliery have been estimated (2005) to be 750 Mt, which at current extraction rates would last for 50 years. In future the colliery can also be extended to the west (Machauvlei area) which has estimated additional reserves of 100 Mt.

2.3.2 Grootegeluk coal

Figure 2.1 shows that the Grootegeluk coal mine (GCM) is located in the Waterberg coalfield and supplies 15 Mt/a of steam coal to the Eskom Matimba power station, 1 Mt/a metallurgical coal for Exxaro’s Corex and Blast Furnace plants and 0.5 Mt sized steam coal for use in chain grate stoker-fired boilers. The coal obtained for this study is the steam coal supplied to the Matimba power station.

The Waterberg coalfield has vast in situ coal resources estimated to be more than those of the Witbank and Highveld coalfields combined (Pinheiro *et al.*, 1999). The recoverable coal reserves using conventional extraction technologies are estimated to be 15.5 Bt (Jeffrey, 2005, after Bredell, 1987). The coal in the Waterberg coalfield is present in two coal sequences. The upper sequence (Grootegeluk formation) is ± 60 m thick and contains seven thin coal seams that are interlaminated with carbonaceous mudstone, siltstone and sandstone. The GCM is located in the area of the coalfield where the Grootegeluk formation is shallow, and therefore surface mining techniques are used to extract the coal.

Due to the embedded and intercalated nature of the coal, siltstone and mudstone bands in the Grootegeluk formation, the ash content of the extracted coal (ROM) is high (± 55%). Before being transported to the Matimba power station, the coal is washed (beneficiated) in order to reduce the ash content from ± 55% (as mined) to ± 35%. Discards with an ash content of ± 75% are produced during the washing process. The GCM is currently being expanded to supply an additional 15 Mt/a of beneficiated coal to the new Eskom Medupi power station which is scheduled to start operation in 2014.

The lower coal sequence of the Waterberg coalfield (Vryheid formation) is 55 m thick and contains four coal seams that are thicker than the seams in the upper sequence. The coal in the lower coal sequence (Vryheid formation) is, however, more difficult to extract due to the greater depth of the Vryheid formation (250–400 m). Exxaro is currently developing underground extraction of the Vryheid formation.

2.4 Results of standard coal characterisation tests

Characterisation results for New Vaal and Grootegeluk coals using standard methods are reported in this section. A description of these methods is given by Engelbrecht (2008). The coal characterisation tests selected are those that were considered relevant to the current investigation, namely the fluidised bed gasification of coal. The possible effect of coal properties on the operation and performance of fluidised bed coal gasifiers is discussed in each analyses section. Relationships between the results of the various characterisation methods are also explored. The analyses of the New Vaal and

Grootegeluk coals are compared to the analyses of six other high-ash South African coals that are utilised by Eskom and Sasol for power and synfuel production. The analyses of the six other South African coals were obtained from Pinheiro *et al*. (1999), and comparisons were therefore only made for the analysis given in this report and not for all the analyses carried out on Grootegeluk and New Vaal coals.

2.4.1 Proximate, ultimate and calorific value analyses

The proximate, ultimate and calorific value analyses allow mass and energy balances to be calculated for coal utilisation processes which are required for the modelling of these processes.

The results of the proximate, ultimate and calorific value analyses carried out by Advanced Coal Technologies (Pretoria) and the methods used are given in Table 2.3.

Table 2.3: Proximate analysis, ultimate analysis and calorific value

	Method	New Vaal	Grootegeluk
Proximate analysis			
Ash content (wt.%)	ISO 1171	37.50	31.70
Inherent moisture (wt.%)	SABS 925	5.91	1.90
Volatile matter (wt.%)	ISO 562	20.74	28.30
Fixed carbon (wt.%)	By difference	35.85	38.10
Ultimate analysis			
Carbon (wt.%)	ISO 12902	44.07	52.93
Hydrogen (wt.%)	ISO 12902	3.54	4.11
Nitrogen (wt.%)	ISO 12902	0.98	1.19
Sulphur (wt.%)	ISO 19759	0.66	1.17
Oxygen (wt.%)	By difference	7.34	7.00
Calorific value			
Gross calorific value (MJ/kg)	ISO 1928	17.71	21.41

Table 2.3 shows that the selected coals have low calorific values and high ash contents. Due to the higher ash content of New Vaal coal, it has a lower calorific value than Grootegeluk coal. According to the SABS grading system (CKS 561 –

1982), which grades coal based on calorific value, the New Vaal and Grootegeluk coal are both classified as grade D coals.

Although fluidised bed gasifiers are known for their ability to process grade D coals, the high ash content of these coals could have a negative impact on the efficiency of the gasifier.

Table 2.4 shows that the ash content and calorific value of Grootegeluk coal is similar to the ash content of six other coals utilised by Eskom and Sasol.

Table 2.4: Proximate and ultimate analysis of selected Eskom and Sasol coals

	Eskom power station coals				**Sasol coals**	
Colliery	Matla	Duvha	Kriel	New Denmark	Bosjes-spruit	Syfer-fontein
Power station	Matla	Duvha	Kriel	Tutuka	Sasol 1 & 2	
Proximate analysis						
Ash content (wt.%)	33.4	32.5	30.4	31.6	32.8	28.3
Inherent moisture (wt.%)	3.5	1.8	4.9	3.5	3.9	5.6
Volatile matter (wt.%)	21.0	19.9	21.9	21.9	21.6	22.0
Fixed carbon (wt.%)	42.1	45.8	42.8	43.0	41.7	44.1
Ultimate analysis						
Carbon (wt.%)	50.66	58.70	50.99	52.08	50.48	52.18
Hydrogen (wt.%)	2.65	3.33	2.76	2.80	2.74	2.75
Nitrogen (wt.%)	1.07	1.27	1.25	1.40	1.23	1.30
Sulphur (wt.%)	0.74	1.10	0.72	1.25	1.61	0.75
Oxygen (wt.%)	7.97	3.14	8.98	7.37	7.24	9.12
Calorific value						
Calorific value (MJ/kg)	18.60	21.10	19.93	19.95	19.65	19.62

New Vaal coal, however, has a slightly higher ash content and a resulting lower calorific value than the other coals. On the other hand, Grootegeluk coal has a higher volatile matter content than the other coals.

2.4.2 Ash melting temperatures and ash analysis

The ash melting temperatures and chemical analyses of the ash were carried out by XRD Analytical and Consulting (Pretoria) and the results are given in Table 2.5 together with the measurement methods that were used.

Table 2.5: Ash melting temperatures and mineral oxides in the ash

	New Vaal	**Grootegeluk**
Ash melting temperature	In accordance with ASTM D 1857	
DT (°C)	1 600	1 350
ST (°C)	1 600	1 410
HT (°C)	1 600	1 480
FT (°C)	1 600	1 500
Mineral oxides in the ash	In accordance with ASTM D 3682	
SiO_2 (%)	56.70	68.60
Al_2O_3 (%)	31.70	20.05
Fe_2O_3 (%)	2.61	5.59
P_2O_5 (%)	0.25	0.08
TiO_2 (%)	1.55	0.72
CaO (%)	2.50	0.71
MgO (%)	0.76	0.83
K_2O (%)	0.44	1.25
Na_2O (%)	0.19	0.12
Minerals phases in the ash	CCSEM (Oboirien, 2011)	
Kaolinite (%)	80.78	38.66
Quartz (%)	13.70	49.73
Mica (%)	0.0	8.05
Rutile (%)	3.32	0.44
Siderite (%)	0.0	0.54

(All percentages are given as wt.%)

Table 2.5 shows that the ash softening temperatures (ST) of the selected coals are both above 1 300 °C. Clinkering of these coals in a fluidised bed gasifier, which normally operates below 1 000 °C, is therefore not expected to occur provided the formation of hotspots in the gasifier is avoided. The ash analysis shows that the ash consists mainly

of SiO_2 and Al_2O_3, and that the ash melting temperature increases with increasing Al_2O_3 content. CCSEM analysis of the ash shows that the dominate mineral phases in the ash are kaolinite and quartz and that New Vaal coal contains significantly higher amounts of kaolinite than quartz. Only small amounts of mica, rutile and siderite were observed in the mineral matter of New Vaal and Grootegeluk coals.

The melting points and mineral oxides in the ash of selected Eskom and Sasol coals are given in Table 2.6.

Table 2.6: Ash melting temperatures and mineral oxides in the ash of selected Eskom and Sasol coals

	Eskom power station coals				**Sasol coals**	
Colliery	Matla	Duvha	Kriel	New Denmark	Bosjes-spruit	Syfer-fontein
Power station	Matla	Duvha	Kriel	Tutuka	Sasol 1 & 2	
Ash melting Temperature						
DT (°C)	1 400	1 460	1 300	1 510	1 290	1 250
ST (°C)	1 450	1 500	1 310	1 540	1 320	1 300
HT (°C)	1 480	1 560	1 320	1 550	1 360	1 310
FT (°C)	1 500	1 600	1 350	1 570	1 400	1 320
Mineral oxides in the ash						
SiO_2 (%)	48.2	55.2	55	55.5	57	54.6
Al_2O_3 (%)	26.4	28.6	23.3	26.2	23.3	24.4
Fe_2O_3 (%)	4.33	5.22	3.9	6.98	5.75	4.35
P_2O_5 (%)	0.98	0.64	0.96	0.19	0.3	0.53
TiO_2 (%)	1.51	1.66	1.65	1.34	1.09	1.54
CaO (%)	9.71	3.11	8.17	3.23	4.86	6.27
MgO (%)	1.93	1.07	1.28	1.21	1.68	2.28
K_2O (%)	0.77	0.90	0.95	1.22	1.05	0.87
Na_2O (%)	0.46	0.10	0.14	0.4	0.44	0.47

(All percentages are given as wt.%)

Table 2.6 shows that the ash softening temperatures (ST) of other coals utilised by Eskom and Sasol are also above 1 300 °C and increase with an increase in Al_2O_3 content in the ash. The CaO content of the other coals is on average higher than the CaO content of Grootegeluk and New Vaal coals, indicating possible better retention of sulphur-containing species during fluidised combustion and gasification of the other coals (Grubor *et al.*, 2003).

2.4.3 Petrographic analysis and rank

Coal is a non-homogenous substance and consists of discernible components called *macerals*. The three maceral groups that are recognised are vitrinite, liptinite and inertinite (Du Cann, 2006). These are distinguished from one another by differences in reflectance, colour, morphology, shape and size.

Due to the higher hydrogen content of liptinite and vitrinite compared to inertinite, they produce more volatiles when heated than inertinite. Coals that are high in liptinite and vitrinite contents therefore have higher volatile matter contents (Borrego *et al*., 2000). Coals that have high vitrinite contents produce porous chars compared to coals that have high inertinite contents, which generally produce dense low-porosity chars.

Vitrinite reflectance analysis has been found to be a reliable method to determining the rank of coal (Neavel, 1979). The vitrinite random reflectance increases as the rank of the coal increases and is independent of the vitrinite content and grade of the coal. Coal rank is a measure of the degree of metamorphism (coalification) that a coal has experienced and increases with maturity of the coal. It is known that the combustion and gasification reactivity of coal decreases as the rank of coal increases. The vitrinite random reflectance can therefore be used as an indicator of the relative reactivity of coal (Alonso *et al.*, 2001; Cloke and Lester, 1994).

The petrographic analysis was carried out by Petrographics SA (Pretoria) in accordance with the ISO 7404-3 method. The maceral contents and vitrinite random reflectance of the selected coals are shown in Table 2.7.

Table 2.7: Petrographic analysis

	New Vaal	Grootegeluk
Vitrinite (vol.% daf[1])	26	83
Liptinite (vol.% daf)	3	5
Reactive inertinite (vol.% daf)	23	2
Inert inertinite (vol.% daf)	48	10
Total inertinite (vol.% daf)	71	12
Vitrinite random reflectance (%)	0.56	0.67

[1] Dry ash free

Figure 2.2 shows that according to the rank classification system by Du Cann (2006), the rank of New Vaal coal is medium-rank bituminous (D), and the rank of Grootegeluk coal is medium-rank bituminous (C). The higher volatile matter content of Grootegeluk coal (Table 2.3) is due to its higher liptinite and vitrinite contents compared to New Vaal coal.

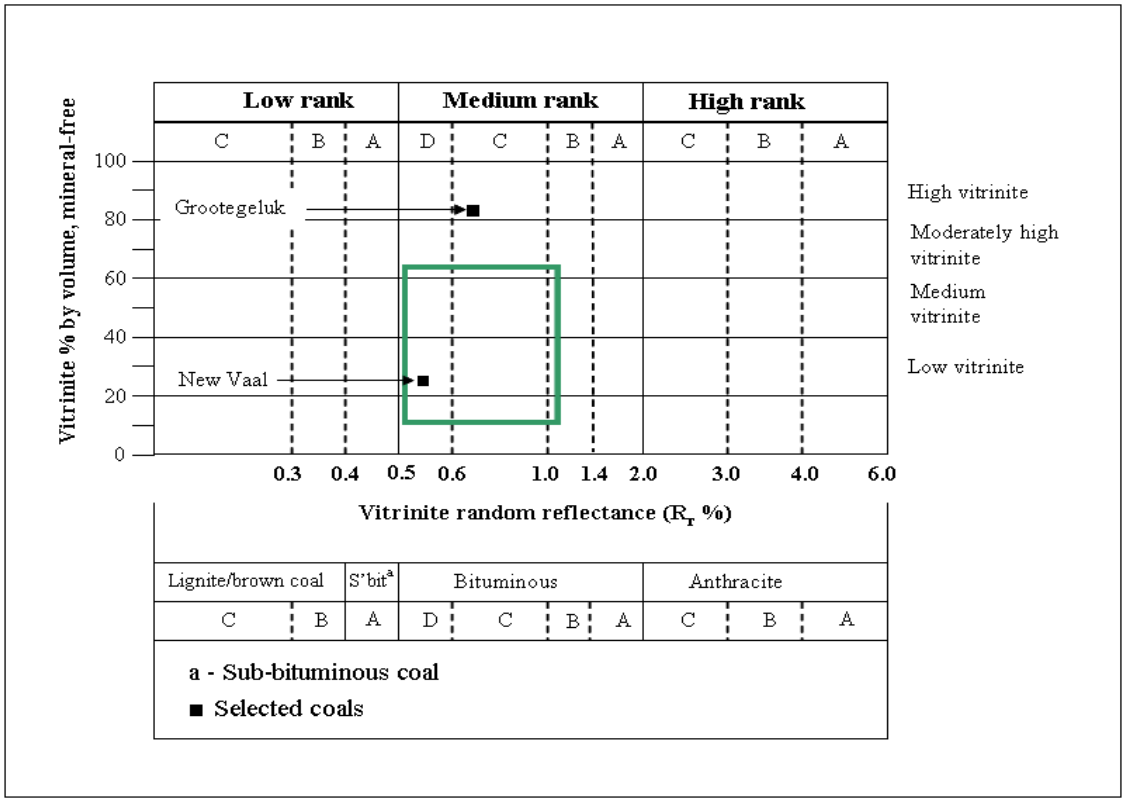

Figure 2.2: Rank classification system using vitrinite random reflectance

Table 2.7 and Figure 2.2 show that New Vaal coal has a lower vitrinite random reflectance ($R_{r)}$ than Grootegeluk coal, which indicates that New Vaal is a less mature coal than Grootegeluk coal, despite both being classified as medium-rank coals. Table 2.7 shows that New Vaal coal has a significantly higher inertinite content than Grootegeluk coal. The higher inertinite content of New Vaal coal, however, does not necessarily mean that it has a lower reactivity than that of Grootegeluk coal (Borrego *et al.*, 2000).

Pinheiro *et al.* (1999) reported that 95% of South African coals fall within the green square shown in Figure 2.2.

A comparison of the petrographic analyses of New Vaal and Grootegeluk coals with other South African coals shows that Grootegeluk coal has a notably higher vitrinite content and that New Vaal coal has a relatively high reactivity as indicated by its low vitrinite reflectance. From Table 2.8 it appears that the lower vitrinite random reflectance (higher reactivity) coals are utilised by Sasol in coal gasifiers.

Table 2.8: Petrographic analysis of other South African coals

	Eskom power station coals				**Sasol coals**	
Colliery	Matla	Duvha	Kriel	New Denmark	Bosjes-spruit	Syfer-fontein
Power station	Matla	Duvha	Kriel	Tutuka	Sasol 1 & 2	
Maceral composition (daf)						
Vitrinite (vol.%)	33	17	32	28	30	25
Liptinite (vol.%)	3	6	4	3	2	5
Reactive inertinite (vol.%)	21	27	18	22	20	23
Inert inertinite (vol.%)	43	50	46	47	48	47
Vitrinite random reflectance (%)	0.64	0.75	0.65	0.64	0.57	0.63

2.4.4 Structural and physical properties

The internal surface area of coal consists of micropores (< 2 nm), mesopores (2 - 50 nm) and macropores (> 50 nm). Coal has a wide range of pore size distributions and the relative percentage of each type depends on the origin and rank of the coal (Gan *et al.*, 1972). During devolatilisation existing pores are enlarged and new pores are developed, with the latter giving a larger internal surface area. The pore structure, pore size distribution and the internal surface area of char affect the reactivity of char during combustion and gasification. (Miura *et al.*, 1989).

The surface area of coal and chars is most often measured using the BET (Brunauer, Emmett and Teller) method, with nitrogen as the adsorbing gas. The method consists of measuring the equilibrium adsorption pressure of N_2 and relating it to the amount of N_2 adsorbed and therefore to the surface area. A nitrogen-based BET measures the surface area of the meso- and macropores. In order to measure the surface area of the micropores, CO_2 is used as the adsorbing gas.

For cylindrical pores the porosity of coal can be estimated using equation (2.1). Equation (2.1) was derived using surface area and volume calculations (Engelbrecht, 2007).

$$\varepsilon_c = \frac{d_{pore} S_{BET} \rho_c}{40000} \qquad (2.1)$$

The bulk density of low-porosity coals (ε_c < 5%) can be measured using the water displacement method (Engelbrecht, 2007).

The structural and physical properties of the selected coals and their chars are given in Table 2.9. From Table 2.9 it can be seen that the surface area and porosity of the coals and their chars decrease with increasing rank. The higher-rank Grootegeluk coal experienced more extensive coalification (pressure and time) and therefore has a lower surface area, porosity and vitrinite random reflectance compared to New Vaal coal. The higher bulk density of New Vaal coal can be attributed to its higher mineral matter (ash) content.

Table 2.9: Structural and physical properties of selected coals and their chars

	New Vaal		Grootegeluk	
	Coal	Char	Coal	Char
BET (N_2) surface area (m^2/g)[1]	7.01	28.10	0.38	8.60
Bulk density (kg/m^3)[2]	1 700	-	1 570	-
BET pore diameter (nm)[1]	11.3	11.4	101.1	28.5
BET porosity (%)[3]	3.4	12.8	1.5	9.6

[1] Carried out by Protechnik Laboratories (Pretoria) using the BET method

[2] Measured by the CSIR (Pretoria) using the method described in Appendix B.1

[3] Calculated from BET surface area, BET pore diameter and bulk density using the method described in Appendix B.2

2.4.5 Free swelling index and Roga index

These indices are used to indicate the caking and agglomerating nature (tendency to deform and stick together) of the coal – the scales are FSI 0 – 9 and RI 0 – 90 (Thomas, 1986). Coals that have a FSI of 0 and a RI of 0 do not cake or agglomerate. To determine the FSI by the ISO 501 method, one gram of finely powdered coal (250 μm) is rapidly heated to 820 °C and the silhouette of the resulting coke button is compared with a series of standard profiles. The FSI of the sample is the number of the standard profile (0 – 9) which it most closely resembles.

Table 2.10 shows that Grootegeluk coal is weakly caking, whereas New Vaal coal is non-caking by nature.

Table 2.10: Free swelling index and Roga index of selected coals

	New Vaal	Grootegeluk
Free swelling index (FSI)[1]	0	1
Roga index (RI)[2]	0	10

[1] Measured by Advanced Coal Technologies (Pretoria) using the ISO 501 method

[2] Measured by Advanced Coal Technologies (Pretoria) using the ISO 335 method

It has been found by other investigators (Du Cann, 2006) that high-ash, high-inertinite and low-volatile bituminous coals tend to be non-caking by nature. Severe agglomeration of the two selected coals in a fluidised bed gasifier is therefore not expected to occur.

2.4.6 Hardgrove grindability index

The Hardgrove grindability index (HGI) of coal is a measure of how difficult or easy it is to grind the coal to smaller sizes (ISO 5074). In general, the HGI of coal varies between 20 and 110, a lower value indicating that the coal is difficult to grind and a higher value that it is easy to grind finer. On the whole, lignite and anthracite are more resistant to grinding (i.e. have low indices) than are bituminous coals (Brown and Hiorns, 1963). The HGI is important for fluidised bed gasification since it could be an indicator of the relative amount of fines that will be generated in the gasifier due to abrasion and attrition (Engelbrecht, 2008).

The Hardgrove grindability index was measured by Advanced Coal Technologies (Pretoria) using the ISO 5074 method and is given in Table 2.11.

Table 2.11: Hardgrove grindability index (HGI)

	New Vaal	**Grootegeluk**
Hardgrove grindability index	66	47

Table 2.11 shows that New Vaal coal has a significantly higher HGI than Grootegeluk coal, indicating that more fines could be generated during the fluidised bed gasification of New Vaal coal, which could have a negative impact on the gasification efficiency.

The Hardgrove grindability index of other South African coals is given in Table 2.12. Table 2.12 shows that the HGI values of the other South African coals fall between the HGI values of Grootegeluk and New Vaal coals.

Table 2.12: Hardgrove grindability index (HGI) of other South African coals

	Eskom power station coals				Sasol coals	
Colliery	Matla	Duvha	Kriel	New Denmark	Bosjes-spruit	Syfer-fontein
Power station	Matla	Duvha	Kriel	Tutuka	Sasol 1 & 2	
HGI	55	50	64	67	61	57

2.4.7 Particle size analysis

The coal received from the mines was crushed and screened to produce coal with a size range of 0.7 to 4.0 mm which is suitable for feeding to a fluidised bed gasifier. The size distributions within the 0.7 to 4.0 mm range for each of the fluidised bed gasification tests described in Chapter 4 are given in Appendix D.2.11 (New Vaal coal) and Appendix D.2.12 (Grootegeluk coal).

2.5 Coal characterisation and fluidised bed gasifier modelling

The coal characterisation results that are required as input to the fluidised bed gasifier model described in Chapter 5 are:

- Proximate and ultimate analysis (Table 2.3).
- Calorific value of the coal (Table 2.3).
- Particle size analysis (Appendices D.2.11 and D.2.12).

The characterisation results given in the following tables are not required as input to the model but have been included since they could relate to fluidised bed gasifier performance in a non-quantitative manner:

- Table 2.5 (Ash melting point and ash analysis).
- Table 2.7 (Petrographic analysis).
- Table 2.9 (Structural and physical properties).
- Table 2.10 (Caking properties).
- Table 2.11 (Hardgrove grindability index).

2.6 Summary of coal characterisation

The results of the proximate and calorific value analyses of the two coals selected for this study show that they have high ash contents and low calorific values and are therefore classified as grade D coals. Based on the rank classification system using vitrinite random reflectance, the rank of New Vaal coal is medium-rank bituminous (D) and the rank of Grootegeluk coal is medium-rank bituminous (C).

Ash melting temperature analyses show that the ash softening temperatures (ST) of both coals are above 1 300 °C. Free swelling index (FSI) and Roga index (RI) analyses show that both coals have a low caking tendency. Clinkering and agglomeration of these coals in a fluidised bed gasifier, which normally operates below 1 000 °C, is therefore not expected to occur, provided that the formation of hotspots in the gasifier is avoided.

The results of petrographic, surface area and porosity analyses indicate that New Vaal coal could have a higher gasification reactivity than Grootegeluk coal. The higher Hardgrove grindability index (HGI) of New Vaal coal indicates that more fines could be generated in a fluidised bed gasifier than Grootegeluk coal.

Comparison of the analysis of the two coals selected for this study with the analysis of six other South African coals utilised by Eskom and Sasol show that the six other coals are also grade D, medium-rank coals with high ash melting temperatures.

Comparison of the petrographic analysis of New Vaal and Grootegeluk coals with other South African coals show that Grootegeluk coal has a notably higher vitrinite content, and that New Vaal coal has a relatively higher reactivity as indicated by its lower vitrinite reflectance.

2.7 Chapter 2 references

ALONSO, M.J.G. BORREGO, A.G. AND MENENDEZ, R. (2001b). A reactivity study of chars obtained at different temperatures in relation to their petrographic characteristics. *Fuel Processing Technology* 69:257–272.

ARNOLD, B.J. (2013). Coal formation. In: OSBORNE, D., *The Coal Handbook: Towards Cleaner Production*, Volume 1, Coal Production, Chapter 2, Woodhead Publishing Limited, 31–52.

BORREGO, A.G., MARBÁN, G., ALONSO, M.J.G., ÁLVAREZ, D. AND MENÉNDEZ, R. (2000). Maceral effects in the determination of proximate volatiles in coals. *Energy & Fuels* 14: 117-126.

BROWN, R.L. AND HIORNS, F.L. (1963). Mechanical properties. In: LOWRY, H.H., *Chemistry of Coal Utilization – Supplementary Volume*, Chapter 3, New York: Wiley, 119–149.

CLOKE, M. AND LESTER, E. (1994). Characterisation of coals for combustion using petrographic analysis. A review. *Fuel* 73:315–320.

DU CANN, V.M. (2006). A brief introduction to some basic aspects of coal and organic petrology. South African Bureau of Standards report.

ENGELBRECHT, A.D. (2008). Characterisation and fluidised bed gasification of selected high-ash South African coals. Master's dissertation, North-West University, South Africa.

ENGELBRECHT, A.D. (2007). Clean coal technology – Fine coal gasification progress report. CSIR report, DMS number 133570.

ERGUN, S. (1979). Coal classification and characterization. In: WEN, C.Y. AND SANLEE L.E., (Eds), *Coal Conversion Technology*, Chapter 1, Massachusetts: Addison-Wesley, 1–56.

FALCON, R. (2013). Coal petrography. In: OSBORNE, D., *The Coal Handbook: Towards Cleaner Production*, Volume 1, Coal Production, Chapter 3, Woodhead Publishing Limited, 53–79.

GAN, H., NANDI, S.P. AND WALKER, P.L. (1972). Nature of the porosity in American coals. *Fuel* 51:272.

GRUBOR, B., MANOVIC, V. AND OKA, S. (2003). An experimental and modeling study of the contribution of coal ash to SO_2 capture in fluidized bed combustion. *Chemical Engineering Journal* 96:157–169.

HATTINGH, B.B. (2012). Product evaluation and reaction modelling for the devolatilization of large coal particles. Doctoral thesis. North-West University, South Africa.

HORSFALL, D.W. (1993). Coal Preparation and Usage. Parklands: Coal Publications (Pty) Ltd.

JEFFREY, L. (2005). Challenges associated with further development of the Waterberg coalfield. *Journal of the South African Institute of Mining and Metallurgy* 105: 453 – 457.

LAYBOURNE, R.A. AND WATTS, R. (1990). The development and application of strip mining to previously mined underground coal workings. *Journal of the South African Institute of Mining and Metallurgy* 90: 187–197.

MIURA, K., HASHIMOTO, K. AND SILVESTON, P.L. (1989). Factors affecting the reactivity of coal chars during gasification, and indices representing reactivity. *Fuel* 68:1461.

NEAVAL, R.C. (1979). Origin, petrography, and classification of coal. In: ELLIOTT, M.A., *Chemistry of Coal Utilization*, Chapter 3, New York: Wiley, 91–158.

OBOIRIEN, B. (2011). Gasification of high-ash coals and chars from South African coals. Doctoral thesis. University of the Witwatersrand, South Africa.

PINHEIRO, H.J., PRETORIUS, C.C., BOSHOFF, H.P. AND BARKER, O.B. (1999). A techno-economic and historical review of the South African coal industry in the 19th and 20th centuries and analysis of coal product samples of South African collieries 1998–1999. Coal Bulletin 113. Issued by the South African Bureau of Standards (SABS) and the Department of Minerals and Energy (DME).

THOMAS, K.M. (1986). Characterisation of coal for gasification processes. In: FIGUEIREDO, J.L. AND MOULIJN, J.A., *Carbon and Coal Gasification*, Dordrecht: Martinus Nijhoff Publishers, 421–453.

2.8 Chapter 2 and Appendix B nomenclature

d_{pore}	average pore diameter by BET analysis	nm
R_r	vitrinite random reflectance	(%)
R_s	reactivity index of char	h^{-1}
S_{BET}	surface area of coal by BET analysis	$m^2.g^{-1}$
X	fractional conversion of fixed carbon in coal	-

Greek letters

β	grain model structural parameter	-
ε_c	porosity of coal	(%)

$\tau_{0.5}$	time for 50% fixed carbon conversion	h
ρ_c	coal density	$kg.m^{-3}$

Acronyms/Abbreviations

ASTM	American Society for Testing and Materials
BET	Brunauer, Emmett and Teller
Bt	Billion tons
CSIR	Council for Scientific and Industrial Research
CCSEM	Computer-controlled scanning electron microscopy
daf	Dry and ash free
DT	Deformation temperature
Eskom	Electricity Supply Commission (South Africa)
FSI	Free swelling index
FT	Fluid temperature
GCM	Grootegeluk coal mine
GWe	Gigawatt electrical
HT	Hemispherical temperature
HGI	Hardgrove grindability index
ISO	International Standards Organization
Myr	Million years
Mt	Million tons
Mt/a	Million tons per annum
RI	Roga index
ROM	Run-of-mine
SABS	South African Bureau of Standards
Sasol	Suid Afrikaanse Steenkool en Olie
ST	Softening temperature

CHAPTER 3 BENCH-SCALE GASIFICATION AND DEVOLATILISATION EXPERIMENTS

3.1 Introduction

This chapter describes bench-scale experiments carried out on New Vaal and Grootegeluk coals to obtain parameters (coal-dependent) for equations that calculate the rates of:

- the char-steam gasification reaction,
- the char-CO_2 gasification reaction
- and the coal devolatilisation process.

These equations are sub-models that are included in the fluidised bed coal gasifier model described in Chapter 5. Section 3.2 describes the thermogravimetric analyser experiments that were carried out to determine parameters for the Johnson char-steam rate equation. Section 3.2 includes a literature review, description of the thermogravimetric analyser, experimental programme, tests results and parameter estimation for New Vaal and Grootegeluk coals. In Section 3.3 thermogravimetric analyser data generated by Engelbrecht (2008) is applied to obtained parameters for a first-order char-CO_2 gasification rate equation. In Section 3.4 the evolution rates of devolatilisation products of each coal are determined using a 50 mm fluidised bed reactor. Section 3.4 includes a literature review, description of the 50 mm fluidised bed reactor, tests results, model development and determination of devolatilisation model parameters for New Vaal and Grootegeluk coals. A summary of the bench-scale gasification and devolatilisation experiments is given in Section 3.5.

3.2 Char-steam gasification kinetics

3.2.1 Literature review

Selected bench-scale studies on the steam gasification of coal char that have been carried out since 1984 are given in Table 3.1.

3.2.1.1 Motivation for investigations

The rates of coal char gasification with steam and CO_2 are relatively slow compared to coal combustion and devolatilisation. The study of these reactions and the factors that affect their rate is therefore important since they are rate limiting in terms of the overall gasification process and determine the carbon conversion that can be achieved in a coal gasifier (Roberts and Harris, 2006).

3.2.1.2 Objectives of the investigations

Investigations have been carried out to determine the effect of the following factors on the steam gasification rate of coal chars:

- Temperature, pressure and steam concentration.
- Coal properties such as rank, alkali metals in the coal ash, char pore structure and surface area development during gasification.
- Addition of catalyst to the char.
- Coal devolatilisation conditions (temperature, pressure and rate).
- Competition between steam and CO_2 for active reaction sites on the surface of the char.
- Inhibiting effect of reaction products (CO and H_2) on the gasification rate.

In addition to the above the objectives, many of the investigation have been carried out to determine appropriate char-steam rate equations that can be incorporated into coal gasifier simulation models.

Table 3.1: Summary of selected coal char-steam gasification studies

Investigator	Date	Country	No. of coals	Coal rank	Primary objective of investigation	Reactor	Sample mass (g)	Particle size (mm)	Gas flow Nl/mim	Reacting gases	Temp (°C)	Pressure (MPa)
Satoshi [8]	2013	Japan	3	Bituminous	RM[1]	PDTF[2]	0.005	0.04	0.4	CO_2, H_2O	900–1 400	0.1
Coetzee	2013	SA[3]	1	Bituminous	CE[4]	TGA[5]	3 – 6	3 – 10	1.4	H_2O	800–875	0.09
Chen	2012	China	1	Lignite	DV[6]	TGA	0.3	0.07 – 0.1	3.0	CO_2, H_2O	1 000	0.09
Huang	2010	China	1	Lignite	RM	TGA	0.01	0.2	1.4	H_2O, H_2,CO_2, CO	850 –950	0.1
Wang	2009	China	1	Bituminous	CE	TGA	0.2	0.15	0.5	H_2O	750–1 000	0.1
Roberts	2007	Australia	3	Bituminous	RM	TGA	0.15	0.6 – 1.0	-	H_2O, H_2,CO_2, CO	850–900	0.1–1.0
Wu	2006	China	1	Various	RM	FB	7.0	3 – 6	0.50	H_2O	900–1 200	0.1
Zhang	2006	China	6	Anthracite	CP[7]	TGA	0.005	0.1	0.1	H_2O, CO_2	920–1 050	0.1
Everson	2005	SA	2	Bituminous	RM	TGA	0.1	0.02– 0.06	0.04	H_2O, CO_2	800 – 950	0.09
Ye	1997	Australia	2	Sub-bituminous	CP	TGA	4.0	0.8 – 3.0	-	H_2O, CO_2	714 – 892	0.1
Goyal	1989	USA	1	Bituminous	RM	TGA	-	0.4 – 0.8	-	H_2O, H_2, CO, CO_2	925 – 1 038	0.4–2.8
Kwon	1988	Korea	1	Lignite	CE	TGA	-	0.2 – 0.4	-	H_2O	700 – 800	0.1
Takarada	1985	Japan	34	Various	CP	TGA	-	1.0 – 2.0	-	H_2O	750	0.1
Mühlen	1984	Germany	1	Lignite	RM	TGA	0.5	-	-	H_2O, H_2,CO_2, CO	800–1 000	0.1–7.0

[1] Reaction modelling
[2] Pressurised drop tube furnace
[3] South Africa
[4] Effect of catalyst addition
[5] Thermogravimetric analyser
[6] Effect of coal devolatilisation conditions
[7] Effect of coal properties
[8] The names given in Tables 3.1 are the first authors of the coal char - steam gasification studies. Details of the papers are given in Chapter 3 references.

3.2.1.3 Reactors used for gasification experiments

Table 3.1 shows that the majority of bench-scale experiments were carried out using a thermogravimetric analyser. Thermogravimetric analysis involves placing a char sample (prepared from the parent coal) in a heated furnace at the required temperature and gas atmosphere (CO_2, H_2O, CO, H_2 and N_2). The mass loss of the sample is recorded as a function of time to allow the gasification rate to be calculated. Table 3.1 shows that for the selected investigations the char sample masses varied between 0.005 g and 7.0 g, char particles sizes varied between 0.02 and 10 mm and reacting gas flows varied between 0.1 and 3 Nl/min.

In studies that were aimed at measuring the intrinsic gasification rate, char sample mass, char particle size and reacting gas flow were selected in order to avoid external and internal diffusion effects. The effect of sample mass, particle size and reacting gas flow on diffusion was pre-tested by Huang *et al*. (2010) in order to minimise diffusion effects during their experiments. The investigation by Goyal *et al*. (1989) avoided diffusion by selecting reacting gas flows that were sufficiently high relative to the gasification rates so that the reacting gas conversion was less than 1% (differential reactor). Studies that were carried out at high temperature and high pressure using reactive coals (lignite) resulted in high gasification rates, and in these cases smaller char particle diameters and smaller sample masses were selected in order to avoid diffusion effects. Studies that were carried out at high pressure needed to account for the buoyancy effect of the high-density gas on the sample weight in the calculation of the gasification rates (Mühlen *et al*., 1985; Roberts and Harris, 2006).

3.2.1.4 Results of bench-scale char-steam gasification studies reported in the literature

Effect of coal properties on gasification rates

The primary objective of the study by Takarada *et al*. (1985) was to study the effect of coal rank on the steam gasification reactivities of coal char. Thirty-four coals with a wide variation in rank were selected from eight countries. Another selection criterion was that the coals with similar rank should have varying ash contents. The dry ash-free carbon content (C_{daf}) of the coals was used as the indicator of its rank. It was found that coals that have C_{daf} values above 78% (high-rank coals) have low reactivities. For C_{daf} values below 78% (low-rank coals), a definitive increase in reactivity was observed. Although coals in the 65% < C_{daf} < 78% range have significantly higher reactivities than coals in the 78% < C_{daf} < 83% range, the correlation between the reactivity value and C_{daf} in the 65% < C_{daf} < 78% is not good. It was found that in the 65% < C_{daf} <78 % range the reactivity of the chars was well correlated with the sum of the calcium and sodium contents of the ash in the coal.

Zhang *et al*. (2006) studied the gasification reactivities of six Chinese anthracite chars in steam and CO_2, and found that during steam gasification the reactivities of the chars are well correlated with the volatile matter contents of the parent coals. The CO_2 gasification reactivities seemed to be more dependent on the catalytic effect of inherent minerals in the anthracite (alkali index). They also found that the reactivity during steam gasification was about 10 times higher than during CO_2 gasification, which is a higher ratio than for bituminous and lignite chars. The higher steam gasification reactivity was attributed to the higher percentages of micropores in anthracite chars compared to bituminous and lignite coals. Micropores are more accessible to steam than to CO_2, which results in higher steam-to-CO_2 reactivity ratios for anthracite chars compared to bituminous and lignite coal chars.

Effect of catalyst addition to the char on gasification rates

Wang *et al*. (2009) investigated the gasification of Chinese bituminous coal chars with the addition of K_2CO_3. It was found that with the addition of 17.5 wt.% K_2CO_3 to the char sample, the gasification rate at 750 °C was the same as the un-catalysed rate at 1 100 °C. During the catalytic gasification at 750 °C, the hydrogen production

increased and the production of CO and CH_4 decreased markedly. An oxygen transfer and intermediate hybrid mechanism was proposed to explain the increase in gasification rate at lower temperatures when K_2CO_3 was added to the char.

Kwon *et al*. (1988) investigated the gasification of an Australian lignite char at 750 °C using Na_2CO_3, K_2CO_3 and Li_2CO_3 as catalysts. At 3% by weight addition of the catalysts the catalytic activities were ranked as $Na_2CO_3 > K_2CO_3 < Li_2CO_3$. For catalytic gasification with Na_2CO_3, K_2CO_3 and Li_2CO_3, the reactivity indices were respectively 2.8, 2.0 and 1.68 times higher than in non-catalytic gasification.

Coetzee *et al*. (2013) investigated the steam gasification of a bituminous South African coal at temperatures between 800 °C and 875 °C with the addition of K_2CO_3 as a catalyst. The coal was impregnated with K_2CO_3 solution, which increased the potassium content from 0.05 wt.% (raw coal) to 0.83 wt.% (impregnated coal). It was found that at lower temperatures the effect of catalyst addition was the most pronounced, resulting in an increase of up to 40% in gasification rates.

Effect of devolatilisation conditions on gasification rates

Chen *et al*. (2012) carried out steam gasification tests on Chinese lignite chars that were prepared in a drop tube furnace (DTF) and in a fixed-bed tubular furnace (FBTF) at 1 000 °C with particle heating rates of 10 000 °C/s and 10 °C/min respectively. Steam gasification experiments carried out on these chars using a mixture containing 33 vol.% steam and 67 vol.% N_2 at 1 000 °C shows that the char prepared in the DTF has a reactivity index 90% higher than that of the char prepared in the FBTF.

Coal char steam reaction kinetics

Many of the studies of the steam gasification of coal chars were aimed at obtaining rate equations that adequately describe the gasification rate of char particles under conditions present in coal gasifiers. Obtaining an adequate rate equation is complicated by the fact that for a particular coal the rate of char-steam gasification is not only dependent on the steam concentration and temperature in the gasifier, but

also on the concentration of other gases in the gasifier, with CO_2, CO and H_2 having the most significant effect.

Roberts and Harris (2007) in their investigation found that at a pressure of 1.0 MPa, steam and CO_2 compete for active sites on the char surface, which means that the presence of CO_2 has an inhibiting effect on the steam gasification rate. Everson *et al*. (2005) found that during the gasification of a high-ash South African coal at atmospheric pressure the CO_2 and steam gasification reactions occur on separate sites, and observed no CO_2 inhibition of the steam reaction. The investigation by Chen *et al*., (2012) concluded that the char-steam reaction was independent of the char-CO_2 reaction, although the char-CO_2 reaction was inhibited by the char-steam reaction. On the other hand, the investigation by Satoshi *et al*. (2013) concluded that the char-CO_2 and char-steam reactions partially share active sites, i.e. they do not take place on separate sites or common sites.

There is general consensus among investigators that the presence H_2 and CO inhibit the char-steam gasification reaction. Although H_2 and CO do not react with the char, they adsorb on active sites, rendering them unavailable for steam gasification and thereby lowering the gasification rate.

Many investigators have used Langmuir-Hinshelwood (LH)-type rate equations to describe the char-steam and char-CO_2 gasification rates since they include the effects of temperature, pressure and concentrations of H_2O, CO_2, CO and H_2. The general form of these equations is given in Figure 3.1 for reactions occurring on separate sites, common sites and partially shared sites. In equations (3.1) to (3.3) shown in Figure 3.1, F(X) is a char conversion model that describes the effect of structural changes in the char on the gasification rate as conversion progresses. The homogenous model and the random pore model are char conversion models that have often been used and are described by equations (3.4) and (3.5).

$$F(X) = (1 - X)^{\beta} \qquad (3.4)$$

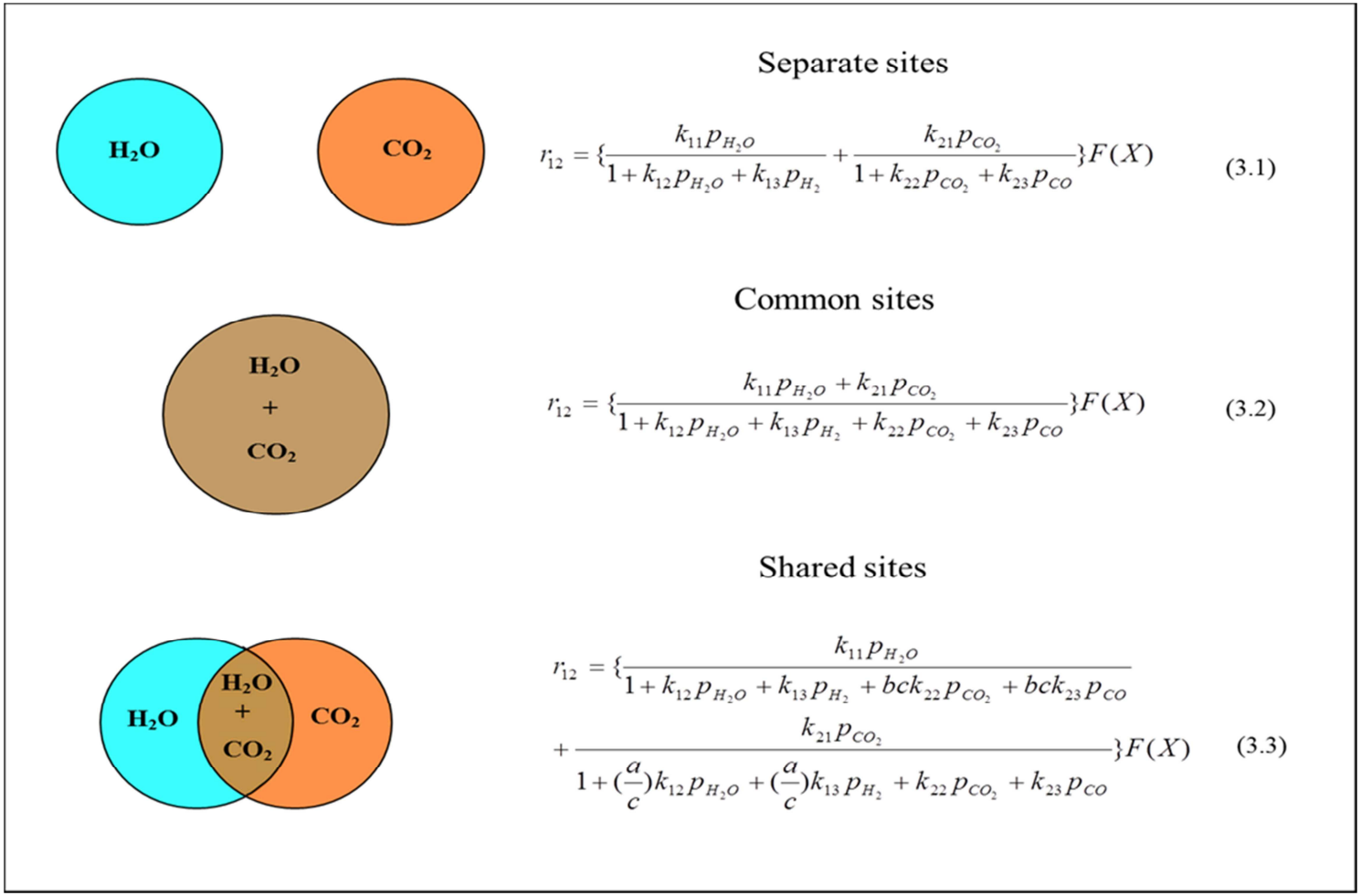

Figure 3.1: Langmuir-Hinshelwood rate equations for various coal char-steam reaction mechanisms

$$F(X) = (1-X)\sqrt{1+\psi \ln(1-X)} \qquad (3.5)$$

The reaction rate constants in equations (3.1) to (3.3) are given by equation (3.6).

$$k_{ij} = A_{ij} e^{-\frac{E_{ij}}{RT}} \qquad (i = 1, 2 \quad j = 1\text{-}3) \qquad (3.6)$$

3.2.1.5 Johnson char-steam gasification rate equation

The Johnson rate equation has often been used to calculate the rate of the char-steam gasification reaction in fluidised bed coal gasifier models. The condition under which the Johnson equation was developed is similar to the operating condition of fluidised coal bed gasifiers and the equation only has one parameter (f_L), which makes it easier to use compared to the Langmuir-Hinshelwood equations.

Development of the Johnson equation started in 1975 at the Institute of Gas Technology (USA) using a high-pressure thermogravimetric analyser in which ± 100 American bituminous coals were tested.

Tests were carried at temperatures of 797 °C – 1 000 °C, pressures of 0.1 – 7.0 Mpa and particle sizes of 0.1 – 1.4 mm in gas mixtures containing varying amounts of H_2O, CO, H_2 and CH_4. The final expression developed by Johnson to calculate the fractional char conversion rate was first published in his book *Kinetics of coal gasification* in 1979 (Johnson, 1979) and is given by equation (3.7)

$$\frac{dX}{dt} = f_L k_I F(X) \qquad (3.7)$$

In equation (3.7) f_L is the relative reactivity factor of the coal char and is dependent on the properties of the parent coal and the temperature at which the char was prepared. Johnson recommended an empirical correlation to calculate the relative reactive factor for bituminous coal chars, which is given by equation (3.8).

$$f_L = 6.2Y_c(1-Y_c).\exp\left[-\frac{9340}{R}\left(\frac{1}{T}-\frac{1}{T_p}\right)\right] \quad (3.8)$$

In equation (3.8) Y_c is the mass fraction dry ash-free carbon content of the coal, T is the gasification temperature and T_p is the temperature at which the chars were prepared.

The effect of gas concentrations and temperature on the char conversion rate is given by k_I and is expressed by equation (3.9). Equation (3.9) shows that the inhibiting effects of CO and H_2 are included in the Johnson rate equation.

$$k_I = \frac{\exp\left(9.0201-\frac{12910}{T}\right)\left(1-\frac{p_{CO}p_{H_2}}{p_{H_2O}K_{eq1}}\right)}{60.\left[1+\exp\left(-22.216+\frac{24881}{T}\right)\left(\frac{1}{p_{H_2O}}+16.35\frac{p_{H_2}}{P_{H_2O}}+43.5\frac{p_{CO}}{p_{H_2O}}\right)\right]^2} \quad (3.9)$$

In equation (3.9) K_{eq1} is the water-gas shift reaction equilibrium constant and is given by equation (3.10).

$$\log_{10}K_{eq1} = 7.49-\frac{7070}{T} \quad (3.10)$$

In equation (3.7), F(X) is a structural factor and is given by equation (3.11). The structural factor is incorporated to account for the effect of structural changes in the char particles on the gasification rate as conversion (X) progresses.

$$F(X) = (1-X)^{2/3}\exp(-\alpha X^2) \quad (3.11)$$

In equation (3.11) α is a structural parameter and is given by equation (3.12).

$$\alpha = \frac{52.5p_{H_2}}{1+54.3p_{H_2}}+\frac{0.521p_{H_2}^{0.5}\,p_{H_2O}}{1+0.707p_{H_2}+0.5p_{H_2}^{0.5}p_{H_2O}} \quad (3.12)$$

3.2.2 Experimental apparatus, procedure and programme

In this section a description is given of the thermogravimetric analyser (TGA) at the North-West University (NWU) that was used to carry steam gasification tests on New Vaal and Grootegeluk chars. The experimental procedure that was followed to carry out the tests and the experimental programme are also described.

Description of thermogravimetric analyser

The tests were carried out on the thermogravimetric analyser that was used by Coetzee *et al.* (2013) to produce the results presented in the paper detailed in Table 3.1. A schematic representation of the apparatus is shown in Figure 3.2. The thermogravimetric analyser was designed and constructed by staff and students at the North West University and consists of a gas supply system, a vertical tube furnace, a precision balance with a sample holder attached and a data acquisition interface.

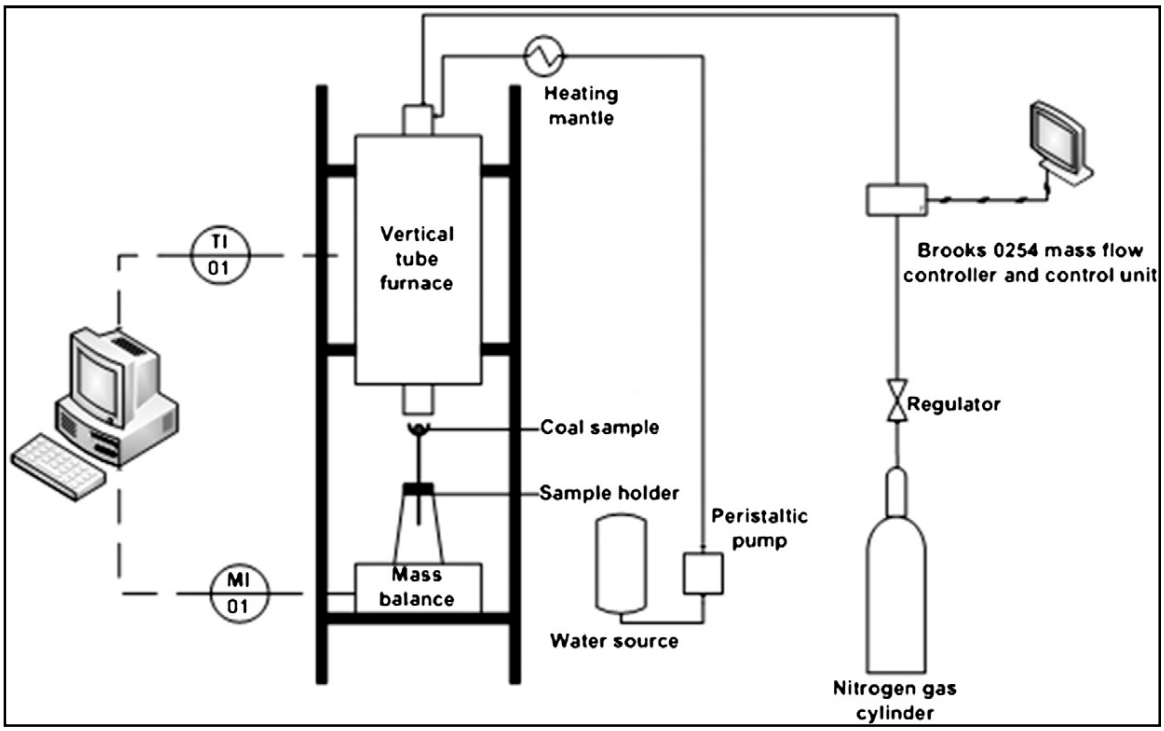

Figure 3.2: Schematic representation of the TGA (Coetzee *et al.*, 2013)

Experimental procedure

Coal samples received from New Vaal and Grootegeluk coal mines were crushed and screened (0.85 mm < d_p < 1.2 mm) into representative batches for the thermogravimetric analyser experiments. Test chars were prepared prior to the steam

gasification tests by devolatilisation of the coal samples in a nitrogen atmosphere. Since the devolatilisation temperature and heating rate have an effect on the reactivity of the chars, the chars were subjected to rapid devolatilisation in order for them to be representative of conditions in a pilot-scale fluidised bed gasifier. The New Vaal char was prepared by inserting the coal sample into a nitrogen-blanketed furnace that had been pre-heated to 950 °C. The coal sample was kept in the furnace for 20 minutes, which is sufficient time for complete devolatilisation of the coal. Due to the caking properties of Grootegeluk coal, the char samples were prepared at 980 °C using a 50 mm fluidised bed reactor described in Section 3.4.3. Although New Vaal and Grootegeluk chars were prepared in different furnaces, it is expected to have little effect on their relative reactivity factor (f_L) since in both furnaces the coal was heated rapidly to the charring temperature.

For the char-steam gasification experiments, the vertical tube furnace of the thermogravimetric analyser was heated to the required temperature at a rate of 20 °C/min with simultaneous introduction of nitrogen at 1.5 Nl/min. The char sample (± 1.0 g) was placed in the sample holder and when the furnace stabilised at the required temperature the furnace was lowered over the sample. After an additional holding period, the experiment was started when steam and the CO/H_2 mixture were introduced at the top of the tube furnace. A type K thermocouple was located directly above the sample in the tube furnace to ensure isothermal conditions during char gasification. The mass loss of the sample was recorded by the data acquisition system and the experiment was continued until no further mass loss was observed. The reaction data (time, temperature and mass) was copied to an Excel® file for data processing.

Experimental programme

The experimental programme was designed to obtain parameters for the Johnson rate equation given in Section 3.2.1.5. Temperatures and gas concentrations were selected that are representative of coal gasification in a fluidised bed. Hydrogen and carbon monoxide were added to the reacting gas mixture so that the inhibiting effect of these gases could be included in the rate equations. Reaction conditions for tests on New Vaal and Grootegeluk chars is given in Table 3.2.

Table 3.2: Reaction conditions used for thermogravimetric analyser experiments

				New Vaal char			Grootegeluk char		
Reacting gas mixtures (vol.%)				Temperature (°C)			Temperature (°C)		
H_2O	H_2	CO	N_2	850	900	950	880	920	980
20	5	5	70	NV1[1]	NV4	NV7	GG1[2]	GG4	GG7
30	10	10	50	NV2	NV5	NV8	GG2	GG5	GG8
40	20	20	20	NV3	NV6	NV9	GG3	GG6	GG9
30	0	0	70			NV10			
40	0	0	60					GG10	

[1] NV1 to NV10: Test 1 to test 10 on New Vaal char

[2] GG1 to GG10: Test 1 to test 10 on Grootegeluk char

For each test the char particle size was 0.85 – 1.2 mm, the coal sample mass was (±)1 000 mg and the N_2 flowrate was 1 200 ml.min^{-1}(NTP). The tests were carried out at ambient pressure which was assumed to be approximately 87.5 kPa (absolute).

Hydrogen and carbon monoxide were added by adding a gas mixture containing 50 vol.% hydrogen and 50 vol.% carbon monoxide to a steam/nitrogen mixture. The concentrations of the two gases (H_2 and CO) were therefore equal for all tests (0, 5, 10 and 20 vol.%).

Since the Johnson char-steam rate equation only has one parameter (f_L), ten tests on each coal as given in Table 3.2 was considered sufficient to estimate the value of f_L. Tests were, therefore, not conducted which investigated the effect of varying the H_2O concentration at constant CO and H_2 concentrations.

3.2.3 Experimental results and discussion

3.2.3.1 Normalisation and processing of experimental data

The experiment on New Vaal char at 950 °C, using a reacting gas mixture of 30 vol.% H_2O, 10 vol.% H_2, 10 vol.% CO and 50 vol.% N_2 (NV8), is described in this section to demonstrate how the experimental data were processed in order to obtain plots of char conversion vs. time for each char, temperature and reacting gas mix. The results of all the experiments are given in Section 3.2.3.2.

Data obtained from a thermogravimetric analyser are in the form of mass as a function of time, as shown in Figure 3.3 for the tests on New Vaal char at 950 °C referred to above. The residue obtained from the experiment agrees within ± 5% with the ash content of the char.

The experimental data shown in Figure 3.3 were normalised by expressing the char conversion variation on an ash-free basis according to equation (3.13) (Kaitano, 2007)

$$X = \frac{m_0 - m_t}{m_0 - m_{ash}} \tag{3.13}$$

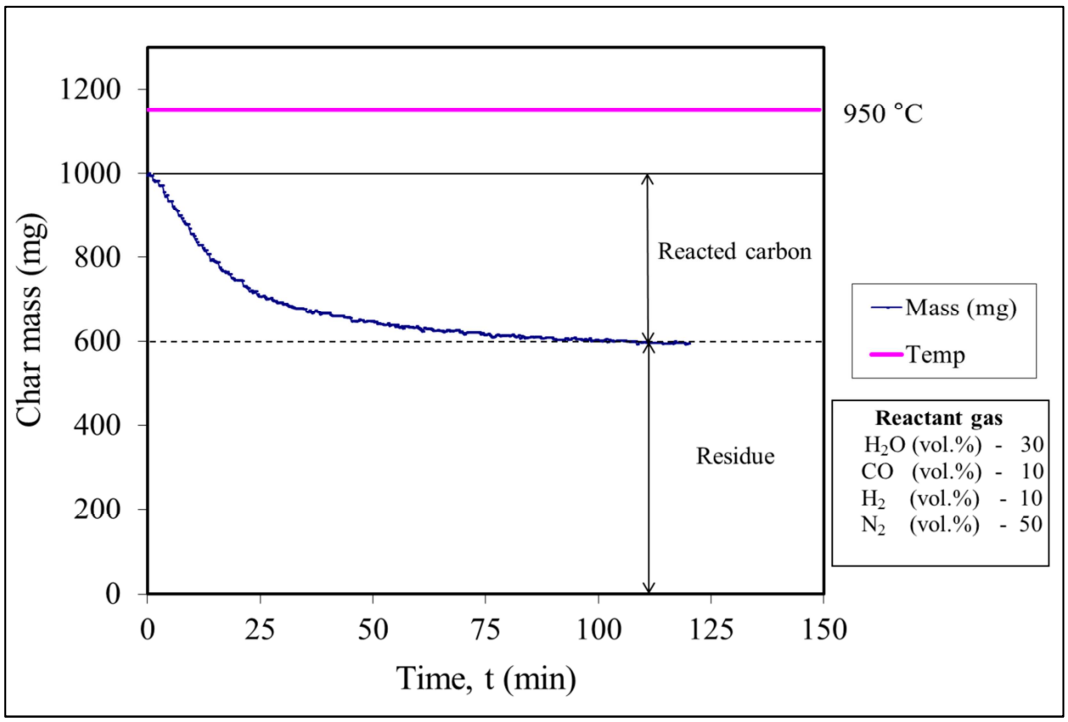

Figure 3.3: Isothermal gasification of New Vaal char at 950 °C and 87.5 kPa

A typical normalised result derived from the data in Figure 3.3 is shown in Figure 3.4.

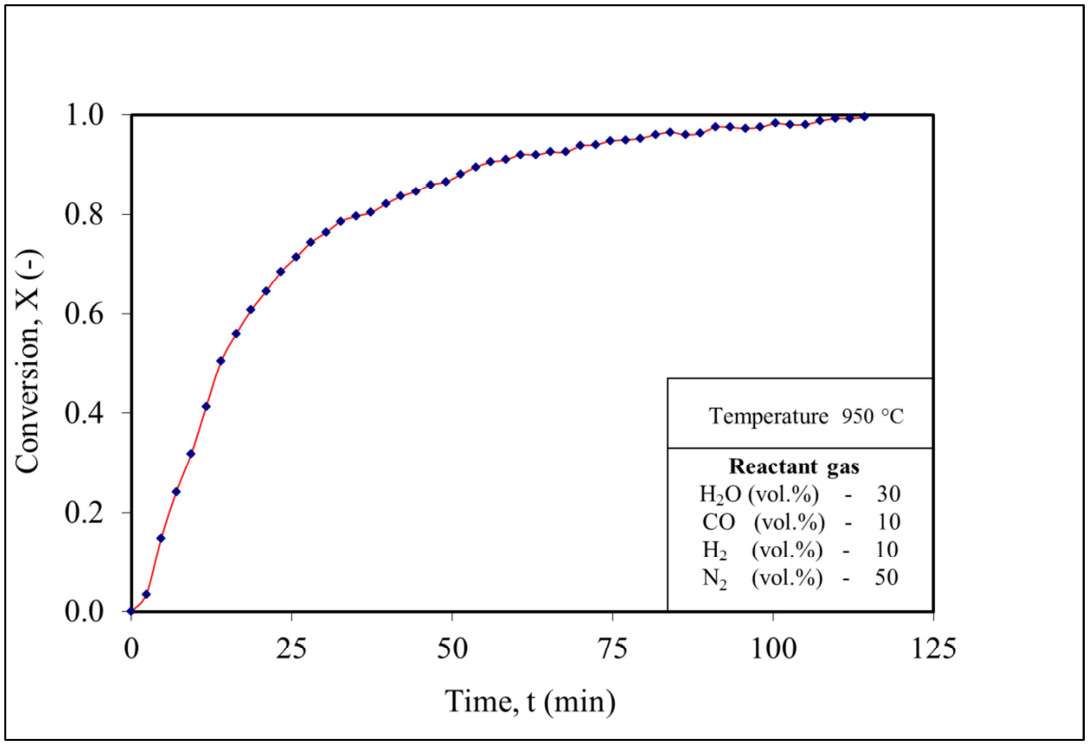

Figure 3.4: Normalised char conversion as a function of time

For each test, fifty data points were used for the calculation of f_L given in Section 3.2.4. Fifty data points were considered to be sufficient, since using two hundred data points resulted in a difference of less than ± 3% in the calculated value of f_L, which is within the repeatability of the experiments (± 5%).

3.2.3.2 Results of char-steam thermogravimetric analyser experiments

The effect of temperature on the char-steam gasification rate of New Vaal and Grootegeluk char is given in Figure 3.5. For these tests (NV3, NV6, NV9, GG3, GG6 and GG9) a constant reacting gas concentration was used containing 40 vol.% H_2O, 20 vol.% H_2, 20 vol.% CO and 20 vol.% N_2.

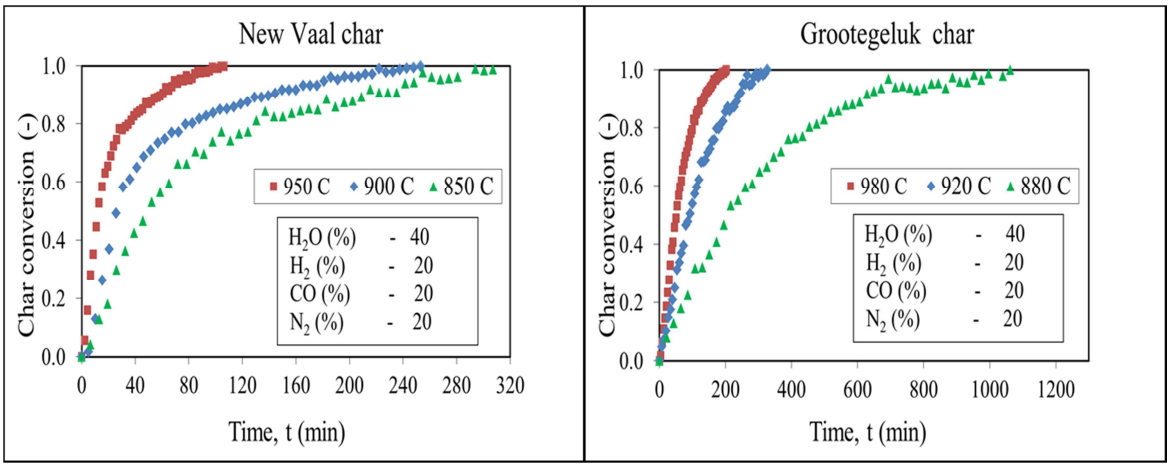

Figure 3.5: Effect of temperature on the steam gasification of char at 87.5 kPa

Figure 3.5 shows that the char gasification rate increases with an increase in temperature for both New Vaal and Grootegeluk chars, and that New Vaal char is more reactive than Grootegeluk char since New Vaal char requires less time to reach a fractional char conversion of 1. Similar results was obtained by Takarada *et al.* (1985), who studied the gasification reactivity of 34 coals having different dry ash-free carbon contents (C_{daf}). The results of the tests using reacting gas mixes one (20 vol.% H_2O, 5 vol.% H_2, 5 vol.% CO, 70 vol.% N2) and two (30 vol.% H_2O, 10 vol.% H_2, 10 vol.% CO, 50 vol.% N2) are given in Appendix C.1.

The inhibiting effect of CO and H_2 on the steam gasification rate of New Vaal and Grootegeluk chars is shown in Figure 3.6. The tests on New Vaal char (NV8 and NV 10) were carried out at a constant temperature of 950 °C, and the tests on Grootegeluk char (GG 9 and GG 10) were carried out at a constant temperature of 980 °C.

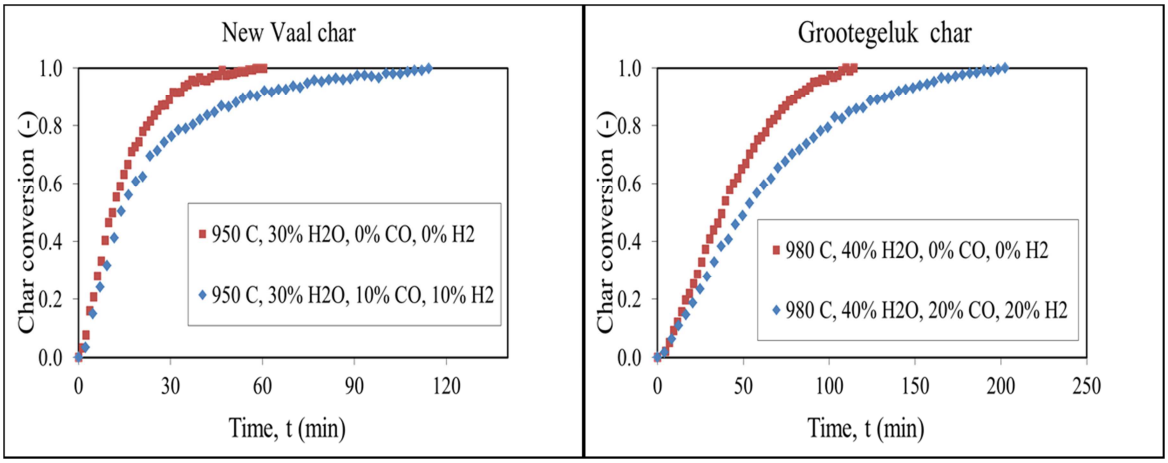

Figure 3.6: Effect of CO and H_2 on the steam gasification of char at 87.5 kPa

Figure 3.6 shows that for both New Vaal and Grootegeluk chars, the time to reach 100% conversion increased by a factor of ± 2 when CO and H_2 were added to the H_2O/N_2 mixture, which clearly illustrates their inhibiting effect on the steam gasification rate. The studies of Everson *et al*. (2006), Goyal *et al*. (1989) and Mühlen *et al*. (1985) also observed the inhibiting effect of CO and H_2 on the steam gasification rate of coal chars.

The effect of increasing the steam concentration of the reacting gas on the gasification rate of New Vaal and Grootegeluk chars is shown in Figure 3.7. The tests on New Vaal char (NV7, NV8 and NV9) were carried at a constant temperature of 950 °C, and the tests on Grootegeluk char (GG7, GG8 and GG9) were carried out at a constant temperature of 980 °C. Figure 3.7 shows that in this case an increase in the steam concentration does not result in a significant increase in the gasification rate since the concentration of the inhibiting gases (CO and H_2) was also increased. The effect of steam concentration on the gasification rate at 900 °C and 850 °C for New Vaal char and 920 °C and 880 °C for Grootegeluk char is shown in Appendix C.2. A similar trend is observed at the lower temperatures as that shown in Figure 3.7.

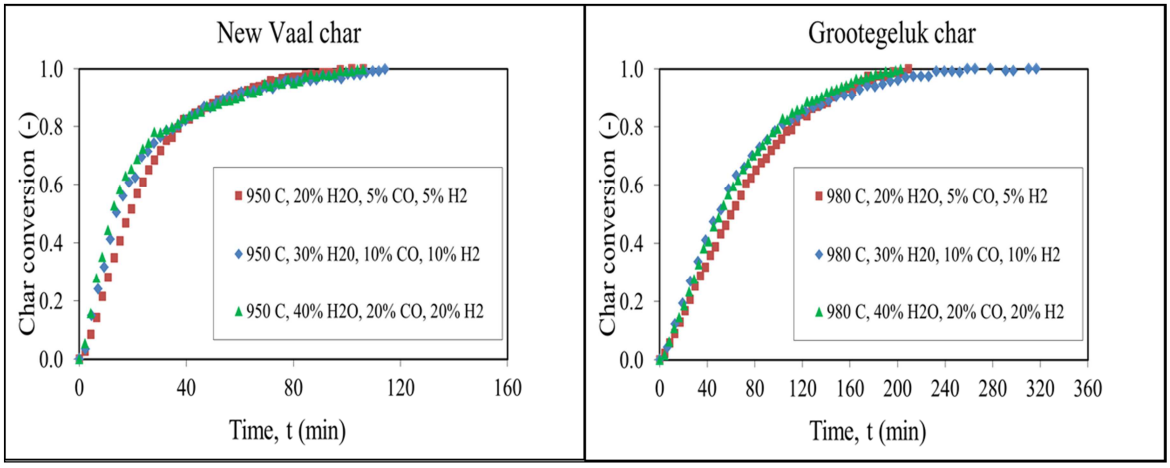

Figure 3.7: Effect of H_2O concentration on the steam gasification of char at 87.5 kPa

Although similar gasification rates were obtained for these sets of tests, (Figure 3.7, Figure C.2 (a) and Figure C.2 (b)) they can be used to estimate the value of f_L, since the inhibiting effects of CO and H_2 are included in the Johnson char-steam rate equation.

3.2.4 Determination of the Johnson rate equation parameter

In this section the thermogravimetric analyser data are used to determine the relative reactivity factor (f_L) for New Vaal and Grootegeluk chars. The reactive factor (f_L) is used as a parameter in the Johnson rate equation which is used in the fluidised bed model (Chapter 5) to calculate the rate of the steam char gasification reaction.

Data processing

A description of the Johnson equation is given in Section 3.2.1.5 of the char-steam gasification literature survey. The abbreviated form of the Johnson equation is given by equation 3.14.

$$\frac{dX}{dt} = K_J F(X) \tag{3.14}$$

Where K_J is the lumped reaction rate constant of the Johnson equation and is given by equation (3.15).

$$K_J = f_L k_I \tag{3.15}$$

Equation (3.7) can be rearranged to produce equation (3.16).

$$t(X) = \frac{1}{K_J}\int_0^X \frac{1}{F(X)} dX \tag{3.16}$$

Numerical integration of equation (3.16) produces a graph of fractional char conversion (X) as a function of time (t).

The value of K_J for each thermogravimetric analyser test is obtained by minimising the squared difference between the conversion values (X^m) determined experimentally using the thermogravimetric analyser data and the values (X^p) calculated using equation (3.16). The objective function (Φ_{KJ}) that is minimized is given by equation (3.17).

$$\Phi_{K_J} = \sum_{i=1}^{50} \left[(X^m)_i - (X^p)_i \right]^2 \qquad (3.17)$$

The measured and predicted values using the Johnson equation for New Vaal char (NV2, NV5 and NV8) and Grootegeluk char (GG2, GG5 and GG8) are given in Figure 3.8.

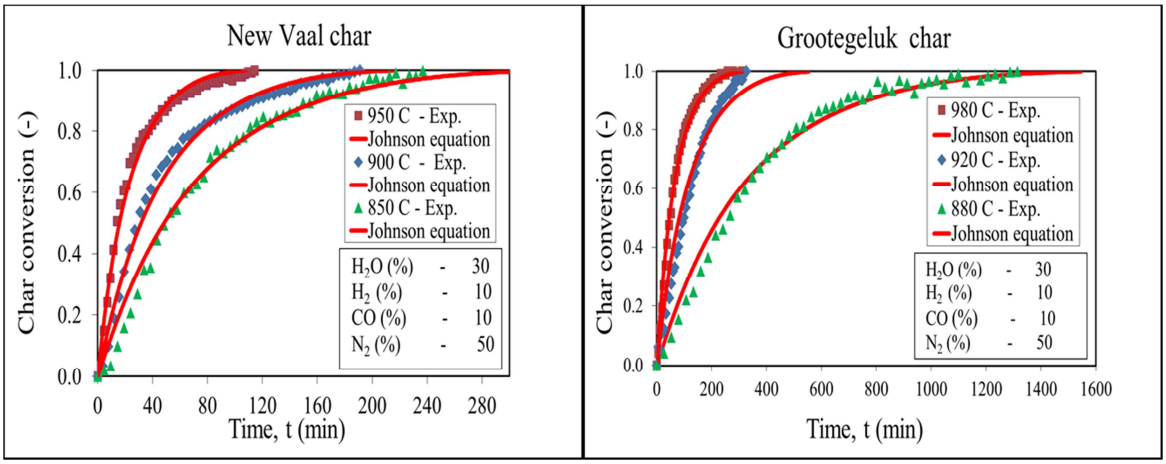

Figure 3.8: Experimental and predicted conversions using the Johnson equation

The value of f_L was estimated by minimising the squared difference between the measured and predicted values of K_J (equation (3.18)).

$$\Phi_{f_l} = \sum_{i=1}^{10} w_i \left[(K_J^m)_i - (K_J^p)_i \right]^2 \qquad (3.18)$$

Due to the large difference (two orders of magnitude) between the lowest and highest measured values of K_J, weighted least squared regression is applied which reduces the effect of the larger values of K_J on the objective function (Φ_{f_L}).

In this case the weighting factor is given by equation (3.19), which normalises the difference between the measured and predicted values of K_J using the average of the measured and predicted values of K_J (Engineering Statistics Handbook).

$$w_i = \left(\frac{2}{(K_J^m)_i + (K_J^p)_i} \right)^2 \qquad (3.19)$$

Table 3.3 and Table 3.4 show that the best fit values of f_L in the Johnson equation using the experimental thermogravimetric analyser data generated for New Vaal and Grootegeluk chars are 8.65 and 1.91 respectively.

Table 3.3 shows that for Grootegeluk char the values of f_L determined from the thermogravimetric analyser experimental data and the empirical equation (3.8) recommended by Johnson have the same order of magnitude.

Table 3.3: Johnson rate equation relative reactivity factor (f_L)

	New Vaal	Grootegeluk
TGA experimental data	8.65 ± 0.4	1.91 ± 0.1
Johnson empirical equation	1.20	1.00

However, for New Vaal coal the value of f_L determined from the thermogravimetric analyser data is an order of magnitude higher than the value determined using the Johnson correlation. A possible explanation for this finding is that Grootegeluk coal is a medium-rank bituminous coal and the Johnson correlation to predict f_L was developed using American medium-rank bituminous coals. The rank classification system using vitrinite reflectance given in Figure 2.2 (Chapter 2) shows that New Vaal coal is close to the boundary line that separates bituminous and sub-bituminous coals. Reactivity tests on New Vaal char using CO_2 as the reacting gas shows that it has a reactivity as high as some lignite coals (Engelbrecht, 2008), which could explain why the Johnson empirical correlation under-predicts f_L in the case of New Vaal coal.

Table 3.4: Experimental and calculated values of K_J for New Vaal coal to minimise Φ_{fL}

Test no.	Temperature (° C)	H_2O (%)	H_2 (%)	CO (%)	N_2 (%)	k_I x 60 (min^{-1})	K_J x 1000 measured (min^{-1})	K_J x 1000 predicted[1] (min^{-1})	Weighted deviation	f_L determined for each test
NV1	850	20	5	5	70	0.0001988	12.33	1.72	2.281	62.0
NV2	850	30	10	10	50	0.0001527	13.82	1.32	2.726	90.5
NV3	850	40	20	20	20	0.0000820	11.88	0.71	3.150	145.0
NV4	900	20	5	5	70	0.0017047	15.17	14.75	0.001	8.9
NV5	900	30	10	10	50	0.0020999	21.88	18.16	0.034	10.4
NV6	900	40	20	20	20	0.0011786	19.45	10.19	0.390	16.5
NV7	950	20	5	5	70	0.0106577	37.83	92.19	0.699	6.8
NV8	950	30	10	10	50	0.0105856	42.34	91.57	0.540	3.6
NV9	950	40	20	20	20	0.0068583	46.29	59.32	0.061	4.0
NV10	950	30	0	0	70	0.0326409	63.65	282.34	1.598	2.0

[1] $f_L = 8.65$

(All percentages are given as vol.%)

Table 3.5: Experimental and calculated values of K_J for Grootegeluk coal to minimise Φ_{fL}

Test no.	Temperature (° C)	H_2O (%)	H_2 (%)	CO (%)	N_2 (%)	k_I x 60 (min^{-1})	K_J x 1000 measured (min^{-1})	K_J x 1000 predicted[1] (min^{-1})	Weighted deviation	f_L determined for each test
GG1	880	20	5	5	70	0.0007885	2.76	1.51	0.344	3.5
GG2	880	30	10	10	50	0.0006114	2.93	1.17	0.740	4.8
GG3	880	40	20	20	20	0.0003342	3.59	0.64	1.948	10.8
GG4	920	20	5	5	70	0.0038114	7.24	7.29	0.000	1.9
GG5	920	30	10	10	50	0.0038930	8.18	7.45	0.009	2.1
GG6	920	40	20	20	20	0.0017777	9.07	3.40	0.826	5.1
GG7	980	20	5	5	70	0.0229061	13.29	43.81	1.143	0.6
GG8	980	30	10	10	50	0.0255561	14.57	48.88	1.170	0.6
GG9	980	40	20	20	20	0.0143426	15.78	27.43	0.291	1.1
GG10	920	40	0	0	60	0.0541740	19.82	103.61	1.843	0.4

[1] $f_L = 1.91$

(All percentages are given as vol.%)

3.3 Char-CO_2 gasification kinetics

Selected bench-scale studies on the char-CO_2 gasification reaction are given in Table 3.1. Many of these studies (Satoshi *et al*., 2013; Roberts and Harris, 2007; Everson *et al*., 2006; Mühlen *et al*., 1985) have used the Langmuir-Hinshelwood (LH) rate equations (Figure 3.1) to model the char-CO_2 gasification reaction.

The rate equation that was selected to be incorporated into the fluidised bed coal gasifier model described in Chapter 5 is given here as equation (3.20), which is a simplified version of the LH equations. It was also used by Ye *et al.* (1997) to calculate the rate of the char-CO_2 reaction.

$$\frac{dX}{dt} = k_{0CO_2} \exp\left(\frac{-E_{CO_2}}{RT}\right) p_{CO_2} (1-X)^{\beta} \qquad (3.20)$$

Equation (3.20) is based on the following assumptions:

- The char-steam and char-CO_2 reactions occur on separate sites (Everson *et al.*, 2005).
- Due to the low rate of the char-CO_2 reaction compared to the char-steam and char-O_2 reactions, the inhibiting effects of CO on the rate of the char-CO_2 reaction are not accounted for in the rate equation.
- The reaction order is one with respect to the CO_2 partial pressure (p_{CO2}).
- The grain model ($(1-X)^{\beta}$) adequately describes the effect of char conversion (X) on the rate of the char-CO_2 gasification reaction.

Data from the thermogravimetric analyser tests on New Vaal and Grootegeluk coals (Engelbrecht, 2008) were used to obtain values for the parameters in equation (3.20).The parameters in equation (3.20) are:

- the pre-exponential factor (k_{0CO2}),
- Arrhenius activation energy (E_{CO2})
- and grain model parameter (β).

Figure 3.9 shows the results of the thermogravimetric analyser tests carried out at 875 °C, 900 °C, 925 °C and 950 °C on New Vaal and Grootegeluk chars.

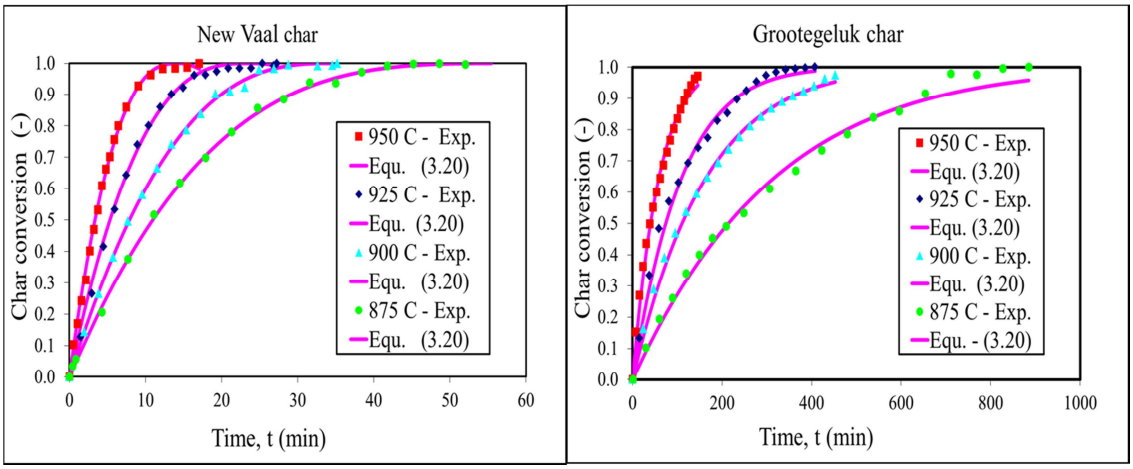

Figure 3.9: Thermogravimetric analyser test results at 87.5 kPa in 100% CO_2

Parameters for equation (3.20) were obtained by minimising the difference between the experimental and predicted char conversion values (Engelbrecht, 2008) as shown in Figure 3.9. Parameters for New Vaal and Grootegeluk chars are given in Table 3.6.

Table 3.6: Parameters for the char-CO_2 gasification rate equation

Char	E_{CO2} (kJ/mol)	$\ln(k_{0CO2})$ ($atm^{-1}s^{-1}$)	β
New Vaal	180	11.82	0.64
Grootegeluk	252	16.54	0.92

The char conversion rates calculated by the Johnson equation (equation (3.7)) for the char-steam reaction and the char-CO_2 reaction (equation (3.20)) are expressed as dX/dt (fractional char conversion rate). Conversion of dX/dt (s^{-1}) to r_j ($kmol.m^{-3}.s^{-1}$), which are the units required by the fluidised bed gasifier model described in Chapter 5, is given in Appendix E.2.1.

3.4 Fluidised bed coal devolatilisation experiments

3.4.1 Introduction

The objective of the bench-scale experiments described in this section was to develop a simplified coal devolatilisation sub-model suitable for the fluidised bed coal gasifier model described in Chapter 5. Due to the relatively high volatile matter content of high-ash South African coals (20-30%), the volatile matter has a significant influence on the composition and flow of the gas produced by fluidised bed gasifiers when gasifying these coals. The purpose of the devolatilisation sub-model is to estimate the evolution rate of gaseous species resulting from coal devolatilisation under typical fluidised bed coal gasification conditions

3.4.2 Literature review

Coal is a complex, non-homogenous organic material containing inclusions of inorganic matter (ash) incorporated in the structure. The organic part of coal consists of large aromatic clusters linked by hydrocarbon and O-N-S chains of differing bond strength, which decompose and release decomposition products upon heating (Howard, 1981). The final products of coal devolatilisation are char, tar, light oils and hydrocarbon gases.

The evolution rate and distribution of devolatilisation products are affected by the properties of the coal (including particle size), the coal heating rate, the peak devolatilisation temperature, the gases in which devolatilisation occurs and the pressure (Seebauer *et al.*, 1997; Solomon *et al.*, 1988).

Due to the complexity of the chemical and physical transformations that take place during devolatilisation, many fluidised bed coal gasification models use empirical correlations based on bench-scale experimental data to predict the devolatilisation products. (Loison and Chauvin, 1964; Yeboah, 1980; Ma *et al.*, 1988; Lee *et al.*, 1998).

Yeboah (1980) and Lee *et al*. (1998) used bench-scale fluidised bed reactors to generate devolatilisation data on Texas lignite, Illinois No. 6 bituminous coal and an Australian sub-bituminous coal. Details of these investigations are given in Table 3.7

Table 3.7: Selected bench-scale fluidised bed devolatilisation experiments

Investigator	Coal particle size (mm)	Sand particle size (mm)	Fluidising gas	Reactor diameter (mm)	Fluidising velocity (m/s)	Temp-erature (°C)
Yeboah (1980)	0.25-0.50	0.2 - 0.3	Nitrogen	50	0.25 -0.30	425 - 875
Lee *et al*. (1998)	0.3-1.0	0.27	Nitrogen	100	0.6- 0.8	750 - 900

Table 3.7 shows that the investigations were carried out using nitrogen as the fluidising gas in order to create an inert atmosphere in the reactor, thereby minimising char conversion by means of gas char-H_2O and char-CO_2 gasification reactions.

These investigations show that the coal type and temperature have the most significant effect on the evolution rates of gaseous species. The general trend observed is that as the temperature is increased the volume concentrations of H_2 and CO increase while the CH_4 and CO_2 volume concentrations decrease.

Advanced commercial coal devolatilisation models such as FLASHCHAIN (Maffei *et al.*, 2013) are capable of predicting the products of devolatilisation based on the physical and chemical properties of the parent coal. These advanced models were, however, not considered suitable for the present study since:

- The fluidised bed gasifier model described in Chapter 5 is focused on predicting the thermal performance of the gasifier, which does not require the evolution rates of minor species such as HCN, NH_3, NO_X, SO_X and tar.

- The advanced models have significantly longer computational times.

To create devolatilisation conditions that are representative of those in a bubbling fluidised bed coal gasifier, a bench-scale fluidised bed reactor at the CSIR was used to generate coal-specific devolatilisation data for Grootegeluk and New Vaal coals.

3.4.3 Description of the bench-scale fluidised bed reactor

A schematic representation of the bench-scale fluidised bed reactor at the CSIR is given in Figure 3.10 and a photograph is shown in Figure 3.11. The fluidised bed reactor consists of a 50 mm diameter 310 stainless steel pipe with a length of 1 800 mm. The reactor is heated by two electric heaters, each with a rating of 3 kW.

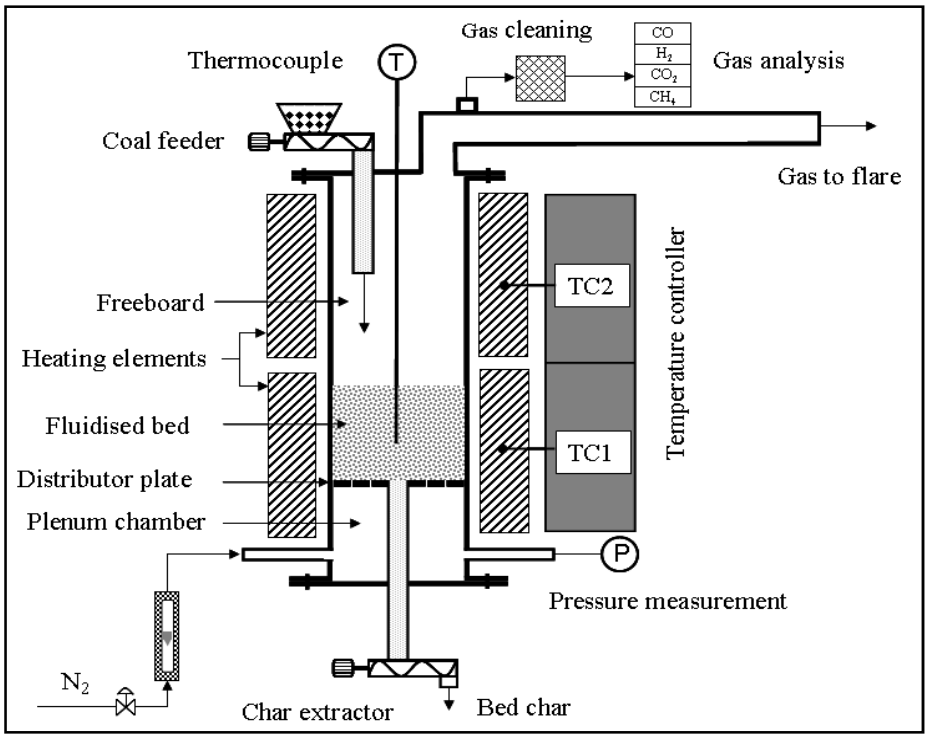

Figure 3.10: Bench-scale fluidised bed reactor flow diagram

The temperature in the bed and freeboard zones can be controlled independently by regulating the heat input to the bed and freeboard heaters separately. The distributor of the fluidised bed consists of a 5 mm thick 310 stainless steel disc containing eight holes (2 mm) for distribution of the fluidising gas. Screw feeders are used for coal feeding and char extraction from the bed. The temperature of the bed is measured by means of a thermocouple inserted through the roof of the reactor. Gas exiting the

reactor to the flare is sampled and cleaned using the apparatus shown in Figure 4.6 (Chapter 4) before flowing to the analysers specified in Table 4.4 (Chapter 4).

Figure 3.11: Bench-scale fluidised bed reactor at the CSIR

3.4.4 Experimental programme

The bench-scale fluidised bed reactor was used to devolatilise the coal in an inert (N_2) atmosphere at temperatures between 880 °C and 973 °C. An inert atmosphere is used to ensure that the gases that evolve are from the devolatilisation of coal alone and not from combustion and gasification reactions.

An experimental run is started by loading a 100 g batch of silica sand (0.4 – 0.8 mm) into the reactor. Incipient (minimum) fluidisation conditions are produced in the bed by introducing nitrogen at 20 Nl/min.

The reactor is heated to the operating temperature (900 °C – 975 °C) by the electric heaters. Due to the increase in the temperature, the superficial gas velocity increases

to ± 0.85 m/s which is approximately 5 times the minimum fluidising velocity. A mixture of 50% coal and 50% silica sand is fed continuously to the bed at a rate of ± 1.5 kg/h. The coal is mixed with silica sand in order to prevent agglomeration and defluidisation of the bed. The bed height is maintained at a constant level by draining bed material (char and sand) from the bed by means of the char extraction screw. A test is continued for ± 1 h to ensure that the composition of the gas produced by the reactor stabilises for at least ½ h, during which time measurements are taken.

Tests were carried out at temperatures between 880 °C and 973 °C with char residence times of ± 9.5 min, which allows sufficient time for complete devolatilisation of the coal (Ross *et al*., 2000). Other operating variables such as coal particle size and fluidising velocity were selected so that the tests would be representative of the pilot-scale fluidised bed gasification tests carried out on New Vaal and Grootegeluk coal described in Chapter 4.

3.4.5 Experimental results

The results of the fluidised bed devolatilisation tests are given in Table 3.8. The values shown in Table 3.8 are average values obtained during ½ h of stable operation.

Table 3.8, Figure 3.12 and Figure 3.13 show that for both New Vaal and Grootegeluk coals the CO and H_2 concentration of the gas produced during devolatilisation increased with an increase in temperature, while the CH_4 and CO_2 concentrations decreased with an increase in temperature. Grootegeluk coal produced higher concentrations of CH_4 and lower concentrations of CO, H_2 and CO_2 than New Vaal coal.

Table 3.8: Bench-scale fluidised bed devolatilisation tests

Coal	**New Vaal**			**Grootegeluk**		
Test number	**1**	**2**	**3**	**1**	**2**	**3**
Mid-bed temperature (ºC)	880	932	955	887	950	973
Char residence time (min)	9.3	9.3	9.3	9.8	9.8	9.8
Coal feed rate (kg/h)	0.73	0.73	0.73	0.70	0.70	0.70
Coal particle size (mm)	0.8 – 1.2	0.8 – 1.2	0.8 – 1.2	0.8 – 1.2	0.8 – 1.2	0.8 – 1.2
Sand feed rate (kg/h)	0.73	0.73	0.73	0.70	0.70	0.70
Sand particle size (mm)	0.5 - 0.8	0.5 - 0.8	0.5 - 0.8	0.5 - 0.8	0.5 - 0.8	0.5 - 0.8
Nitrogen flow (Nm^3/h)	1.2	1.2	1.2	1.2	1.2	1.2
Fluidising velocity (m/s)	0.83	0.87	0.88	0.83	0.88	0.90
Bed pressure drop (Pa)	900	900	900	900	900	900
Dynamic bed height (mm)[1]	230	230	230	230	230	230
Measured dry gas composition						
CO (vol.%)	3.2	4.2	5.1	3.0	4.1	4.3
H_2 (vol.%))	8.5	10.2	12.0	7.4	9.4	9.8
CH_4 (vol.%)	1.0	0.9	0.8	4.3	3.4	3.4
CO_2 (vol.%)	1.3	1.3	1.4	0.5	0.4	0.3
N_2 + others[2] (vol.%)[3]	86.1	83.4	80.7	84.7	82.6	82.2
Nitrogen-free gas composition[4]						
CO (vol.%)	22.8	25.2	26.3	19.8	23.4	24.1
H_2 (vol.%)	60.8	61.5	61.9	48.5	54.3	55.2
CH_4 (vol.%)	6.8	5.2	4.3	28.2	19.8	19.0
CO_2 (vol.%)	9.6	8.0	7.5	3.5	2.5	1.7

[1] Expanded bed height at the operating fluidising velocity

[2] Others are < 0.4 vol.% and include H_2S, COS, NH_3, HCN and C_2^+

[3] (N_2 + others) by difference

[4] Gas composition normalised to CO, H_2, CH_4 and CO_2

3.4.6 Devolatilisation sub-model development

Based on the data given in Table 3.8, Figure 3.12 and Figure 3.13, the molar evolution rates of CO, CH_4, CO_2, H_2, H_2S and N_2 as a result of coal devolatilisation can be estimated using the sub-model described in Appendix C.3.

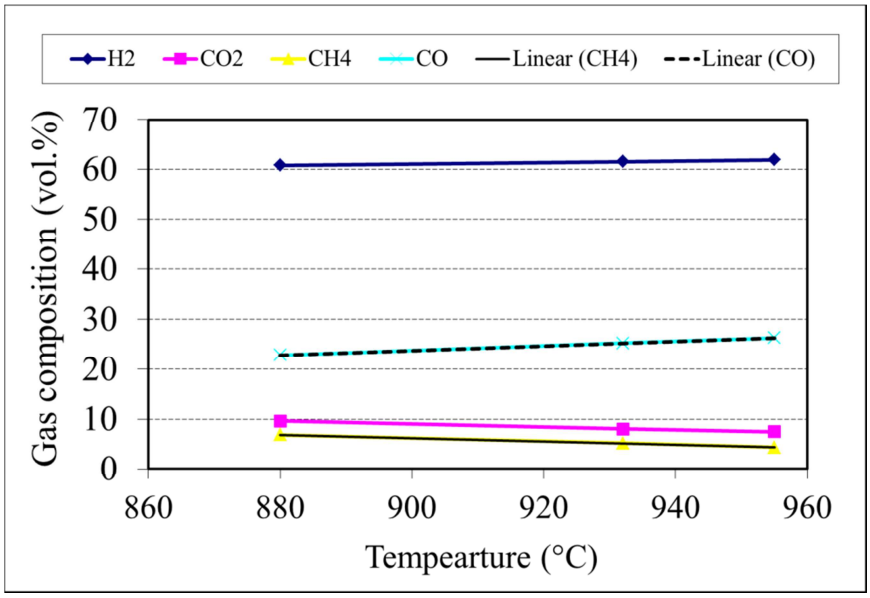

Figure 3.12: Dry and nitrogen-free gas composition – New Vaal coal

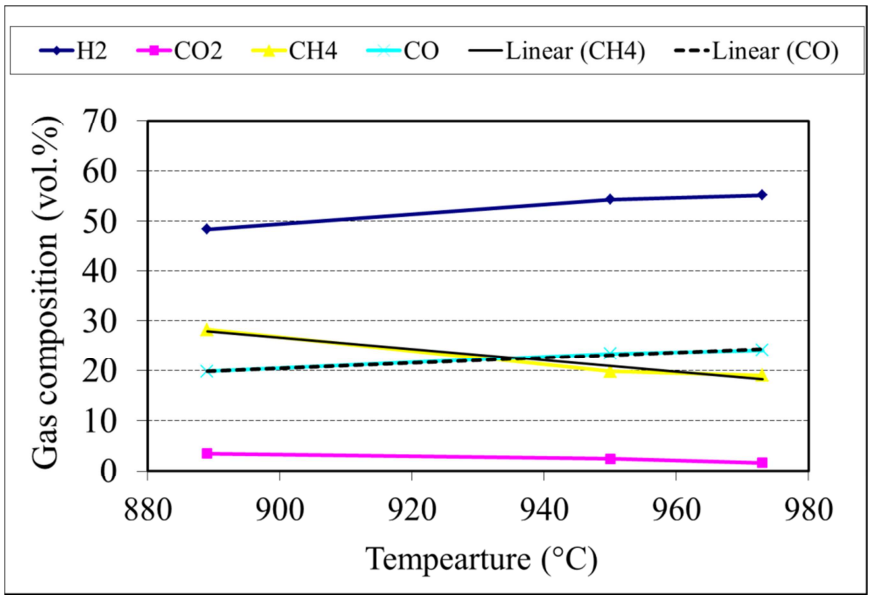

Figure 3.13: Dry and nitrogen-free gas composition – Grootegeluk coal

3.5 Summary of bench-scale gasification and devolatilisation experiments

Parameters were obtained for the Johnson char-steam rate equation using a thermogravimetric analyser. The rate equation to be included in the fluidised bed gasifier model described in Chapter 5 is given by equation (3.7).

$$\frac{dX}{dt} = f_L k_1 F(X) \qquad (3.7)$$

In equation (3.7) the relative reactivity parameter (f_L) was found to be 8.65 and 1.91 for New Vaal and Grootegeluk coals respectively.

It could be concluded that themorgravimetric analyser data are required to estimate the values of f_L for high-ash South African coal chars since the correlation recommended by Johnson to estimate f_L, which is based on the dry ash-free carbon content of the coal (Y_c), results in a significant under-prediction of f_L in the case of New Vaal coal.

Parameters were obtained for a first-order char-CO_2 gasification rate equation using the data generated by Engelbrecht (2008). The results of the tests show that:

- The char-CO_2 gasification rate is approximately 10 to 15 higher for New Vaal coal than for Grootegeluk coal.
- The char-CO_2 gasification rate is approximately 5 to 10 times lower than the char-steam gasification rate for both coals.

Devolatilisation tests were carried out on Grootegeluk and New Vaal coals using a bench-scale fluidised bed devolatilisation reactor. The devolatilisation yields of the two coals differed in that Grootegeluk coal produced higher concentrations of CH_4 and lower concentrations of CO, H_2 and CO_2 compared with New Vaal coal.

3.6 Chapter 3 references

CHEN, C., WANG, J., LIU, W., ZANG, S., YIN, J., LUO, G. AND YAO, H. (2012). Effect of pyrolysis condition on the char gasification with mixtures of CO_2 and H_2O. *Proceedings of the Combustion Institute* 34: 2453–2460.

COETZEE, S., NEOMAGUS, H.W.J.P., BUNT, J.R. AND EVERSON, R.C. (2013). Improved reactivity of large coal particles by K_2CO_3 addition during steam gasification. *Fuel Processing Technology* 114: 75–80.

ENGELBRECHT, A.D. (2008). Characterisation and fluidised bed gasification of selected high-ash South African coals. Master's dissertation, North-West University, South Africa.

EVERSON, R.C., NEOMAGUS, H.W.J.P., KASAINI, H. AND NJAPHA, D. (2006). Reaction kinetics of pulverised coal-chars derived from inertinite-rich coal discards: Gasification with carbon dioxide and steam. *Fuel* 85: 1076–1082.

GOYAL, A., ZABRANSKY, R.F. AND REHMAT, A. (1989). Gasification kinetics of Western Kentucky bituminous coal char. *Industrial & Engineering Chemistry Research 28*: 1767–1778.

Engineering Statistics Handbook. Chapter 4 – process modelling. http://www.itl.nist.gov/div898/handbook//pmd/section4/pmd432.htm

HOWARD, J.B. (1981). Fundamentals of coal pyrolysis and hydropyrolysis. In: *Chemistry of Coal Utilization, second supplementary volume*, Chapter 12, John Wiley & Sons, New York.

HUANG, Z., ZHANG, J., ZHAO, Y., ZANG, H., YUE, G., SUDA, T. AND NARUKAWA, H. (2010). Kinetic studies of char gasification with steam and CO_2 in the presence of CO and H_2. *Fuel Processing Technology* 91: 843–847.

JOHNSON, J.L. (1979). Chapter 1. In: *Kinetics of Coal Gasification*, New York: Wiley.

KAITANO, R. (2007). Characterisation and reaction kinetics of high ash chars derived from inertinite-rich coal discards. Doctoral thesis. North-West University, South Africa.

KWON, T-W., KIM, S.D. AND FUNG, D.P.C. (1988). Reaction kinetics of char-CO_2 gasification. *Fuel* 67: 530–535.

LEE, J.M., KIM, Y.J., LEE, W.J. AND KIM, S.D. (1998). Coal gasification kinetics derived from pyrolysis in a fluidized bed reactor. *Energy* 23: 475–488.

LOISON, R. AND CHAUVIN, R. (1964). Pyrolyse rapide du charbon. *Chemie et Industrie* 91: 269.

MA, R.P., FELDER, R.M. AND FERREL, J.F. (1988). Modelling a pilot-scale fluidised bed coal gasification reactor. *Fuel Processing Technology* 19: 265–290.

MAFFEI, T., FRASSOLDATI, A., CUOCI, A., RANZI, E. AND FRAVELLI, T. (2013). Predictive one step model of coal pyrolysis for CFD applications. *Proceedings of the Combustion Institute* 34: 2401–2410.

MÜHLEN, H., VAN HEEK, H. AND JUNTGEN, H. (1985). Kinetic studies of steam gasification of char in the presence of CO, CO_2 and H_2. *Fuel* 64: 944–949.

ROBERTS, D.G. AND HARRIS, D.J. (2007). Char gasification in mixtures of CO_2 and H_2O: Competition and inhibition. *Fuel* 86: 2672–2678.

ROBERTS, D.G. AND HARRIS, D.J. (2006). A kinetic analysis of coal char gasification reactions at high pressures. *Energy and Fuels* 20: 2314–2320.

ROSS, M., HEIDENRICH, C.A. AND ZHANG, D.K. (2000). Devolatilisation times of coal particles in a fluidised bed. *Fuel* 79: 873–883.

SATOSHI, U., SHIRO, K. AND SAURO, H. (2013). Modelling coal char gasification in coexistence of CO_2 and H_2O considering sharing of active sites. *Fuel* 103: 14–21.

TAKARADA, T., TAMAI, Y. AND TOMITA, A. (1985). Reactivities of 34 coals under steam gasification. *Fuel* 64: 1438–1442.

SEEBAUER, V., PETEK, J. AND STAUDINGER, S. (1997). Effects of particle size, heating rate and pressure on measurement of pyrolysis kinetics by thermogravimetric analysis. *Fuel* 76: 1277–1282.

SOLOMON, P.R., HAMBLEN, D.G., CARAGELO, R.M., SERIO, M.A. AND DESHPANDE, G.V. (1988). General model for coal devolatilization. *Energy and Fuels* 2: 405–422.

WANG, J., JIANG, M., YAO, Y., ZANG, Y. AND CAO, H. (2009). Steam gasification of coal char catalyzed by K_2CO_3 for enhanced production of hydrogen without formation of methane. *Fuel* 88: 91: 1572–1579.

WU, S., GU, J., LI, Y., WU, Y. AND GAO, J. (2006). The reactivity and kinetics of Yanzhou coal char from elevated pyrolysis temperatures during gasification in steam at 900 – 1 200 °C. *Process safety and environmental Protection* 84(B60): 420-428.

YE, D.P., AGNEW, J.B. AND ZHANG, D.K. (1997). Gasification of South Australian low-rank coal with carbon dioxide and steam: Kinetics and reactivity studies. *Fuel* 77: 1209–1219.

YEOBAH, J.D. (1980). Effects of calcined dolomite on the fluidised bed pyrolysis of coal. *Industrial & Engineering Chemistry Process Design and Development* 19: 646.

ZHANG, L., HUANG, J., FANG, Y. AND WANG, Y. (2006). Gasification reactivity and kinetics of typical Chinese anthracite chars with steam and CO_2. *Energy & Fuels* 20: 1201–1210.

3.7 Chapter 3 and Appendix C nomenclature

a	LH equation weighting parameter	-
A_{ij}	LH equation pre-exponential factors	s^{-1}
b	LH equation weighting parameter	-
C	mass percentage carbon in coal	wt.%
c	LH equation weighting parameter	-
C_{daf}	dry and ash-free carbon in coal	wt.%
C_{fixed}	fixed carbon in coal	wt.%
d	LH equation weighting parameter	-
E_{CO2}	Arrhenius activation energy of the char – CO_2 reaction	$kJ.mol^{-1}$
E_{ij}	LH equation activation energies	$kJ.mol^{-1}$
F(X)	structural factor (char conversion model)	-
f_L	Johnson equation relative reactivity factor	-
G_{coal}	coal flow rate	$kg.h^{-1}$
H	mass percentage hydrogen in coal	wt.%
IH_2O	inherent moisture in the coal	wt.%
K_{eq1}	equilibrium constant in Johnson rate equation	-
k_I	rate constant of Johnson char-steam rate equation	s^{-1}
k_{ij}	LH equation rate constants	s^{-1}
K_J	Johnson equation lumped rate constant	min^{-1}
k_{0CO2}	pre-exponential factor of the char – CO_2 reaction	$atm^{-1}s^{-1}$
m_{ash}	mass of ash/residue	g
m_o	initial mass of char following pyrolysis	g
m_t	mass of coal/char at time t	g
N	mass percentage nitrogen in coal	wt.%
nQ	dry molar gas flowrate	$mol.h^{-1}$
O	mass percentage oxygen in coal	wt.%

p_{CO}	partial pressure of carbon monoxide	atm
p_{CO2}	partial pressure of carbon dioxide	atm
p_{H2}	partial pressure of hydrogen	atm
p_{H2O}	partial pressure of water	atm
R	universal gas constant	$J.mol^{-1}K^{-1}$
r''_j	rate of reaction based on solids volume	$mol.m^{-3}s^{-1}$
T	gas temperature	K
T_p	pre-treatment temperature of char	K
T_C	gas temperature	C
Vf_{gi}	molar flow of gas component i due to coal devolatilisation	$mol.s^{-1}$
V_i	concentration of species i in the volatiles (wet basis)	vol.%
V^d_i	concentration of species i in the volatiles (dry basis)	vol.%
w_i	regression weighting factor	-
X	fractional conversion of fixed carbon in coal	-
X^m	measured fixed carbon conversion	-
X^p	predicted fixed carbon conversion	-
dX/dt	fractional char conversion rate	s^{-1}
Y_c	mass fraction dry ash-free carbon in coal	-

Greek Letters

α	parameter in structural factor of Johnson rate equation	-
β	structural factor of the grain model	-
ψ	random pore model structural parameter	-
Φ	objective function	-

Acronyms/Abbreviations

DTF	Drop tube furnace
FB	Fluidised bed
FBTF	Fixed bed tubular furnace
ISO	International Standards Organization
LH	Langmuir-Hinshelwood

NWU	North-West University
No.	Number
SABS	South African Bureau of Standards
TGA	Thermogravimetric analyser/analysis

CHAPTER 4 PILOT-SCALE FLUIDISED BED COAL GASIFICATION

4.1 Introduction

In this chapter a detailed investigation is conducted into the gasification of coal in pilot-scale fluidised bed gasifiers. Section 4.2 reviews selected pilot- and bench-scale fluidised bed coal gasification studies that have been reported in the literature. In Section 4.3 the pilot-scale fluidised bed gasifier at the CSIR and its operation are described. The experimental programme and the results of tests carried out on the pilot-scale fluidised bed gasifier at the CSIR are presented in Sections 4.4 and 4.5. Finally, a summary of the pilot-scale fluidised bed gasification of coal is given in Section 4.6.

4.2 Literature review

Selected pilot and bench-scale fluidised bed coal gasification investigations that have been reported in the literature since 1982 are given in Table 4.1 and Table 4.2. Table 4.1 gives details regarding the operating conditions and performance of the gasifiers. Table 4.2 gives details regarding the dimensions and configuration of the gasifiers.

4.2.1 Motivation for investigations

The motivation given by most of the investigators for their work is that fluidised bed coal gasifiers can potentially be applied for efficient and clean generation of electricity using Integrated Gasification Combined Cycles (IGCC). Other investigators have given as their motivation the generation of industrial fuel gas (Gutierrez and Watkinson, 1982; Belyaev *et al.*, 2003) and syngas (Rhinehardt *et al.*, 1987; Purdy *et al.*, 1984) using fluidised bed coal gasifiers.

Table 4.1: Summary of selected experimental bubbling fluidised bed coal gasification studies

Investigator	Year	Country	Coal	Average coal particle size (mm)	Gasification agents	Gasification Agents temperature (°C)	Superficial gas velocity (m/s)	Gasifier pressure (kPa)	Gasifier temperature (°C)	Fixed carbon conversion (%)	Calorific value of gas (MJ/Nm^3)
Engelbrecht[1]	2010	South Africa	Bituminous	1.2–2.4	Air/steam	159–202	1.9–2.2	90	925–950	52–86	2.5–3.0
Xiao	2007	China	Bituminous	1.6–2.0	Air/steam	270–300	1.2–1.3	500	940–980	62–69	4.2–4.7
Bhattacharya	2006	Australia	Lignite	N/R	O_2/air/steam	N/R	0.7–1.4	900	750–920	70–87	4.0 *
Jing	2005	China	Bituminous & anthracite	0.5–0.6	Air/steam	N/R	N/R	101	880–920	65–80	2.6–3.1
Ashman	2005	Australia	Lignite	0.5–2.0	Air/steam	500–600	0.5–0.7	100	837–850	79–88	4.7–5.4
Huang	2003	China	Sub-bituminous	0.9–3.0	Air/steam	N/R	0.8–1.0	500–1 400	880–980	73–78	4.6–5.1
Belyaev	2003	Russia	Bituminous	1.0–3.0	O_2/air/steam	N/R	N/R	101	850–1 250	30–75	3.5–6.1
Ocampo	2003	Colombia	Bituminous	0–1.2	Air/steam	355–420	N/R	101	812–872	58–69	2.7–3.0
Paterson	1997	United Kingdom	Bituminous & lignite	N/R	Air/steam	N/R	N/R	1 300	960–980	71–79	3.9–4.8
Chatterjee	1995	India	Bituminous & coke breeze	0–2.0	Air/steam	N/R	0.5–1.0	101	750–1 000	50–80	4.0–4.5
Goyal	1990	United States	Bituminous	0.5	Air/steam	N/R	1.2 –1.3	1000 – 2 700	960–1 000	80–90	2.3–3.9
Saffer	1988	France	Spanish anthracite	0.8–1.2	Air/steam	208–555	0.7–1.0	101	818–945	21–69	2.2–3.4
Rhinehardt	1987	United States	Lignite	0.2–0.9	O_2/steam	527	N/R	810	747–927	80–97	9.3–11.1
Neogi	1986	United States	Bituminous	0.3	Steam	N/R	N/R	101	550–850	N/R	8.0–9.7
Purdy	1984	United States	Sub-bituminous	0.7	O_2/steam	527	N/R	790–828	924–981	64–90	14.0
Gutierrez	1982	Canada	N/R	0.5–4.8	Air/steam	N/R	1.0–1.4	101	750–902	25–66	1.4–2.9

[1] The names given in Tables 4.1 and 4.2 are the first authors of the papers that describe the correlations and models. Details are given in Chapter 4 references.

N/R Not reported * Lower heating value

Table 4.2: Details of bench and pilot-scale bubbling fluidised bed gasifiers used by investigators

Investigator	Coal feedrate (kg/h)	Estimated thermal rating (kW)	Gasifier dimensions (m)	Gasifier height (m)	Fluidised bed height (m)	Tapered bed section	Ratio of freeboard to bed area	Distributor type	Coal feeding position	Insulation	Fines recycle
Engelbrecht	23–29	140	0.20 x 0.20	4.0	0.8	No	4	Nozzle cap	Above bed	Refractory	No
Xiao	320–330	2248	0.45 Ø	10.5	2.1–3.6	No	2	Spouting nozzle	In bed	Refractory	Yes
Bhattacharya	250	1200	0.30 Ø	5.5	N/R	Yes	1	N/R	In bed	Refractory	Yes
Jing	5	30	0.10 Ø	4.4	N/R	No	1	N/R	N/R	Fibreglass wool	No
Ashman	< 20	90	0.20 Ø	2.55	0.9	No	2.5	N/R	In bed	Electrical heating	No
Huang	62–135	937	0.20 Ø	3.0	1.0	No	2.25	N/R	In bed	Refractory	No
Belyaev	0.2–1	6	0.04 Ø	N/R	N/R	No	1	N/R	In bed	Electrical heating	No
Ocampo	6–8	64	0.22 Ø	2.0	N/R	No	1	Perforated plate	In bed	Refractory	No
Paterson	216–246	1700	0.30 Ø	6.6	3.0	Yes	2.25	Spouting nozzle	In bed	Refractory	No
Chatterjee	10	75	0.20 x 0.20	2.0	0.6	No	1	Perforated plate	Above bed	Refractory	No
Goyal	208	1400	0.20 Ø	4.7	1.5–2.3	Yes	6	Spouting nozzle	In bed	Refractory	No
Saffer	4–11	85	0.18 Ø	1.5	0.4–0.5	No	4	Perforated plate	In bed	Fibreglass wool	No
Rhinehardt	18–30	170	0.15 Ø	N/R	0.6–1.0	No	1	Nozzle cap	Above bed	Fibreglass wool	No
Neogi	N/R	N/R	0.1 Ø	0.55	0.1	No	2	Perforated plate	Above bed	Electrical heating	No
Purdy	18–30	170	0.15 Ø	N/R	0.6–1.0	No	1	Nozzle cap	Above bed	Fibreglass wool	No
Gutierrez	3.6–7.2	60	0.15 Ø	1.2	0.2–0.6	No	1	Perforated plate	Above bed	Fibreglass wool	No

N/R Not reported
Ø Diameter

The advantages of fluidised bed gasifiers given are:

- Coal flexibility in terms of ash content and ash fusion temperature (Huang *et al.*, 2003; Belyaev *et al.*, 2003; Engelbrecht *et al.*, 2010; Chatterjee *et al.*, 1995; Paterson, 1997).
- Operation at lower temperatures is possible, which
    - reduces sensible heat losses (Bhattacharya, 2006; Goyal *et al.*, 1990),
    - avoids vaporisation of alkali species in the ash and therefore reduces corrosion of syngas coolers (Bhattacharya, 2006; Xiao *et al.*, 2007),
    - reduces construction and maintenance costs (Huang *et al.*, 2003)
    - and reduces oxygen consumption (Huang *et al.*, 2003).
- Limestone can be added for the in-bed capture of hydrogen sulphide and sulphur dioxide (Ocampo *et al.*, 2003; Paterson, 1997; Goyal *et al.*, 1990).

4.2.2 Objectives of investigations

Most of the investigators conducted their studies in order to evaluate the performance of a particular coal or a number of different coals in a fluidised bed gasifier. The effect of operating variables such as temperature, pressure, coal particle size, bed height and limestone addition on the fixed carbon conversion, gas composition, fines generation and bed agglomeration has been studied.

Investigations have also been carried out in order to generate data that can be used for the validation of fluidised bed coal gasifier models (Chatterjee *et al.*, 1995; Ashman *et al.*, 2005; Saffer *et al.*, 1988 Rhinehardt *et al.*, 1987; Paterson, 1997).

4.2.3 Pilot-scale and bench-scale equipment used for investigations

Details of the bench-scale and pilot-scale fluidised bed gasifiers used to conduct the investigations are summarised in Table 4.2. This table shows that the diameters of the fluidised beds are between 0.04 and 0.45 m, and the heights are between 1.2 and 10.5 m. In ± 50% of the studies the fluidised bed gasifiers have expanded freeboards, with the highest expansion ratio being equal to 6.

4.2.4 Results of selected pilot-scale fluidised bed gasifier studies

4.2.4.1 Fixed carbon conversion

Table 4.1 shows that the fluidised bed coal gasification studies were conducted using lignite, sub-bituminous, bituminous and anthracite coals. It is clear that with the lower-rank coals (Bhattacharya *et al.*, 2006; Ashman *et al.*, 2005; Huang *et al.*, 2003; Rhinehardt *et al.*, 1987; Purdy *et al.*, 1984), higher fixed carbon conversions were obtained than with the higher rank coals (Xiao *et al.*, 2007; Jing *et al.*, 2005; Ocampo *et al.*, 2003; Gutierrez and Watkinson, 1982). The highest fixed carbon conversion was achieved with lignite (97%) and the lowest with anthracite (21%). It was found that the fixed carbon conversion increases with bed temperature, and of the operating variables investigated, bed temperature has the most significant effect on the fixed carbon conversion. The maximum temperature is, however, limited to 950 – 1 000 °C to prevent agglomeration and clinkering of the bed (Xiao *et al.*, 2007; Chatterjee *et al.*; 1995, Bhattacharya, 2006). Xiao *et al.* (2007) concluded from their work that fixed carbon conversion increases with increases in fluidised bed height since this increases the residence time of char (ash) particles in the gasifier. Huang *et al*. (2003) investigated the effect of pressure on fixed carbon conversion at a fixed coal flowrate. They found that fixed carbon conversion increases up to a pressure of 1.2 MPa and concluded that, at pressures higher than 1.2 MPa, the rate of the gasification reaction is limited by gas diffusion. Jing *et al.* (2005) and Chatterjee *et al.* (1995) found that a higher steam concentration in the gasifier had a positive effect on fixed carbon conversion.

It is concluded by the majority of the investigations that the attrition of char and the subsequent elutriation of high carbon fines from the gasifier have a limiting effect on the maximum fixed carbon conversion that can be achieved. The attrition rate of char increases with increased brittleness of the char and higher fluidising velocities (Bhattacharya, 2006). Closer examination of Table 4.2 shows that only two of the investigators recycled fines to the gasifier. It is not clear whether the other investigators thought that recycling of fines would not be effective or that it would introduce unnecessary complications into the system. The investigators who did recycle fines did not report the effect of fines recycling on fixed carbon conversion.

4.2.4.2 Gas composition

Table 4.1 shows that higher gas calorific values were obtained in the cases where oxygen and steam were used as the gasification agents (Rhinehardt *et al.*, 1987; Purdy *et al.*, 1984). The investigators who used oxygen-enriched air and steam (Bhattacharya, 2006; Belyaev *et al.*, 2003) obtained higher calorific values than those who used air and steam as the gasification agents. The highest calorific value that was achieved was 14 MJ/Nm^3 (Purdy *et al.*, 1984) and the lowest was 1.4 MJ/Nm^3 (Gutierrez and Watkinson, 1982).

In the cases where air and steam were used as the gasification agents, the calorific value of the gas increased when the temperature was increased to between 925 and 950 °C due to the increase in fixed carbon conversion. At higher temperatures the calorific value of the gas decreases since the nitrogen in the additional air that is required to increase the temperature has a diluting effect on the gas and more unconverted fines are elutriated. In the cases of oxygen and steam gasification, the gas calorific value (CV) did not decrease at higher temperatures since the diluting effect of nitrogen was not present. Huang *et al.* (2003) and Chatterjee *et al.* (1995) concluded that the methane in the gas is produced only from the volatiles in the coal and that the CO and H_2 in the gas are produced from the reactions of H_2O and CO_2 with the char and also from the volatiles in the coal.

Several investigators have added limestone to the bed in order to capture H_2S and reduce its concentration in the gas. Goyal *et al.* (1990) and Paterson (1997) reported sulphur-capture efficiencies of between 60% and 90% at temperatures of 970 °C for gasification tests conducted on high- and low-rank coals. Ocampo *et al.* (2003), however, reported lower sulphur-capture efficiencies of 20% to 30% at temperatures of 870 °C and 840 °C for gasification tests conducted on a Colombian bituminous coal. Significant concentrations of NH_3 (1 600 ppm) were detected in the gas by Bhattacharya (2006) in gasification tests conducted on Australian lignites. Addition of dolomite to the bed reduced the NH_3 concentration by ± 50%.

4.2.4.3 Bed agglomeration and clinkering

Bed agglomeration and clinker formation were experienced by Bhattacharya *et al.* (2006), Ashman *et al.* (2005), Huang *et al.* (2003), Paterson (1997), Chatterjee *et al.* (1995) and Gutierrez and Watkinson (1982) during the course of their test work. Agglomeration of char and clinker formation resulted in defluidisation of the bed and subsequent termination of the tests. The following possible explanations were given for the occurrence of bed agglomerates and clinkers:

- Bed temperature is too high.
- Ash fusion temperature of the coal is too low.
- High caking index of the coal.
- Fluidising velocity is too low.
- Segregation of oversize coal particles to the distributor.
- Bed is too high.
- Oxygen concentration of the reactant mix is too high.

Bhattacharya (2006) subjected the agglomerates to X-ray diffraction (XRD) analysis and found the presence of silicates with low melting points. He concluded that these are formed due to the high sodium content of the coal ash. Some investigators found that the addition of limestone or dolomite can in some instances prevent the formation of agglomerates. No reasons why limestone can be effective for agglomeration control have been given.

4.2.5 Data for model calibration and validation

Saffer *et al.* (1988) reported detailed results of 17 tests that were conducted on Spanish anthracite at different operating conditions. These results were given in sufficient detail to be able to determine the parameters for a fluidised bed gasification model. The results of four tests on bituminous coal reported by Xiao *et al.* (2007) are also given in sufficient detail to allow model parameters to be fitted to a model.

Other investigators (Paterson, 1997; Chatterjee *et al.*, 1995; Neogi *et al.*, 1986) have used their data to validate models that were developed by their own research institutes and universities. However, their data have not been reported in sufficient detail to allow other investigators to use it to validate their own models. The results of experiments conducted by Ashman *et al.* (2005) on Victorian lignite were used to validate a model developed at the University of Adelaide, Australia. A description of the model is given by Yan *et al.* (1998) and Ross *et al.* (2005).

Overall, investigators concluded that the development of a model is required to understand and simulate the effect of complex interactions of input variables on the performance of a bubbling fluidised bed coal gasifier.

4.2.6 Fluidised bed coal gasification with oxygen-enriched air

Table 4.1 shows that gasification of high-ash bituminous coals with air and steam in a fluidised bed gasifier results in a low calorific value (LCV) gas (Engelbrecht *et al.*, 2010; Jing *et al.*, 2005). The reasons given for the low calorific value of the gas is that in order to heat the inert ash to the temperature of the bed more air is required, which results in dilution of the gas due to the introduction of nitrogen with the additional air. Low flame temperatures are produced during the combustion of an LCV gas, which reduce its utilisation efficiency.

In an attempt to increase the calorific value of the gas during fluidised bed gasification of low-grade coals, Belyaev *et al.* (2003) proposed the use of oxygen-enriched air and steam as gasification agents. Tests were carried out in a 40 mm diameter bench-scale fluidised bed reactor and calorific values of 6.1 MJ/Nm^3 were obtained with an oxygen concentration of 33 vol.% in the enriched air.

The promising results obtained by Belyaev *et al.* (2003) contributed to the decision to use oxygen-enriched air and steam for the fluidised bed gasification of high-ash South African coals using the pilot-scale fluidised bed gasifier at the CSIR. This gasifier has a larger bed area (32 times larger) than the 40 mm diameter bench-scale gasifier used by Balyaev *et al*. (2003).

4.3 Description of the pilot-scale fluidised bed coal gasifier

A pilot-scale fluidised bed coal gasifier (FBG) at the CSIR was used to conduct fluidised bed gasification tests on two selected high-ash South African coals using oxygen-enriched air and steam as the gasification agents. The pilot plant, previously used to carry out tests with air and steam as the gasification agents, was retrofitted so that oxygen-enriched air and steam could be used as the gasification agents. A description of the fluidised bed gasifier used for the air and steam gasification tests is given by Engelbrecht (2008). The description that follows includes the changes that were made during the latest upgrade of the fluidised bed gasifier to allow tests to be conducted using oxygen-enriched air and steam as the gasification agents.

4.3.1 Plant and process description

A flow diagram of the fluidised bed gasifier pilot plant is given in Figure 4.1 and a photograph of it is shown in Figure 4.2. The specifications of the fluidised bed gasifier pilot plant are given in Table 4.3.

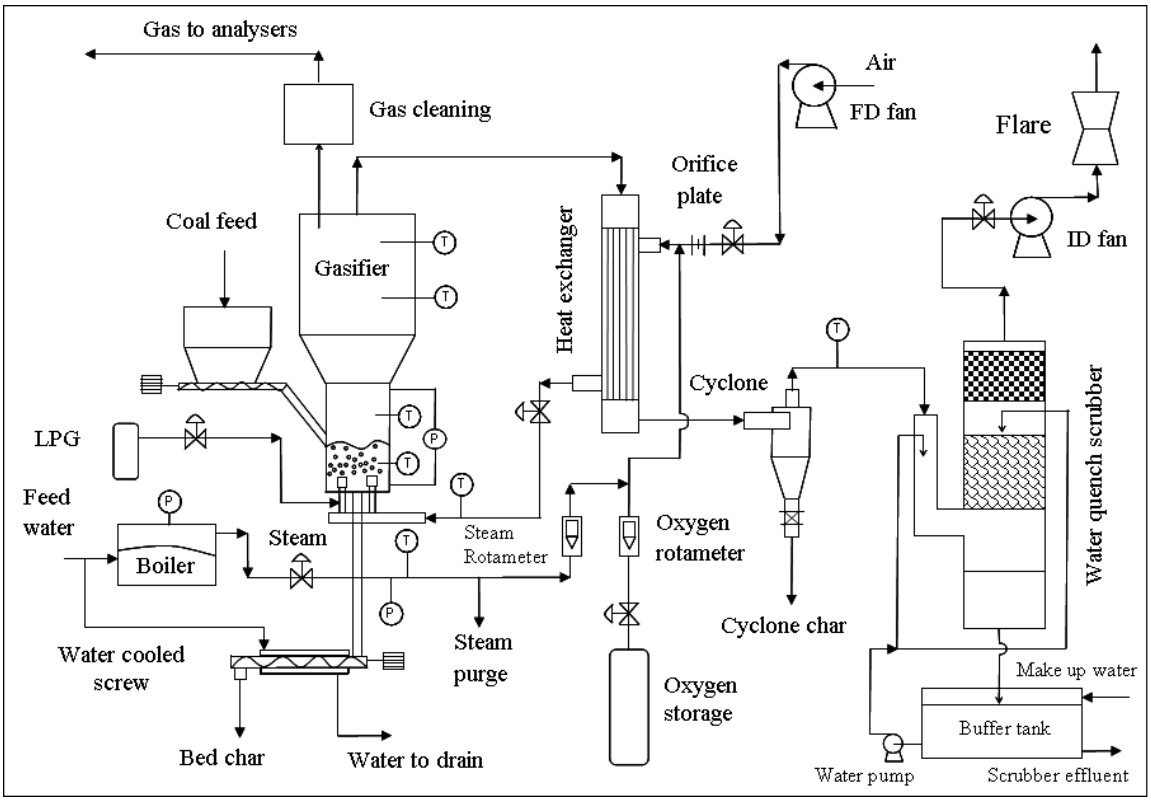

Figure 4.1: Flow diagram of the fluidised bed gasifier pilot plant

Coal, air, oxygen and steam are the input streams to the process which produces the output streams of gas and char (ash). Coal is fed to the gasifier by means of a screw conveyor (Appendix D.1.1) at a height of 1.3 m above the distributor. To prevent coal from accumulating and blocking (due to caking) the exit of the feed chute, air is pulsed to this area at 2 min intervals. Steam is generated in an electrode boiler (Appendix D.1.2) and is mixed with air and oxygen before being introduced into the gasifier via the distributor. The gas produced during the gasification process is used to preheat the air, oxygen and steam by means of a shell-and-tube heat exchanger. Char is removed from the bed (bed char) by means of a water-cooled screw conveyor (Appendix D.1.3) and from the gas (cyclone char) by means of a cyclone (Appendix D.1.4) which is placed after the shell-and-tube heat exchanger. A water quench scrubber (Appendix D.1.5) is used to remove fine dust particles that were not captured by the cyclone and to condense excess steam from the gas. The cold, clean and dry gas is combusted (flared) before it is vented to the atmosphere (Appendix D.1.6).

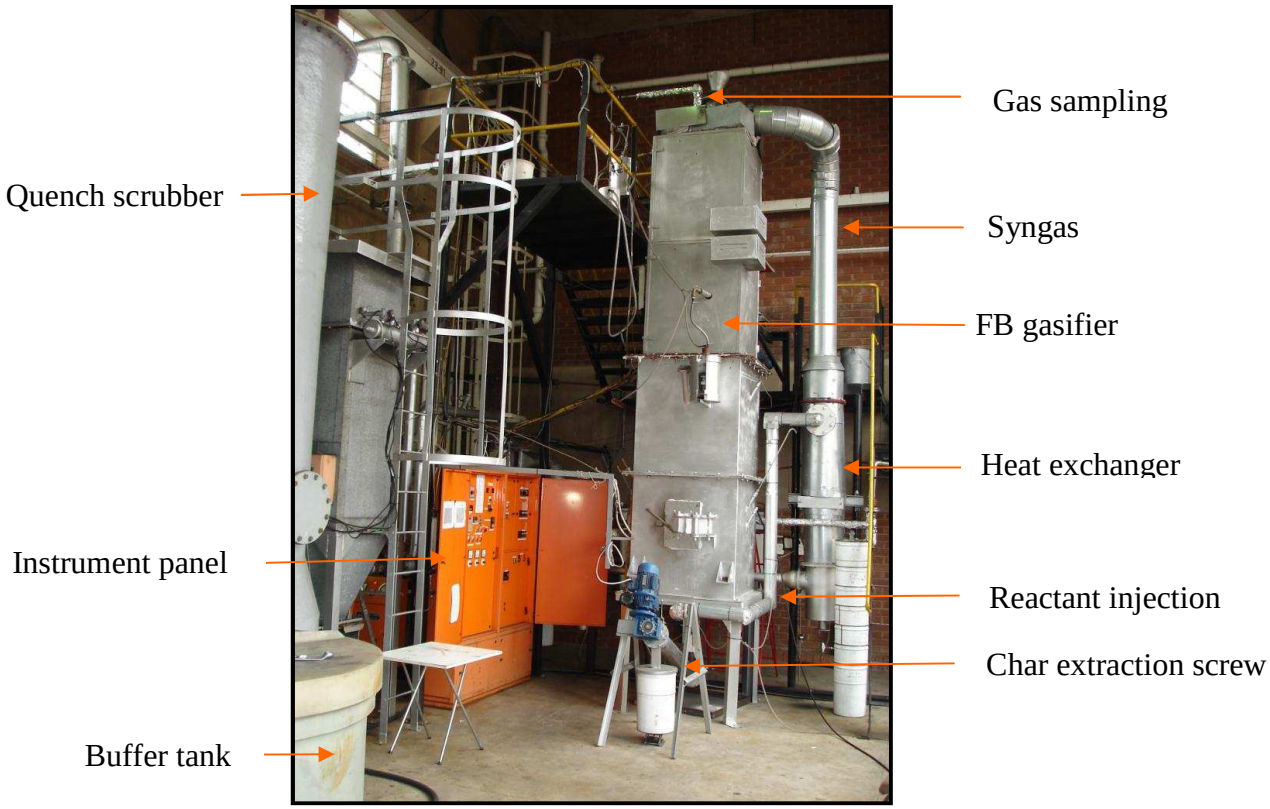

Figure 4.2: Fluidised bed gasifier pilot plant at the CSIR

Table 4.3: Specifications of the FBG pilot plant

Operating pressure	Atmospheric (90 kPa)
Bed dimensions (m)	0.2 × 0.2 (square)
Freeboard dimensions (m)	0.4 × 0.4 (square)
Furnace height (m)	4 (2 m bed & 2 m freeboard)
Fluidised bed height (m)	< 1.3
Coal feedrate (kg/h)	15–35
Thermal rating (kW)	140
Coal particle size (mm) (d_{50})	1.0–2.5
Coal CV (MJ/kg)	10–25
Air flowrate (Nm^3/h)	15–30
Oxygen flowrate (kg/h)	4–10
Steam flowrate (kg/h)	10–25
Bed temperature (°C)	850–1 000
Air, oxygen and steam temperature (°C)	200–300
Fluidising velocity (m/s)	1.2–2.5

4.3.1.1 Fluidisation

In a fluidised bed coal gasifier, the char particles are suspended (fluidised) by the gas stream flowing upwards in the furnace. In order for the bed to be 'well fluidised', it is recommended that the gas velocity in the bed be greater than three times the minimum fluidising velocity (U_{mf}) of the char particles. The minimum fluidising velocity can be obtained by solving equation (4.1) for U_{mf} (Geldart, 1986).

$$1.75\rho_g U_{mf}{}^2 + \frac{150(1-\varepsilon)\mu}{d_p} U_{mf} = (\rho_{char} - \rho_g) g d_p \varepsilon^3 \qquad (4.1)$$

Calculated values of U_{mf} as a function of char particle size (d_p) and density (ρ_{char}) are given in Appendix D.1.7.

4.3.1.2 Fluidised bed gasifier distributor

An important component of a fluidised bed gasifier is the gas distributor. It distributes the fluidising gas (air, oxygen and steam) uniformly across the bed area to provide 'smooth' fluidisation of the bed. In order to ensure that the gas is distributed uniformly across the bed, it is essential to design the distributor so that the gas passing through it has a sufficiently high pressure drop. It is recommended that, at design conditions, the ratio of distributor pressure drop to bed pressure drop should be greater than 0.30 ($\Delta P_D/\Delta P_B > 0.30$). Diagrams of the fluidised bed gasifier gas distributor and details of the nozzle are given in Figures 4.3 and 4.4. A photograph showing the distributor removed from the bed is given in Appendix D.1.8.

Equation (4.2) can be used to calculate the distributor pressure drop (British Standard 1042).

$$\Delta P_D = (\frac{\rho_g}{2}).(\frac{v}{C_d})^2 \qquad (4.2)$$

The pressure drop of the distributor shown in Figure 4.3 was measured for different air flowrates and is given in Appendix D.1.9. Equation (4.2) was fitted to the data and a value for the discharge coefficient (C_d) of 0.67 was obtained for the fluidised bed gasifier distributor nozzle shown in Figure 4.4.

Another essential design feature of a distributor is that it should prevent bed solids from falling through the distributor into the gas distribution pipes when the bed is de-fluidised (slumped). Since the angle of repose of the bed char is greater than 30°, it is recommended that the value of θ shown in Figure 4.4 should be less than 30° to prevent back-flow of solids into the gas distribution pipes (plenum). The angle of repose is the angle formed by a heap of char on a flat surface.

4.3.1.3 Furnace details

The internal dimensions of the fluidised bed gasifier and the location of the thermocouples and pressure probes are given in Figure 4.5. This figure shows that the fluidised bed gasifier has a 0.2 m x 0.2 m bed section, which expands to a 0.4 m x 0.4 m freeboard section.

Coal particles enter the furnace via the coal feed chute drop into the fluidised bed section and are rapidly (15 – 30 s) devolatilised to produce char. The char particles move rapidly up and down between the gasification and combustion zones in the bed. The combustion zone is limited to the lower 15 – 20% of the bed above the air and steam distributor and is rich in oxygen. Due to the high rate of the exothermic combustion reaction, the temperature in the bottom of the combustion zone can be up to ±150 °C higher than in the middle of the bed where the endothermic gasification reactions are dominant.

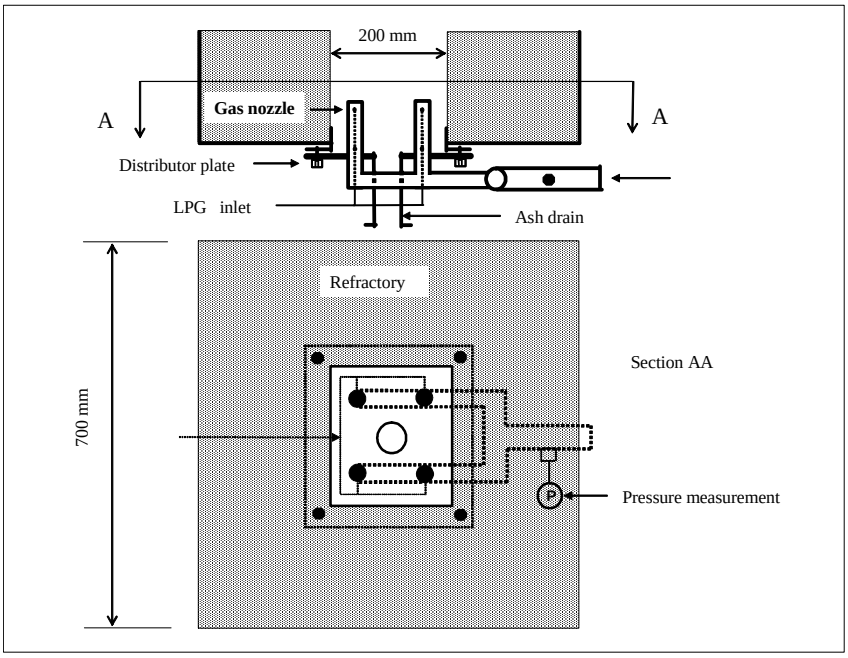

Figure 4.3: Fluidised bed gasifier distributor layout

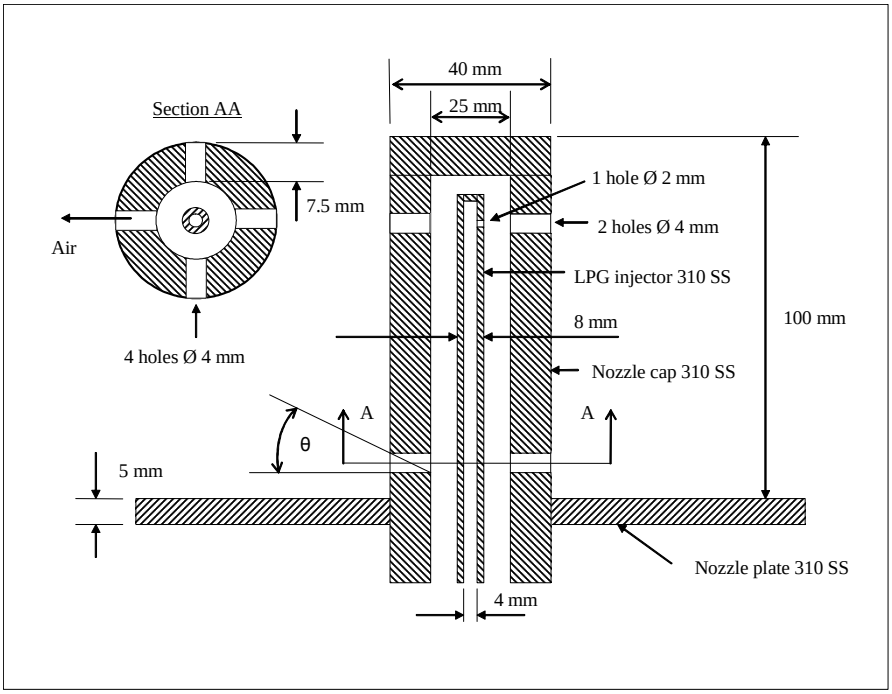

Figure 4.4: Details of distributor nozzle

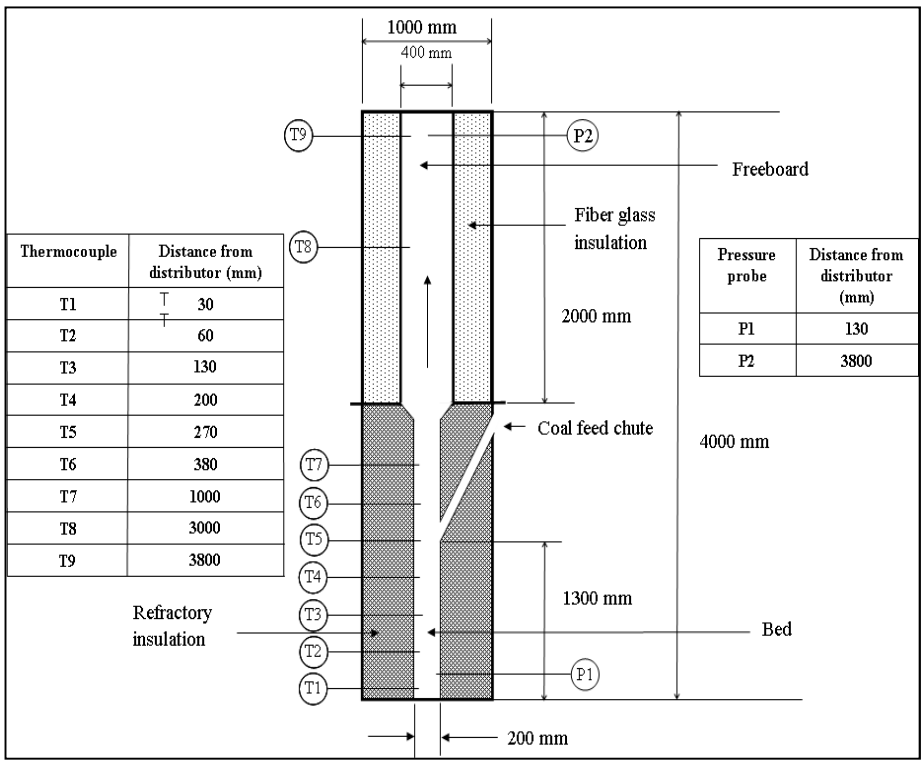

Thermocouple	Distance from distributor (mm)
T1	30
T2	60
T3	130
T4	200
T5	270
T6	380
T7	1000
T8	3000
T9	3800

Pressure probe	Distance from distributor (mm)
P1	130
P2	3800

Figure 4.5: Dimensions of the fluidised bed gasifier furnace

Due to the fluidising action of the bed, the char particles experience attrition and break down into smaller particles. When the particles are small enough, they are entrained into the freeboard section (upper part) of the furnace. Due to the expanded nature of the freeboard, the gas velocity decreases and the particles fall back to the bed, resulting in internal circulation of particles between the bed and the freeboard. Further breakdown of the char particles results in their entrainment to the top of the freeboard (gas outlet) and they are elutriated from the furnace. However, a significant proportion of the char particles (40 – 60%) are not elutriated from the furnace and these are drained from the bottom of the bed in order to maintain a constant fluidised bed height.

4.3.2 Fluidised bed start-up and control

The fluidised bed gasifier is started up by adding 15 kg of silica sand (0.4 – 0.85 mm) to the furnace. The silica sand is fluidised by starting the forced-draught (FD) and induced-draught (ID) fans. LPG is injected into the fluidised silica sand bed via the nozzles shown in Figure 4.4. The LPG is ignited by means of a pilot flame which is

inserted through the furnace door and directed down towards the bed. When the bed temperature reaches 650 °C, coal addition to the furnace is started. When the temperature reaches 850 °C, LPG injection is stopped, the pilot flame (lance) is removed and the furnace door is closed. The temperature is further increased by coal addition and the furnace is operated in combustion mode (excess air) at 925 °C for 6 h. Operation in combustion mode is required for thermal soaking of the refractories and heating of the freeboard. After 6 h oxygen and steam are introduced into the furnace and the flowrates of coal, air, oxygen and steam are adjusted in order to obtain the required bed temperature, fluidising velocity, level of oxygen enrichment and residence time of char particles in the furnace. The furnace is operated for a further 6 h to allow the bed carbon content and freeboard temperature to stabilise.

During heat-up and the test period, the air and steam flowrates are set at a fixed value which is high enough to maintain good fluidisation and low enough to minimise elutriation of fine char from the furnace ($3 \times U_{mf} < U < 10 \times U_{mf}$). The bed temperature is controlled by increasing or decreasing the oxygen flow. If the oxygen flow increases above a maximum value (determined by the oxygen concentration of the blast which has to be less than 25 vol.% in order to prevent the formation of hotspots), the airflow is decreased and the steam flow is increased. The bed height is controlled by removing char from the bed via the bed extraction screw. The gauge pressure in the furnace is controlled at -20 mmH_2O (-200 Pa) by adjusting the valve before the ID fan. Once stable conditions have been achieved, operating data are recorded and samples are collected for a period of 3 to 4 h.

4.3.3 Measurements and analyses

4.3.3.1 Coal feedrate

The coal screw feeder was calibrated by measuring the rotational speed of the screw shaft and measuring the mass of coal fed in a given time period. During the tests, the coal feedrate is determined by measuring the rotational speed of the screw shaft and using Figure D.1.10 in Appendix D.1.10, which gives the coal feedrate as a function of rotational speed. The accuracy of the coal feedrate measurement is estimated to be

± 1.0 kg/h based on the accuracy of the scale used for the measurement of the coal mass during calibration of the coal screw feeder.

4.3.3.2 Air flowrate

The airflow was measured using a sharp-edged orifice plate (Appendix D.1.11) with pressure tappings at one pipe diameter (D_p) upstream of the orifice plate and half a pipe diameter ($D_p/2$) downstream of the orifice plate. A formula was derived to calculate the airflow using British Standard 1042: 1964, which gives the airflow as a function of the pressure drop over the orifice plate, the temperature and the absolute pressure of the air. The formula and plot of airflow as a function of pressure drop are given in Appendix D.1.12. The accuracy (tolerance) of the airflow measurement is given by British Standard 1042: 1964 and is ± 1.5 Nm^3/h.

4.3.3.3 Steam flowrate

The steam flow was measured using a rotameter with a stainless steel float and tube (Appendix D.1.13). The rotameter was calibrated by monitoring its output reading and measuring the mass of steam that flowed through it in a given time period. The mass of steam was determined by diverting the steam to a drum filled with crushed ice and then measuring the increase in the mass of the drum and its contents. The calibration curve for the steam flow rotameter is given in Appendix D.1.14. The accuracy of the steam flow measurement is estimated to be ± 0.2 kg/h, based on the accuracy of the scale used for the measurement of the condensed steam mass during calibration of the steam orifice plate.

4.3.3.4 Oxygen flowrate

The oxygen flowrate was measured using a rotameter (Appendix D.1.15). A calibration curve for the oxygen rotameter was obtained from the supplier, C&F Technologies (Pty) Ltd (Appendix D.1.16). The accuracy of the oxygen flowrate was therefore assumed to be equal to the value given by the supplier of the rotameter, which is ± 2%.

4.3.3.5 Gas analysis

The gas produced by the fluidised bed is sampled and cleaned using the apparatus shown in Figure 4.6. Gas is sampled from the upper part of the freeboard of the fluidised bed gasifier at a rate of 2.5 Nl/min. In the sampling tube the gas velocity decreases from 0.45 to 0.07 m/s, which reduces the dust concentration of the sample gas since particles greater than 65 μm disengage from the sample gas in the sampling tube. Most of the water and tar in the gas are removed in the water bubbler and gas cooler. Final drying of the sample gas takes place in the water trap and silica gel dryer. Fine char particles are removed using a 2 μm filter before the gas flows to the gas analysers.

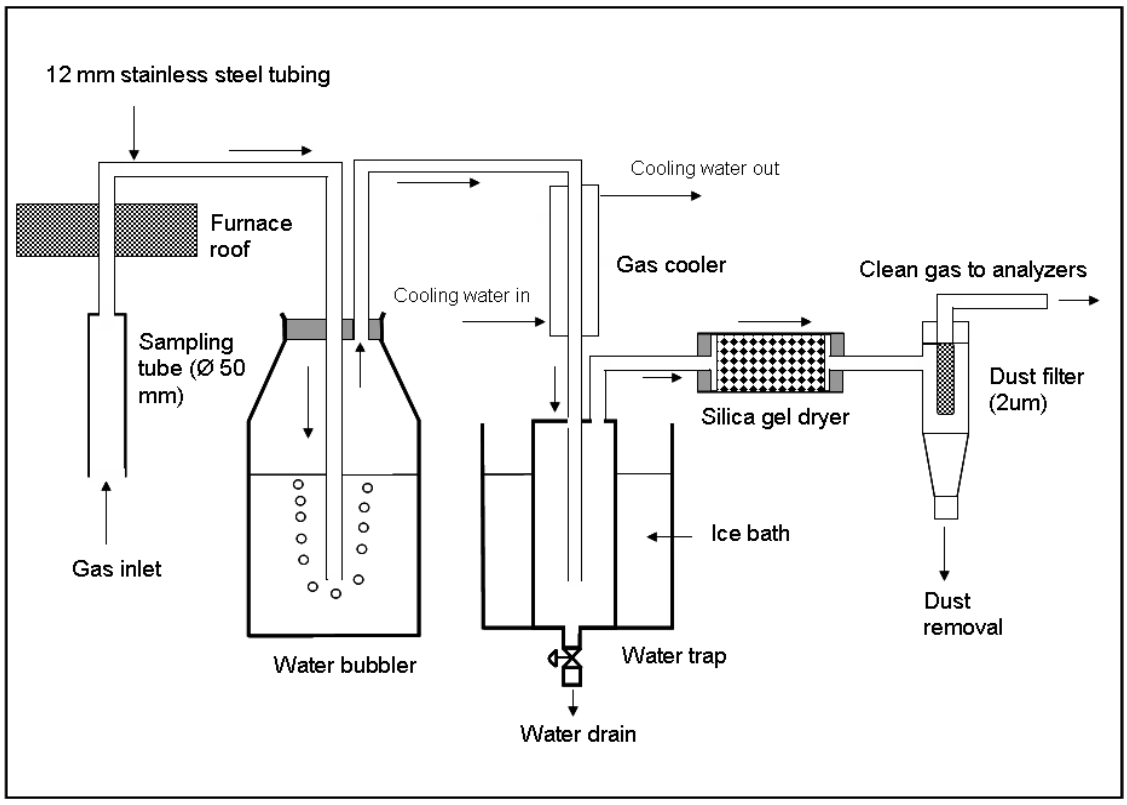

Figure 4.6: Apparatus for gas sampling and cleaning

The cleaned gas is analysed using continuous online gas analysers, the specifications of which are given in Table 4.4. The analysers are shown in Appendix D.1.17 to Appendix D.1.19.

Table 4.4: Specifications of gas analysers

Gas	Supplier	Model	Measurement method	Accuracy
CO	Servomex	4210	Infrared	± 0.25%
H_2	Servomex	K1550	Thermal conductivity	± 0.50%
CH_4	Servomex	4210	Infrared	± 0.10%
CO_2	Servomex	4210	Infrared	± 0.25%
O_2	Hartman and Braun	Magnos 3K	Paramagnetic	± 0.25%

4.3.3.6 Temperature and pressure

The process temperatures and pressures are measured by means of type K thermocouples, low-pressure gauges and manometers. The locations of the temperature and pressure gauges are shown in Figure 4.5. Due to the bubbling action of the bed, the bed pressure drop reading fluctuates by ± 150 Pa.

4.3.3.7 Char flows and char analysis

The mass flowrate of char from the bed and cyclone is determined by collecting and weighing the char produced by the bed and cyclone during the test period. The carbon in the bed and cyclone char is determined by placing 50 g samples in a muffle oven at 950 °C for a period of 6 h. The resulting mass loss allows the carbon in the char to be calculated. Tyler screens are used to determine the size analysis of both the bed and cyclone char. To reduce sampling errors, four samples of the bed char and the cyclone char are taken for each test. The standard deviation of the carbon-in-ash measurements is 1.0%. The char flowrate error is estimated to be 0.2 kg/h (based on the accuracy of the scale used to weigh the bed and the cyclone char produced).

4.4 Fluidised bed gasifier test programme and procedure

Pilot-scale fluidised bed coal gasification tests were carried out on each coal using as gasification agents:

- Oxygen-enriched air and steam.
- Oxygen and steam.

The objectives of the programme were to:

- Assess the performance of New Vaal and Grootegeluk coal in a fluidised bed gasifier in terms of:
  - fixed carbon conversion,
  - analysis of the gas produced,
  - attrition of coal in the bed,
  - analysis of the char produced,
  - and agglomeration of the bed.
- Generate data that could be used to evaluate the predictive capability of a fluidised bed gasifier model

The information given in Tables 4.1 and 4.2 in the literature survey on pilot-scale fluidised bed coal gasification studies (Section 4.2) was used as a guide to select a range of operating conditions for New Vaal and Grootegeluk coals (bituminous coals).

4.4.1 Oxygen-enriched air and steam

The operating conditions using oxygen-enriched air and steam are given in Table 4.5. The residence time and temperature (independent variables) could be varied independently within the limits given in Table 4.5. The residence time is varied by adjusting the coal flow or fluidised bed height and the temperature is varied by adjusting the oxygen flow. The air and steam flowrates are adjusted in order to maintain the fluidising velocity, the oxygen concentration of the blast and the oxygen-enrichment level of the air (dependent variables) within the limits given in Table 4.1. The fluidising velocity is maintained above 1.25 m/s to obtain good mixing in the bed and below 1.84 m/s to reduce attrition and elutriation of fine char from the gasifier. The oxygen concentration of the oxygen, air and steam mixture is maintained above 17.1 vol.% to increase gasification efficiency and below 25 vol.% to reduce the possibility of hotspot and clinker formation in the lower section of the fluidised bed. The oxygen concentration of the enriched air is maintained above 30 vol.% to

increase the calorific value of the gas and below 40 vol.% to reduce the oxygen consumption.

Table 4.5: FGB operating conditions at 90 kPa absolute pressure

Coal	New Vaal	Grootegeluk
Mid-bed temperature (°C)	880–976	876–983
Residence time (min)	16.2–27.7	31.5–48.9
Fluidising velocity (m/s)	1.68–1.77	1.25–1.84
Oxygen in enriched air (vol.%)	37.2–38.7	30.7–38.6
Oxygen in total inlet flow (vol.%)	22.2–24.8	17.1–22.7
Oxygen, steam and air temperature (°C)	275–299	248–294
Coal particle size (mm)	1.4–1.8	1.4–1.7
Fluidised bed height (m)	0.8–1.3	0.86–2.0

For each coal three temperatures and residence times were selected within the limits given in Table 4.5. The selected temperatures and residence times for each coal are given in Tables 4.6 and 4.7.

Table 4.6: Temperatures and residence times selected for New Vaal coal

Residence time (min)	Mid-bed temperature (°C)		
	880	[(944) (943) (940)][2]	976
16.2		Test 2	
[(23.3) (23.4) (23.7)][1]	Test 1	Test 3	Test 5
27.7		Test 4	

[1] Residence times for Tests 1, 3 and 5
[2] Temperatures for Tests 2, 3 and 4

Table 4.7: Temperatures and residence times selected for Grootegeluk coal

Residence time (min)	Mid-bed temperature (°C)		
	876	943	[(976) (983) (979)][2]
[(33.0) (33.4) (31.5)][1]	Test 1	Test 2	Test 3
38.2			Test 4
48.9			Test 5

[1] Residence times for Tests 1, 2 and 3
[2] Temperatures for Tests 3, 4 and 5

For Grootegeluk coal more tests were done at a temperature of ± 980 °C and a residence time of ± 33 min since these conditions were considered to be representative of the conditions that would be used for the industrial gasification of this coal. The experimental designs given in Table 4.6 and 4.7 would therefore not be suitable for the development of a regression or empirical equation using response surface methodology (RSM). However, since the data will be used to validate a fluidised coal gasification model, in this case an RSM experimental design would not necessarily be a requirement (De Souza-Santos, 2010).

The variation in *mean coal particle size* (1.4 – 1.8 mm) shown in Table 4.5 resulted from the crushing procedure (cone crusher) used for preparing the samples received from the mines (< 20 mm). Since the gasification reactions are controlled by the chemical reaction rates and not diffusion controlled for particles less than 2.8 mm, the variation in mean coal particle size is not expected to have a significant effect on the results (Hanson *et al*., 2001; Ye *et al.,* 1997).

A representative four-ton batch of Grootegeluk coal was received from the mine near Lephalale (Ellisras). After the coal had been crushed and screened, it was used to carry out the five tests listed in Table 4.7. However, for New Vaal coal, two batches of two tons were received from the New Vaal colliery near Vereeniging. Tests 1 – 4 were conducted on Batch 1 and Test 5 was conducted on Batch 2. The variation in the analysis of the two batches (Appendix D.2.15) was not considered to be significant in terms of obtaining parameters for a fluidised bed coal gasification model.

4.4.2 Oxygen and steam

Two tests using oxygen and steam as the gasification agents were carried out on the New Vaal and Grootegeluk coals. The conditions used for the tests are given in Table 4.8.

Table 4.8: FGB operating conditions at 90 kPa absolute pressure

Coal	New Vaal	Grootegeluk
Mid-bed temperature (°C)	931	918
Residence time (min)	25.5	35.4
Fluidising velocity (m/s)	1.77	1.92
Oxygen in total inlet flow (vol.%)	19.8	19.0
Oxygen and steam temperature (°C)	183	205
Coal particle size (mm)	1.2	2.1
Fluidised bed height (m)	0.79	1.32

The analysis of the coals used for the tests detailed in Table 4.8 are given in Appendix D.2.15.

4.5 Fluidised bed gasification test results and discussion

4.5.1 Tests using oxygen-enriched air and steam as the gasification agents

The results of the fluidised bed gasification tests on New Vaal and Grootegeluk coal using oxygen-enriched air as the gasification agents are presented in Tables 4.9 and 4.10 respectively. The values shown in these tables are average values obtained during 3 h of stable operation. Figures 4.7 and 4.8 show examples of the temperature and gas concentration profiles during the test period for New Vaal coal at 943 °C and 18.2 min residence time (Test 3). The temperature and gas concentration profiles for Grootegeluk coal at 976 °C and 31.5 min residence time (Test 3) are given in Appendix D.2.1.

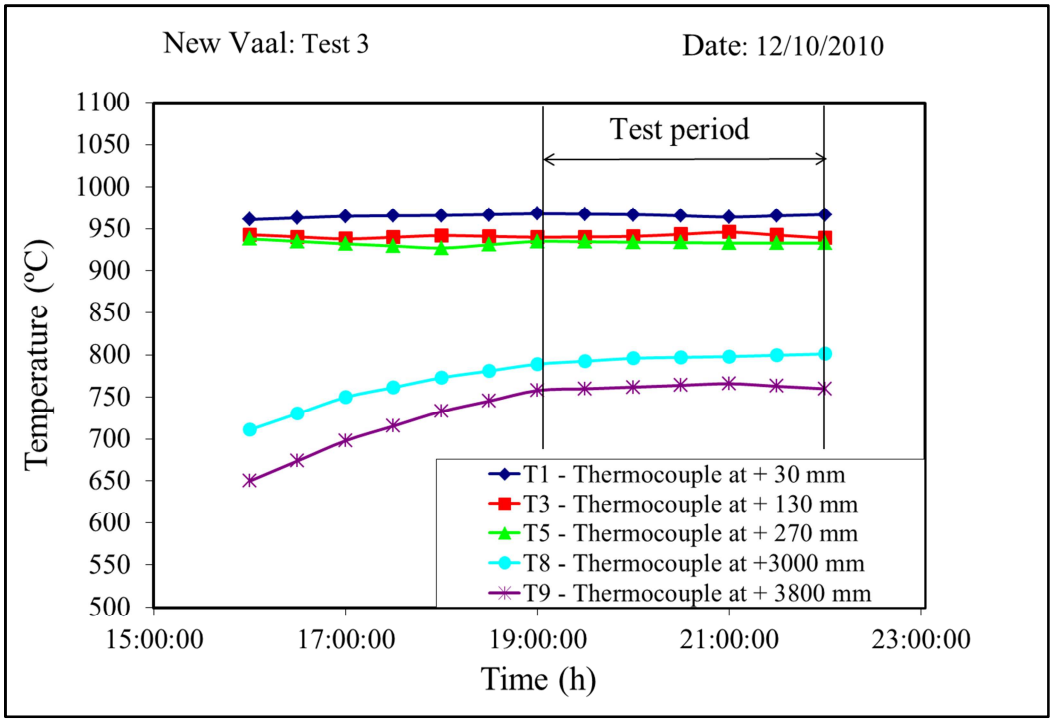

Figure 4.7: FBG temperature profiles for New Vaal coal (Test 3)

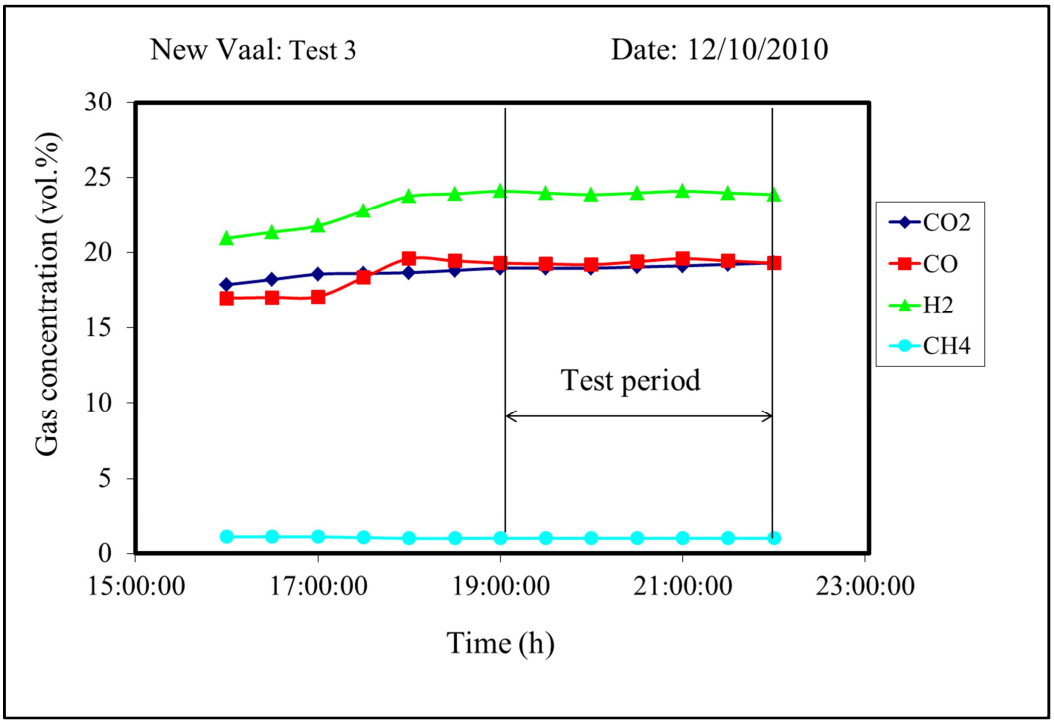

Figure 4.8: FBG gas concentration profiles for New Vaal coal (Test 3)

Table 4.9: Fluidised bed coal gasification tests on New Vaal coal at 90 kPa

Test number	**1**	**2**	**3**	**4**	**5**
Mid-bed temperature - T4 (ºC)	880	944	943	940	976
Char residence time (min)	23.3	16.2	23.4	27.7	23.7
Coal feedrate (kg/h)	32.2	32.2	32.2	26.9	32.2
Airflow (Nm^3/h)	24.19	23.79	24.35	21.90	24.0
Steam flow (kg/h)	16.50	15.60	16.0	16.50	13.90
Oxygen flow (kg/h)	8.9	9.0	9.2	8.7	9.9
Oxygen in enriched air (vol.%)[1]	37.2	37.5	37.5	38.2	38.7
Oxygen in total inlet flow (vol.%)[2]	22.2	22.8	22.8	22.0	24.8
Total inlet flow temperature (ºC)	281	275	299	281	285
Stoichiometric molar ratio[3]	0.36	0.36	0.37	0.41	0.43
Steam: carbon molar ratio	0.78	0.73	0.75	0.93	0.73
Coal particle size (mm)[4]	1.80	1.6	1.40	1.7	1.70
Minimum fluidising velocity (m/s)	0.20	0.17	0.12	0.13	0.18
Fluidising velocity (m/s)	1.68	1.73	1.77	1.69	1.73
Lower bed temperature - T1 (ºC)	908	965	958	958	997
Gasifier exit temperature - T9 (ºC)	735	730	762	743	757
Dry gas composition					
CO (vol.%)	16.6	19.9	19.4	18.9	19.1
H_2 (vol.%)	24.0	24.3	23.9	24.2	22.5
CH_4 (vol.%))	1.3	1.1	1.0	1.0	1.0
CO_2 (vol.%)	20.7	18.8	19.1	20.3	20.2
N_2 + others[5] (vol.%)[6]	37.3	35.8	36.5	35.5	37.1
O_2 (vol.%)	0.1	0.1	0.1	0.1	0.1
Dry gas calorific value (MJ/Nm^3)	5.74	6.12	5.96	5.93	5.77
Dry gas flowrate (Nm^3/h)	51.8	53.1	53.3	49.3	51.7
Bed pressure drop (Pa)[7]	1 905	1 185	1 868	1 839	1 896
Dynamic bed height (m)[8]	1.31	0.80	1.21	1.11	1.15
Char extracted from bed (kg/h)	6.10	5.64	4.81	4.40	6.63
Carbon in bed char (wt.%)	13.70	7.20	4.40	3.21	2.50
Bed char particle size (mm)	0.90	0.81	0.65	0.69	0.81
Char elutriated to cyclone (kg/h)	9.04	8.91	9.67	7.27	7.80
Carbon in cyclone char (wt.%)	24.70	23.24	22.66	19.78	14.90
Cyclone char particle size (µm)	60	62	62	62	70
Char elutriated (%)	59.72	61.24	66.78	62.28	54.10
Fixed carbon conversion (%)	73.41	78.54	79.19	83.63	87.54
Total carbon conversion (%)	78.37	82.54	83.07	86.69	89.49
Cold gas efficiency (%)	53.81	58.75	57.48	63.31	58.75

[1] Oxygen concentration of the combined air and oxygen flow stream
[2] Oxygen concentration of the combined air, oxygen and steam flow stream
[3] Molar ratio of oxygen in the gasification agents with respect to that required for stoichiometric combustion
[4] d_{50} – 50% of the coal mass is less than the d_{50} size (PSDs are given in Appendix D.2.11)
[5] Others are < 0.5 vol.% and include H_2S, COS, SO_2, NH_3, HCN and C_2^+
[6] (N_2 + others) by difference
[7] Pressure difference between P1 and P2 (P1 is 130 mm above the distributor)
[8] Expanded bed height at the operating fluidising velocity

Table 4.10: Fluidised bed coal gasification tests on Grootegeluk coal at 90 kPa

Test number	**1**	**2**	**3**	**4**	**5**
Mid-bed temperature - T4 (ºC)	876	943	976	983	979
Char residence time (min)	33.0	33.4	31.5	38.2	48.9
Coal feedrate (kg/h)	23.0	23.0	23.0	19.6	16.0
Airflow (Nm^3/h)	24.50	22.72	22.10	20.90	15.90
Steam flow (kg/h)	17.8	20.0	18.3	15.0	11.5
Oxygen flow (kg/h)	4.9	7.2	8.5	7.6	6.5
Oxygen in enriched air (vol.%)[1]	30.7	35.3	37.8	37.0	38.6
Oxygen in total inlet flow (vol.%)[2]	17.1	18.6	20.8	21.6	22.7
Total inlet flow temperature (ºC)	256	288	294	274	248
Stoichiometric molar ratio[3]	0.32	0.36	0.39	0.42	0.42
Steam: carbon molar ratio	0.97	1.10	1.00	0.96	0.91
Coal particle size (mm)[4]	1.7	1.7	1.4	1.4	1.7
Minimum fluidising velocity (m/s)	0.26	0.18	0.13	0.11	0.08
Fluidising velocity (m/s)	1.65	1.83	1.82	1.61	1.25
Lower bed temperature -T1 (ºC)	908	958	999	1 003	998
Gasifier exit temperature -T9 (ºC)	747	810	808	768	752
Dry gas composition					
CO (vol.%)	10.5	13.6	16.1	17.0	16.6
H_2 (vol.%)	14.8	18.6	18.6	20.7	20.9
CH_4 (vol.%))	2.9	2.2	1.7	1.4	1.5
CO_2 (vol.%)	20.5	22.3	21.2	20.0	22.8
N_2 + others[5] (vol.%)[6]	51.2	43.2	42.3	40.8	38.1
O_2 (vol.%)	0.1	0.1	0.1	0.1	0.1
Dry gas calorific value (MJ/Nm^3)	4.48	5.07	5.19	5.44	5.45
Dry gas flowrate (Nm^3/h)	38.1	41.9	41.7	40.9	33.3
Bed pressure drop (Pa)[7]	1 964	1 964	1 816	1 816	1 816
Dynamic bed height (m)[8]	2.0	1.96	1.72	1.25	0.86
Char extracted from bed (kg/h)	8.85	5.90	5.05	3.10	3.27
Carbon in bed char (wt.%)	36.30	28.24	21.71	10.80	4.50
Bed char particle size (mm)	1.35	1.05	0.88	0.70	0.52
Char elutriated to cyclone (kg/h)	3.24	5.10	5.17	4.98	2.88
Carbon in cyclone char (wt.%)	49.00	40.10	35.51	30.70	32.40
Cyclone char particle size (µm)	70	72	70	67	67
Char elutriated (%)	26.81	46.38	50.61	61.61	46.86
Fixed carbon conversion (%)	45.21	57.63	66.52	75.06	82.26
Total carbon conversion (%)	60.56	69.50	75.90	82.05	87.23
Cold gas efficiency (%)	34.69	43.19	43.91	52.96	53.03

[1] Oxygen concentration of the combined air and oxygen flow stream

[2] Oxygen concentration of the combined air, oxygen and steam flow stream

[3] Molar ratio of oxygen in the gasification agents with respect to that required for stoichiometric combustion

[4] d_{50} – 50% of the coal mass is less than the d_{50} size (PSDs are given in Appendix D.2.11)

[5] Others are < 0.5 vol.% and include H_2S, COS, SO_2, NH_3, HCN and C_2^+

[6] (N_2 + others) by difference

[7] Pressure difference between P1 and P2 (P1 is 130 mm above the distributor)

[8] Expanded bed height at the operating fluidising velocity

The shaded values given in Tables 4.9 and 4.10 are calculated values and are based on the measured values (unshaded values); the coal analyses are given in Table 2.3 and Table D.2.1. The calculations and estimated errors associated with the calculations are given in Appendix D.2.2 to Appendix D.2.10.

4.5.1.1 Fixed carbon conversion

The effect of temperature on the fixed carbon conversion for New Vaal and Grootegeluk coals is given in Figure 4.9.

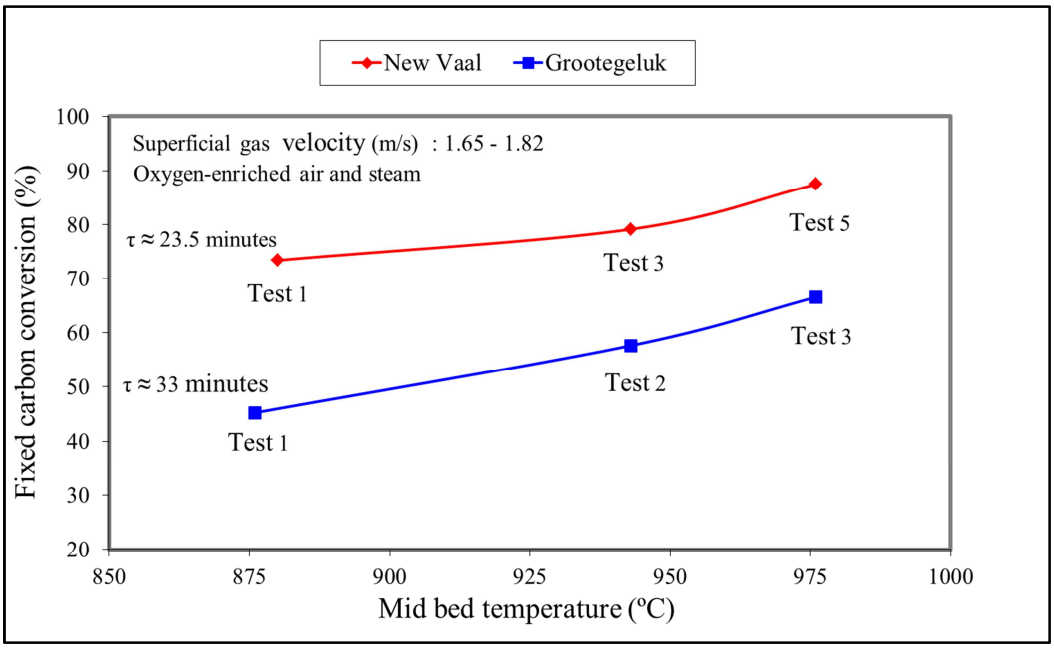

Figure 4.9: Fixed carbon conversion as a function of temperature

Figure 4.9 shows that the fixed carbon conversion achieved in the fluidised bed gasifier pilot plant increases with temperature and that due to the higher reactivity of New Vaal coal, the fixed carbon conversions were higher than those obtained for Grootegeluk coal, despite the residence time being lower (23.5 min versus 33 min). Tables 4.9 and 4.10 show that an increase in the fixed carbon conversion, produced by the higher temperature, results in an increase in the cold gas efficiency. Although the higher temperature would tend to reduce the cold gas efficiency due to sensible heat losses, more chemical energy is transferred to the gas as a result of the higher fixed carbon conversion giving a higher overall cold gas efficiency.

The effect of temperature on fixed carbon conversion is compared with results obtained by other investigators in Figure 4.10. The measurements made by these investigators were also taken at fixed residence times for each study. Figure 4.10 shows that the other investigators also found that the fixed carbon conversion increases with temperature and the reactivity of the coal.

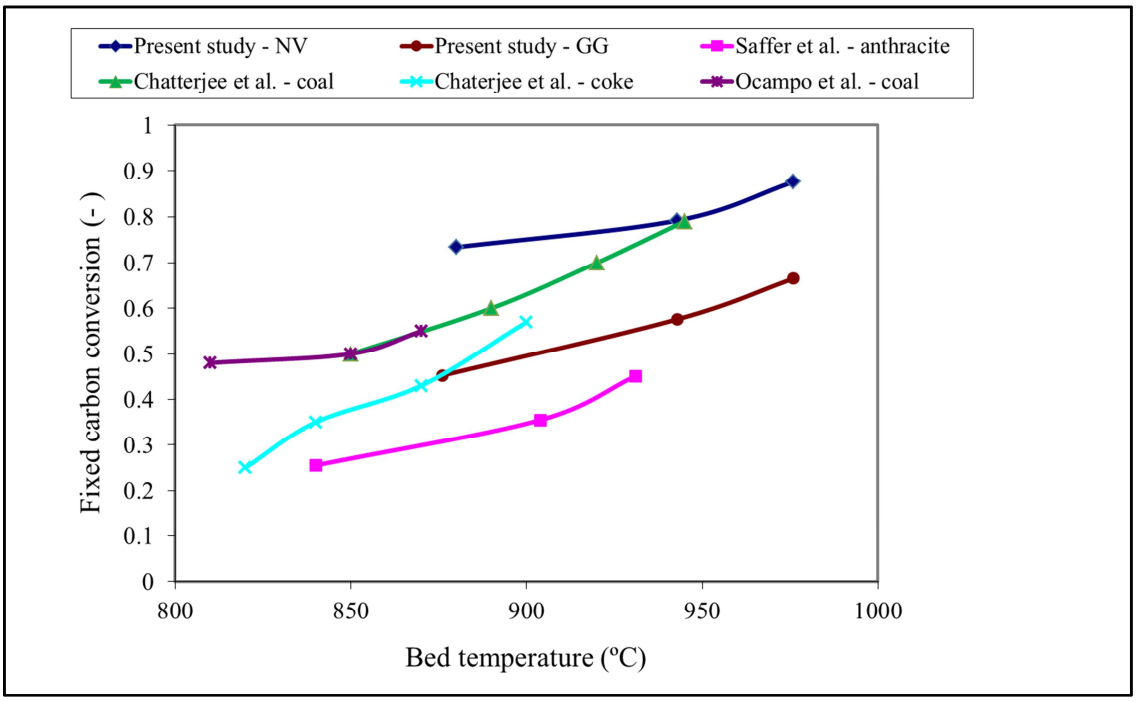

Figure 4.10: Effect of bed temperature on fixed carbon conversion found by other investigators

Table 4.11 presents the slope ($\Delta X/\Delta T$) of the fractional fixed carbon conversion as a function of the temperature graphs obtained by the investigators shown in Figure 4.10. It can be seen that $\Delta X/\Delta T$ varies between 1.1 E -03 and 3.8 E -03 for the various coals tested and that there is no clear relationship between $\Delta X/\Delta T$ and coal reactivity or the temperature range used for a particular investigation.

The effect of residence time on fixed carbon conversion is given in Figure 4.11, which shows that the fixed carbon conversion in the fluidised bed gasifier pilot plant increases when the residence time of char particles in the gasifier is increased.

Table 4.11: Slope of fractional fixed carbon versus temperature graph

Investigator	Fuel	Temperature range (°C)	$\frac{\Delta X}{\Delta T}$ (°C^{-1})
Present study – NV[1]	Bituminous coal	890–980	1.7 E-03
Present study – GG[2]	Bituminous coal	880–980	2.1 E-03
Saffer *et al.*	Anthracite	840–930	2.0 E-03
Chatterjee *et al.*	Bituminous coal	850–945	3.1 E-03
Chatterjee *et al.*	Coke breeze	820–900	3.8 E-03
Ocampo *et al.*	Bituminous coal	810–870	1.1 E-03

[1] New Vaal coal
[2] Grootegeluk coal

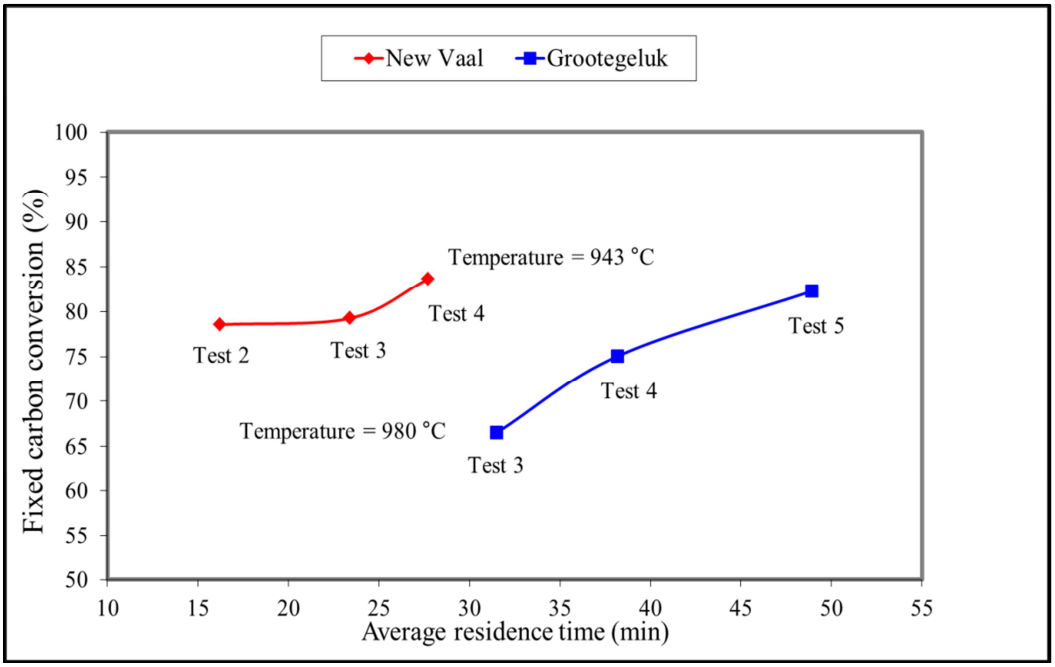

Figure 4:11: Fixed carbon conversion as a function of residence time

Figure 4:11 shows that the fixed carbon conversion of the lower reactivity Grootegeluk coal can be increased to over 80% if the residence time is increased to 48.9 min. The higher fixed carbon conversion is, however, achieved at the expense of plant thermal output since the residence time of char in the gasifier is increased by decreasing the coal feedrate.

Figure 4.11 also shows that, for New Vaal coal at 940 °C and 27.7 min residence time, a fixed carbon conversion of 83.7% was obtained (Test 4). The residence time was decreased to 23.4 min by increasing the coal flowrate and maintaining a constant bed height (Test 3), which had the effect of decreasing the fixed carbon conversion to 79.4%. For Test 2 on New Vaal coal, the residence time was decreased further to 16.2 min by decreasing the bed height and maintaining a constant coal feedrate. In this case the fixed carbon conversion decreased to 78.5%, which is a smaller decrease than expected. This could possibly be explained by the findings of Gururajan and Agarwal (1992) and Yan *et al.*(1998), namely that a large percentage of the fixed carbon is converted in the lower part of the gasifier by the partial oxidation reactions. The fluidised bed gasifier simulation model (Chapter 5) will be used to explore further the effect of bed height on the fixed carbon conversion.

The bed chars produced by the fluidised bed gasifier were subjected to combined petrographic, FTIR and XRD analysis (Oboirien, 2011). The results show that some of the clay minerals in the coal ash had decomposed, resulting in the formation of a range of silicate and alumina-silicate minerals in the char. The presence of fayalite, a low melting point silicate, was detected in Grootegeluk char. The molten matter had penetrated into some of the cracks and pores in the chars (Figure 4.12). These mineral boundaries could have prevented the reacting gases from coming into contact with the carbon, thereby reducing the reactivity of the Grootegeluk char as conversion progressed. In addition to the physical effect on char reactivity, the molten minerals can also react at the char-mineral interface, resulting in a more ordered carbon structure which is less reactive.

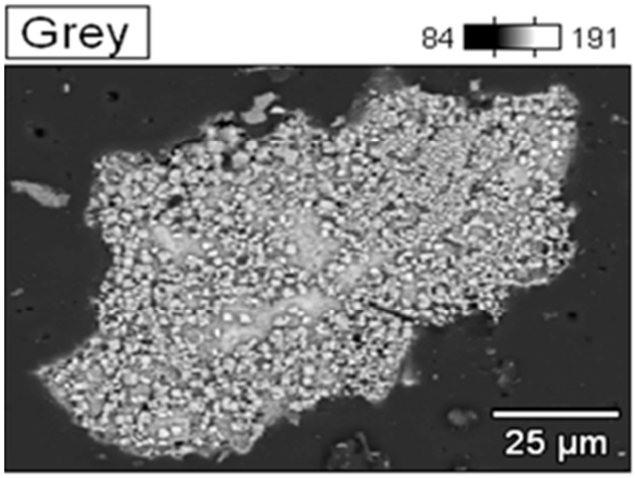

Figure 4.12: SEM image illustrating discrete agglomerate mineral distributions in a Grootegeluk char

4.5.1.2 Calorific value of the gas

Figure 4.13 shows that when oxygen-enriched air and steam are used as the gasification agents, a significant increase in the calorific value of the gas is obtained compared with when air and steam are used as the gasification agents (Engelbrecht, 2008). This can be attributed to the reduced dilution effect of nitrogen on the gas produced when oxygen-enriched air and steam are used as the gasification agents. Figure 4.14 shows that due to the higher calorific value of the gas, a stable high-temperature flame was obtained when the gas was flared (New Vaal - Test 3). The air and steam gasification tests produced an unstable low-temperature flame which required frequent re-ignition by the operator.

It was shown above (Figure 4.9) that an increase in bed temperature results in a significant increase in the fixed carbon conversion. Figure 4.13 shows that the higher fixed carbon conversion produced by the higher temperature translates into a much lower percentage increase in the calorific value of the gas. This can be ascribed to the fact that a large fraction of the energy content (calorific value) of the gas is produced from the volatile matter in the coal, which is not related to the fixed carbon conversion. Higher bed temperatures also increase the sensible heat in the gas and therefore less heat is available as chemical energy, which is required to increase the calorific value of the gas.

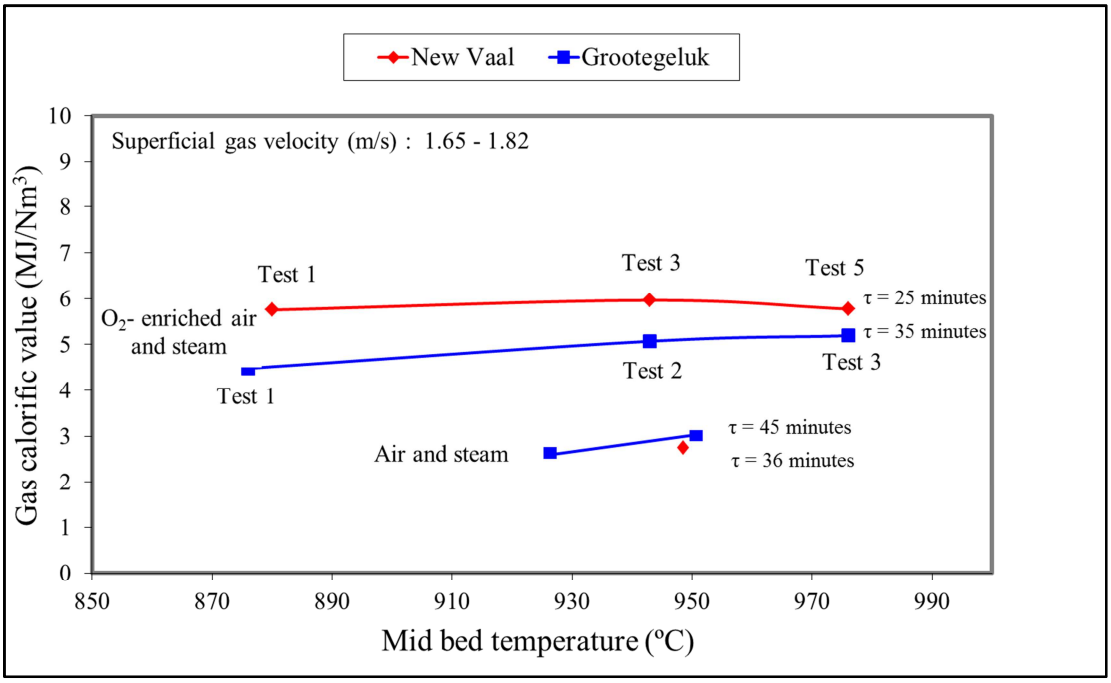

Figure 4.13: Calorific value of the gas as a function of bed temperature

Figure 4.14: Flaring of gas produced by the fluidised bed gasifier

A higher fixed carbon conversion therefore increases the thermal output of the gasifier through an increase in the gas flow, gas temperature and, to a lesser extent, through a higher gas calorific value.

The effect of bed temperature on the gas calorific value obtained by other investigators is presented in Figure 4.15. The tests done by Chatterjee *et al*. (1995) on coke breeze, which has a low volatile matter content (3.5 wt.%), show that an increase in temperature (fixed carbon conversion) produced a significantly higher percentage increase in the calorific value of the gas compared with the tests conducted on coal. This supports the conclusion that the volatile matter in bituminous coal produces a large percentage of the chemical energy of the gas.

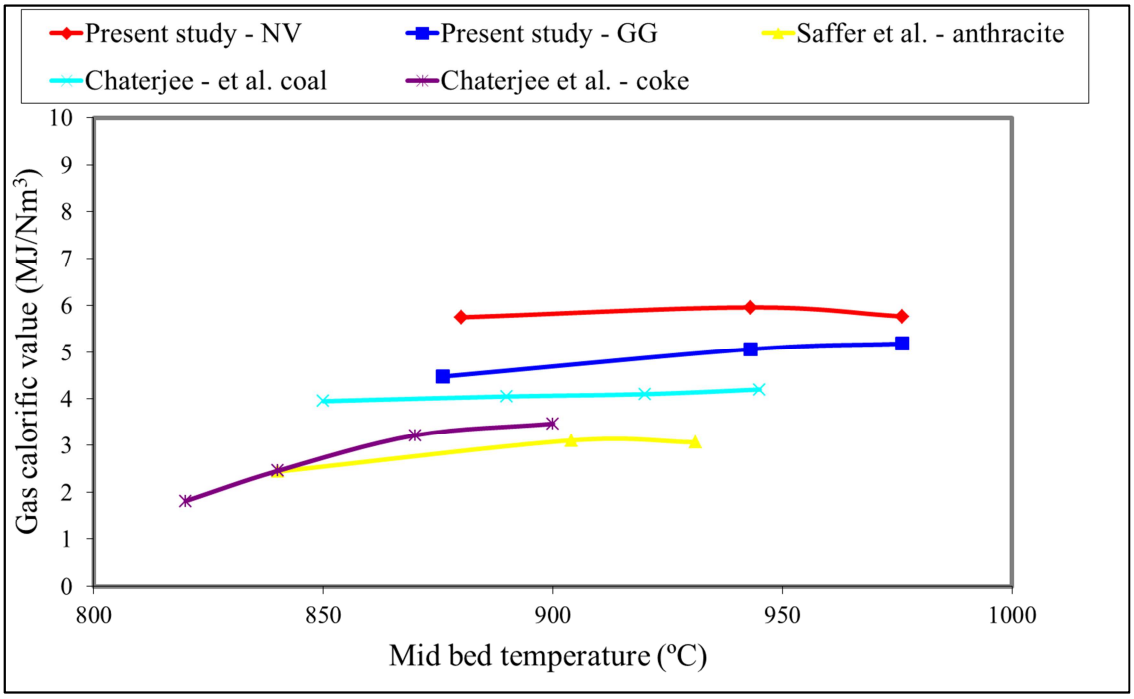

Figure 4.15: Gas calorific values as a function of bed temperature (results from the literature)

4.5.1.3 Bed temperature distribution

The temperature variation in the fluidised bed gasifier as a function of height above the distributor is given in Figure 4.16 for the tests on New Vaal coal. The temperature variations for the tests on Grootegeluk coal, which are similar to the variations found in New Vaal coal, are given in Appendix D.2.14. Figure 4.16 shows that the temperature in the lower part of the bed (< 200 mm) is higher than that in the middle and at the top of the bed. This is due to the high concentration of oxygen and the resulting high rate of the char combustion reaction in the lower part of the bed. The temperature increase at 1 000 mm above the distributor could be due to the air that is injected through the feeder (Appendix D.1.1). Figure 4.16 also shows that the temperature at the top of the fluidised bed gasifier (T9) is ± 175 °C lower than that in the mid-bed (T4). The fluidised bed gasifier's high ratio of surface area to volume results in high heat losses, which is unfortunately a disadvantage suffered by most small fluidised bed pilot plants. Large-scale fluidised beds have a smaller difference (± 30 °C) between the bed and freeboard temperatures since the heat losses are a much lower percentage of the total heat input.

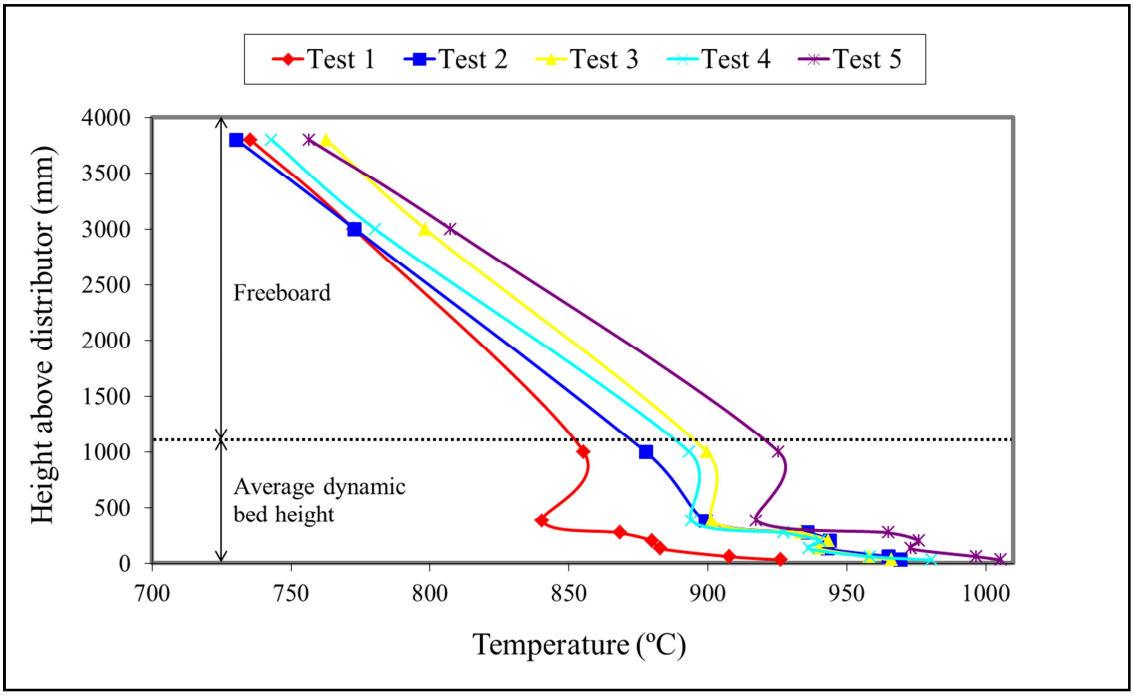

Figure 4.16: FBG temperature as a function of gasifier height for New Vaal coal

Tests carried out using air and steam as the gasification agents (Engelbrecht, 2008) showed that for temperatures above 1 150 °C in the lower part of the bed, agglomeration, clinkering and de-fluidisation of the bed had occurred. The difference between the mid-bed temperature and the lower bed temperature increases when larger particles (> 6 mm) segregate and fall to the bottom of the bed. These particles are not well fluidised and do not move rapidly between the bottom and the top of the bed. The temperature of the larger particles increases since they are not cooled by moving higher up in the bed where the gasification reaction takes place, no oxygen is present and the temperature is lower (Rhemat and Saxena, 1980). When the larger particles reach temperatures approaching the ash fusion temperature of the coal, they can agglomerate, resulting in de-fluidisation of the bed. High temperatures in the lower part of the bed can also be produced by high oxygen concentrations (> 30 vol.%) in the gasification agent mixture (air, oxygen and steam) that is fed to the gasifier (Weimer and Clough, 1980).

For the 10 tests carried out on New Vaal and Grootegeluk coal using oxygen-enriched air and steam as the gasification agents (Tables 4.9 and 4.10), agglomeration and clinkering of the bed was avoided by taking the following precautionary measures:

- The lower bed temperature was maintained below 1 000 °C.
- Feed coal particles larger than 4 mm were removed by screening.
- The oxygen concentration of the gasification agents mixture (oxygen, air and steam) was maintained below 25 vol.%.
- The fluidising velocity was maintained above 1.25 m/s.

4.5.1.4 Thermal fragmentation and attrition of char

The New Vaal and Grootegeluk coals were screened to remove coal particles less than 0.7 mm and greater than 4 mm in size (Appendices D.2.11 and 12) prior to feeding into the fluidised bed gasifier. Tables 4.9 and 4.10 show that due to thermal fragmentation and attrition of the coal in the gasifier, a fine char fraction (0 - 0.25 mm) is produced which is elutriated from the gasifier and captured in the cyclone (cyclone char). The amount of cyclone char produced varied between 27% and 67%

of the total char produced. Factors that affect the cyclone char production are coal properties such as the Hardgrove grindability index (HGI) and conditions in the gasifier such as temperature, residence time and fluidising velocity. The values for the char elutriated, as shown in Table 4.12, are the average values of the five tests on New Vaal and Grootegeluk coal detailed in Tables 4.9 and 4.10. Table 4.12 shows that for approximately similar average operating conditions and feed coal particle sizes, a larger percentage of the char was elutriated in the case of New Vaal coal. This indicates that New Vaal coal is more prone to thermal fragmentation and attrition, which is consistent with the difference between the HGIs of the two coals.

Table 4.12: Effect of HGI of coal on char elutriated from the FBG

Coal	New Vaal	Grootegeluk
Bed temperature (°C)	937	951
Fluidising velocity (m/s)	1.65	1.61
Average coal particle size (mm)	1.64	1.58
Bed char particle size (mm)	0.77	0.90
Cyclone char particle size (µm)	57.2	69.2
Hardgrove grindability index (HGI)	66	47
Char elutriated (%)	60.8	46.4

4.5.1.5 Bed and cyclone char properties

It is necessary to know the properties of the bed and cyclone chars produced by fluidised bed coal gasifiers in order to explore potential disposal and utilisation options for these chars. Utilisation options include applications in construction, agriculture and energy recovery. Due to the high carbon content of the chars produced by fluidised bed gasifiers, the properties that will be discussed here are those relating specifically to the utilisation of the char in combustion and gasification applications for energy recovery. From Table 4.13 it is clear that only a few of the selected studies given in Table 4.1 (from the literature survey) have attempted to characterise the char produced by fluidised bed gasifiers, and only limited data have been reported.

Xiao *et al*. (2007) characterised chars produced from a pressurised pilot-scale fluidised bed gasifier. Figure 4.17 shows a SEM image of bed char produced during

the gasification of a bituminous coal. The reported surface area of the char was 178 m^2/g, which was 54 times larger than the surface area of the coal (3.26 m^2/g).

Table 4.13: Fluidised bed gasifier char properties reported in the literature

Investigators	Char elutriated (%)	Bed char			Cyclone char		
		Carbon content (wt.%)	Size (mm)	Surface area (m^2/g)	Carbon content (wt.%)	Size (mm)	Surface area (m^2/g)
Xiao *et al.*	41–62	22–39	1.0	178	42– 52	0.1	N/R
Bhattacharya	N/R	N/R	1.0	N/R	N/R	0.04	N/R
Huang *et al.*	96	25–70	1.25	N/R	N/R	0.2	N/R
Guterriez *et al.*	22–79	N/R	N/R	N/R	29–80	N/R	N/R

N/R Not reported

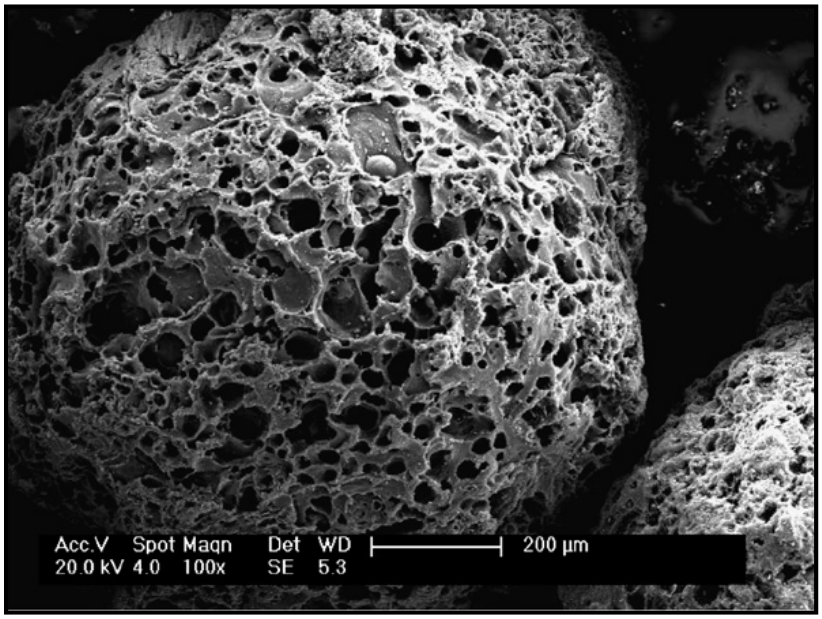

Figure 4.17: SEM image of gasifier bed char produced by Xiao *et al.* (2007)

The char produced by the fluidised bed gasifier was combusted in a pilot-scale fluidised bed combustor and a combustion efficiency of greater than 99% was reported. The high combustion reactivity of the char was attributed to its high surface area which was formed in the fluidised bed gasifier.

Carbon content of char

Tables 4.9 and 4.10 show that the carbon content of the elutriated char (cyclone char) is significantly higher than that of the bed char. A possible explanation for this is that the small particles (< 250 μm) that are generated as a result of thermal fragmentation and attrition are entrained to the freeboard area (above the bed) of the fluidised bed gasifier. The conversion rate (dX/dt) of the char particles in the freeboard is lower than that of the char particles in the bed since:

- there is little or no oxygen present in the freeboard,
- the concentrations of CO_2 and H_2O in the freeboard are lower than in the bed resulting in lower gasification reaction rates,
- the concentrations of CO and H_2 are higher, which inhibits (decreases) the gasification reaction rates,
- the temperature of the freeboard is lower
- and the residence time of particles in the freeboard is lower than the residence time of particles in the bed.

In many situations the generation of fines due to thermal fragmentation and attrition therefore limits the maximum carbon conversion that can be achieved in a fluidised bed gasifier. Test 5 on New Vaal coal illustrates how char attrition and fines generation limit the maximum carbon conversion that can be achieved in a fluidised bed gasifier. Table 4.9 shows that due to the higher temperature and residence time used for Test 5, the carbon content of the bed char is 2.5 wt.% and the fixed carbon conversion is 87.5%. In order to increase the fixed carbon conversion further it would be necessary to reduce the carbon content of the fly-ash (14.9 wt.%) since the carbon content of the bed char is already very low. Due to the lower char gasification rate in the freeboard, increasing the bed temperature and char residence time further would have little effect on the carbon content of the fly-ash.

In order to increase the gasification rate in the freeboard, Gräbner *et al*. (2009) and Brüngel *et al*. (1989) injected oxygen into the freeboard of the gasifier. Since the oxygen is more likely to react with gas rather than with the char, oxygen injection will

increase the freeboard temperature and decrease the calorific value of the gas. This method is therefore not expected to increase the fixed carbon conversion and gasification efficiency significantly since the calorific value of the gas will be lower and the sensible heat losses in the gas will be higher.

The investigations of Xiao *et al*. (2007) and Bhattacharya (2006) were aimed at addressing the fines-generation problem by recycling the char collected by the cyclone back to the gasifier. The effectiveness of this method is questionable since the recycled fines will be rapidly elutriated to the freeboard where the conversion rate is low, as explained above. Recycling of the fines to the bottom of the bed where the oxygen concentration and temperature are high could be a more effective solution to the problem. The distribution of fines to the lower part of the bed and their retention there could, however, be difficult to implement, particularly on a large-scale bubbling fluidised bed gasifier. Effective recycle of char fines to the bottom of the bed could be easier to implement on a circulating fluidised bed gasifier design (Figure 1.6). The high fluidising velocity (7 – 11 m/s) increases the mixing rate and distribution of the recycled char fines in the combustion zone of the gasifier, thereby increasing their conversion rate.

Char density and size

The densities of the cyclone and bed char are plotted against the carbon content of the char in Figures 4.18 and 4.19. It can be seen that the density of the bed char increases with a decrease in the carbon content. However, for the cyclone char no increase in density is observed. The bed chars were subjected to combined petrographic, FTIR and XRD analysis (Oboirien, 2011). The results show that some of the lower-melting-point minerals (clay minerals) had melted and penetrated into the cracks and pores in the chars. Since the low-carbon bed chars were produced when higher temperatures and residence times were used, this could explain the higher density of these chars. The density of the cyclone chars did not increase at lower carbon content, which supports the above conclusion since the cyclone chars are entrained to the freeboard area and are therefore subjected to lower temperatures and residence times.

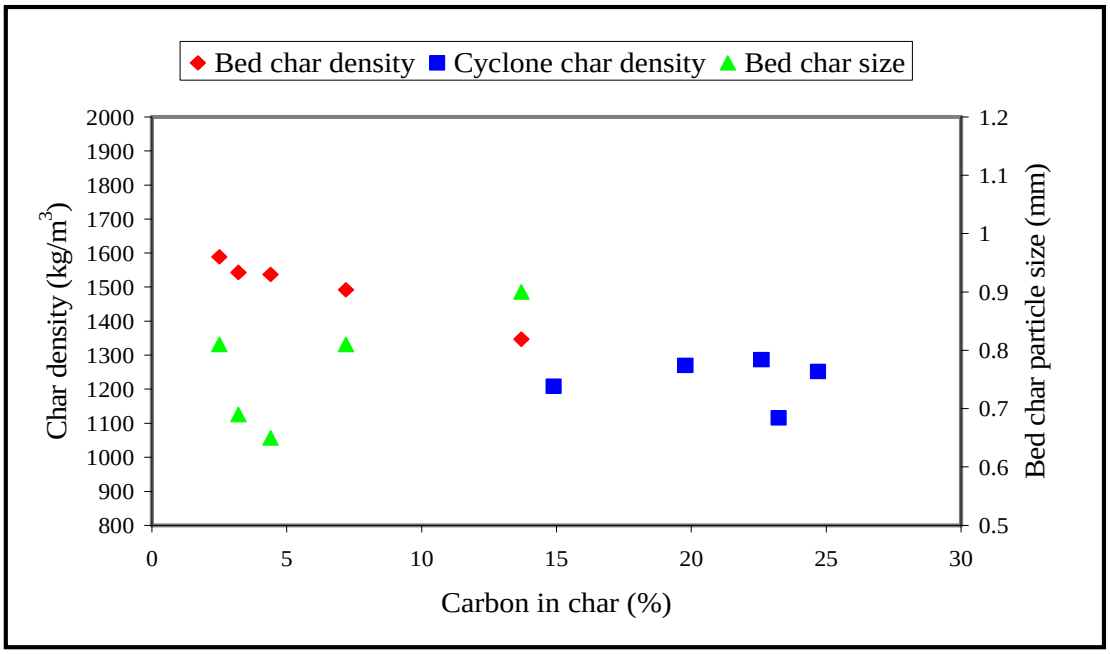

Figure 4.18: Char densities and particle sizes (New Vaal coal)

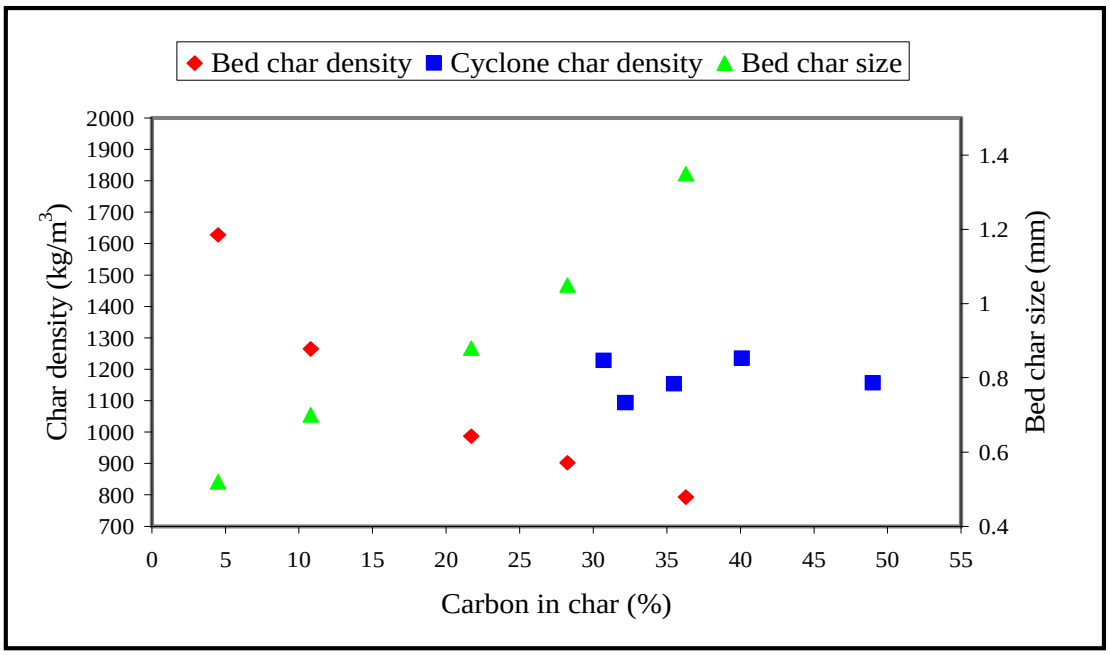

Figure 4.19: Char densities and particle sizes (Grootegeluk coal)

The variation in bed char density with carbon content has implications for the design and operation of fluidised bed coal gasifiers since the minimum fluidising velocity (U_{mf}) is affected by the density of the bed char. The implications in the case of New Vaal coal would be more important because higher bed char densities are not associated with a significant decrease in the char particle size (Figure 4.18). In the

case of Grootegeluk coal, higher bed char densities are associated with a significant decrease in particle size (Figure 4.19), which would counteract the effect of higher bed char density on the calculated minimum fluidising velocity.

4.5.2 Tests using oxygen and steam as the gasification agents

Two further tests were carried out on New Vaal and Grootegeluk coal using only oxygen and steam as the gasification agents, without the addition of air. The objective of the two tests was to investigate the effect of using oxygen and steam as the gasification agents on the fixed carbon conversion and gas calorific value compared with using oxygen-enriched air and steam as the gasification agents. The results of these additional tests are given in Table 4.14. The tests were carried out on batches of coal of which the analysis (Appendix D.2.15) differed slightly from that of the coals used for the tests with oxygen-enriched air and steam as the gasification agents.

4.5.2.1 Fixed carbon conversion

Table 4.14 shows that for Grootegeluk coal a higher fixed carbon conversion was obtained when oxygen and steam were used as the gasification agents compared with the use of oxygen-enriched air and steam (Table 4.10, Test 2). This could possibly be attributed to the higher steam concentration in the gasifier during oxygen and steam gasification compared with oxygen-enriched air and steam gasification. In the case of New Vaal coal, the higher steam concentration in the gasifier did not produce an increase in the fixed carbon conversion (Table 4.9, Test 2), which indicates that the maximum fixed carbon conversion is limited by thermal fragmentation and attrition of coal in the gasifier.

4.5.2.2 Gas calorific value

Due to the absence of nitrogen, the dry gas calorific value was higher when oxygen and steam were used as the gasification agents compared with oxygen-enriched air and steam. A dry gas calorific value of 10.9 MJ/Nm^3 (H_2 – 43 vol.%, CO – 18.2 vol.%, CH_4 – 8 vol.% and CO_2 – 26.4 vol.%) was obtained by Rhinehardt *et al*.

(1987), who carried out fluidised bed gasification tests on West Texas lignite using oxygen and steam as the gasification agents. The higher gas calorific value obtained by these researchers can be attributed to the higher char reactivity and volatile matter of the West Texas lignite that was used.

Table 4.14: Summary of fluidised bed gasification tests using oxygen and steam

Coal tested	New Vaal	Grootegeluk
Mid-bed temperature (ºC)	931	918
Char residence time (min)	25.5	35.4
Coal feedrate (kg/h)	29.4	22.8
Airflow (Nm^3/h)	0.00	0.00
Steam flow (kg/h)	33.0	36.6
Oxygen flow (kg/h)	14.5	15.3
Oxygen and steam temp. (ºC)	183	205
Oxygen in total inlet flow (vol.%)	19.80	19.00
Stoichiometric molar ratio	0.40	0.40
Steam: carbon molar ratio	1.76	2.03
Coal particle size – d_{50} (mm)	1.2	2.1
Fluidising velocity (m/s)	1.77	1.92
Lower bed temperature (ºC)	944	979
Gasifier exit temperature (ºC)	752	740
Dry gas composition		
CO (vol.%)	21.4	21.7
H_2 (vol.%)	34.2	32.6
CH_4 (vol.%)	1.3	4.9
CO_2 (vol.%)	36.2	39.5
O_2 (vol.%)	0.1	0.1
N_2 + others (vol.%)	6.3	0.3
Gas calorific value (MJ/Nm^3)	7.68	9.05
Dry gas flowrate (Nm^3/h)	33.77	26.22
Bed pressure drop (Pa) (P1-P2)	2 180	2 050
Dynamic bed height (m)	1.25	2.11
Char extracted from bed (kg/h)	4.10	5.81
Carbon in bed char (wt.%)	4.20	24.40
Bed char particle size (mm)	0.3	1.1
Char elutriated to cyclone (kg/h)	9.65	4.33
Carbon in cyclone char (wt.%)	17.60	29.80
Cyclone char particle size (μm)	78	48
Char elutriated to cyclone (%)	70.18	42.70
Fixed carbon conversion (%)	81.57	66.70
Total carbon conversion (%)	85.05	77.41
Cold gas efficiency (%)	56.69	49.09

The effect of oxygen concentration in the 'air' on the dry gas calorific value is given in Figure 4.20. The calorific value of the gas when air and steam are used as the gasification agents was obtained from Engelbrecht (2008). Figure 4.20 shows that when the air is enriched to ± 36 vol.% oxygen (15% enrichment), the calorific value of the gas increases from ± 3.0 MJ/Nm^3 to ± 5.5 MJ/Nm^3, which is an increase of 83.3%. When oxygen and steam are used as the gasification agents (100% enrichment), the calorific value of the gas increases further to ± 8.46 MJ/Nm^3, which is a 180% increase. The optimum level of oxygen enrichment, which could be less than 100%, will therefore depend on the eventual utilisation option chosen for the gas, such as for combustion in gas turbines for electricity generation or as synthesis gas for the production of liquid fuels and chemicals.

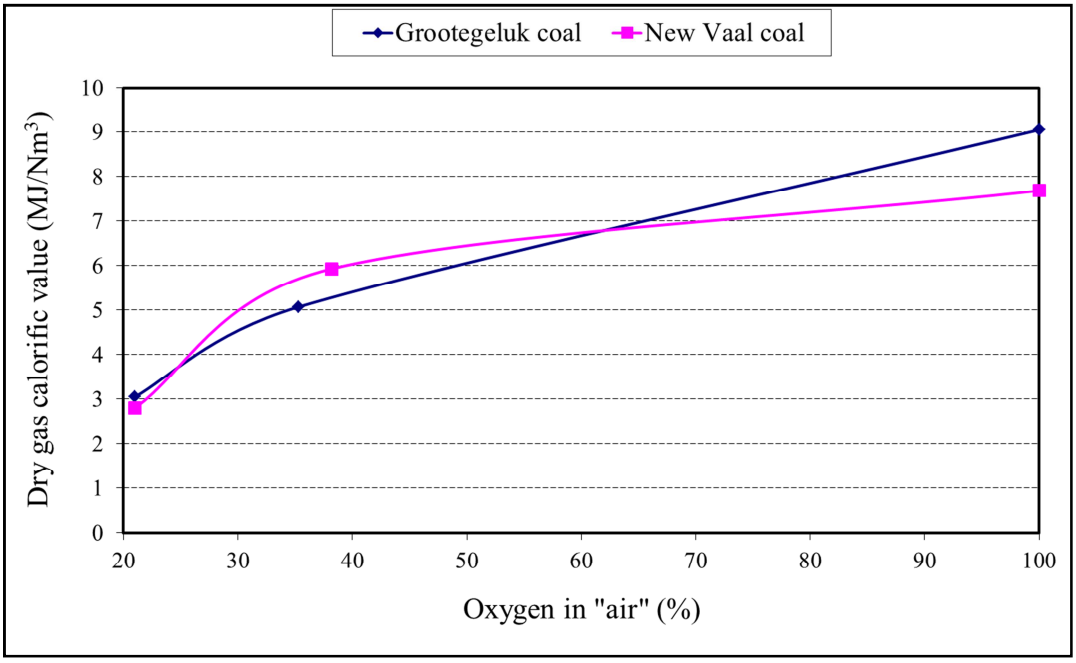

Figure 4.20: Dry gas calorific value as a function of oxygen enrichment

4.6 Summary of pilot-scale fluidised bed coal gasification tests

Pilot-scale bubbling fluidised bed gasification tests were conducted on two high-ash South African coals at temperatures between 880 and 980 °C and an absolute pressure of 90 kPa. Tests were carried out using both oxygen-enriched air and steam, and oxygen and steam as the gasification agents. Stable gasification was achieved for all the operating conditions selected for the tests.

The results of the tests show that the fixed carbon conversion obtained in the gasifier increases with:

- bed temperature,
- steam concentration of the reacting gases,
- residence time of char in the bed
- and reactivity of the coals tested.

An increase in fixed carbon conversion produced a low increase in calorific value of the gas at a constant oxygen-enrichment level. This is attributed to the large fraction of the energy content of the gas (calorific value) that is produced by the volatile matter in the coal, which is not related to fixed carbon conversion. An increase in the oxygen-enrichment level of the air produced a significant increase in the calorific value of the gas, which was attributed to the reduced dilution effect of nitrogen at the higher oxygen-enrichment levels.

The temperature distribution in the bed showed that the temperature in the lower part of the bed is higher (± 50 °C) than the temperature at the top of the bed. This is due to the high concentration of oxygen and the resulting high rate of the char combustion reaction in the lower part of the bed. Agglomeration and clinkering of the bed were avoided by implementing the following precautionary measures:

- The lower bed temperature was maintained below 1 000 °C.
- Coal particles in the feed larger than 4 mm were removed by screening.
- The oxygen concentration of the gasification agents mixture (oxygen, air and steam) was maintained below 25 vol.%.
- The fluidising velocity was maintained above 1.25 m/s.

Due to thermal fragmentation and attrition, fine char (0 – 0.25 mm) is produced which is elutriated from the gasifier and captured in the cyclone. The amount of fine char that is produced depends on the coal properties, such as the Hardgrove grindability

index (HGI), and the conditions in the gasifier, such as the temperature and the fluidising velocity.

The carbon content of the elutriated char (fine char) is significantly higher than that of the bed char since the fine char is elutriated to the freeboard of the fluidised bed where the conversion rate of the char particles is lower than in the fluidised bed for the following reasons:

- There is little or no oxygen present in the freeboard.
- The concentrations of CO_2 and H_2O in the freeboard are lower than in the bed, resulting in lower gasification reaction rates.
- The concentrations of CO and H_2 are higher, which inhibits (decreases) the gasification reaction rates.
- The temperature of the freeboard is lower.
- The residence time of particles in the freeboard is lower than that in the bed.

In many situations the generation of fines due to thermal fragmentation and attrition limits the maximum carbon conversion that can be achieved in a bubbling fluidised bed coal gasifier.

Density measurements carried out on the bed char particles produced by the gasifier show that the density of the char particles increases as their carbon content decreases. Petrographic, FTIR and XRD analysis of the chars showed that due to the higher temperature to which the low-carbon chars were exposed, some of the lower-melting-point minerals (clay minerals) had melted and penetrated into the cracks and pores of the chars, thereby increasing the density of the char particles.

4.7 Chapter 4 references

ASHMAN, P.J., KOSMINSKI, A., BUTTON, S.J. AND MULLINGER, P.J. (2005). Gasification of Victorian Lignite in a Laboratory Scale Fluidised Bed Gasifier. Paper presented at the 5th Asia-Pacific Conference on Combustion, University of Adelaide, Adelaide, Australia, 18–20 July 2005.

BELYAEV, A.A., YAMPOLSKII, Y.P., STARANNIKOVA, L.E., POLYAKOV, A.M., CLARIZIA, G., DRIOLI, E., MARIGLIANO, G., BARBIERI G. (2003). Membrane air separation for intensification of coal gasification process. *Fuel Processing Technology* 80: 119–141.

BHATTACHARYA, S. P. (2006). Gasification performance of Australian lignites in a pressurized fluidized bed gasifier process development unit under air and oxygen-enriched air blown conditions. *Institution of Chemical Engineers Trans. IChemE, Process Safety and Environmental Protection* 84(B6): 453–460.

BRITISH STANDARD 1042. (1964). Methods for the measurement of fluid flow in pipes. Part 1. Orifice plates, nozzles and venturi tubes. British Standards Institution.

BRÜNGEL, N., LAMBERTZ, J. AND THEIS, K.A. (1989). Stages of Development of the HTW Process Regarding its Suitability for Combined-cycle Plants. Rheinische Braunkohlenwerke AG report.

CHATTERJEE, P.K., DATTA, A.B. AND KUNDU, K.M. (1995). Fluidised bed gasification of coal. *The Canadian Journal of Chemical Engineering* 73: 204–210.

DE SOUZA-SANTOS, M.L. (2010). Comprehensive simulator applied to fluidized bed coal gasification. *The Open Chemical Engineering Journal* 4: 68–79.

ENGELBRECHT, A.D. (2008). Characterization and fluidised bed gasification of selected high-ash South African coals. Masters dissertation, North-West University, South Africa.

ENGELBRECHT, A.D., EVERSON, R.C., NEOMAGUS H.W.P.J. AND NORTH, B.C. (2010). Fluidised bed gasification of selected South African coals. *Journal of the South African Institute of Mining and Metallurgy* 110: 225–742.

GELDART, S. (1986). Single particles, fixed and quiescent beds. In: *Gas Fluidization Technology*, Chapter 2, New York, Brisbane, Toronto, Singapore: Wiley, 26.

GOYAL, G., BRYAN, A.B., RHEMAT, A., PATEL, J. (1990). In-situ desulphurization in a fluidized bed coal gasifier. *Energy Sources* 12: 161–179.

GRÄBNER, M., MESSIG, D., UEBEL, K. AND MEYER B. (2009). Development and Modelling of 3rd Generation Gasifiers for Low-rank and High-ash Coals. Paper presented at the International Conference on Coal Science & Technology, Cape Town, South Africa, 26–29 October 2009.

GURURAJAN, V.S. AND AGARWAL, P.K. (1992). Mathematical model of fluidized bed coal gasifiers. *Chem. Eng. Res. Des. Trans.* 70A: 211–237.

GUTIERREZ, L.A. AND WATKINSON, A.P. (1982). Fluidized bed gasification of some Western Canadian coals. *Fuel* 61: 133–138.

HANSON, S., PATRICK, J.W. AND WALKER, A. (2001). The effect of coal particle size on pyrolysis and steam gasification. *Fuel* 81: 531–537.

HUANG, J., FANG, Y., CHEN, H. AND WANG, Y. (2003). Coal gasification characteristic in a pressurized fluidised bed. *Energy & Fuels* 17: 1474–1479.

JING, B., ZHONG, Z., HUANG, Y. AND XIAO, R. (2005). Air and steam coal partial gasification in an atmospheric fluidized bed. *Energy & Fuels* 19: 1619–1623.

NEOGI, D., CHANG, C.C., WALAENDER, W.P., AND FAN, L.T. (1986). Study of coal gasification in an experimental fluidised bed reactor. *AIChE Journal* 32: 17–28.

OBOIRIEN, B. (2011). Gasification of high-ash coals and chars from South African coals. Doctoral thesis. University of the Witwatersrand, South Africa.

OCAMPO, A., ARENAS, E., CHEJNE, F., ESPINEL, J., LONDONO, C., AGUIRRE, J. AND REREZ, J.D. (2003). An experimental study on gasification of Colombian coal in a fluidised bed. *Fuel* 82: 161–164.

PATERSON, N. (1997). Fuel behaviour studies in the air-blown gasification cycle. *Fuel* 76: 1319–1325.

PURDY, M.J., FELDER, R.M. AND FERREL, J.K. (1984). Coal gasification in a pilot-scale fluidized bed reactor. 2. Gasification of New Mexico sub-bituminous coal. *Industrial & Engineering Chemistry Process Design and Development* 23: 287–294.

REHMAT A. AND SAXENA, S.C. (1980). Agglomeration of ash in fluidized-bed gasification of coal by steam-oxygen (or air) mixture. *Industrial & Engineering Chemistry Process Design and Development* 19: 223–230.

RHINEHART, R.R., FELDER, R.M. AND FERREL, J.K. (1987). Coal gasification in a pilot-scale fluidized bed reactor. 3. Gasification of Texas lignite. *Industrial & Engineering Chemistry Research* 26: 2048–2057.

ROSS, D.P., YAN, H-M., ZHONG, Z. AND ZHANG, D-K. (2005). A non-isothermal model of a bubbling fluidised bed coal gasifier. *Fuel* 84: 1469–1481.

SAFFER, M., OCAMPO, A. AND LANGUERIE, C. (1988). Gasification of coal in a fluidised bed in the presence of water vapour and oxygen; an experimental study and a first attempt at modelling the reactor. *International Journal of Chemical Engineering* 28: 46–61.

WEIMER, A AND CLOUGH, D. (1980). Modelling a low pressure steam-oxygen fluidised bed coal gasification reactor. *Chemical Engineering Science* 36: 549–567.

XIAO, R., ZHANG, M., JIN, B., XIAONG Y., ZHOU, H., DUAN, Y., ZHONG, Z., CHEN, X., SHEN, L. AND HUANG, Y. (2007). Air blown partial gasification of coal in a pilot plant pressurized spout-fluid bed reactor. *Fuel* 86: 1631–1640.

YAN, H-M., HEIDENREICH, C. AND ZHANG, D-K. (1998). Mathematical modelling of a bubbling fluidised bed coal gasifier and the significance of 'net flow'. *Fuel* 77: 1067–1079.

YE, D.P., AGNEW, J.B. AND ZHANG, D-K. (1997). Gasification of South Australian low-rank coal with carbon dioxide and steam: Kinetics and reactivity studies. *Fuel* 77: 1209–1219.

4.8 Chapter 4 and Appendix D nomenclature

A_B	gasifier bed area	m^2
A_E	char elutriated to cyclone	%
C	carbon in coal	wt.%
C_{ash}	ash in coal	wt.%
C_{BC}	carbon in bed char	wt.%
C_{EC}	carbon in elutriated char	wt.%
C_d	nozzle discharge coefficient	-
C_{fixed}	fixed carbon in coal	wt.%
$C_{FIXEDCON}$	fixed carbon conversion	%
$C_{TOTALCON}$	total carbon conversion	%
CV_{coal}	calorific value of coal	$MJ.kg^{-1}$
CV_{gas}	calorific value of gas	$MJ.Nm^{-3}$
d_p	char particle diameter/coal particle size	m or mm
d_{50}	mean particle diameter	m or mm
D_p	pipe diameter	m
g	gravitational constant	$m.s^{-2}$
G_{BC}	bed char flowrate	$kg.h^{-1}$
G_{EC}	elutriated char flowrate	$kg.h^{-1}$
G_{char}	char feedrate to gasifier	$kg.h^{-1}$
G_{coal}	coal flowrate	$kg.h^{-1}$
G_{O2}	oxygen flowrate	$kg.h^{-1}$
G_{steam}	steam flowrate	$kg.h^{-1}$
H_b	dynamic bed height	m
H_p	distance from distributor to pressure probe	m
$H_2O:C_{MR}$	steam:carbon molar ratio	-
M_1	bed mass above pressure probe - P1	kg
M_2	bed mass below pressure probe - P1	kg
M_t	total bed mass	kg
N	nitrogen in coal	wt.%
NQ_{gas}	dry gas flowrate	$Nm^3.h^{-1}$
nC	elemental carbon molar flowrate	$mol.h^{-1}$

nEAIR	oxygen and air molar flowrate	$mol.h^{-1}$
nH	elemental hydrogen molar flowrate	$mol.h^{-1}$
nH_2O	steam molar flowrate	$mol.h^{-1}$
nINLET	oxygen, air and steam molar flowrate	$mol.h^{-1}$
nO_2	oxygen molar flowrate	$mol.h^{-1}$
nO	elemental oxygen molar flowrate	$mol.h^{-1}$
nS	elemental shulphur molar flowrate	$mol.h^{-1}$
$O:C_{MR}$	oxygen:carbon molar ratio	-
O	oxygen in coal	wt.%
O_{EAIR}	oxygen concentration of enriched air	vol.%
O_{INLET}	oxygen concentration of total inlet flow	vol.%
P1	gasifier bottom pressure	Pa
P2	gasifier top pressure	Pa
P_B	gasifier pressure	kPa
Q_{air}	air flowrate	Nm^3h^{-1}
Q_{total}	total gas flow at bed conditions	m^3h^{-1}
NQ_{total}	total gas flow to the fluidised bed	Nm^3h^{-1}
S	sulphur in coal	wt.%
T1	bottom bed temperature	°C
T4	mid-bed temperature	°C
T9	gasifier exit temperature	°C
T_b	bed temperature	°C
T_B	fluidised bed temperature	°C
U	superficial gas velocity in the bed	$m.s^{-1}$
U_{mf}	minimum fluidising velocity	$m.s^{-1}$
U_t	terminal falling velocity	$m.s^{-1}$
v	gas velocity through holes in distributor nozzle	$m.s^{-1}$
V_{CH4}	CH_4 concentration of the gas	vol.%
V_{CO}	CO concentration of the gas	vol.%
V_{H2}	H_2 concentration of the gas	vol.%
V_{H2S}	H_2S concentration of the gas	vol.%
X	fractional conversion of fixed carbon in coal	-

Greek letters

ε	bed voidage at bed velocity	-
ε_e	expanded bed voidage	-
τ	residence time of char in the gasifier	min
Ø	diameter	m
Φ_{MR}	stoichiometric molar ratio	-
ΔP_B	bed pressure drop	Pa
ΔP_D	distributor pressure drop	Pa
θ	angle of repose	°
η_{CG}	cold gas efficiency	%
μ	gas viscosity	$kg.m^{-1}s^{-1}$
ρ_{char}	char density	$kg.m^{-3}$
ρ_g	gas density	$kg.m^{-3}$
$\Delta X/\Delta T$	slope of the X vs. T graph	$°C^{-1}$

Acronyms/Abbreviations

BS	British Standard
C_2^+	ethane and higher hydrocarbons
CSIR	Council for Scientific and Industrial Research
CV	calorific value
FBC	fluidised bed combustion
FBG	fluidised bed gasifier
FD	Forced draught
FTIR	Fourier transform infrared
GG	Grootegeluk
HGI	Hardgrove grindability index
ID	Induced draught
IGCC	Integrated gasification combined cycle
LCV	Low calorific value
LPG	Liquefied petroleum gas
N/R	not reported
NV	New Vaal

OTH	other gases
PSD	particle size distribution
RSM	response surface methodology
SEM	scanning electron microscope
SO_x	sulphurous oxides
SS	stainless steel
WGSR	water-gas shift reaction
XRD	X-ray diffraction

CHAPTER 5 FLUIDISED BED COAL GASIFIER MODELLING

5.1 Introduction

In this chapter the modelling of fluidised bed coal gasifiers is investigated. Section 5.2 reviews selected fluidised bed coal gasification modelling studies that have been reported in the literature. In Section 5.3 the development of a fluidised bed coal gasifier rate model, its predictive capability and application are described. Finally, a summary of the modelling of fluidised bed coal gasifiers is given in Section 5.4.

5.2 Literature review

Efforts at modelling fluidised bed coal gasifiers started in earnest in the early 1980s and are well documented in the literature. The purpose of the development of fluidised bed coal gasifier models is to assist with:

- Analysis and optimisation.
- Design and scale-up.
- Operation and control.

Fluidised bed gasifier models that have been developed (with increasing degree of complexity) are mass and energy balance models, equilibrium models and rate models. Although rate models require more time and effort to develop they have enhanced predictive capability, since equations describing the various rate process taking place in the gasifier such as chemical reaction, heat transfer and mass transfer are included in the model.

5.2.1 Models reported in the literature

Tables 5.1, 5.2 and 5.3 present summaries of the fluidised bed coal gasification modelling studies that have been reported in the literature. Tables 5.1 and 5.2 show a summary of the sub-models that have been used to describe the various rate processes

that occur in the gasifier, and Table 5.3 gives a summary of the predictive capability of the models. Fluidised bed coal gasifier models include sub-models for:

- Fluidised bed hydrodynamics.
- Coal devolatilisation.
- Rates of homogeneous and heterogeneous chemical reactions.
- Rates of heat and mass transfer between phases.
- Fragmentation, attrition and elutriation of char.

The sub-models have associated parameters that can be estimated by means of pilot plant or thermogravimetric analyser tests. In addition to the sub-models given above, fluidised bed coal gasifier models also include overall mass and energy balances.

5.2.1.1 Fluidised bed hydrodynamics

A hydrodynamic model is required to describe the flow pattern of gases and solids (mixing) in the gasifier. The flow pattern influences the rates of heat and mass transfer between gases and solids in the fluidised bed.

Table 5.1 shows that the majority of the modellers used the Davison and Harrison (1971) model to describe the hydrodynamic behaviour of the bubbling fluidised bed. The Davison and Harrison (1971) model is based on the two-phase theory of fluidisation, which assumes that the bed consists of two phases, namely the emulsion phase (dense phase) and the bubble phase (dilute phase). The emulsion phase, containing all the solids, remains at incipient (minimum) fluidisation conditions and all gas in excess of that required to maintain incipient fluidisation condition passes through the bed in the bubble phase.

Table 5.1: Summary of selected fluidised bed coal gasification modelling studies – Sub-models I

Investigator	Year	Country	Bubbling bed hydrodynamic model	Devolatilisation model	Heterogeneous reactions				Homogenous reactions	
					Char combustion	Char gasification			WGSR[4]	Gas combustion
						H_2O[1]	CO_2[2]	H_2[3]		
Chejne	2010	Colombia	Two-phase - DH	N/R	Eaton[10]	Roberts	Roberts	Roberts	Biba	Vilienski
Snider	2010	USA	CPFD[5]	N/R	Yoon	Wen	Wen	Wen	Bustamante	Not incl.
Yu	2006	China	TFM & KTGF[6]	N/R	Eaton	Johnson	N/R	Johnson	Biba	Vilienski
Ross	2005	Australia	Two-phase- DH[7]	Loison	La Nauze	Johnson	Ye	Johnson	Karim, Wen	Haslam
Chejne	2002	Colombia	Two-phase- DH	N/R	Eaton	Johnson	N/R	Johnson	Biba	Vilienski
Hamel	2001	Germany	N/R	Anthony	Hobbs	Hobbs	NR	Hobbs	Chen	Jensen
Yan	2000	Australia	Two-phase - DH	Loison	La Nauze	Johnson	Ye	Johnson	Equilibrium	Haslam
Yan	1999	Australia	Two-phase - DH	Loison	La Nauze	Johnson	N/R	Johnson	Karim	Haslam
Yan	1998	Australia	Two-phase - DH	Loison	La Nauze	Johnson	Not incl.[8]	Johnson	Karim,Wen	Haslam
Lee	1998	Korea	Two-phase - DH	Own correlation	Rajan	Kwon	Not incl.	Not incl.	Chen	N/R
Luo	1998	Japan	Three-phase - KL[9]	N/R	Saito	Matsui	Matsui	Not incl.	Chen	Not incl.
Chatterjee	1995	India	Three-phase - KL	Field	Parker	Johnson	Elliott	Johnson	Wen	Not incl.
Ciesielczyk	1994	Poland	Two-phase - DH	Not included	N/R	Johnson	Not incl.	Johnson	N/R	Not incl.
Gururajan	1992	Australia	Two-phase - DH	N/R	N/R	Johnson	N/R	Johnson	Chen, Biba	N/R
de Souza-Santos	1989	Brazil	Two-phase - DH	N/R	Yoon	Johnson	N/R	Johnson	Biba	Vilienski
Ma	1988	USA	Two-phase - DH	Own correlation	Field	Johnson	Not incl.	Johnson	Karim, Wen	Haslam
Saffer	1988	France	Two-phase - DH	Loison	Hamor	N/R	N/R	N/R.	Yoon	Not incl.
Neogi	1986	USA	Two-phase - DH	Yeboah	Biba	Biba	Biba	Not incl.	Equilibrium	Not incl.
Weimer	1980	USA	Three-phase - KL	Loison	N/R	Mayers	Dutta	Not incl.	Karim	Haslam

N/R: Not reported

1 $C + H_2O \Rightarrow H_2 + CO$
2 $C + CO_2 \Rightarrow 2CO$
3 $C + H_2 \Rightarrow CH_4$
4 Water-gas shift reaction
5 Computational particle fluid dynamics
6 Two-fluid model and kinetic theory of granular flow
7 Davidson and Harrison
8 Not included
9 Kunii and Levenspiel
10 The names given in Tables 5.1, 5.2, 5.3 and 5.4 are the first authors of the papers that describe the correlations and models. Details are given in Chapter 5 references.

Table 5.2: Summary of selected fluidised bed coal gasification modelling studies – Sub-models II and features

Investigator	Year	Country	Net gas flow between phases	Mass transfer	Heat transfer		Fines generation and elutriation	Iso or non-iso	Solution method
					Particle - emulsion gas	Emulsion gas - bubble gas			
Chejne	2010	Colombia	Included	Babu	Kunii	Kunii	Yates	Non-iso	ODE
Snider	2010	USA	N/R	N/R	N/R	N/R	N/R	N/R	CFD
Yu	2006	China	N/R	N/R	N/R	N/R	N/R	Non-iso	CDF
Ross	2005	Australia	Included	Sit	N/R	N/R	Rhinehardt	Non-iso	Finite element
Chejne	2002	Colombia	Included	Babu	Kunii	Kunii	Wen	Non-iso	ODE
Hamel	2001	Germany	N/R	N/R	N/R	N/R	N/R	Non-iso	ODE
Yan	2000	Australia	Included	Sit	N/R	N/R	Rhinehardt	Iso	Finite element
Yan	1999	Australia	Included	Sit	N/R	N/R	Rhinehardt	Iso	Finite element
Yan	1998	Australia	Included	Sit	N/R	N/R	Rhinehardt	Iso	Finite element
Lee	1998	Korea	Included	N/R	N/R	N/R	N/R	Non-iso	ODE
Luo	1998	Japan	Not included	KL	Kunii	Kunii	Horio	Iso	ODE
Chatterjee	1995	India	Not included	KL	Kunii	Kunii	Not included	Iso	ODE
Ciesielczyk	1994	Poland	Not included	N/R	N/R	N/R	N/R	Non-iso	ODE
Gururajan	1992	Australia	Included	KL	Kunii	Kunii	Not included	Iso	ODE
de Souza-Santos	1989	Brazil	Included	Sit	Gelperin	Kunii	Wen	Non-iso	ODE
Ma	1988	USA	Not included	Wen & Fan	Ranz	Kunii	Rhinehardt	Non-iso	Finite element
Saffer	1988	France	Not included	Kobayashi	N/R	N/R	N/R	Iso	ODE
Neogi	1986	USA	Not included	Kobayashi	N/R	N/R	N/R	Iso	ODE
Weimer	1980	USA	Not included	KL	Ranz	Kunii	Chen	Non-iso	ODE

N/R Not reported
Non-iso Non isothermal
Iso Isothermal
CFD Computational fluid dynamics
ODE Ordinary differential equations

Correlations used by modellers to estimate the minimum fluidising velocity include those by Geldart (1986) and Sit and Grace (1981) which are given in Appendix E.1.1.1

The gases in the bubble phase have been assumed to be in plug flow; however, the gases in the emulsion phase have been modelled either as a plug flow reactor (Ciesielczyk and Gawdzik, 1994; Chatterjee *et al.*, 1995; Ma *et al.*, 1988; Yan *et al.*, 1999) or as a continuously stirred tank reactor (CSTR) (Gururajan and Agarwal, 1994; Saffer *et al.*, 1988; De Sousa Santos *et al.*, 1989; Weimer and Clough, 1980). In all the models given in Table 5.1 the solids have been assumed to be well mixed within the emulsion phase. Figure 5.1 shows a schematic diagram representing the model where all gases in both the bubble and emulsion phases are assumed to be in plug flow, and the solids are well mixed within the emulsion phase.

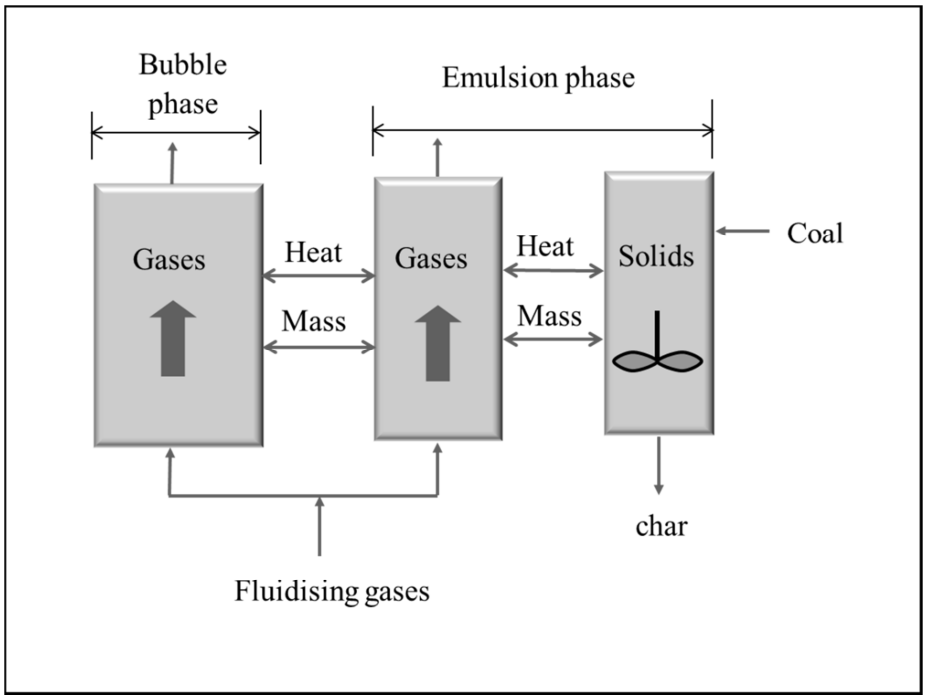

Figure 5.1: Schematic representation of the two-phase model of fluidisation

In a fluidised bed bubbles form as soon as the gas velocity exceeds the minimum fluidisation velocity. The bubble diameter is one of the most important parameters in the modelling of the hydrodynamics of a fluidised bed since it affects the bubble rise velocity, the bubble fraction of the bed, solids mixing, and mass transfer between the bubble and emulsion phases. Due to bubble coalescence, the bubble diameter

increases as a function of height in the bed. The majority of the modellers used the well-known correlation of Mori and Wen (1975) to estimate the bubble diameter as a function of operating variables and bed height. The correlation of Mori and Wen (1975) is given in equations (5.1) – (5.3).

The minimum bubble diameter is given by equation (5.1).

$$D_{B0} = 0.872[\frac{A_B(U - U_{mf})}{n_d}]^{0.4} \quad (5.1)$$

The maximum bubble diameter is given by equation (5.2).

$$D_{BM} = 1.64[A_B(U - U_{mf})]^{0.4} \quad (5.2)$$

The bubble diameter as a function of bed height (z) is given by equation (5.3).

$$d_b = D_{BM} - (D_{BM} - D_{B0})\exp(\frac{-0.3z}{D_t}) \quad (5.3)$$

Gururajan and Agarwal (1994) used the correlation of Darton *et al*. (1977) to estimate the bubble diameter. These equations are given in Appendix E.1.1.2

The rising velocity of bubbles in the bed is related to the bubble diameter by equation (5.4) (Davidson and Harrison, 1971).

$$U_b = U - U_{mf} + 0.71(gd_b)^{0.5} \quad (5.4)$$

The bubble fraction of the bed (δ) can be calculated by applying the two-phase theory of fluidisation, which assumes that all gas in excess of that required to maintain incipient fluidisation condition passes through the bed in the bubble phase.

$$A_B(U - U_{mf}) = A_B\delta U_b \quad (5.5)$$

Solving for δ gives:

$$\delta = \frac{U - U_{mf}}{U_b} \tag{5.6}$$

When the bubble diameter increases to 60% of the bed diameter (d_t) the bubbles are treated as slugs, and the rise velocity of the slugs is calculated using equation (5.7) (Ormiston *et al*., 1965). Since the bed diameter of pilot-scale fluidised bed reactors is often less than 0.5 m, slugs develop in the bed and equation (5.8) will give a better estimation of the bubble fraction of the bed than equation (5.6).

$$U_s = U - U_{mf} + 0.35(gd_b)^{0.5} \tag{5.7}$$

$$\delta = \frac{U - U_{mf}}{U_s} \tag{5.8}$$

The total bubble volume of the bed can be estimated using equation (5.9).

$$V_B = A_B \int_0^{H_b} \delta(z).dz \tag{5.9}$$

Substituting equations (5.4) and (5.6) gives the following equation for a bubbling bed:

$$V_B = A_B \int_0^{H_b} \frac{U - U_{mf}}{U - U_{mf} + 0.71(gd_b)^{0.5}}.dz \tag{5.10}$$

In equation (5.10) the bubble diameter (d_b) can be obtained as a function of bed height (z) by using equation (5.3), which allows equation (5.10) to be integrated either analytically or numerically.

The fractional bed expansion can be calculated from the total bubble volume (V_B) using equation (5.11).

$$B_E = \frac{V_B}{V_B + A_B H_{mf}} \tag{5.11}$$

Table 5.2 shows that Gururajan and Agarwal (1994), Yan *et al*. (1998) and Ross *et al*. (2005) included the concept of net gas flow into the hydrodynamics of their models. Net gas flow was included since the total gas volume in the emulsion phase increases due to combustion and gasification reactions and devolatilisation of coal particles. The generated gas was assumed to flow from the emulsion phase into the bubble phase, and Yan found that this flow is in the range of 71% – 87% relative to the feed gas rate. The large net gas flow rate can change the hydrodynamics of the bed and thus affect the rates of heat and mass transfer between the phases.

More recently numerical methods have gained popularity in modelling the multiphase gas-solid flows in fluidised beds. The model by Snider *et al*. (2010) uses an extension of the Eulerian-Lagrangian computational particle fluid dynamics (CPFD) methodology to model the hydrodynamics of a fluidised bed gasifier, and Yu *et al*. (2007) used the two-fluid model (TFM), including the kinetic theory of granular flow (KTGF), to model the gas-solids flows. Although these methods are an exciting new field of growing importance, there is some doubt (Grace and Abba, 2005) as to whether they currently have better predictive capability than simpler methods/models requiring less computational time, such as the two-phase model of Davidson and Harrison (1971).

5.2.1.2 Coal devolatilisation

Due to the relatively high content of volatile matter (20 – 45 wt.%) of bituminous, sub-bituminous and lignite coals, the volatile matter has a significant influence on the composition and flow of the gas produced by fluidised bed gasifiers when gasifying these coals. A fluidised bed gasifier simulation model therefore needs to incorporate a sub-model which predicts the composition and flow of gases and tars that are produced during devolatilisation.

The composition and flow of gases produced by the devolatilisation of coal are affected by the heating rate of coal particles, the maximum devolatilisation temperature, the gases in which devolatilisation occurs, the pressure, particle size and coal type. Due to the many complex reactions that occur during devolatilisation, fluidised bed coal gasifier modellers have resorted to the use of empirical correlations to predict the composition and flow of gases produced by devolatilisation. Table 5.1 shows that the majority of the investigators used the empirical correlation of Loison and Chauvin (1964), which is given by equation (5.12).

$$
\begin{aligned}
X_{H_2} &= 0.157 - 0.868X_{MV} + 1.388(X_{MV})^2 \\
X_{CH_4} &= 0.201 - 0.469X_{MV} + 0.241(X_{MV})^2 \\
X_{CO} &= 0.428 - 2.653X_{MV} + 4.845(X_{MV})^2 \\
X_{CO_2} &= 0.135 - 0.90X_{MV} + 1.906(X_{MV})^2 \\
X_{H_2O} &= 0.409 - 2.389X_{MV} + 4.554(X_{MV})^2 \\
X_{tars} &= -0.325 + 7.279X_{MV} - 12.880(X_{MV})^2
\end{aligned}
\qquad (5.12)
$$

It is surprising that the correlation of Loison and Chauvin (1964) has been used by so many investigators – this correlation does not include the effect of temperature on the composition of the volatiles and predicts a significantly higher tar yield than would be expected for a fluidised bed coal gasifier.

Table 5.1 shows that Lee *et al*. (1998) and Ma *et al*. (1988) developed their own empirical correlations to predict the products of devolatilisation which are applicable to the coals that they used in their investigations. It can be seen from these correlations (Appendix E.1.2.1 and Appendix E.1.2.2) that the gas yield and composition are predicted as a function of gasifier temperature. Neogi *et al*. (1986) used data developed by Yeboah (1980) for Illinois No. 6 coal, which is the coal they (Neogi *et al*., 1986) used for their fluidised bed gasification experiments and modelling work. The composition of the volatiles measured by Yeboah (1980) for Illinois No. 6 coal at temperatures between 600 °C and 800 °C is given in Appendix E.1.2.3.

The models of Ross *et al*. (2005), Yan *et al*. (1998), Saffer *et al*. (1988) and Weimer and Clough (1980) assume that the volatiles are well distributed in the emulsion phase following the assumption of well-mixed solids. The assumption of uniform distribution of volatiles in the emulsion phase seems to be justified since an investigation by Ross *et al*. (2000) has shown that 1.75 mm Bowman coal particles require approximately 10 seconds for complete devolatilisation in a fluidised bed at 950 °C. The investigation of Stein *et al*. (2000) shows that at typical fluidised bed gasification conditions the vertical particle velocities are approximately 1 m/s, which allows uniform distribution of volatiles throughout the emulsion phase in a period of 10 seconds. Uniform distribution of volatiles in the emulsion phase means that a significant percentage of the volatiles will be consumed by combustion in the lower part of the bed where the oxygen concentration is high. The volatiles (H_2 and CO) released into the upper part of the bed can inhibit the rate of the gasification reactions as will be discussed in Section 5.2.1.3.

The models of Ma *et al*. (1988), Gururajan *et al*. (1992) and Saffer *et al*. (1988) assume that the volatiles are released instantaneously at the top of the bed and combine with the gases that are produced by the combustion and gasification in the bed to produce the product gas stream. The assumption of instantaneous volatile release at the top of the bed is questionable, as shown by the studies of Ross *et al*. (2000) and Stein *et al*. (2000).

5.2.1.3 Rates of chemical reactions

As shown in Table 5.1, chemical reactions taking place in a fluidised bed coal gasifier consist of heterogeneous reactions and homogeneous reactions. Heterogeneous reactions occur in the emulsion phase and homogeneous reactions occur both in the emulsion and bubble phases of the fluidised bed.

Heterogeneous reactions

Heterogeneous reactions include reactions between gases and the carbon in the char particles. Heterogeneous reactions that have been included by the majority of the modellers are:

$C + \varphi O_2 \rightarrow 2(1-\varphi)CO + (2\varphi - 1)CO_2$ (5.13)

$C + H_2O \rightarrow CO + H_2$ (5.14)

$C + CO_2 \rightarrow 2CO$ (5.15)

$C + 2H_2 \rightarrow CH_4$ (5.16)

Other modellers (Yan *et al*., 1999; Ma *et al*., 1988; de Souza-Santos, 1989) have also included the reaction of hydrogen and oxygen with sulphur and nitrogen in the coal to form COS, H_2S, NH_3, NO and SO_2. These reactions are given in Appendix E.2.6.

Char combustion (reaction (5.13))

Although uncertainties still exist about many aspects of char combustion, the current view of the char combustion mechanism is that oxygen diffuses from the bulk gas to the char surface where it reacts to form CO, which then burns in the gas phase surrounding the char particle. Oxygen also diffuses through the pores in the char and reacts on the interior surfaces of the char particle. The combustion rate is therefore likely to be controlled by film diffusion in the bulk gas surrounding the char particle, pore diffusion inside the char particle and reaction on the exterior and interior surfaces of the coal particle.

Fluidised bed combustors (FBCs) operate using air/coal feed ratios that are high enough so that the only product of combustion is CO_2 and the value of φ in equation (5.13) is equal to 1. Fluidised bed gasifiers, however, operate using a lower air/coal ratio (sub-stoichiometric) so that both CO and CO_2 are formed and the value of φ in equation (5.13) is within the range $0.5 < \varphi < 1$ (Yan and Zhang, 2000). Due to the uncertainty associated with the value of φ, it is often treated as a fitting parameter in many of the models given in Table 5.1; the value of φ is estimated based on minimising the square of the errors between the measured and predicted values of gasification performance variables.

The modelling studies of Yan *et al*. (1999) assumed that due to the relatively large particle size of char used in fluidised bed gasification (0.5 – 3 mm) and the high rate of the surface reaction, the rate of combustion of char is controlled by film diffusion and is equal to the mass transfer rate of oxygen to the particle surface. The equations

of La Nauze and Jung (1982), which are based on film diffusion, were used to calculate the char combustion rate.

$$r_{O_2} = \varphi k_{ep}\left(\frac{p_{O_2}}{R(T_e + 273)}\right) \tag{5.17}$$

$$k_{ep} = \frac{D_g}{d_p}\left[2\varepsilon_{mf} + 0.69\left(\frac{u_g}{\rho_g D_g}\right)^{1/3}\left(\frac{d_p v_g \rho_g}{\mu_g \delta}\right)^{1/2}\right] \tag{5.18}$$

The model of Ma *et al*. (1988) uses the rate expression proposed by Field (1969) for the combustion of bituminous and sub-bituminous coal chars. The rate expression includes a diffusion rate coefficient (k'_d) which depends on the rate of transport of oxygen to the external surface area of the particle and a surface reaction rate coefficient (k'_s) which expresses the combined effects of chemical reactivity and internal pore diffusion.

$$r_{O_2} = k_{O_2} p_{O_2} \tag{5.19}$$

$$\frac{1}{k_{O_2}} = \frac{1}{k_d} + \frac{1}{k_s} \tag{5.20}$$

$$k_d = \frac{0.00533}{d_p \varphi}\left(\frac{T_e + 273}{1600}\right)^{0.75} \tag{5.21}$$

$$k_s = 7252000\left(-\frac{17976}{T_s + 273}\right) \tag{5.22}$$

Several modellers used Arrhenius-type expressions of the form given in equation (5.23) to calculate the char combustion rate. These equations would probably be applicable to cases in which the surface reaction is rate controlling (smaller particles at a lower temperature).

$$\frac{dX}{dt} = k_o \exp(\frac{-E}{RT}) P_{O_2}^n .F(X) \quad (5.23)$$

The models of Snider *et al*. (2010) and Luo *et al*. (1997) assume that the reaction order (n) and the structural factor (F(X)) are equal to one. The models of Chejne and Hernandez (2002), Yu *et al*. (2006) and Weimer and Clough (1980) include a reaction order but also assume that the structural factor is equal to one. The model of Lee *et al*. (1998) includes both a reaction order and structural factor. The structural factor used by Lee *et al*. (1998) is given in equation (5.24) and describes the structural change of the particle according to the shrinking core model.

$$F(X) = (1-X)^{2/3} \quad (5.24)$$

The values of k_o and E in equation (5.23) were obtained from literature based on thermogravimetric analyser tests done on the coals that they were using or on coals that were similar to the coals that they were using. In some cases k_o was used as a fitting parameter in fluidised bed coal gasifier models, i.e. the values of k_o were estimated based on minimising the square of the errors between the measured and predicted values of gasification performance variables.

Char gasification

Char-steam gasification (reaction (5.14))

Table 5.1 shows that the majority of the modellers used the Johnson (1979) equation to calculate the rate of the char-steam gasification reaction. Johnson (1979) used a thermo balance reactor to measure the gasification rates of bituminous coal chars over a wide range of temperatures (797 °C – 1 097 °C) and pressures (0.1 – 7 MPa) in gas mixtures containing varying amounts of CO, CO_2, H_2, H_2O and CH_4. Equation (5.25) gives the expression developed by Johnson to calculate the char conversion rate as a result of steam gasification.

$$\frac{dX}{dt} = f_L k_I F(X) \quad (5.25)$$

In equation (5.25), f_L is the relative reactivity factor of the coal char, F(X) is a structural factor that describes the effect of char conversion on the gasification rate and k_I describes the effect of temperature and the partial pressure of H_2O, CO and H_2 on the gasification rate. Expressions for F(X) and k_I used by Johnson (1979) are given in Appendix E.1.3.1. Since the intrinsic surface steam gasification rate of bituminous coal chars is several orders of magnitude lower that the combustion rate, Johnson's kinetic expression (equation (5.25)) does not incorporate the effects of external and intra-particle gas diffusion resistances. The inhibiting effects of CO and H_2 on the steam gasification rate of coal chars are included in the k_I term of equation (5.25) as shown in Appendix E.1.3.1.

The relative reactivity factor (f_L) is dependent on the reactivity of the char. Johnson (1979) recommended a correlation, based on the dry ash-free carbon content of the coal, the gasification temperature and pre-treatment temperature of the char to estimate f_L, which is given by equation (5.26).

$$f_L = 6.2Y_c(1-Y_c).\exp\left[-\frac{9340}{R}\left(\frac{1}{T}-\frac{1}{T_p}\right)\right] \qquad (5.26)$$

Most of the modellers, however, used f_L as fitting parameters in their models, since equation (5.26) was developed using American bituminous coal chars and would not necessarily be applicable to sub-bituminous coals and lignites.

Other modellers (Luo *et al*., 1997; Chejne and Hernandez, 2002; Hamel and Krumm, 2001) used Langmuir-Hinshelwood-type rate equations to calculate the char-steam gasification rates. These equations have the form:

$$\frac{dX}{dt} = \frac{k_{H_2O1}[p_{H2O}]}{1+k_{H_2O2}[p_{H2O}]+k_{H_2O3}[p_{H2}]+k_{H_2O4}[p_{CO}]}F(X) \qquad (5.27)$$

Equation (5.27) shows that due to the presence of the partial pressure of H_2 and CO in the denominator of the equation, the inhibiting effects of these gases have been taken into account in the calculation of the char-steam gasification rate. The disadvantage of

this type of rate equation is that it has four parameters (k_{H2O1}, k_{H2O2}, k_{H2O3} and k_{H2O4}) compared to the Johnson equation, which only has one (f_L). The model developed by Luo *et al*. (1997) uses kinetic parameters determined by Matsui *et al*. (1985), using a thermogravimetric analyser for 'SS 5' coal, which is one the coals they used for their experimental and modelling work.

Lee *et al*. (1998), Neogi *et al*. (1986) and Weimer and Clough (1980) used the Arrhenius equation similar to equation (5.23). The use of this equation, which does not include the inhibiting effects of CO and H_2, is questionable since many investigations (Goyal *et al*., 1989; Njapha, 2003; Everson *et al*., 2006; Roberts and Harris, 2007; Huang *et al*., 2010) have confirmed the strong inhibiting effects of the reaction products CO and H_2 on the char-steam gasification rate.

Char-CO_2 gasification (equation (5.15))

Studies by Ye *et al*. (1997) found that the char-CO_2 gasification rate (Boudourd reaction) is significantly lower (3 to 10 times) than the char-steam gasification rate. Due to the lower char-CO_2 gasification rate, reaction models used to calculate the char-CO_2 gasification rate usually do not account for external and internal particle diffusion of CO_2.

The models of Luo *et al*. (1997) and Chatterjee *et al*. (1995) use expressions of the Langmuir-Hinshelwood type developed by Matsui *et al*. (1987) and Elliott (1981) respectively to calculate the char-CO_2 gasification rate. The general form of these equations, which accounts for the inhibiting effect of CO, is given by equation (5.28).

$$\frac{dX}{dt} = \frac{k_{CO_2 1} p_{CO_2}}{1 + k_{CO_2 2} p_{CO} + k_{CO_2 3} p_{CO_2}} F(X) \qquad (5.28)$$

The models of Ross *et al*. (2005), Yan and Zhang (2000), Neogi *et al*. (1986) and Weimer and Clough (1980) simply use first-order rate equations of the Arrhenius type (equation (5.23)) to calculate the char-CO_2 gasification rate. The models of Ross *et al*. (2005) and Yan and Zhang (2000) use the expression developed by Ye *et al*. (1998), which includes a structural factor F(X) given by equation (5.29). The models of Neogi

et al. (1986) and Weimer and Clough (1980) assume that F(X) = 1, which is questionable since it is well known that that the char reactivity decreases with the extent of conversion (X).

$$F(X) = (1-X) \tag{5.29}$$

The exclusion of the inhibiting effect of CO from the rate expressions of an atmospheric pressure model is not likely to have a significant impact on model predictions since the rate of the char-CO_2 gasification reaction is low and the CO-inhibiting effect at low pressure is not as strong as in the case of the char-steam gasification reaction (Mühlen *et al*., 1985).

Several investigators (Yan *et al*., 1998; Lee *et al*., 1998; Ciesielczyk and Gawdzik, 1994; Ma *et al*., 1988) did not include the char-CO_2 reaction in their models. The reason given is that the char-CO_2 reaction is not an 'independent reaction'. It is interesting to note that Yan did include the char-CO_2 reaction in later versions of his model (Yan *et al*., 1999; Yan and Zhang, 2000).

H_2-char gasification reaction (reaction (5.16))

Table 5.1 shows that the majority of the modellers used the Johnson (1979) equation to calculate the rate of the H_2-char gasification (methanation) reaction. The form of this equation is similar to the H_2O-char rate expression and is given by equation (5.30)

$$\frac{dX}{dt} = f_L k_{II} F(X) \tag{5.30}$$

The k_{II} term in equation (5.30), which is different from the k_{II} term in equation (5.25), is given in Appendix E.1.3.2

At pressures below 1 MPa (10 bar) the rate of the H_2-char reaction is several orders of magnitude slower that the H_2O-char reaction (Johnson, 1979). Modellers who developed atmospheric pressure models (Lee *et al*., 1998; Luo *et al*., 1997; Neogi *et*

al., 1986; Weimer and Clough, 1980) therefore did not include the H_2-char reaction in their models.

Homogeneous reactions

Homogenous reactions are gas-gas reactions that take place in the interstitial gas phase, the bubble phase and the freeboard of the fluidised bed. Homogeneous reactions that have been included by the majority of the modellers are:

Water-gas shift reaction:

$$CO + H_2O \rightleftharpoons CO_2 + H_2 \qquad (5.31)$$

Gas combustion reactions:

$$CO + 1/2O_2 \rightarrow CO_2 \qquad (5.32)$$

$$H_2 + 1/2O_2 \rightarrow H_2O \qquad (5.33)$$

$$CH_4 + 2O_2 \rightarrow 2H_2O + CO_2 \qquad (5.34)$$

Water-gas shift reaction (equation (5.31))

Table 5.1 shows that the majority of the modellers used the correlations of Karim and Mohindra (1974) and Chen *et al*. (1987) to calculate the rate of the reversible water-gas shift reaction. The rate expression of Karim and Mohindra (1974) is shown in equation (5.35).

$$r_{wgs} = k_{wgsb} C_{CO} C_{H_2O} - \left(\frac{k_{wgsb}}{K_{wgs}} \right) C_{CO_2} C_{H_2} \qquad (5.35)$$

$$k_{wgsb} = (2.978E10).\exp\left(\frac{-44388}{T} \right) \qquad (5.36)$$

$$K_{wgs} = \exp\left(-4.33 + \frac{4577.8}{T} \right) \qquad (5.37)$$

Positive values of r_{wgs} indicate that the forward reaction is taking place and negative values favour the reverse reaction. At equilibrium conditions, the value of r_{wgs} is equal to zero. The rate expression of Chen *et al*. (1987) is given in Appendix E.1.4.1

The models of Yan *et al*. (1998), Chatterjee *et al*. (1995) and Ma *et al*. (1988) assume that the water-gas shift reaction in the emulsion phase occurs on the surface of the char particles and that it is catalysed by iron in the ash present in the char. A second rate expression developed by Wen and Tseng (1979) was therefore included by them to calculate the rate of the catalysed water-gas shift reaction in the emulsion phase (equation (5.38)).

$$r_{wgsc} = f_{wgs} k_{wgse} \left(y_{CO} - \frac{y_{H_2} y_{CO_2}}{y_{H_2O} K_{wgs}} \right) p_{atm} \qquad (5.38)$$

$$k_{wgse} = (1.26E11).\exp\left(\frac{13971}{T}\right) \qquad (5.39)$$

In equation (5.38), f_{wgs} is an adjustable parameter which is dependent on the catalytic activity of the ash in the coal.

The assumption of Neogi *et al*. (1986) that the water-gas shift reaction is at equilibrium is questionable since the rate of the reaction in the bubble phase, which accounts for the greater part of the gas volume (± 80 vol.%) in the reactor, is too low (equation (5.35)) to reach equilibrium.

Gas combustion reaction

Table 5.1 shows that the rate expressions of Haslam (1923) have been used extensively in the literature to calculate the rate of the simultaneous combustion of CO and H_2. The reactions given by equations (5.40) and (5.41) are trimolecular and the oxygen consumption rates are first-order with respect to oxygen.

$$r_{CO} = k_{CO} C_{CO}{}^2 C_{O_2} \qquad (5.40)$$

$$r_{H_2} = k_{H_2} C_{H_2}{}^2 C_{O_2} \qquad (5.41)$$

$$k_{CO} = (2.4602E-12).\exp\left(\frac{-21137}{T} + 24.74414\right) T^3 \qquad (5.42)$$

Haslam (1923) found that in the temperature range 900 °C – 1 500 °C the ratio of the reaction rate constants is approximately equal to 0.35.

$$\frac{k_{co}}{k_{H_2}} \approx 0.35 \qquad (5.43)$$

Yan *et al*. (1998) assumed that the combustion rate of CH_4 is equal to the combustion rate of CO given by equation (5.40).

5.2.1.4 Interphase mass transfer and heat transfer

Mass transfer

In a fluidised bed coal gasifier reactants (O_2 and H_2O) are transferred from the bubble phase to the emulsion phase where they react with the char particles. The reaction products (CO, H_2 and CO_2) are transferred from the emulsion phase to the bubble phase. The rate of transfer of the gaseous species mainly depends on the differences between their concentrations in the bubble and emulsion phases, the bubble velocity and the bubble diameter. Smaller bubbles generally have higher interchange coefficients due to their larger surface area-to-volume ratio.

Sit and Grace (1981) developed a correlation to calculate the interchange coefficient between bubbles and interstitial gas in a bubbling fluidised bed.

$$K_{be} = \frac{U_{mf}}{3d_b} + \left(\frac{4D_g \varepsilon_{mf} U_b}{\pi d_b^{\,3}} \right)^{0.5} \qquad (5.44)$$

The molar transfer rate of species *i* from the bubble gas to the emulsion gas is given by equation (5.45).

$$n_i = K_{be}(C_i^{\,b} - C_i^{\,e}) \qquad (5.45)$$

Equations by Kunii and Levenspiel (1969) and Wen and Fan (1975) have also been used by modellers to calculate the mass interchange coefficient and are given in

Appendix E.1.5.1. The equation of Kunii and Levenspiel (1969) is an extension of the two-phase model of Davison and Harrison (1971), and includes a cloud phase at the boundary of the bubble and emulsion phases. The equations allow for resistances in series at the bubble and cloud boundaries.

Heat transfer

In fluidised bed gasifiers heat transfer occurs between char particles and emulsion gas and between emulsion gas and bubble gas. The heat transfer rates are required to calculate the bubble and emulsion phase gas temperatures as a function of bed height.

Particle-emulsion gas heat transfer

The heat transfer coefficient between burning particles in a fluidised bed and the emulsion gas can be obtained by the correlation proposed by Ranz and Marshall (1952).

$$h_p = \frac{2.0 k_g}{d_p} \qquad (5.46)$$

Bubble-emulsion gas heat transfer

The heat interchange coefficient between the bubble and emulsion gas can be calculated using the equations derived by Kunii and Levenspiel (1969).

$$H_{bc} = 4.5\left(\frac{U_{mf} Cc_{pg}}{d_b}\right) + 5.85\left(\frac{\left(k_g Cc_{pg}\right)^{0.5} g^{0.25}}{d_b^{1.25}}\right) \qquad (5.47)$$

$$H_{ce} = 6.78\left(\frac{\varepsilon_{mf} k_g Cc_{pg} u_b}{d_b^{3}}\right)^{0.5} \qquad (5.48)$$

$$\frac{1}{H_{be}} = \frac{1}{H_{bc}} + \frac{1}{H_{ce}} \qquad (5.49)$$

5.2.1.5 Fines generation and elutriation

Fines are generated in a fluidised bed coal gasifier due to primary fragmentation, attrition and secondary fragmentation of the feed coal (Zhang *et al*., 2002). Primary fragmentation occurs during rapid heating and devolatilisation of coal particles after they have been injected into the gasifier. Rapid heating and devolatilisation creates thermal stresses and internal pressure which weaken the structure of the char particle (Syred *et al.*, 2007). The fragile char particles experience attrition due to particle-particle collisions, particle-wall collisions and interaction with gas-jets from the distributor. Secondary fragmentation occurs when the char particle structure is further weakened due to internal combustion and gasification reactions. The amount of fines generated as a result of fragmentation/attrition depends on coal properties such as volatile matter content and hardness and operating conditions such as temperature, fluidising velocity and char residence time. The amount of fines generated and the final particle size of char in the gasifier affect the hydrodynamics of the bed, the combustion reaction rates and the elutriation of unconverted char particles from the bed and subsequent entrainment by the gas to the gasifier exit.

Due to the complexity of the fragmentation and attrition processes, fluidised bed gasifier modellers have resorted to empirical correlations to obtain the final particle size of the char in the gasifier. In his investigations, Ma (1989) estimated the particle size of the bed char based on the particle size of the feed coal using a linear expression given by equation (5.50).

$$d_{p,char} = a_p + b_p d_{p,coal} \qquad (5.50)$$

The constants a and b in equation (5.50) depend only on the physical properties of the coal since the effects of operating conditions such as temperature, fluidising velocity and residences on the bed char particle size were not included in his model.

The models of Chejne and Hernandez (2002) and Chejne *et al*. (2010) assume that the particle size distribution is dependent on coal properties and the fractional char conversion. Solution of the model equations therefore involves iteration loops to calculate the final particle size, fixed carbon conversion and gasifier temperature.

Other modellers have not reported nor included a correlation to calculate the particle size of the bed char – they presumably estimated or assumed the bed char particle size, which is a model input.

The models of Chejne *et al*. (2010) and Luo *et al*. (1997) give correlations to calculate the entrainment rate of char particles from the fluidised bed gasifier and the solids fraction of the freeboard. Chejne *et al*. (2010) assumed that fines will be entrained from the gasifier if their terminal falling velocity is smaller than their velocity in the freeboard. The assumption of Chejne *et al*. (2010), however, will only apply if the gasifier exit is above the transport disengaging height. The equations to calculate the terminal falling velocity are given in Appendix E.1.6. The model of Luo *et al.* (1998) assumes that the solids fraction above the transport disengaging height, which is given by equation (5.51), is zero.

$$TDH = 4.47 d_b^{\,0.5} \tag{5.51}$$

The solids fraction at a height lower than the transport disengaging height is given by equation (5.52):

$$\gamma_f = \gamma_{fo} \exp\left[-a(z - H_b)\right] \tag{5.52}$$

With "a" being a decay constant determined by equation (5.53).

$$a = \frac{1.65 + 3100 d_p - 0.3}{U} \tag{5.53}$$

5.2.1.6 Model development and solution procedure

The rate models given in Table 5.2 are developed by carrying out mass and energy balances over an incremental vertical section (height) of the gasifier. This results in coupled first-order differential equations with the gasifier height (z) as the independent variable and the gas species concentrations and temperature as the dependent variables.

The model equations are solved by means of two nested iterative loops (Ma *et al*., 1988; Ross *et al*., 2005). The convergence variables are temperature of the bed solids (T_s) in the outer loop and fixed carbon conversion (X) in the inner loop. The initial values of T_s and X are assumed to be constant throughout the bed based on the assumption of perfectly mixed solids. The outlet gas concentrations of the gasifier are obtained by solving the system of differential equations that are derived from the incremental mass and energy balances. Using the calculated outlet gas concentrations of the gasifier, a new fixed carbon conversion is obtained by means of an overall mass balance over the gasifier. The new calculated fixed carbon conversion is compared to the initial guessed value, and a new fixed carbon conversion is guessed using the Wegstein method (Ma *et al*., 1988). This procedure is repeated until the difference between the calculated value and the guessed value is less than 0.5%. When convergence of the inner loop has been declared, the final fixed carbon conversion is used to calculate bed solids temperature by means of an overall energy balance over the gasifier. The calculated bed solids temperature is compared to the initial guessed bed solids temperature and a new temperature is guessed using the Wegstein method. The inner and outer loops are solved repeatedly (iterated) until the difference between the calculated and guessed temperature is less than 0.5%. This gives the final fixed carbon conversion, bed solids temperature and molar flow rates of gaseous species leaving the gasifier. More details of the development and solution procedure of a fluidised bed coal gasifier model are given in Section 5.3.

The models of Chejne and Hernandez (2002) and Chejne *et al*. (2010) include a third iterative loop that solves the diameter of the char particles as the inner loop. It is expected that inclusion of a third loop will increase the computation time significantly, which has to be justified against increased predictive capability.

5.2.1.7 Model parameters

Quantities appearing in the equations of mathematical models usually consist of variables and parameters. The variables are usually the inputs and outputs of the system. Parameters are ‘constants’ that are introduced into models which characterise the inherent properties or nature of the system (Bard, 1974).

Rate equations, which are used to describe the rate of combustion and gasification reaction in a fluidised bed coal gasifier, have parameters that are characteristic of the coal that is gasified. In the overall energy balance equation, a parameter is introduced to describe the heat losses from the gasifier and is characteristic of the size and shape of the gasifier.

Many of the fluidised bed gasifier models that were developed before 1995 (Table 5.1) have at least four parameters. The parameters in the model of Ma *et al.* (1988) are the char-steam gasification reactivity factor (f_L), the combustion product distribution coefficient (φ), the rate of the catalytic water-gas shift reaction (f_{wgs}) and the heat losses from the gasifier (Q). Later models of Yan and Zhang (2000) and Ross *et al.* (2005) eliminated φ as a parameter, since they found that if homogeneous gas combustion is included in the model equations, φ can be fixed at 0.85 with little effect on model prediction. The rate of the catalytic water-gas shift reaction (f_{wgs}) was also eliminated as a model parameter, since it was assumed that the gas in the emulsion phase is in equilibrium. These models were therefore reduced to only two parameters.

5.2.1.8 Comparisons of model predictions from the literature with experimental results

Table 5.3 shows that only two modellers have not compared their model predictions with experimental results. The experimental results that the modellers used were results from the literature and results generated in-house using pilot-scale fluidised bed coal gasifiers. A summary of model prediction is given in Table 5.3. The model of de Souza-Santos (1989) compared simulation results to fluidised bed combustion data. The data of the model were, however, later compared to fluidised bed coal gasification data of Ocampo *et al.* (2003) reported in de Souza-Santos (2010).

The following procedure was followed by many of the modellers to evaluate the predictive capability of their models.

1) Parameters for the model are estimated by minimising the sum of squared deviations between predicted and measured gasifier performance variables for a number of experiments on a particular coal. The objective function to be minimised is given by equation (5.54).

Table 5.3: Summary of selected fluidised bed coal gasification modelling studies – Comparison with experimental data

Investigator	Year	Country	Comparison with experimental data	Number of tests	Number of parameters	Percentage deviation in gas conc.[1] (%)	Method of comparison	Reported predictive capability
Chejne	2010	Colombia	Yes - Kawabata	6	N/R	8 – 30	Percentage error in gas conc.	Satisfactory
Snider	2010	USA	No	N/R	N/R	N/R	N/R	N/R
Yu	2006	China	Yes - Ocampo	6	N/R	5 – 20	Percentage error in gas conc.	Good
Ross	2005	Australia	Yes - Xiao	1	3	1 – 11	Percentage error in gas conc.	Good
Chejne	2002	Colombia	Yes - Ocampo	6	N/R	3 – 58	Percentage error in gas conc.	Satisfactory
Hamel	2001	Germany	Yes - Kurkela	7	N/R	0 – 15	Percentage error in gas conc.	Satisfactory
Yan	2000	Australia	Yes - Several[2]	20	3	N/R	N/R	N/R
Yan	1999	Australia	Yes - Several [2]	20	3	0 – 20	Percentage error in gas conc.	Favourable
Yan	1998	Australia	Yes - Newman	3	3	N/R	N/R	Good
Lee	1998	Korea	Yes - Park	N/R	N/R	N/R	N/R	Capable
Luo	1998	Japan	Yes - In-house data	5	2	± 5	On graphs	Good
Chatterjee	1995	India	Yes - In-house data	32	N/R	± 12	On graphs	Satisfactory
Ciesielczyk	1994	Poland	Yes - Banchik	N/R	N/R	N/R	N/R	Satisfactory
Gururajan	1992	Australia	Yes - Several[3]	20	2	0 – 20	Percentage error in gas conc.	Satisfactory
de Souza-Santos	1989	Brazil	Yes - Ocampo	2	N/R	0 – 37	Percentage error in gas conc.	Reasonable
Ma	1988	USA	Yes - In-house data	12	4	0 – 10	Percentage error in gas conc.	Good
Saffer	1988	France	Yes - In-house data	17	N/R	0 – 100	Percentage error in gas conc.	Satisfactory
Neogi	1986	USA	Yes - In-house data	5	N/R	0 – 84	In tables	Satisfactory
Weimer	1980	USA	Yes - Newman	N/R	N/R	N/R	N/R	Reasonable

N/R Not reported

1 Concentration

2 Saffer *et al.*, Kawabata *et al.*, Goyal *et al.* and Newman

3 Saffer *et al*, Kawabata *et al.*, Goyal *et al*

$$Z = \sum_{n=1}^{N} \sum_{o=1}^{O} \left(\frac{x_{on}^{e} - x_{on}^{p}}{x_{on}^{e}} \right)^{2} \qquad (5.54)$$

2) The values of the estimated parameters obtained for a particular coal are used in the model to predict the carbon conversion, bed temperature and concentration of gas species (performance variables) for each experiment. The measured and predicted values are compared using parity plots with the format given in Figure 5.2, which shows the predictive capability of the model by Saffer *et al*. (1988) for the hydrogen concentration of the gas.

The general trend observed in earlier models of Neogi *et al*. (1986), Saffer *et al*. (1988), Ciesielczyk and Gawdzik (1994) and Chatterjee *et al*. (1995) are that they over-predict the H_2 and CO concentrations and under-predict the CO_2 concentration of the syngas. Table 5.2 shows that these models do not include the homogeneous combustion reactions. Later models of Yan *et al*. (1999), Hamel and Krumm (2001) and Chejne *et al*. (2010), which include the homogenous combustion reaction, have better predictive capability of H_2, CO and CO_2.

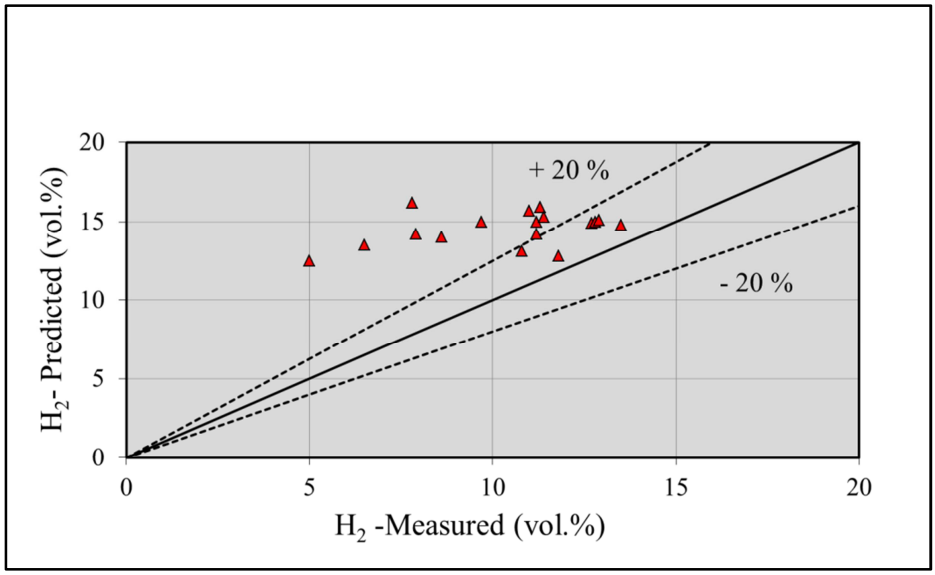

Figure 5.2: Measured and predicted hydrogen concentrations in the gas

Ma *et al*. (1988) and Chejne and Hernandez (2002) concluded that the deviation between measured values and values predicted by their models can be attributed to the uncertainty of the empirical devolatilisation model that they used. Hamel and Krumm (2001) and Ross *et al*.

(2005) concluded that better reaction models for char combustion are required to improve the predictive capability of their models.

5.2.1.9 Sensitivity analysis

In addition to evaluating the predictive capability of their models, researchers have also used their models (using estimated parameters) to investigate the trends in performance variables when input conditions are varied. Ma *et al*. (1988) investigated the effect of oxygen/carbon feed ratio, steam/carbon feed ratio, bed height and gasifier pressure on fixed carbon conversion, bed temperature, gas production rate and H_2/CO ratio in the gas. They found that increasing the oxygen/carbon feed ratio while keeping the fluidising velocity and steam/carbon feed ratio constant increased the bed temperature and the fixed carbon conversion. Increasing the steam/carbon feed ratio decreased the bed temperature and fixed carbon conversion. The H_2/CO ratio increases with lower O_2/carbon ratios and higher steam/carbon ratios

Weimer and Clough (1980) found that increasing the reactant feed rate while keeping the oxygen/steam ratio and coal feed rate constant increased the temperature and fixed carbon conversion and decreased the H_2/CO ratio in the product gas. Increasing the oxygen/steam ratio while keeping the fluidising velocity constant increased the temperature, fixed carbon conversion and maximum temperature in the high-temperature zone above the distributor.

5.2.2 Summary of the literature review of fluidised bed coal gasifier modelling

Fluidised bed coal gasification models are well documented in the literature and consist mainly of equilibrium models and rate models. Rate models often have better predictive capability than equilibrium models since they can predict the fixed carbon conversion, bed temperature and concentration of gas species in the gasifier. Rate models include sub-models for:

- Fluidised bed hydrodynamics.
- Coal devolatilisation.
- Rates of heterogeneous and homogeneous and chemical reactions.
- Rates of heat and mass transfer between phases.
- Fragmentation, attrition and elutriation of char.

The two-phase theory of Davidson and Harrison (1971) has been used by most of the models to describe the hydrodynamics of a fluidised bed coal gasifier. More recently, the computational particle fluid dynamics (CPFD) methodology has gained popularity in modelling the hydrodynamics of fluidised bed gasifiers.

Due to the complexity of the devolatilisation process, many modellers have used empirical correlations from the literature to predict the composition and flow of gases produced by the devolatilisation of coal. Others have developed their own coal-dependent devolatilisation correlations using bench-scale equipment.

Char combustion and steam gasification of char are responsible for more than 90% of the fixed carbon conversion in a fluidised bed coal gasifier. The combustion rate of char has been described by sub-models that are based on film diffusion alone, and by models that include film diffusion, pore diffusion and intrinsic reactivity of the coal. Steam gasification of char has been mostly described by the Johnson equation and Langmuir-Hinshelwood-type expressions. The Johnson equation is the most popular since it only has one parameter, whereas the Langmuir-Hinshelwood equation can have up to six parameters.

Measurements have shown that the gases at the exit of fluidised bed coal gasifiers are seldom in equilibrium, and therefore many models include a rate expression that calculates the rate of the reversible water-gas shift reaction in the gasifier. The rate of the water-gas shift reaction in the emulsion phase has been assumed to be catalysed by the ash in the char particles, and a different rate expression has been used than for the bubble phase.

Comparison of model results with experimental data has shown that many of the earlier models over-predict the concentration of CO and H_2 in the gas and under-predict the concentration of CO_2 in the gas. Later models that included net flow of gases from the emulsion phase to the bubble phase and homogeneous gas combustion obtained lower deviations between the measured and the predicted gas compositions. Other modellers have concluded that the predictive capability of their models can be improved by including better sub-models for coal devolatilisation, char combustion and fragmentation of char.

5.3 Model development, validation and application

5.3.1 Introduction

The literature survey in Section 5.2 forms the basis for the development of a fluidised bed coal gasifier rate model which will be referred to as 'the model'. The sub-models and correlation used to describe the various rate processes in the gasifier were selected from Tables 5.1 and 5.2. The criteria used for selection of the correlations are based on their applicability to high-ash South African coals and the availability of the rate expressions in the literature. Model assumptions, formulation of model equations and solution procedures are based mainly on the papers of Ma *et al*. (1988), Gururajan and Agarwal (1994), Yan *et al*. (1999) and Ross *et al*. (2005).

The results of the pilot-scale fluidised bed gasification tests reported in Chapter 4 and the results reported by Engelbrecht (2008) were used to evaluate the predictive capability of the model. The model is applied to analyse the variation of gas concentrations and temperature in the bed and to evaluate the effect of major operating variables on gasifier performance.

5.3.2 Model assumptions

Gasification of coal in a fluidised bed is a complex process and simplifying assumptions are required in order to assist with the formulation of a model for the process. The model formulation is based on the following assumptions, which are mainly related to the hydrodynamic behaviour of the bed described in Section 5.2.1.1:

1) The hydrodynamic behaviour of the fluidised bed is modelled by the two-phase theory of fluidisation, that is, the fluidised bed consists of a bubble phase and an emulsion phase that can be further divided into an interstitial gas phase and a solid phase.

2) The emulsion phase, containing all the solids, remains at incipient (minimum) fluidisation conditions and all gas in excess of that required to maintain incipient fluidisation condition in the emulsion phase passes through the bed in the bubble phase.

3) All gases in both the emulsion and bubble phases are assumed to be in plug flow. The solids are perfectly mixed in the emulsion phase and have a uniform temperature, size, density and carbon content throughout the bed.

4) The gas generated in the emulsion phase due to heterogeneous reactions and coal devolatilisation which is in excess of that required to maintain minimum fluidisation conditions flows to the bubble phase (net flow).

5) Mass transfer between the bubble phase and the emulsion phases is due to both molecular diffusion (driven by concentration differences) and convection (net flow from the bubble to the emulsion phase).

6) The fluidised bed is one-dimensional, with variations in conditions (gas temperature, gas concentrations, bubble size, bubble velocity, bubble fraction, reaction rates and transfer rates) occurring only in the vertical direction (z).

7) Volatiles released from the coal are uniformly distributed in the emulsion phase following the assumption of perfectly mixed solids.

8) The fluidised bed has a uniform carbon content which is equal to the carbon content of the combined bed and cyclone char streams.

9) Transition from bubbling to slugging bed hydrodynamics occurs at a height in the bed where the bubble diameter increases to 60% of the bed diameter.

10) The syngas produced by the gasifier consist of N_2, CO_2, H_2O, H_2, CO, CH_4 and H_2S. The formation of minor gas components such as NH_3, HCN, NO, COS, SO_2, C_2H_6 and tars are not included in the model. The minor gas components represent less than 2 vol.% of the total gas volume.

11) The gasifier operates at atmospheric pressure and the gases behave ideally.

5.3.3 Sub-models selected for rate processes

A summary of the sub-models used by the fluidised bed gasifier model to describe the various rate processes that take place in the fluidised bed is given in Table 5.4. Sections 5.3.3.1 to 5.3.3.6 discuss the rationale for selecting the various sub-models given in Table 5.4.

5.3.3.1 Hydrodynamics

The two-phase model of Davidson and Harrison has been included to describe the hydrodynamic behaviour of the bubbling fluidised bed gasifier. The gases in both the bubble and emulsion phases have been assumed to be in plug flow. The majority of the investigators listed in Table 5.1 have concluded that due to the high bubble velocity in fluidised bed gasifiers, the assumption of plug flow in the bubble phase is justified. They have also concluded that the emulsion gas is neither in plug flow or well mixed, but that plug flow is a better assumption than perfect mixing.

Many of the hydrodynamic models given in Table 5.1 (literature survey) include a jetting region to account for vertical jets originating from perforated plate distributors. Jetting region hydrodynamics has not been included for the region immediately above the distributor since the model is applicable to fluidised beds that have nozzle cap distributors as shown in Figure 4.4, which produce horizontal jets. Slugging bed hydrodynamics has been included in the model when the bubble diameter increases to 60% of the bed diameter, and the correlation of Ormiston *et al*. (1965) is used to calculate the slug fraction of the bed.

5.3.3.2 Devolatilisation

The advantage of this model over most other models (Table 5.1) is that it includes an option to input coal-specific devolatilisation data. A detailed description of the bench-scale reactor that was used to generate devolatilisation data for New Vaal and Grootegeluk coals and the development of the correlations to estimate the products of devolatilisation are given in Chapter 3.4 and Appendix C.3.1.

Table 5.4: Summary of sub-models and correlations used in the fluidised bed coal gasifier model

Sub-model		Correlation	Equation
Hydrodynamics	Minimum fluidising velocity	Geldart	(E.1.1.1a)
	Bubble diameter	Mori and Wen	(5.3)
	Bubble velocity	DH[1]	(5.4)
	Bubble fraction	DH	(5.6)
	Slug fraction	Ormiston	(5.8)
Devolatilisation		CSIR – Chapter 3.4	(C.3.12)
Heterogeneous reactions	Char combustion	La Nauze and Jung	(5.17)
	Char-steam gasification	Johnson	(3.7)
	Char-CO_2 gasification	Ye, Agnew and Zhang	(3.20)
	Char-H_2 gasification	Johnson	(5.30)
Homogeneous reactions	Non-catalytic WGSR[2]	Karim and Mohindra	(5.35)
	Catalytic WGSR	Wen and Tseng	(5.38)
	CO combustion	Haslam	(5.40)
	H_2 combustion	Haslam	(5.41)
	CH_4 combustion	Haslam	(5.40)
Interphase mass transfer	Emulsion to bubble transfer by diffusion	Sit and Grace	(5.44)
	Net flow	Derived from Yan	(E.2.2e)
Interphase heat transfer	Particle to emulsion	Ranz and Marshall	(5.46)
	Emulsion to bubble	Kunii and Levenspiel	(5.49)
Attrition		Ma	(5.50)
Elutriation		Geldart	(E.1.6a)
Freeboard void fraction		Horio	(5.52)
Transport and thermodynamic properties		Appendix (E.2.5)	several

[1] Davidson and Harrison [2] Water-gas shift reaction

5.3.3.3 Heterogeneous reactions

Char combustion

As discussed in Section 5.2.1.3, the correlation of La Nauze and Jung (1982) is applicable to cases where the char combustion rate is controlled by film diffusion and is equal to the mass transfer rate of oxygen to the particle surface. Film diffusion would be the rate controlling

step in the case of reactive coals that have a particle size in the range of ±0.5 – ±3 mm, which is typical for fluidised bed coal gasification.

Char-steam gasification

The advantages of the Johnson rate equation are that it was developed using bituminous coals, it has only one parameter (f_L) and accounts for the inhibiting effects of CO and H_2 on the char-steam reaction rate. The values of f_L of 8.65 and 1.9 for New Vaal and Grootegeluk coals respectively were obtained using a thermogravimetric analyser (Chapter 3.2).

Char-CO_2 gasification

The rate equation of Ye *et al*. (1997), which was referred to in Chapter 3.3 and Section 5.2.1.3, is used to calculate the rate of the char-CO_2 gasification reaction.

$$\frac{dX}{dt} = k_{0CO_2} \exp\left(\frac{-E_{CO_2}}{RT}\right) p_{CO_2} (1-X)^{\beta} \qquad (3.20)$$

The parameters in equation (3.20) are the pre-exponential factor (k_{0CO2}), Arrhenius activation energy (E_{CO2}) and grain model structural factor (β) that were obtained for New Vaal and Grootegeluk chars by means of thermogravimetric analyser tests (Engelbrecht, 2008) and are given in Table 5.5.

Table 5.5: Parameters for the char-CO_2 gasification rate equation

Char	E_{CO2} (kJ/mol)	$\ln(k_{0CO2})$ ($atm^{-1}s^{-1}$)	β
New Vaal	180	11.82	0.64
Grootegeluk	252	16.54	0.92

Char-H_2 gasification

The Johnson rate equation (equation (5.30)) has been included in the model to calculate the rate of the char-hydrogen gasification reaction. This equation uses the relative reactivity factors (f_L) that were obtained for the char-steam gasification reaction (Chapter 3), i.e. 8.65 for New Vaal coal and 1.9 for Grootegeluk.

5.3.3.4 Homogeneous reactions

Table 5.1 (literature survey) shows that the rate expressions of Haslam (1923) and Karim and Mohindra (1974) have been used extensively in fluidised bed coal gasifier models to calculate the rate of the gas combustion reactions and the non-catalytic water-gas shift reaction. The rate constants in these equations are not dependent on the properties of the coal, therefore values given in the literature were used.

A rate expression by Wen and Tseng (1979) is used to calculate the rate of the catalysed water-gas shift reaction in the emulsion phase. The equation includes a parameter (f_{wgs}) which is dependent on the catalytic activity of the ash in the coal. For the present study, estimation of f_{wgs} for New Vaal and Grootegeluk coals by means of laboratory experiments was not attempted. Instead, a value proposed by Ma (1988) for bituminous coals ($f_{wgs} = 5.7 \times 10^{-5}$) was used.

5.3.3.5 Interphase mass transfer

The correlation of Sit and Grace (1981) is used to calculate the interphase mass transfer coefficient since it is applicable to particles that have a minimum fluidising velocity greater than 0.2 ms^{-1}, which would typically be the case for particles in a fluidised bed coal gasifier.

As explained in Sections 5.2.1.1 (Hydrodynamics) and 5.3.2 (Model assumptions), net flow occurs when gas flows from the emulsion phase to the bubble phase because of excess gas being generated in the emulsion phase due to combustion reactions, gasification reactions and coal devolatilisation. Yan *et al*. (1998) was the first investigator to include net flow into his model. Equation (E.2.6a) derived in Appendix E.2.2 to calculate the net flow is based on the description of net flow given by Yan *et al*. (1998).

5.3.3.6 Interphase heat transfer

The correlations of Ranz and Marshall (1954) and Kunii and Levenspiel (1969) are well established in the literature for the calculation of the particle-to-emulsion and emulsion-to-bubble heat transfer.

5.3.4 Formulation of model equations

The notation convention used in formulating the model equations is given below:

- Gas components O_2, N_2, CO_2, H_2O, H_2, CO, CH_4 are represented by the subscripts i = 1, 2, 3, 4, 5, 6, 7.

- Reactions (5.13), (5.14), (5.15), (5.16), (5.31), (5.32), (5.33) and (5.34) are represented by the subscripts j = 1, 2, 3, 4, 5, 6, 7, 8.

- The stoichiometric coefficient of component i in reaction j is represented by v_{ij}. For reactants v_{ij} is negative and for products it is positive.

The reactions of sulphur are not considered and the H_2S concentration of the product gas is calculated by assuming that all the sulphur in the coal forms H_2S.

Formulation of the model equations is based on mass and energy balances over an incremental horizontal section of the bed with a thickness of Δz as shown in Figure 5.3. The figure shows that the outlet flows and temperature from an incremental horizontal section of the bed are the inlet flows to the next incremental section.

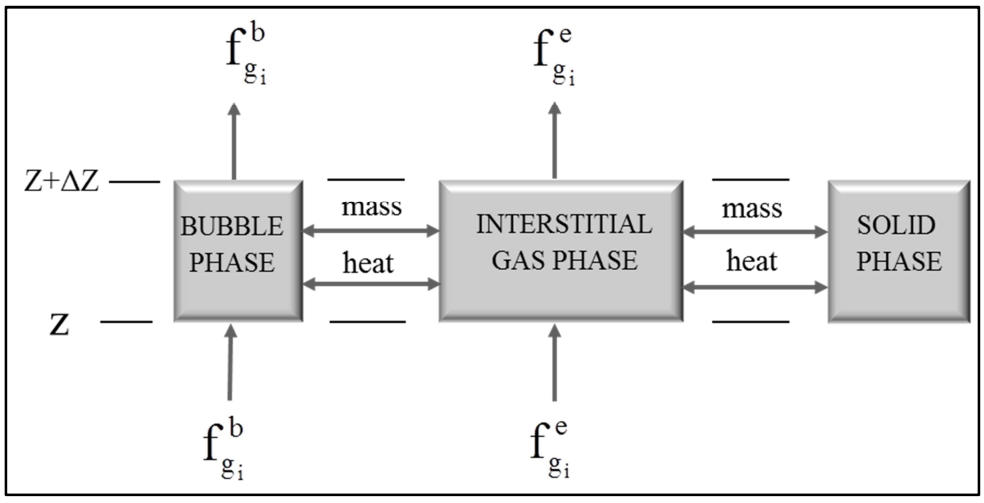

Figure 5.3: Incremental horizontal section of the fluidised bed

5.3.4.1 Mass balance equations

A mass balance for an incremental horizontal section of the bed can be expressed as follows:

$$\left\{\begin{array}{c}\text{output molar}\\ \text{flow from}\\ \text{increment}\end{array}\right\}=\left\{\begin{array}{c}\text{input molar}\\ \text{flow to}\\ \text{increment}\end{array}\right\}+\left\{\begin{array}{c}\text{moles}\\ \text{generated}\\ \text{by reaction}\end{array}\right\}+\left\{\begin{array}{c}\text{net molar input}\\ \text{by interphase}\\ \text{mass transfer}\end{array}\right\}+\left\{\begin{array}{c}\text{molar}\\ \text{input by}\\ \text{net flow}\end{array}\right\}+\left\{\begin{array}{c}\text{molar}\\ \text{input from}\\ \text{volatiles}\end{array}\right\}$$

Bubble phase

Written in symbols, the bubble phase mass balance becomes:

$$f_{gi}^{b}\,|_{z+\Delta z}=f_{gi}^{b}\,|_{z}+\delta A_B\Delta z\sum_{j=5}^{8}v_{ij}r_j+\delta A_B\Delta z(K_{be})_b(C_i^e-C_i^b)+NF_Iy_i^e$$

$$\text{For } i = 1, 2,\ldots..,7 \qquad (5.55)$$

Equation (5.55) does not include a volatiles flow term since the volatiles are released into the interstitial gas of the emulsion phase following the assumption of well-mixed solids.

Emulsion phase

Written in symbols, the emulsion phase mass balance becomes:

$$f_{gi}^{e}\,|_{z+\Delta z}=f_{gi}^{e}\,|_{z}+(1-\delta)\varepsilon_{mf}A_B\Delta z\sum_{j=5}^{8}v_{ij}r_j+(1-\delta)(1-\varepsilon_{mf})A_B\Delta z\sum_{j=2}^{4}v_{ij}r_j''$$

$$(1-\delta)(1-\varepsilon_{mf})A_B\Delta z a_s\sum_{j=1}^{1}v_{ij}r_j'+\delta A_B\Delta z(K_{be})_b(C_i^b-C_i^e)-NF_Iy_i^e+Vf_{gi}\left(\frac{\Delta Z}{H_b}\right)$$

$$\text{For } i = 1, 2, \ldots, 7 \qquad (5.56)$$

Equation (5.56) shows that the net flow term and the volatiles flow term have been included, therefore the equation is different to the equation used by Ma (1989), which did not take into account net flow and volatiles released into the interstitial gas phase. The bubble fraction (δ) in equations (5.55) and (5.56) is calculated using equation (5.6).

5.3.4.2 Energy balance equations

An energy balance for an incremental horizontal section of the bed can be expressed as follows:

$$\left\{\begin{matrix}\text{heat output}\\ \text{by molar}\\ \text{flow}\end{matrix}\right\}=\left\{\begin{matrix}\text{heat input}\\ \text{by molar}\\ \text{flow}\end{matrix}\right\}+\left\{\begin{matrix}\text{heat}\\ \text{generated}\\ \text{by reactions}\end{matrix}\right\}+\left\{\begin{matrix}\text{net heat input}\\ \text{by interphase}\\ \text{heat transfer}\end{matrix}\right\}+\left\{\begin{matrix}\text{heat}\\ \text{input by}\\ \text{net flow}\end{matrix}\right\}-\left\{\begin{matrix}\text{Heat losses}\\ \text{through wall}\\ \text{of reactor}\end{matrix}\right\}$$

Bubble phase

Written in symbols, the bubble phase energy balance becomes:

$$\sum_{i=1}^{7} f_{gi}^{b}\Delta H_{gi}^{b}\,|_{z+\Delta z}=\sum_{i=1}^{7} f_{gi}^{b}\Delta H_{gi}^{b}\,|_{z}-\delta A_{B}\Delta z\sum_{j=5}^{8} r_{j}\Delta H_{rj}^{0}+\delta A_{B}\Delta z(H_{be})_{b}(T^{e}-T^{b})$$

$$+NF_{I}c_{pe}(T_{e}-25)-\delta\pi D_{e}\Delta z h_{w}(T^{s}-T_{a}) \qquad (5.57)$$

Emulsion phase

Written in symbols, the emulsion phase energy balance becomes:

$$\sum_{i=1}^{7} f_{gi}^{e}\Delta H_{gi}^{e}\,|_{z+\Delta z}=\sum_{i=1}^{7} f_{gi}^{e}\Delta H_{gi}^{e}\,|_{z}-(1-\delta)\varepsilon_{mf}A_{B}\Delta z\sum_{j=5}^{8} r_{j}\Delta H_{rj}^{0}$$

$$-(1-\delta)(1-\varepsilon_{mf})A_{B}\Delta z\sum_{j=2}^{4} r_{j}^{''}\Delta H_{rj}^{0}-(1-\delta)(1-\varepsilon_{mf})A_{B}\Delta z a_{s}\sum_{j=1}^{1} r_{j}^{'}\Delta H_{rj}^{0}$$

$$+\delta A_{B}\Delta z(H_{be})_{b}(T^{b}-T^{e})+(1-\delta)(1-\varepsilon_{mf})A_{B}\Delta z a_{s}h_{p}(T^{s}-T^{e})$$

$$-NF_{I}c_{pe}(T_{e}-25)+(1-\delta)\pi D_{e}\Delta z h_{w}(T^{e}-T_{a}) \qquad (5.58)$$

In equation (5.58) the interphase heat transfer consists of transfer between the emulsion phase and the bubble phase and between solids and the interstitial gas of the emulsion phase.

Expansion and conversion ($\Delta z \rightarrow 0$) of equations (5.55) – (5.58) to differential equations produces 16 first-order ordinary differential equations ((5.59) – (5.74)). The independent variable is the height in the fluidised bed (z) and the dependent variables are:

- Molar flowrates of O_2, N_2, CO_2, H_2O, H_2, CO, and CH_4 in the bubble and emulsion phases (f^{b}_{gi} and f^{e}_{gi} for i = 1, 2,…..,7).

- Temperature of the bubble and emulsion phases (T^b and T^e).

Emulsion phase

Oxygen

$$\frac{df_{O_2}^e}{dz} = -\phi A_B(1-\delta)(1-\varepsilon_{mf})\left(\frac{6}{d_p}\right)r_1^{'} - A_B(1-\delta)\varepsilon_{mf}\left(\frac{r_6}{2}+2r_8+\frac{r_7}{2}\right)$$
$$+\delta A_B(K_{be})_b\left(C_{O_2}^b - C_{O_2}^e\right) - NF_R y_{O_2}^e \qquad (5.59)$$

Nitrogen

$$\frac{df_{N_2}^e}{dz} = \delta A_B(K_{be})_b\left(C_{N_2}^b - C_{N_2}^e\right) - NF_R y_{N_2}^e + \frac{Vf_{N_2}}{H_b} \qquad (5.60)$$

Carbon dioxide

$$\frac{df_{CO_2}^e}{dz} = +(2\phi-1)A_B(1-\delta)(1-\varepsilon_{mf})\left(\frac{6}{d_p}\right)r_1^{'} + A_B(1-\delta)\varepsilon_{mf}\left(r_6+r_8+r_{wgsc}\right) - A_B(1-\delta)(1-e_{mf})r_3$$
$$+\delta A_B(K_{be})_b\left(C_{CO_2}^b - C_{CO_2}^e\right) - NF_R y_{CO_2}^e + \frac{Vf_{CO_2}}{H_b} \qquad (5.61)$$

Steam

$$\frac{df_{H_2O}^e}{dz} = -(1-\delta)(1-e_{mf})A_B r_2^{''} + A_B(1-\delta)\varepsilon_{mf}\left(r_7+2r_8-r_{wgsc}\right)$$
$$+\delta A_B(K_{be})_b\left(C_{H_2O}^b - C_{H_2O}^e\right) - NF_R y_{H_2O}^e + \frac{Vf_{H_2O}}{H_b} \qquad (5.62)$$

Hydrogen

$$\frac{df_{H_2}^e}{dz} = (1-\delta)(1-e_{mf})A_B\left(r_2^{''}-2r_4^{''}\right) - A_B(1-\delta)\varepsilon_{mf}\left(r_7-r_{wgsc}\right) + \delta A_B(K_{be})_b\left(C_{H_2}^b - C_{H_2}^e\right)$$
$$-NF_R y_{H_2}^e + \frac{Vf_{H_2}}{H_b} \qquad (5.63)$$

Carbon monoxide

$$\frac{df_{CO}^{e}}{dz} = (1-\delta)(1-e_{mf})A_B\left(r_2^{''} + 2r_3^{''} + 2(1-\varphi)(\frac{6}{d_p})r_1^{'}\right) - A_B(1-\delta)\varepsilon_{mf}\left(r_6 + r_{wgsc}\right)$$
$$+ \delta A_B(K_{be})_b\left(C_{CO}^{b} - C_{CO}^{e}\right) - NF_R y_{CO}^{e} + \frac{Vf_{CO}}{H_b} \qquad (5.64)$$

Methane

$$\frac{df_{CH_4}^{e}}{dz} = (1-\delta)(1-e_{mf})A_B\left(r_4^{''}\right) - A_B(1-\delta)\varepsilon_{mf}\left(r_8\right) + \delta A_B(K_{be})_b\left(C_{CH_4}^{b} - C_{CH_4}^{e}\right)$$
$$- NF_R y_{CH_4}^{e} + \frac{Vf_{CH_4}}{H_b} \qquad (5.65)$$

Temperature

$$\frac{dT^e}{dz} = [\ -(1-\delta)(1-e_{mf})A_B\left(r_2^{''}\Delta H_2^0 + r_3^{''}\Delta H_3^0 + r_4^{''}\Delta H_4^0 + (\frac{6}{d_p})r_1^{'}\Delta H_1^0 - (\frac{6}{d_p})h_p(T^s - T^e)\right)$$
$$-(1-\delta)e_{mf}A_B\left(r_6\Delta H_6^0 + r_7\Delta H_7^0 + r_8\Delta H_8^0 + r_{wgsc}\Delta H_5^0\right) + \delta A_B(H_{be})_b(T^b - T^e) - NF_R(T_e - 25)c_{pe}$$
$$-(1-\delta)\pi D_e h_w(T^e - T_a)\ ] \Big/ \left[f_g^e c_{pe}\right] \qquad (5.66)$$

Bubble phase

Oxygen

$$\frac{df_{O_2}^{b}}{dz} = -A_B\delta\left(\frac{r_6}{2} + \frac{r_7}{2} + 2r_8\right) + \delta A_B(K_{be})_b\left(C_{O_2}^{e} - C_{O_2}^{b}\right) + NF_R y_{O_2}^{e} \qquad (5.67)$$

Nitrogen

$$\frac{df_{N_2}^{b}}{dz} = +\delta A_B(K_{be})_b\left(C_{N_2}^{e} - C_{N_2}^{b}\right) + NF_R y_{N_2}^{e} \qquad (5.68)$$

Carbon dioxide

$$\frac{df_{CO_2}^{b}}{dz} = +A_B\delta\left(r_6 + r_8 + r_{wgs}\right) + \delta A_B(K_{be})_b\left(C_{CO_2}^{e} - C_{CO_2}^{b}\right) + NF_R y_{CO_2}^{e} \qquad (5.69)$$

Steam

$$\frac{df^{e}_{H_2O}}{dz} = +A_B\delta\left(r_7 + 2r_8 - r_{wgs}\right) + \delta A_B (K_{be})_b \left(C^{e}_{H_2O} - C^{b}_{H_2O}\right) + NF_R y^{e}_{H_2O} \qquad (5.70)$$

Hydrogen

$$\frac{df^{b}_{H_2}}{dz} = -A_B\delta\left(r_7 - r_{wgs}\right) + \delta A_B (K_{be})_b \left(C^{e}_{H_2} - C^{b}_{H_2}\right) + NF_R y^{e}_{H_2} \qquad (5.71)$$

Carbon monoxide

$$\frac{df^{b}_{CO}}{dz} = -A_B\delta\left(r_6 + r_{wgs}\right) + \delta A_B (K_{be})_b \left(C^{e}_{CO} - C^{b}_{CO}\right) + NF_R y^{e}_{CO} \qquad (5.72.)$$

Methane

$$\frac{df^{b}_{CH_4}}{dz} = -A_B\delta\left(r_8\right) + \delta A_B (K_{be})_b \left(C^{e}_{CH_4} - C^{b}_{CH_4}\right) + NF_R y^{e}_{CH_4} \qquad (5.73)$$

Temperature

$$\frac{dT^{b}}{dz} = \left[-\delta A_B\left(r_6\Delta H^{0}_{6} + r_7\Delta H^{0}_{7} + r_8\Delta H^{0}_{8} + r_{wgs}\Delta H^{0}_{5}\right) + \delta A_B (H_{be})_b (T^{e} - T^{b}) + NF_R (T_e - 25)c_{pe} \right.$$
$$\left. - \delta\pi D_e h_w (T^{b} - T_a) \right] \Big/ \left[f^{b}_{g} c_{pb} \right] \qquad (5.74)$$

The boundary conditions are the molar flowrates and temperature of the gases entering the fluidised bed via the distributor. The differential equations were solved using the MATLAB® ode45 differential equation solver which gives the values of the dependent variables as a function of bed height (z).

5.3.5 Model solution procedure

The calculation procedure used in the model consists of two nested iteration loops. (Ma *et al*., 1988; Ross *et al*., 2005). The convergence variables are temperature of the bed solids (T_s) in the outer loop and fixed carbon conversion (X) in the inner loop. The initial values of T_s and X are guessed and assumed to be constant throughout the bed based on the assumption of perfectly mixed solids. Values of T_s and X are required for the inner loop calculations which involve solving the system of differential equations (Equations (5.59) to (5.74)) using the

MATLAB® ode45 solver. From the solution of the differential equations, which gives the molar flowrates of the gas species as a function of bed height, the molar flowrates of CO_2, CO and CH_4 at the top of the bed are obtained. Using the molar flowrates of CO_2, CO and CH_4 at the top of the bed, a new fixed carbon conversion is obtained by means of an overall carbon balance over the gasifier (Appendix E.2.3). The new calculated fixed carbon conversion is compared to the initial guessed value and a new fixed carbon conversion is guessed using the method given in Appendix E.2.3. The new fixed carbon conversion is used for the next inner loop calculation. This procedure is repeated until the difference between the calculated and the guessed values of X is less than 0.1%. When convergence of the inner loop has been declared, the final fixed carbon conversion is used to calculate the bed solids temperature (T_s) by means of an overall energy balance over the gasifier (Appendix E.2.4). The calculated bed solids temperature is compared to the initial guessed bed solids temperature and a new temperature is guessed using the method given in Appendix E.2.4. The inner and outer loops are solved repeatedly (iterated) until the difference between the calculated and previously guessed temperature is less than 0.5°C. This gives the final fixed carbon conversion, bed solids temperature and molar flow rates of gaseous species leaving the gasifier. A flowchart of the computational procedure of the model is given in Figure 5.4.

The model code was developed in MATLAB® and run on a 64-bit personal computer. Input data were read and output data were written to Excel spreadsheet files. Several other options were included in the model to make it more flexible. The model options that can be selected are:

1) Both the solids temperature (T_s) and the fixed carbon conversion (X) are constant.
2) The solids temperature (T_s) is constant and the fixed carbon conversion (X) is solved by iteration.
3) Both the solids temperature (T_s) and the fixed carbon conversion (X) are solved by iteration.

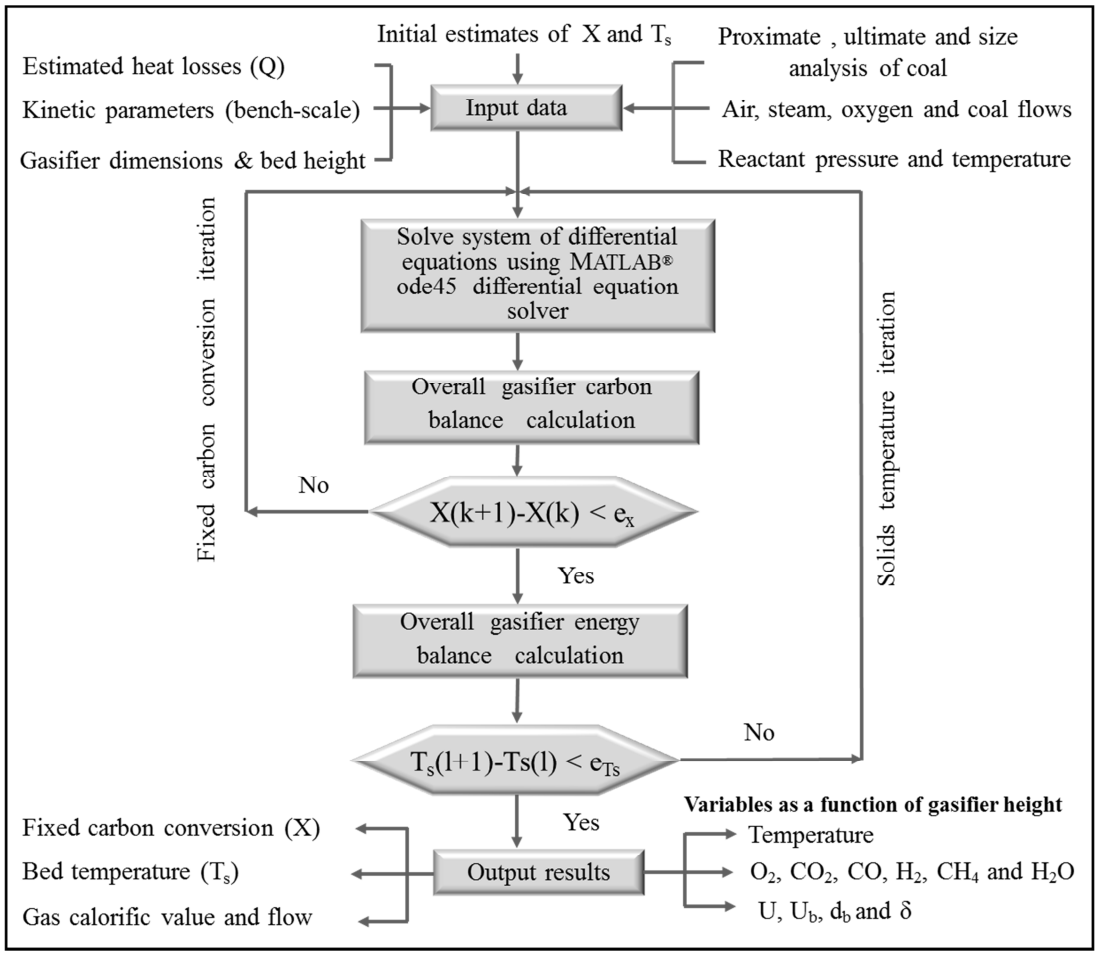

Figure 5.4: Flowchart of the model computational procedure

Options 1) and 2) always converge; however, in the case of option 3 if the initial guessed value of the solids temperature (T_s) is far too high or too low, the calculated temperature to be used for the next iteration could be outside the valid range of the kinetic expressions leading to arithmetic overflows or underflows. The problem can be solved by changing the initial guessed value of the solids temperature after carrying out a few exploratory runs using options 1) and 2).

5.3.6 Testing and validation of the model

In this section the predictive capability of the model is evaluated by using the results of the pilot scale fluidisation tests reported in Chapter 4 and the results reported by Engelbrecht (2008). The difference between the measured and predicted results of all the tests is used to evaluate the validity of the model. Model validation has been defined to mean: "Substantiation that a computerized model within its domain of applicability possesses a

satisfactory range of accuracy consistent with the intended application of the model" (Schlesinger, 1979). In this case the 'intended application' of the model is design, optimisation and scale-up of fluidised bed coal gasifiers.

5.3.6.1 Model parameters

Parameters in fluidised bed coal gasifier models are usually associated with the rates of the gasification reactions, coal devolatilisation and the dimensions of the gasifier. The approach that has been proposed for the present study is to estimate the model parameters by means of bench-scale gasification and devolatilisation tests (Chapter 3) and a heat loss calculation (Appendix E.2.8). The estimated model parameters are given in Table 5.6.

Table 5.6: Estimated model parameters for Grootegeluk and New Vaal coals

Model parameters			New Vaal		Grootegeluk		Reference
Char-steam gasification	f_L		8.65		1.91		Chapter 3.2
Char- CO_2 gasification	$\ln(k_{0CO2})$		11.82		16.54		Chapter 3.3
	E_{CO2}		180		252		
	β		0.64		0.94		
Devolatilisation	a_{CO}	b_{CO}	35.8	-0.033	-27.5	0.053	Chapter 3.4 & Appendix C.3.2
	a_{CH4}	b_{CH4}	-17.9	0.046	131	-0.116	
Gasifier heat losses	Q		37.0 ± 9.0				Appendix E.2.8

5.3.6.2 Predictive capability

The predictive capability of the model is evaluated by comparing model predictions with the results of the seven tests on Grootegeluk and New Vaal coals.

Simulation runs were carried out using the estimated value of Q (37.0 MJ/h) and with the lower and upper confidence limits, i.e. 28.0 MJ/h and 46.0 MJ/h. The results of the simulation runs on New Vaal and Grootegeluk coal are given in Tables 5.7 and 5.8. The values given in Tables 5.7 and 5.8 are the average deviations between the measured and predicted performance variables using the seven tests on each of the two coals.

Table 5.7: Predictive capability of the model for New Vaal coal

Q (MJ/h)	Difference between measured and predicted performance variables (%)							
	Tempe-rature	Fixed carbon conversion	CO	H_2	CH_4	CO_2	Calorific value	Total[1]
28.0	2.4	3.7	17.0	6.6	26.7	16.8	12.0	18.1
37.0	**2.5**	**7.4**	**8.4**	**3.8**	**29.1**	**13.3**	**6.8**	**16.7**
46.0	3.9	12.4	6.9	3.5	31.5	10.6	3.5	19.8

[1] Total of the temperature, fixed carbon and calorific value deviations. Although methane (CH_4) and carbon dioxide (CO_2) have larger percentage deviations, they have little effect on the performance of a fluidised bed coal gasifier since the concentration of methane is low (± 1.5 vol.%) and CO_2 has no energy value.

Simulation runs with Q set at 37.0 MJ/h for New Vaal coal (Table 5.7) show that:

- The deviations between the measured and predicted temperature, fixed carbon conversion and calorific value are less than 10%.

- The deviations between the measured and predicted CH_4 and CO_2 values are 29.6% and 13.1% respectively.

Simulation runs with Q set at 37.0 MJ/h for Grootegeluk coal (Table 5.8) shows that the deviations between the measured and predicted fixed carbon conversion and gas calorific value are higher than 10%. For Grootegeluk coal lower deviations (< 10%) between the measured and predicted temperature, fixed carbon conversion and calorific value of the gas are obtained with Q set at 46.0 MJ/h.

Table 5.8: Predictive capability of the model for Grootegeluk coal

Q (MJ/h)	Difference between measured and predicted performance variables (%)							
	Tempe-rature	Fixed carbon conversion	CO	H_2	CH_4	CO_2	Calorific value	Total[1]
28.0	1.4	15.8	21.0	21.1	39.9	17.3	19.1	36.2
37.0	**1.2**	**10.4**	**12.3**	**18.9**	**41.0**	**13.0**	**14.3**	**25.9**
46.0	4.6	6.9	6.0	17.2	42.5	7.8	9.7	21.1

[1] Total of the temperature, fixed carbon and calorific value deviations

Additional simulation runs were carried out for values of Q outside the confidence limits given above and are presented in Appendix E.2.7.

The deviations between the measured and predicted performance variables for each of the seven tests on New Vaal and Grootegeluk coals using heat loss values (Q) of 37.0 MJ/h and 46.0 MJ/h respectively are presented in Tables 5.9 – 5.10 and Figures 5.5 – 5.12.

Table 5.9: Experimental and predicted gasifier performance variables for New Vaal coal (Q = 37.0 MJ/h)

Performance variable	Oxygen-enriched air and steam										Oxygen and steam		Air and steam		Average deviation (%)
	Test 1		Test 2		Test 3		Test 4		Test 5						
	Exp.[1]	Mod.[2]	Exp.	Mod.	Exp.	Mod.	Exp.	Mod.	Exp.	Mod.	Exp.	Mod.	Exp.	Mod.	
Temperature (°C)	880	917	944	939	943	944	940	929	976	961	931	869	948	919	2.45
Fixed carbon conversion (%)	73.4	69.2	78.5	68.3	79.2	71.7	83.7	80.8	87.5	87.0	81.6	70.3	85.8	80.7	7.41
Dry gas composition															
CO (vol.%)	16.60	18.72	19.90	19.55	19.40	20.07	18.90	19.16	19.10	21.66	21.40	21.27	11.10	13.95	8.44
H_2 (vol.%)	24.00	24.25	24.30	24.56	23.90	24.14	24.20	23.94	22.50	22.82	34.20	37.51	8.60	9.54	3.76
CH_4 (vol.%)	1.30	1.35	1.10	1.60	1.00	1.40	1.00	1.32	1.00	1.40	1.30	1.84	0.70	0.70	29.15
CO_2 (vol.%)	20.70	17.12	18.80	17.01	19.10	16.61	20.30	18.04	20.20	17.09	36.20	38.14	15.80	12.48	13.25
H_2S (vol.%)	-	0.28	-	0.29	-	0.28	-	0.26	-	0.36	-	0.49	-	0.20	-
Calorific value (MJ/kg)	5.74	6.05	6.12	6.29	5.96	6.22	5.93	6.04	5.77	6.28	7.71	8.30	2.82	3.30	6.84

[1] Exp. - Experimental

[2] Mod. - Model

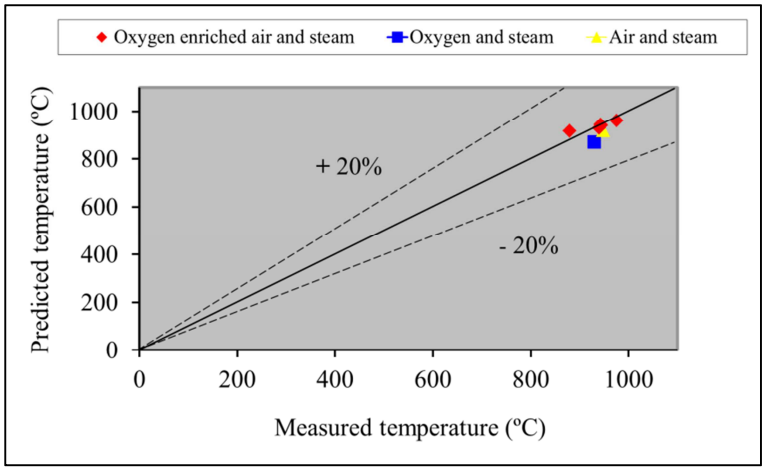

Figure 5.5: Experimental and predicted temperatures – New Vaal coal

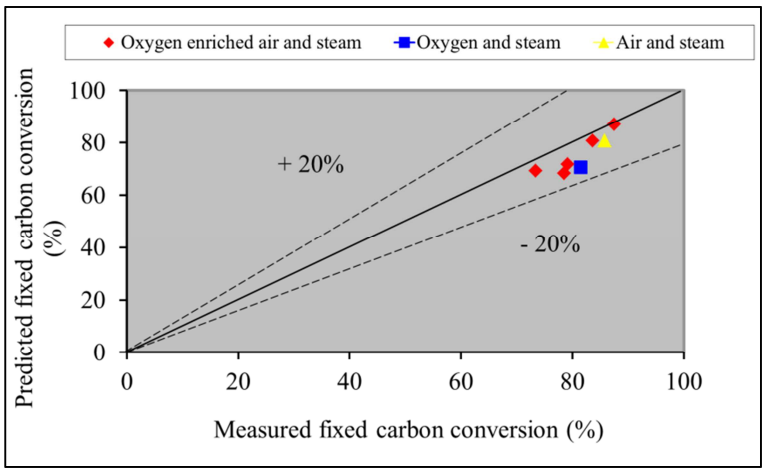

Figure 5.6: Experimental and predicted fixed carbon conversions – New Vaal coal

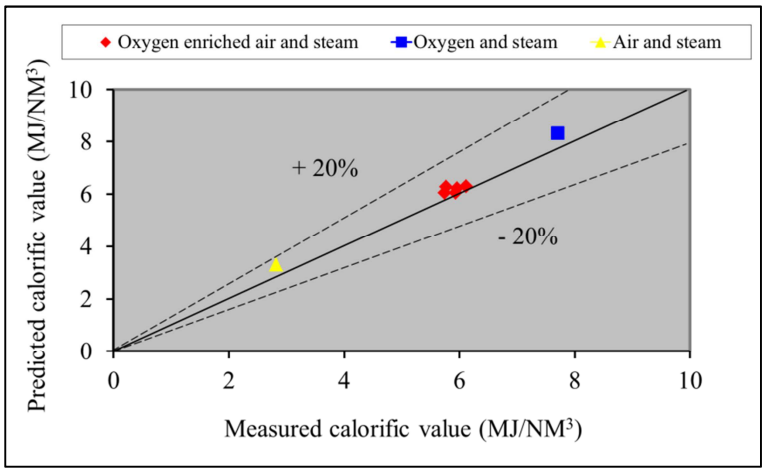

Figure 5.7: Experimental and predicted gas calorific values – New Vaal coal

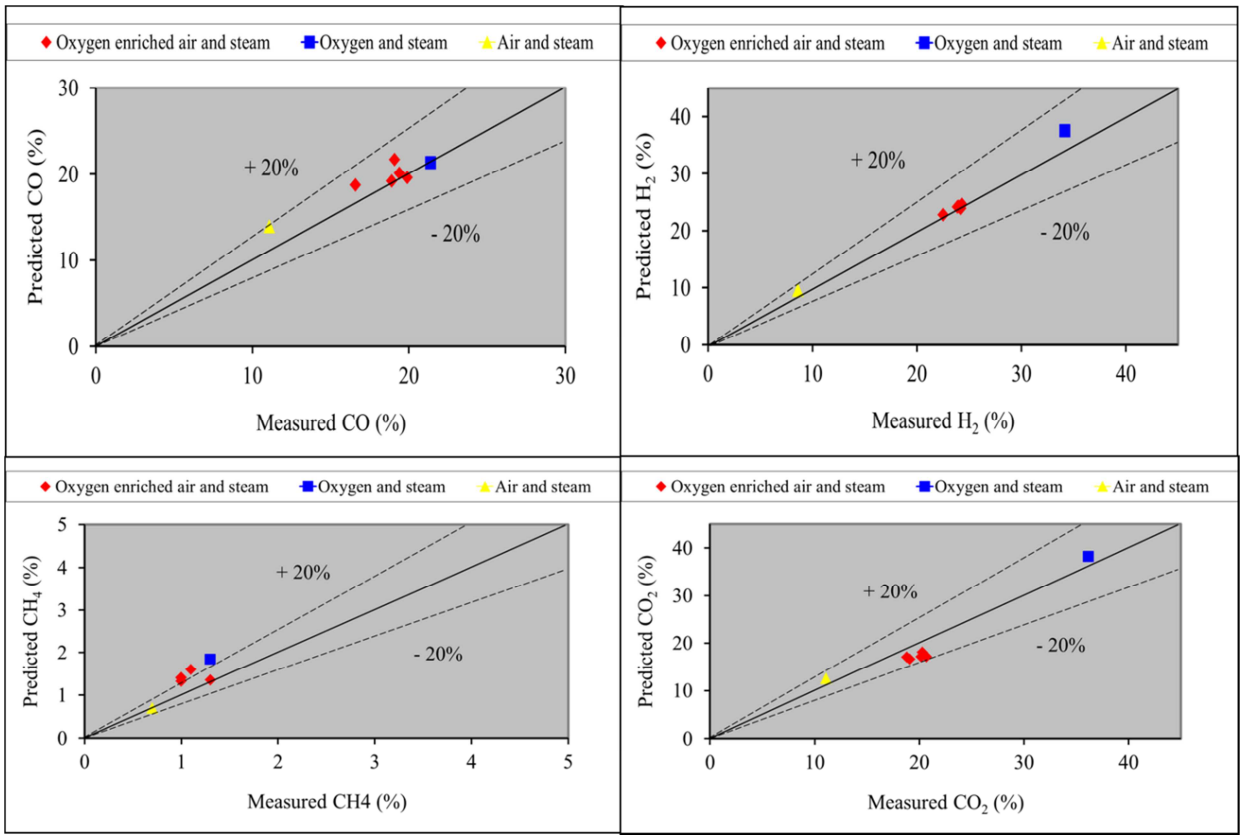

(All gas concentrations are given as vol.%)

Figure 5.8: Experimental and predicted gas concentrations – New Vaal coal

Table 5.10: Experimental and predicted gasifier performance variables for Grootegeluk coal (Q = 46.0 MJ/h)

Performance variable	Oxygen-enriched air and steam										Oxygen and steam		Air and steam		Average deviation (%)
	Test 1		Test 2		Tests 3		Test 4		Test 5						
	Exp.[1]	Mod.[2]	Exp.	Mod.	Exp.	Mod.	Exp.	Mod.	Exp.	Mod.	Exp.	Mod.	Exp.	Mod.	
Temperature (°C)	876.0	808.3	943.0	913.1	976.0	947.8	983.0	951.2	979.0	904.9	918.0	900.9	953.0	900.6	4.57
Fixed carbon conversion (%)	45.2	47.7	57.6	58.6	66.5	72.0	75.1	77.9	82.3	73.4	66.7	70.8	67.0	58.9	6.89
Dry gas composition															
CO (vol.%)	10.5	10.4	13.6	13.3	16.1	16.9	17.0	17.0	16.6	15.2	21.7	17.3	10.2	10.6	5.95
H_2 (vol.%)	14.8	21.4	18.6	21.8	18.6	22.3	20.7	20.6	20.9	19.7	32.6	38.3	9.5	10.9	17.16
CH_4 (vol.%)	2.9	2.5	2.2	2.5	1.7	2.6	1.4	2.6	1.5	2.5	4.9	4.0	1.1	1.6	42.45
CO_2 (vol.%)	20.5	18.8	22.3	19.9	21.2	19.4	20.0	19.3	22.8	20.8	39.5	37.3	14.9	13.5	7.81
H_2S (vol.%)	0.4	0.4	0.4	0.4	0.4	0.4	0.4	0.4	0.4	0.4	0.8	0.8	0.4	0.4	-
Calorific value (MJ/kg)	4.47	5.11	5.06	5.52	5.18	6.11	5.43	5.90	5.45	5.50	9.04	8.83	3.04	3.47	9.66

[1] Exp. - Experimental

[2] Mod. - Model

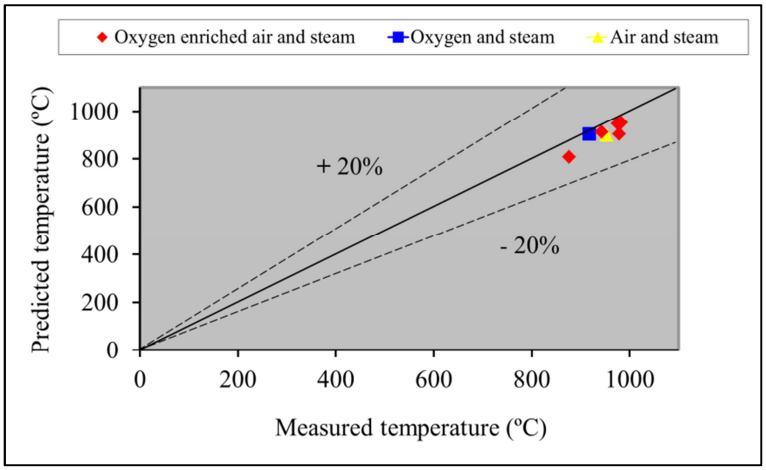

Figure 5.9: Experimental and predicted temperatures – Grootegeluk coal

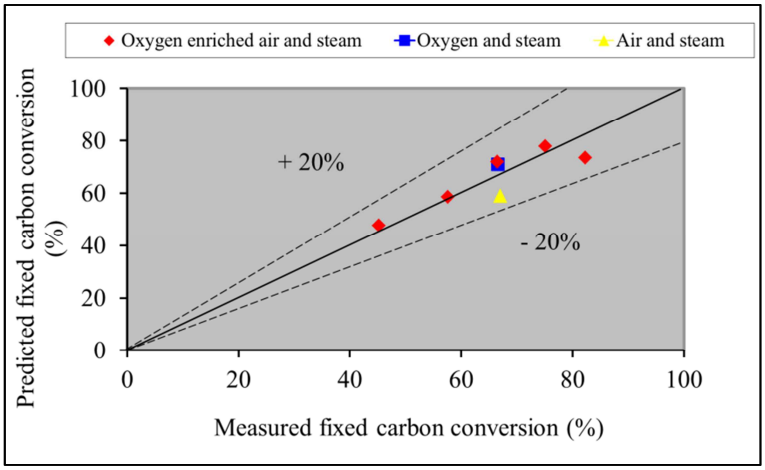

Figure 5.10: Experimental and predicted fixed carbon conversions – GG coal

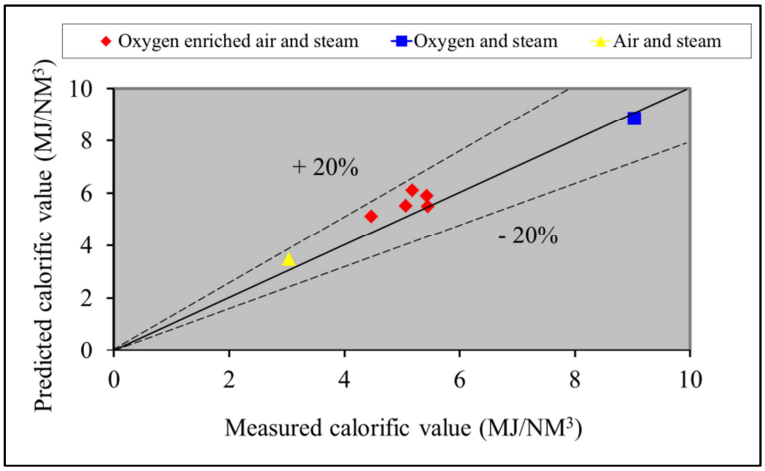

Figure 5.11: Experimental and predicted gas calorific values – Grootegeluk coal

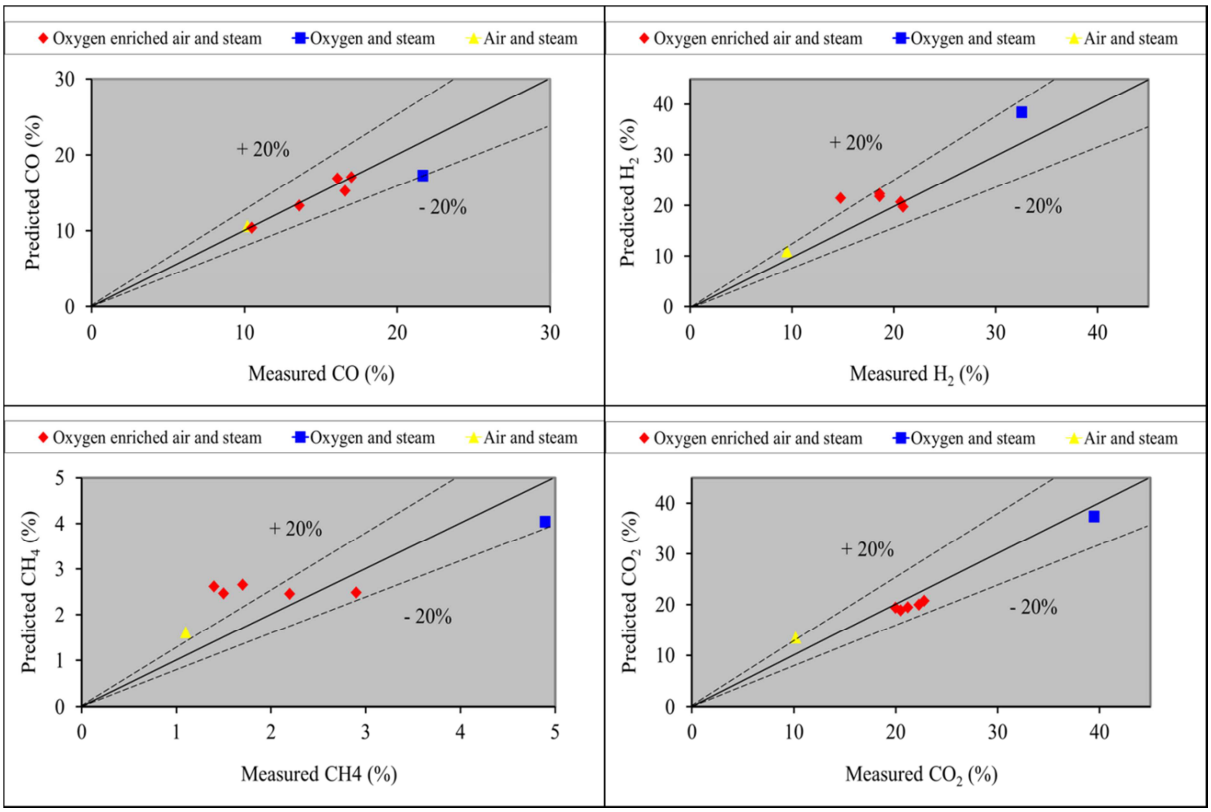

(All gas concentrations are given as vol.%)

Figure 5.12: Experimental and predicted gas concentration – Grootegeluk coal

Differences between experimental results and results predicted by the model shown in Figures 5.5 – 5.12 can be attributed to:

- Assumption inherent in the model given in Section 5.3.2.
- Uncertainty in the values of the model parameters determined by means of bench-scale experiments and heat loss calculations.
- Accuracy (tolerances) of the instruments used for measuring the pilot plant data.

Figures 5.6, 5.8, 5.11 and 5.12 show that the model over-predicts the calorific value of the gas due to over-prediction of CO, H_2 and CH_4 in the product gas. Over-prediction of CO, H_2 and CH_4 could be due to one of the model assumptions (3), which is that all the gases in the bubble and emulsion phases are in plug flow. It appears that in reality a certain degree of back-mixing of gases from the gasification zone higher in the bed to the combustion zone (lower 20% of the bed) takes place. In the combustion zone

CO, H_2 and CH_4 react with oxygen, which results in a lower concentration of these gases in the product gas than predicted by the model.

Over-prediction of H_2 and CH_4 could also be attributed to the model assumption (9) which assumes that the gas produced by the gasifier does not contain NH_3, HCN, C_2H_6, C_2H_4 and tar. The model includes the carbon and hydrogen in these compounds in the predicted H_2 and CH_4 concentrations of the product gas.

It can be concluded that for both coals the total deviation between the measured and predicted temperature, fixed carbon conversion and calorific value of the gas are satisfactory for values of Q in the range 37.0 – 46.0 MJ/h, which are within the calculated (heat loss calculation) estimation limits of Q. A satisfactory deviation (accuracy) is defined in terms of the intended application of the model, which in this case is design, optimisation and scale-up.

The model can therefore be used to predict the performance of other coals in fluidised bed coal gasifiers for which pilot-plant data are not available. The model parameters for these simulations can be estimated by conducting bench-scale tests on these coals and carrying out heat loss calculations on the gasifiers as described in Appendix E.2.8.

5.3.7 Analysis of model output

The advantage of rate models is that they can calculate the values of the performance variables as a function of gasifier height. Test 4 on Grootegeluk coal given in Table 4.10 is used in this section to illustrate a simulation run using the model. Figures 5.13 to 5.20 show model outputs as a function of bed height (z). Analysis of these figures provides useful insights into and understanding of coal gasification in a fluidised bed.

Figure 5.13 shows that all the oxygen in the input gas (air and oxygen) is consumed in the lower 20% of the bed. The reactions that are dominant in this area of the bed (the so-called active zone) are the heterogeneous char combustion reaction (5.13) in the emulsion phases and the homogeneous gas combustion reactions in the bubble and the emulsion phases (equations (5.32) – (5.34)). The high combustion rate of char, CO, H_2 and CH_4 results in a rapid decrease in the O_2 concentration and a rapid increase in

the CO_2 concentration with bed height. The concentration of H_2O increases slightly due the combustion of H_2 and CH_4.

In the upper 80% of the bed the char-H_2O and char-CO_2 reactions (equations (5.14) and (5.15)) are dominant, resulting in an increase in the CO and H_2 concentrations and a decrease in the CO_2 and H_2O concentrations. The concentration increase of CH_4 in the upper 80% of the bed is due to the release of volatiles into the emulsion gas. In the lower 20% of the bed, the volatiles released into the emulsion gas are partially consumed by oxygen.

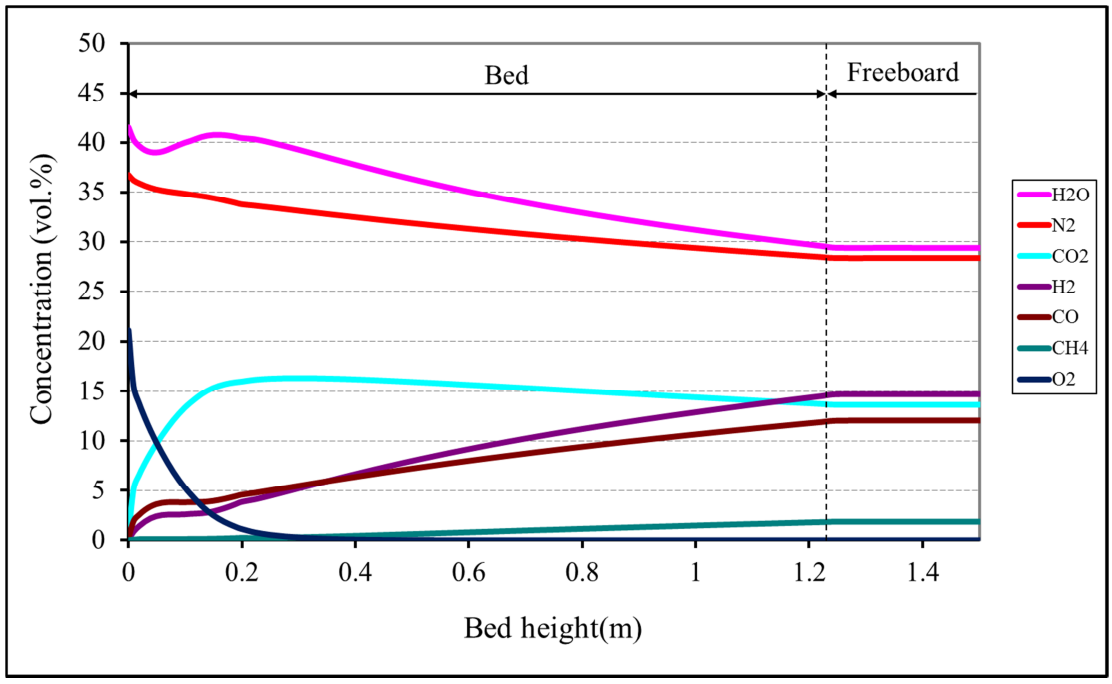

Figure 5.13: Average of bubble and emulsion phase gas concentrations in the bed

The specific reaction rates per unit surface area of char particles for the combustion and gasification reactions are given in Figure 5.14. Figure 5.14 shows that although the char-steam gasification reaction is dominant in the upper 80% of the bed, the rate decreases with an increase in bed height due to higher concentrations of CO and H_2 higher in the bed, which have an inhibiting effect of the char-steam gasification rate (Johnson rate equation).

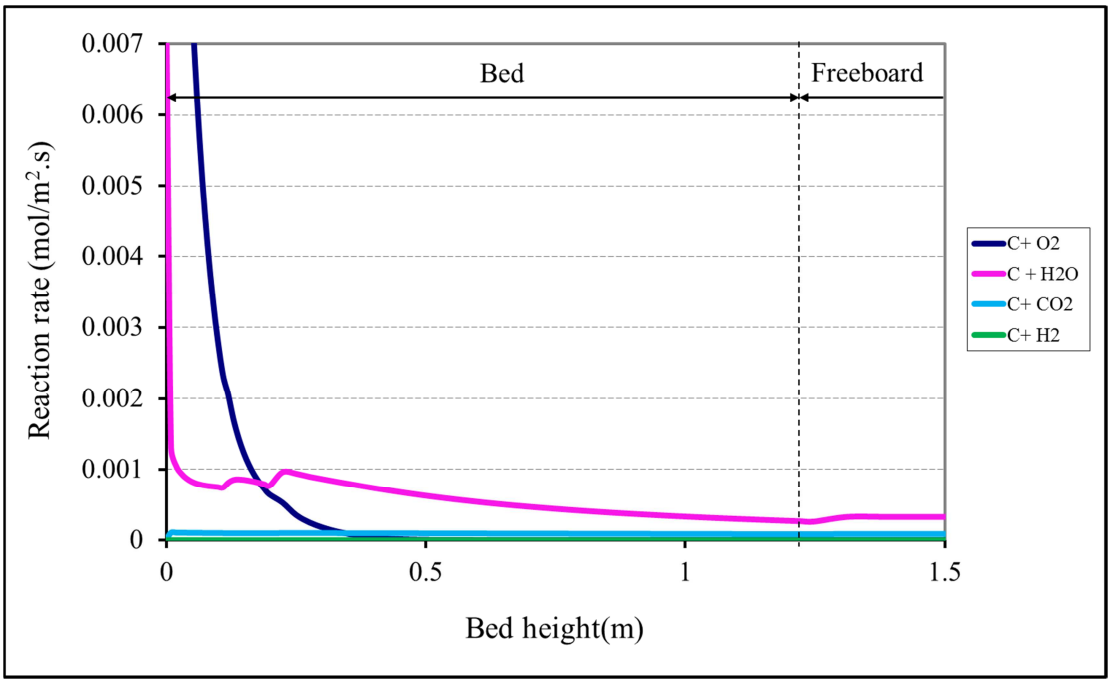

Figure 5.14: Specific reaction rates in the bed

Figure 5.15 shows that due to the high rate of the combustion reactions in the lower part of the bed the predicted temperatures of the bubble gas and the interstitial gas in the emulsion phase are significantly higher than the solids temperature. Above a height of 0.4 m in the bed, the predicted bubble and emulsion gas temperatures are almost equal to the solids temperature following the assumption of isothermal well-mixed solids.

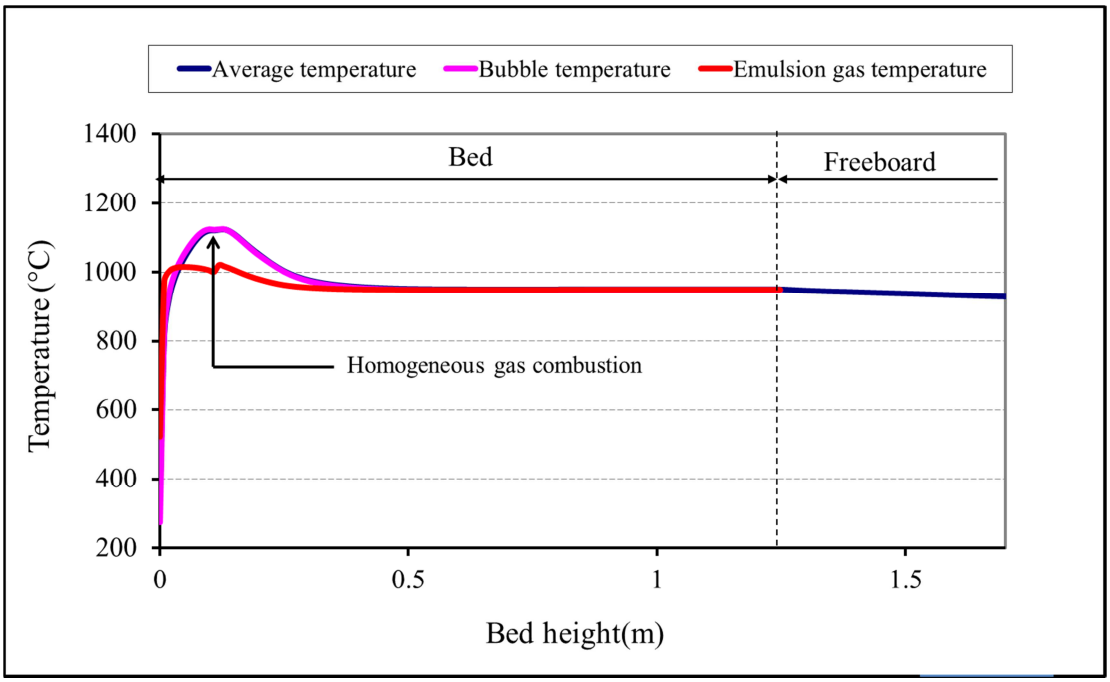

Figure 5.15: Gas temperatures in the bed

The cumulative conversion rate of fixed carbon below a given height in the gasifier is given in Figure 5.16. The figure shows that in the lower 20% of the bed the fixed carbon conversion rate by combustion and gasification reactions is 4.32 kg/h. In the upper 80% of the bed, the fixed carbon conversion rate by gasification reactions (the char combustion rate is zero) is 1.34 kg/h. For fluidised bed coal gasifiers it appears that the 80/20 rule applies; ± 80% of the fixed carbon conversion takes place in the lower 20% of the bed. This could explain why a 40% decrease in bed height had little effect on the measured fixed carbon conversion (Table 5.10) obtained for Test 4 compared to Test 3 using New Vaal coal.

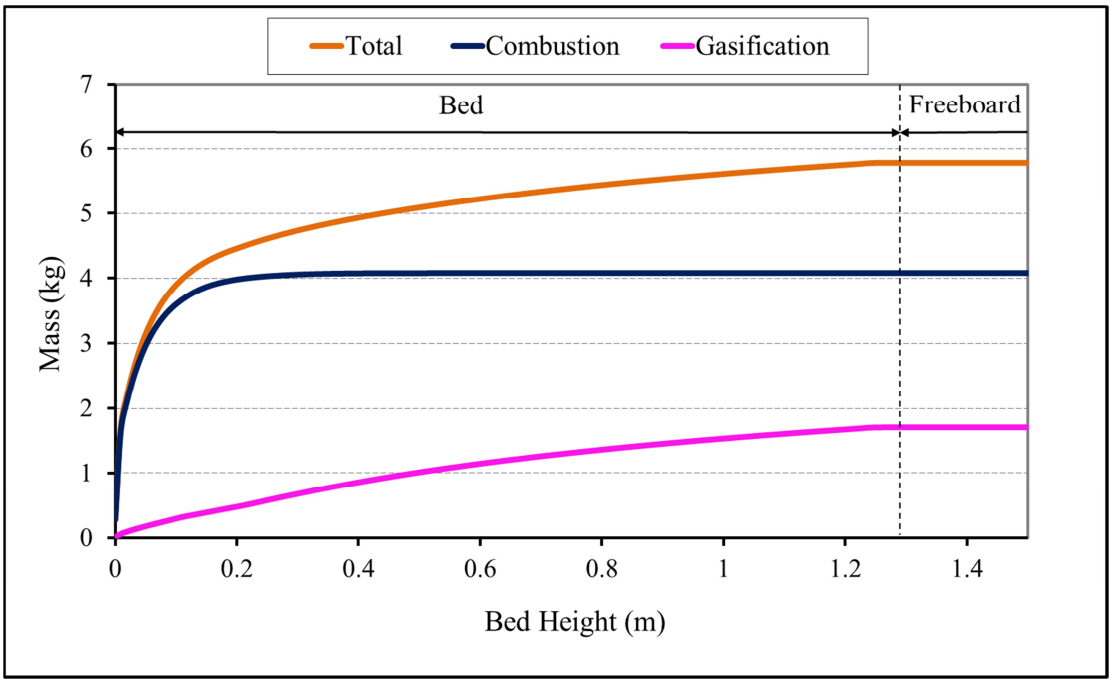

Figure 5.16: Carbon conversion by combustion and gasification

Figures 5.14 and 5.17 show that the char-CO_2 gasification rate is significantly lower that the char-H_2O gasification rate. This is consistent with the results of Ye *et al.* (1997), who studied char-CO_2 and char-H_2O gasification kinetics using a thermogravimetric analyser.

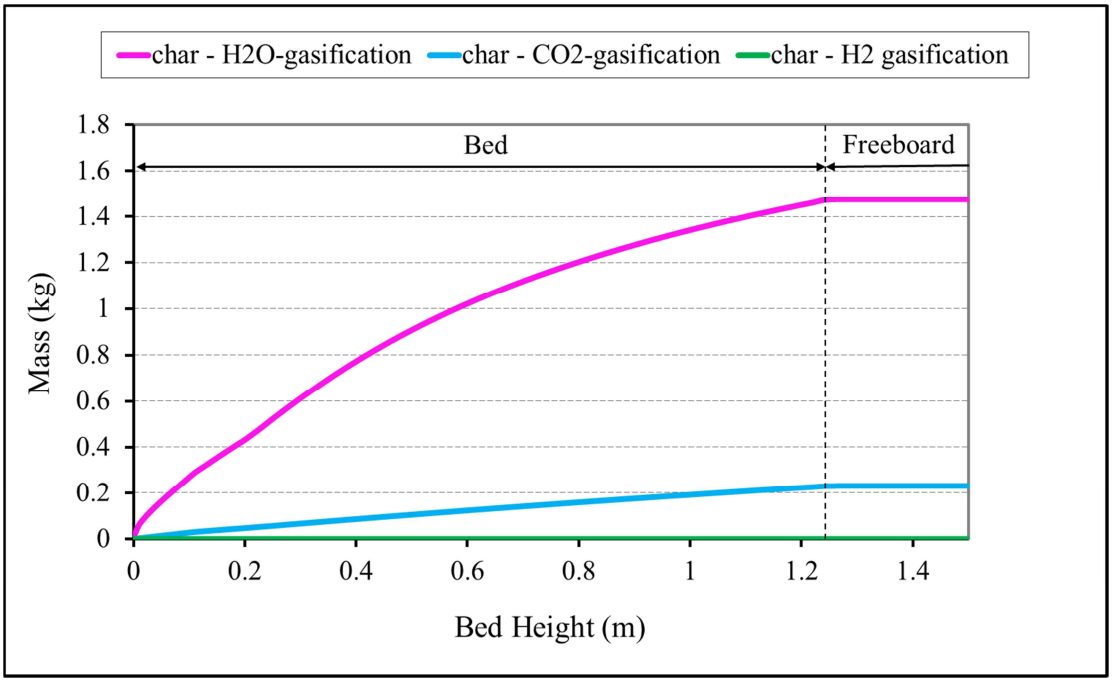

Figure 5.17: Carbon conversion by gasification reactions

Figure 5.18 shows that a large percentage of the bed consists of bubbles and that the total void fraction of the bed is close to 85%. A CFD study by Pain *et al.* (2001) of slugging fluidised bed behaviour found that the total solids volume fraction of slugging beds are typically between 10 and 20%. The increase in void fraction of the bed at 0.1 m above the distributor is the result of transition from bubbling to slugging fluidisation due to the bubble diameter increasing to 60% of the equivalent bed diameter. The typical voidage of a fixed bed gasifier is ± 45%, meaning that significantly higher coal residence times are possible in a fixed bed gasifier compared to a fluidised bed gasifier for a given bed volume.

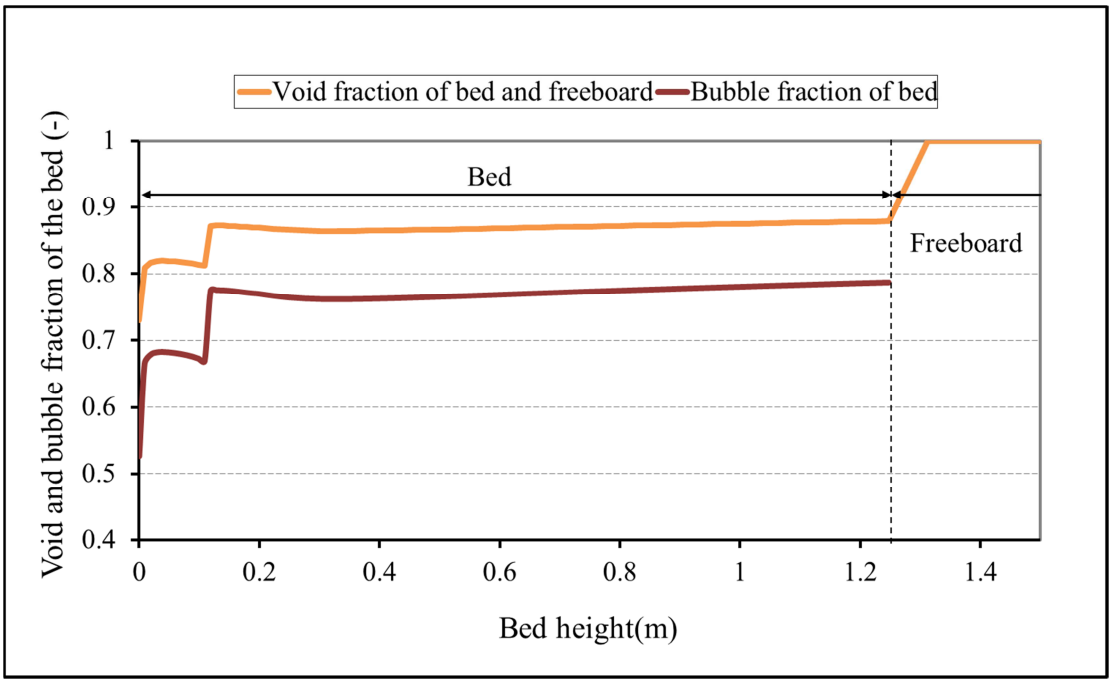

Figure 5.18: Bubble and total void fraction of the bed

Figures 5.19 and 5.20 show that the water-gas shift reaction proceeds in both the forward and reverse directions (negative values) in the bed and that equilibrium is reached at the top of the bed due to the high rate of the water-gas shift reaction in the emulsion phase. Due to the low rate of the water-gas shift reaction in the freeboard (un-catalysed) and the temperature decrease in the freeboard due to heat losses, the gas composition at the gasifier exit is therefore not in equilibrium.

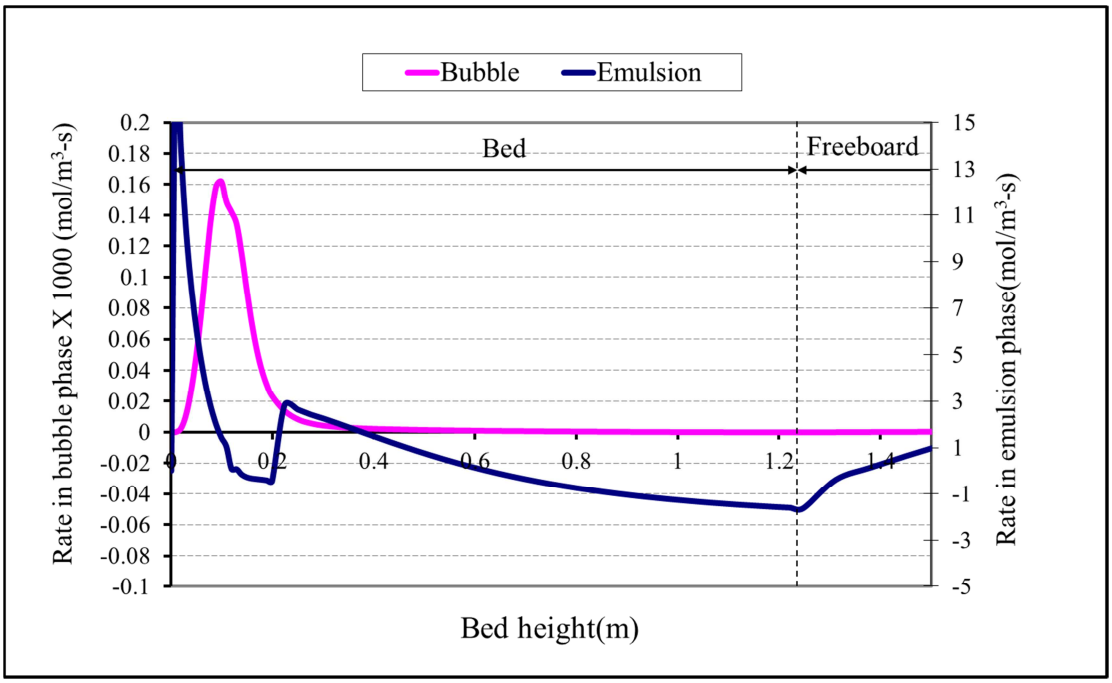

Figure 5.19: Rate of the water-gas shift reaction in the bubble and emulsion phases

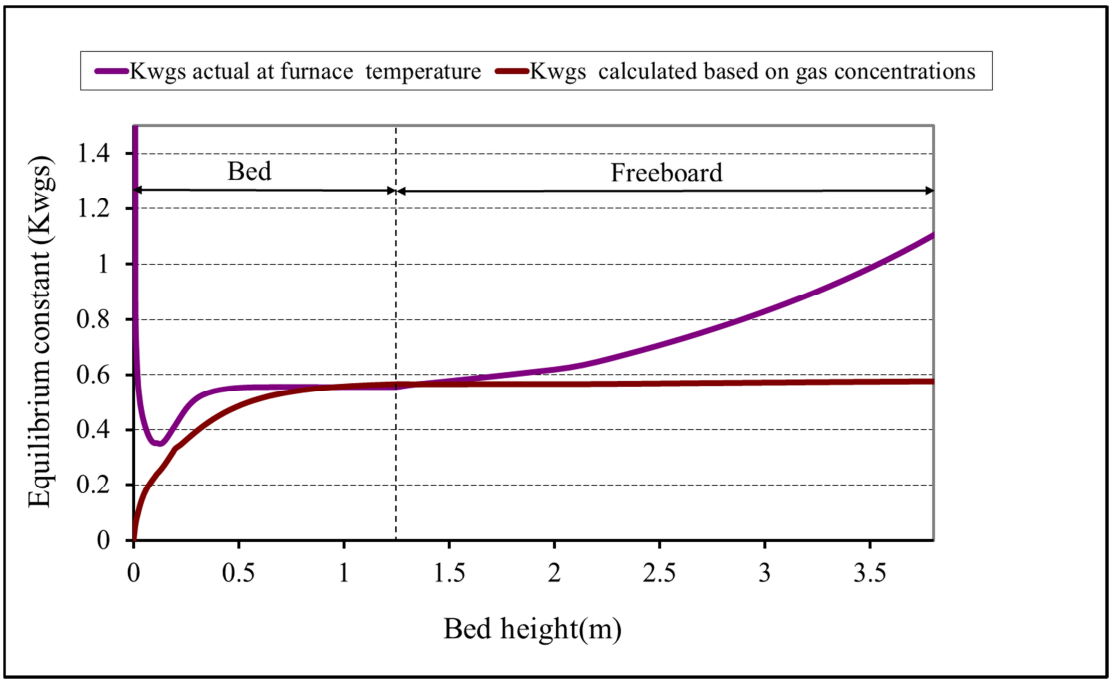

Figure 5.20: Calculated and actual values of the water-gas shift reaction equilibrium constant

Tables 5.11 and 5.12 provide more useful model outputs showing the relative amounts of char converted by combustion and gasification reactions for New Vaal and Grootegeluk coals. It is clear that due to the higher char reactivity of New Vaal coal a greater portion of the char (44.70%) is converted by gasification reactions than for Grootegeluk coal (20.30%). Due to the low char reactivity of Grootegeluk coal at 808 °C (Test1 simulation) the char conversion by gasification reactions is low (±1.0%) resulting in a low fixed carbon conversion (45.2%). Tables 5.11 and 5.12 also shows that a significant percentage of the input oxygen is consumed by homogeneous gas combustion reactions and that the percentage is greater in the case of New Vaal coal (43.98%) than Grootegeluk coal (31.81%). This is due to the higher reactivity of New Vaal coal, which produces higher concentrations of CO and H_2 in the active zone (high O_2 concentration), resulting in higher rates of the homogeneous combustion reaction. Yan and Zhang (2000) also found from their modelling work that homogeneous combustion increases as the coal rank decreases.

The significance of the above observations is that they explain why the calorific value of the gas produced by fluidised bed gasifiers is significantly lower (± 30%) than that produced by fixed bed gasifiers (Parekh, 1982). Due to the plug flow nature of gases and solids in a fixed bed gasifier, the combustion, gasification and devolatilisation zones are essentially separated, which minimises homogeneous gas combustion and produces lower CO_2 concentrations and higher H_2, CO and CH_4 concentrations. Another advantage of minimising homogeneous gas combustion is that more O_2 is available for char combustion, which increases the fixed carbon conversion.

Table 5.11: Percentage of char, oxygen and steam converted by various reactions (New Vaal coal)

Performance variable	Oxygen-enriched air and steam					Oxygen and steam	Air and steam	Average
	Test 1	Test 2	Test 3	Test 4	Test 5			
Char conversion by combustion (%)[1]	52.90	49.49	42.25	52.36	47.38	72.20	70.49	**55.30**
Char conversion by gasification (%)[2]	47.10	50.51	57.75	47.64	52.62	27.80	29.51	**44.70**
Oxygen consumption by char combustion (%)[3]	62.25	57.04	50.31	63.39	60.42	19.20	79.53	**56.02**
Oxygen consumption by gas combustion (%)[4]	37.75	42.96	49.69	36.61	39.58	80.80	20.47	**43.98**
Steam conversion (%)[5]	10.67	18.74	16.65	11.38	19.82	3.55	7.29	**12.59**

Table 5.12: Percentage of char, oxygen and steam converted by various reactions (Grootegeluk coal)

Performance variable	Oxygen-enriched air and steam					Oxygen and steam	Air and steam	Average
	Test 1	Test 2	Test 3	Test 4	Test 5			
Char conversion by combustion (%)[1]	99.00	67.80	65.04	70.16	88.87	76.09	90.97	**79.70**
Char conversion by gasification (%)[2]	1.00	32.20	34.96	29.84	11.13	23.91	9.03	**20.30**
Oxygen consumption by char combustion (%)[3]	76.61	56.33	57.63	66.66	80.00	64.91	75.15	**68.19**
Oxygen consumption by gas combustion (%) [4]	23.39	43.67	42.37	33.34	20.00	35.09	24.85	**31.81**
Steam conversion (%)[5]	0.12	7.39	10.64	9.99	3.23	3.48	3.23	**5.44**

[1] Reaction (5.13)
[2] Reactions (5.14), (5.15) and (5.16)
[3] Reaction (5.13)
[4] Reactions (5.32), (5.33) and (5.34)
[5] Reactions (5.14) and (5.31)

5.3.8 Sensitivity analysis

The pilot-scale fluidised bed gasification tests described in Sections 4.2 and 4.3 in Chapter 4 investigated the effect of bed temperature, char residence time and oxygen enrichment level on the fixed carbon conversion and calorific value of the gas produced in a fluidised bed coal gasifier. In this section the model is used to predict the effect of other operating variables such as input gas (air, oxygen and steam), temperature, dynamic bed height and char particle size on the performance of the gasifier. These variables are likely to be manipulated during the design and operation of fluidised bed gasifiers.

Simulation runs were carried out using Grootegeluk coal and operating conditions similar to those used for Test 4 (Table 4.10). The model parameter determined in Section 5.3.6.1 for Grootegeluk coal and given in Table 5.6 was used for the simulation runs.

5.3.8.1 Temperature of the input gas

Figure 5.21 shows that increasing the temperature of the input gas (air, oxygen and steam) from 250 °C to 550 °C results in a relatively low predicted increase in the calorific value of the gas (± 9.3%) and gasification efficiency (± 6.0%). When the input gas temperature is increased, the oxygen flow to the gasifier must be decreased in order to maintain the bed temperature at 981 °C. Since char combustion plays a major role in the conversion of fixed carbon in a fluidised bed gasifier (Figure 5.16), the reduced oxygen flow results in a decrease in the fixed carbon conversion and therefore a moderate increase in the calorific value of the gas and the gasification efficiency as shown in Figure 5.21.

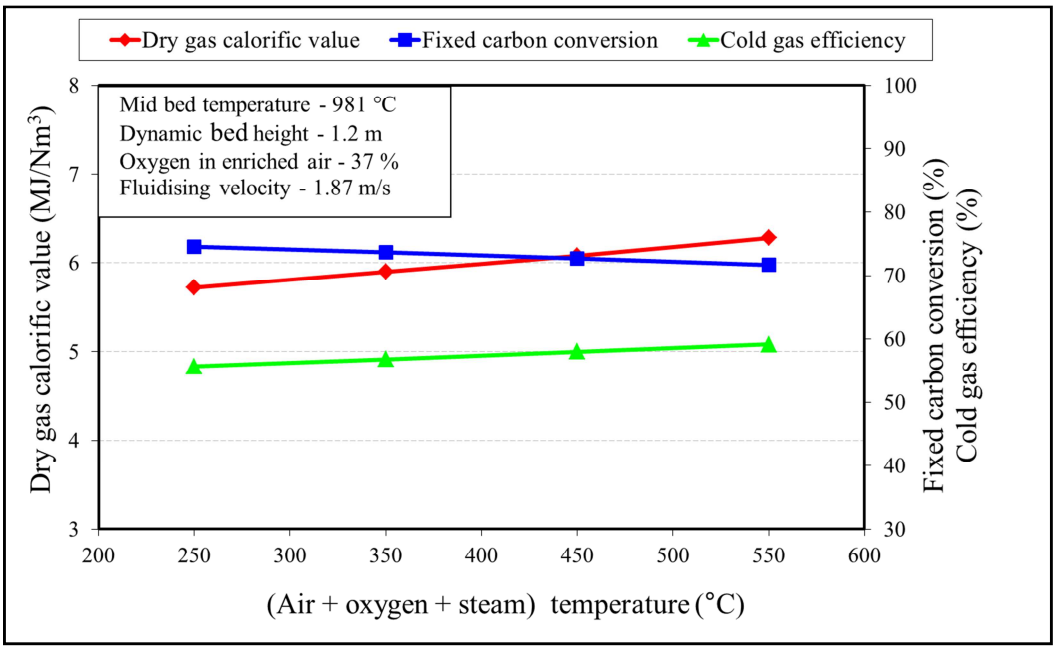

Figure 5.21: Effect of reactant temperature on gasifier performance

The major benefit derived from increasing the input gas temperature is the cost saving as a result of the lower oxygen requirement (± 20%) of the gasifier.

5.3.8.2 Dynamic bed height

Figure 5.22 shows the predicted fixed carbon, calorific value of the gas and gasification efficiency that would be obtained if the gasifier were operated at various bed heights between 0.4 and 2.0 m. It is clear from Figure 5.22 that if the bed height were increased by 0.8 m from 0.4 to 1.2 m, the resulting increase in the fixed carbon conversion would be ±14%. A further 0.8 m increase in the bed height from 1.2 m to 2 m would result in a significantly lower increase (± 6.5%) in the fixed carbon conversion since at higher bed heights:

- the concentrations of CO and H_2 are higher, which slows down (inhibits) the rate of the gasification reactions (equation (5.25)).
- the concentrations of CO_2 and H_2O are lower, which results in lower gasification rates (equations (5.25) and (5.58)).

- the bubble diameter increases, which increases the void fraction of the bed and the rate of transfer of reactants (CO_2 and H_2O) from the bubble phase to the emulsion phase (equation (5.43)).

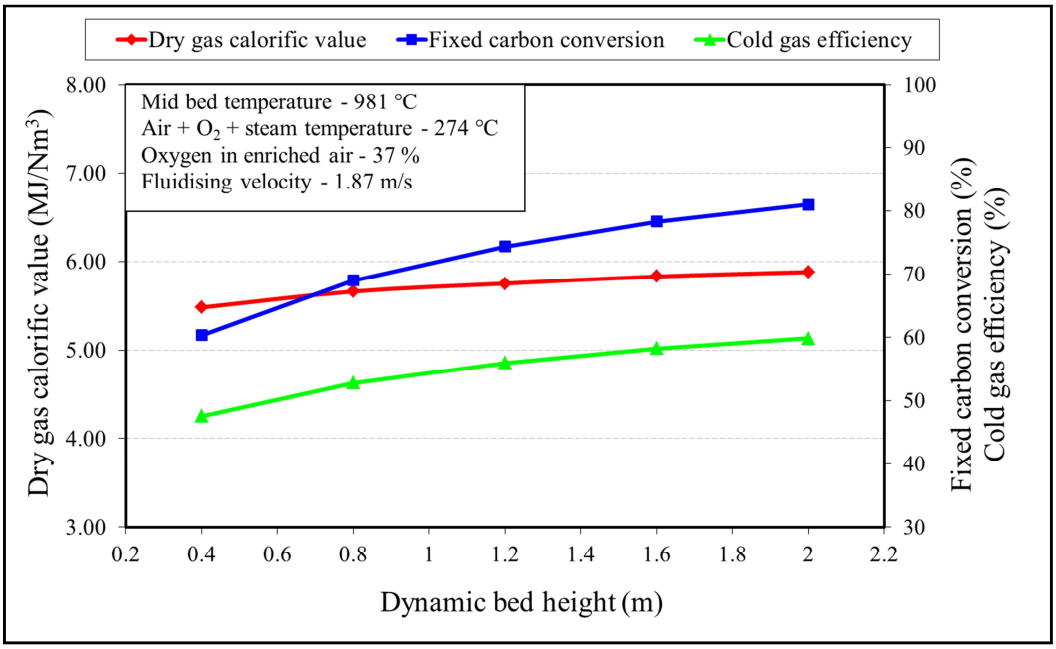

Figure 5.22: Effect of dynamic bed height on gasifier performance

Little benefit is therefore derived from operating atmospheric bubbling fluidised bed coal gasifiers at dynamic bed heights higher than ± 2 m since such deep beds are known to have certain undesirable properties such as:

- Higher particle segregation rates that can result in bed de-fluidisation.
- Higher particle attrition rates.
- Higher pressure drop.

5.3.8.3 Char particle size

Figure 5.23 shows that the predicted fixed carbon conversion increases by ± 5% when the char particle size is increased from 0.6 to 1.5 mm. This may appear contradictory to what would be expected since the char combustion rate expression of La Nauze and Jung (1982) given by equation (5.17), which is used by the model, calculates lower char combustion rates (mol/s) for larger char particles. The two-phase hydrodynamic

model of Davidson and Harrison, however, calculates a higher solids fraction (lower voidage) in the active zone of the bed (bottom 20% of the bed where oxygen is present) for larger char particles, and an overall higher combustion rate of char is calculated in the active zone, producing a slightly higher overall fixed carbon conversion.

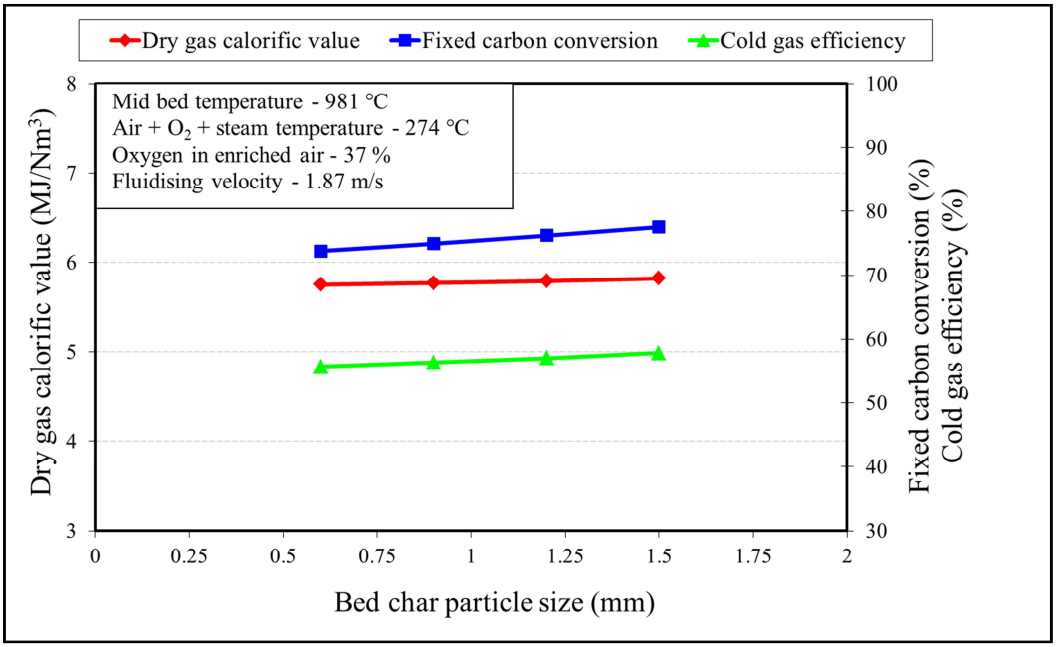

Figure 5.23: Effect of char particle size on gasifier performance

5.4 Summary of fluidised bed gasifier modelling

Based on a review of models reported in the literature since 1980, a fluidised bed coal gasifier model was developed. The model is based on sub-models and correlations that describe the various rate processes that take place in the gasifier, which include fluidised bed hydrodynamics, rates of chemical reaction, coal devolatilisation, interphase mass transfer and heat transfer.

The model formulation is based on 16 first-order ordinary differential equations that were derived by carrying out incremental mass and energy balances over the fluidised bed. The equations were solved using the MATLAB® ode45 differential equation solver. The solution of the equations gives the concentration of the gas species and temperatures in the fluidised bed as a function of bed height.

Parameters associated with the gasification reactions and the devolatilisation process for New Vaal and Grootegeluk coals were obtained by means of bench-scale tests described in Chapter 3. The heat losses from the gasifier were estimated by means of heat loss calculations described in Appendix E.2.8.

The results of the fluidised bed gasification tests reported in Chapter 4 were used to evaluate the predictive capability of the model by comparing the difference between the measured and predicted performance variables. The average difference between the experimental and predicted temperature, fixed carbon and gas calorific value of the gas is less than 10%. The over-prediction of the CO, H_2 and CH_4 could be attributed to the assumption of plug flow of gases in the emulsion phase and the exclusion of hydrogen and carbon-containing gas species such as NH_3, HCN, C_2H_6 and tar from the model formulation. It was concluded that the model has satisfactory predictive capability for its intended use, namely the design, optimisation and scale-up of fluidised bed gasifiers.

The advantage of rate models is that in addition to being able to predict the fixed carbon conversion they predict gas component concentrations and rates of chemical reactions as a function of bed height in the gasifier, and therefore provide useful insights into and understanding of coal gasification in a fluidised bed. Simulations using Grootegeluk coal show that:

- Char and gas combustion reactions are dominant in the lower 20% of the bed, resulting in a rapid decrease in the O_2 concentration and a rapid increase in the CO_2 concentration.

- Due to the high rate of the combustion reactions in the lower part of the bed, a high-temperature zone exists in this part of the bed, which is ± 180 °C higher than the mid-bed temperature. This indicates that although the temperature in the middle of the bed could be below the ash-softening temperature of the coal, it is not always a guarantee that bed agglomeration and clinkering will not occur.

- In the upper 80% of the bed the char gasification reactions are dominant, resulting in an increase of the CO and H_2 concentrations and a decrease in the CO_2 and H_2O concentrations.

- Due to the high rate of the combustion reaction, 80% of the fixed carbon is converted in the lower 20% of the bed. This explains why increasing the bed height often has little effect on the fixed carbon conversion.

- In a fluidised bed gasifier a significant percentage of the inlet oxygen (± 30%) is consumed by the gas combustion reactions, which has a negative effect on the gas calorific value and the fixed carbon conversion that can be achieved.

- The water-gas shift reaction occurs in both the forward and reverse directions and is seldom at equilibrium at the gasifier outlet. This explains why rate models have superior predictive capability compared with equilibrium models which assume that the water-gas shift is at equilibrium at the gasifier exit.

The model was used to predict the effect of variations in reactant temperature, dynamic bed height and char particle size on the performance of the fluidised bed gasifier. The sensitivity analysis showed that:

- Increasing the reactant gas (air, oxygen and steam) temperature from 250 °C to 550 °C results in a relatively low increase in the calorific value of the gas (± 9.3%) and the gasification efficiency (± 6.0%) since the fixed carbon conversion decreases due to the lower oxygen input required to maintain a constant bed temperature.

- Increasing the dynamic bed height results in a relatively low increase in the fixed carbon conversion since at higher bed heights the CO and H_2 concentrations are higher, which inhibits the rate of the gasification reactions, and the bed voidage is higher due to the larger bubble diameter.

- Although increasing the char particle size reduces the rate of the char combustion reaction, it results in a higher bed density (lower void fraction) in the active zone (lower 20% of the bed), producing a higher overall fixed carbon conversion in the gasifier for a constant char residence time (bed pressure drop).

5.5 Chapter 5 and Appendix E references

ANTHONY, D.B. AND HOWARD, J.B. (1976). Coal devolatilisation and hydro-gasification. *American Institute of Chemical Engineers Journal* 22: 625–656.

BABU, S.P., SHAB, B. AND TALWAKAR, A. (1974). Fluidisation correlations for coal gasification materials – minimum fluidisation velocity and bed expansion ratio. *American Institute of Chemical Engineers Symposium Series 74*: 105–113.

BANCHIK, I.N., SUBRAMANIAM, J.K. AND MARTEN, J.H. (1979). Pressure reaction cuts gasification costs. *Hydrocarbon Processing* 121: 10.

BARD, Y. (1974). Non-linear parameter estimation. New York: Academic Press Philadelphia: Balaban Publishers.

BIBA, V. (1978). Mathematical model for the gasification of coal under pressure. *Industrial & Engineering Chemistry Process Design and Development* 17: 92.

BUSTAMANTE, H. AND ENICK, R.M. (2004). Kinetics of the homogeneous reverse water-gas shift reaction at high temperature. *American Institute of Chemical Engineers Journal* 50: 1028–1041.

CHATTERJEE, P.K., DATTA, A.B. AND KUNDU, K.M. (1995). Fluidised bed gasification of coal. *The Canadian Journal of Chemical Engineering* 73: 204–210.

CHEJNE, F. AND HERNANDEZ, J.P. (2002). Modelling and simulation of coal gasification process in a fluidised bed. *Fuel* 81:1687–1702.

CHEJNE, F., LOPERA, E. AND LONDONO, C. (2010). Modelling and simulation of coal gasification process in a pressurized fluidized bed. *Fuel* 90: 399–411.

CHEN, W.J., SHEU, F.R. AND SAVAGE, R.L. (1987). Catalytic activity of coal ash on steam methane reforming and water-gas shift reactions. *Fuel Processing Technology* 16: 279–288.

CIESIELCZYK E. AND GAWDZIK, A. (1994). Non-isothermal fluidised bed gasifier model for char gasification taking into account bubble growth. *Fuel* 73:105–111.

COULSON, J.M. AND RICHARDSON, J.F. (1977). Heat Transfer. In: *Chemical Engineering* Volume one, Chapter 7, New York: Pergamon Press.

DARTON, R.C., LA NAUZE, R.D. AND DAVIDSON, J.F. (1977). Bubble growth due to coalescence in fluidised beds. *Transaction of the Institution of Chemical Engineers* 55: 274.

DAVIDSON, J.F. AND HARRISON, D. (1971). *Fluidization.* London and New York: Academic Press.

DE SOUZA-SANTOS, M.L. (2010). Comprehensive simulator applied to fluidized bed coal gasification. *The Open Journal of Chemical Engineering* 4: 68–79.

DE SOUZA-SANTOS, M.L. (1989). Comprehensive modelling and simulation of fluidized boilers and gasifiers. *Fuel* 68: 1507–1521.

DUTTA, S. AND WEN, C.Y (1977). Reactivity of coal and char in oxygen-nitrogen atmosphere. *Industrial & Engineering Chemical Process Design and Development* 16: 31–37.

EATON, A.M., SMOOT, L.D., HILL, S.C. AND EATOUGH, V.N. (1999). Components formulation, solutions, evaluations and applications of comprehensive combustion models. *Progress in Energy and Combustion Science* 25: 387–436.

ELLIOTT, M.A. (1981). *Chemistry of Coal Utilisation*, 1566–1569. John Wiley & Sons, New York.

EVERSON, R.C., NEOMAGUS, H.W.J.P., KASAINI, H. AND NJAPHA, D. (2006). Reaction kinetics of pulverised coal-chars derived from inertinite-rich coal discards: Gasification with carbon dioxide and steam. *Fuel* 85: 1076–1082.

ENGELBRECHT, A.D. (2008). Characterisation and fluidised bed gasification of selected high-ash South African coals. Master's dissertation, North-West University, South Africa.

FIELD, M.A. (1969). Rate of combustion of size-graded char fractions from a low-rank coal between 1 200 K and 2 000 K. *Combustion and Flame* 13: 237–252.

FIELD, M.A. (1970). Measurement of the effect of rank on combustion rate of pulverized coal. *Combustion and Flame* 14: 237–248.

FIELD, M.A., GILL, D.W., MORGAN, B.B. AND HAWKSLEY, P.G.W. (1967). Combustion of pulverized coal. Banberry, UK: Cheney and Sons.

GELDART, S. (1986). Single particles, fixed and quiescent beds. In: *Gas Fluidization Technology*, Chapter 2, New York, Brisbane, Toronto, Singapore: Wiley, 26.

GELPERIN, N.I., EINSTEIN, V.G AND KWASHA, A. (1967). Fluidisation technique fundamentals. *Izd.Khimia* Moscow, USSR.

GOYAL, A., ZABRANSKY, R.F. AND REHMAT, A. (1989). Gasification kinetics of Western Kentucky bituminous coal char. *Industrial & Engineering Chemistry Research* 28: 1767–1778.

GRACE, J.R. AND ABBA, I.A. (2005). Recent progress in the modelling of fluidised bed reactors. Proc. Industrial Fluidisation South Africa, Johannesburg, South Africa, 16 November.

GURURAJAN, V.S. AND AGARWAL, P.K. (1992). Mathematical model of fluidized bed coal gasifiers. *Chem. Eng. Res. Des. Trans.* 70A: 211–237.

HAMEL, S. AND KRUMM, W. (2001). Mathematical modelling and simulation of bubbling fluidised bed gasifiers. *Powder Technology* 120: 105–112.

HAMOR, R.J., SMITH, I.W. AND TYLER, R.J. (1973). Kinetics of the combustion of pulverized brown coal char between 630 and 1220 K. *Combustion and Flame* 21: 153.

HASLAM, R.T. (1923). The simultaneous combustion of hydrogen and carbon monoxide. *Industrial and Engineering Chemistry* 15: 679–681.

HOBBS, M.L., RADULOVIC, P.T. AND SMOOT, L.D. (1992). Modelling fixed bed coal gasifiers. *American Institute of Chemical Engineers Journal* 38: 681–702.

HORIO, A., TAKI, Y.S., HSIEH, I. AND MUCHI, M. (1980). Elutriation and particle transport through the freeboard of a gas-solid fluidized bed. In: GRACE, J.R. AND MATSEN J.M., *Fluidization*, New York: Plenum, 158.

HSU, S.T. (1962). Thermal Radiation. In: *Engineering Heat Transfer*, Chapter 5, New York: Toronto, London: Van Nostrand Reinhold.

HUANG, Z., ZHANG, J., ZHOA, Y., ZHANG, H., YUE, T., SUDA, T. AND NARUKAWA, M. (2010). Kinetic studies of char gasification by steam and CO_2 in the presence of H_2 and CO. *Fuel Processing Technology* 91: 843–847.

JENSEN, A., JOHNSSON, J.E., ANDRIES, J., LAUGHLIN, K., READ, G. AND MAYER, M. (1995). Formation of NO_x in pressurized fluidised bed combustion of coal. *Fuel* 74: 1555–1569.

JOHNSON, J.L. (1979). Chapter 1. In: *Kinetics of Coal Gasification*, New York: Wiley.

KARIM, G.A. AND MOHINDRA, D.J. (1974). A kinetic investigation of the water-gas shift reaction in homogeneous systems. *Journal of the Institute of Fuel* 47: 219.

KAWABATA, J., YUMIYAMA, M., TAZAKI, Y., HONMA, S., TAKEDA, S. AND YAMAGUCHI, H. (1981). Performance of a pressurized two-stage fluidized bed gasification process for production of low-Btu gas from coal char. *Chemical Engineering Communications* 11: 335–345.

KOBAYASHI, H. AND ARAI, H. (1967). Determination of gas cross-flow coefficient between the bubble and emulsion phases by means of measuring residence-time distribution of fluid in a fluidised bed. *Kagaku Kogaka Ronbunshu* 31: 239.

KUNII, D. AND LEVENSPIEL, O. (1969). Industrial applications. In: *Fluidization Engineering*, Chapter 2, New York: Krieger Publishing Co.

KURKELA, P. AND STAHLBERG, D. (1992). Air gasification of peat, wood and brown coal in a pressurized fluidized bed reactor. Carbon conversion, gas yield and tar formation. *Fuel Processing Technology* 31: 219.

KWON, T.W., KIM, S.D. AND FUNG, D.P. (1988). Reaction kinetics of char-CO_2 gasification. *Fuel* 67: 530–535.

LA NAUZE, R.D. AND JUNG, K. (1982). Kinetics of the combustion of petroleum coke particles in a fluidised bed combustor. 19th International Symposium on Combustion, The Combustion Institute, Pittsburgh, USA.

LEE, J.M., KIM, Y.J., LEE, W.J. AND KIM, S.D. (1998). Coal gasification kinetics derived from pyrolysis in a fluidized bed reactor. *Energy* 23: 475–488.

LI, X., GRACE, J.R., WATKINSON, A.P., LIM, C.J. AND ERGUEDENLER, A. (2001). Equilibrium modelling of gasification: A free energy minimization approach and its application to a circulating fluidized bed coal gasifier. *Fuel* 80: 195–207.

LILEY, P.E. AND GAMBILL W.R. (1980). Physical and chemical data. In: PERRY, R.H. and CHILTON, C.H. (1980) *Chemical Engineers Handbook,* 5th edition, Section 3, New York: McGraw-Hill, 119–125.

LOISON, R. AND CHAUVIN, R. (1964). Pyrolyse rapide du charbon. *Chemie et Industrie* 91: 269.

LUO, C.H., AOKI, K., UEMIYA, S. AND KOYIMA, T. (1998). Numerical model of a jetting fluidized bed reactor and a comparison with the experimental data. *Fuel Processing Technology* 55: 193–218.

MA, R. (1989). Modelling a fluidized bed coal gasification reactor. Doctoral thesis, North Carolina State University, USA.

MA, R.P., FELDER, R.M. AND FERREL, J.F. (1988). Modelling a pilot-scale fluidised bed coal gasification reactor. *Fuel Processing Technology* 19: 265–290.

MATSUI, I., KOMJIMA, T., KUNNI, D. AND FURUSAWA, T. (1987). Study of char gasification by carbon dioxide: 2. Continuous gasification in a fluidized bed. *Industrial & Engineering Chemistry Research* 26: 95–100.

MATSUI, I., KUNNI, D. AND FURUSAWA, T. (1985). Study of fluidized bed steam gasification of char by thermogravimetrically obtained kinetics. *Chemical Engineering Journal* 18: 105–113.

MAYERS, M.A. (1934). Rate of reduction of carbon dioxide by graphite. *Journal of the American Chemical Society* 56: 70–76.

MORI, S. AND WEN, C.Y., (1975). Estimation of bubble diameter in gaseous fluidized beds. *American Institute of Chemical Engineers Journal* 21: 109–115.

MÜHLEN, H., VAN HEEK, H. AND JUNTGEN, H. (1985). Kinetic studies of steam gasification of char in the presence of CO, CO_2 and H_2. *Fuel* 64: 944–949.

NEAVAL, R.C. (1979). Origin, petrography, and classification of coal. In: ELLIOTT, M.A., *Chemistry of Coal Utilization*, Chapter 3, New York: Wiley, 91–158.

NEOGI, D., CHANG, C.C., WALAENDER, W.P., AND FAN, L.T. (1986). Study of coal gasification in an experimental fluidised bed reactor. *AIChE Journal* 32: 17–28.

NEWMAN, P. (1948). Oxygen in the production of hydrogen or synthesis gas. *Industrial and Engineering Chemistry* 40: 559.

NJAPHA, D. (2003). Determination of the kinetic models and associated parameters for the low temperature combustion and gasification of high-ash coal chars. Doctoral thesis, North-West University, South Africa.

OCAMPO, A., ARENAS, E., CHEJNE, F., ESPINEL, J., LONDONO, C., AGUIRRE, J. AND PEREZ, J.D. (2003). An experimental study on gasification of Colombian coal in a fluidised bed. *Fuel* 82: 161–164.

ORMISTON, R.M., MITCHELL, F.R.G. AND DAVIDSON, J.F. (1965). The velocities of slugs in fluidised beds. *Transaction of the Institution of Chemical Engineers* 43: 209–216.

PAIN, C.C., MANSOORZADEH, S., AND DE OLIVEIRA, C.R.E. (2001). A study of bubbling and slugging fluidised beds using a two-fluid granular temperature model. *International Journal of Multiphase Flow* 27: 527–551.

PAREKH, R.D. (1982). Handbook of gasifiers and gas treatment systems. DOE Contract Report, DOE/ET/10159-T2 DE83 004846, September.

PARK, K.Y., SON, Y.C., AND PARK, W.H. (1987). An experimental study on the intrinsic combustion kinetics of Korean anthracite by thermogravimetric analysis. *Hwahak Konghak* 25: 345.

PARKER, A.S. AND HOTTEL, H.C. (1936). Combustion rate of carbon. *Industrial and Engineering Chemistry* 28: 1334–1341.

PINTO, F., ANDRÉ, R.N., LOPES, H., FRANCO, C., CAROLINA, C. GALHETAS, M., MIRANDA, M. AND GULYURTLU, H. (2012). Comparison of pilot-scale gasification installation performance when air or oxygen is used as gasification medium. 2 – Sulphur and nitrogen compounds abatement. *Fuel* 97: 770 –782.

RAJAN, R.R. AND WEN, C.Y. (1980). A comprehensive model for fluidized bed coal combustors. *American Institute of Chemical Engineers Journal* 26: 642–655.

RANZ, W.E. AND MARSHALL, W.R. (1952). Evaporations of drops, Part II. *Chemical Engineering Progress* 48: 173–180.

REID, R.C., PRAUNITZ, J.M. AND SHERWOOD, T.K. (1973). *The Properties of Gases and Liquids*, 3rd edition, New York: McGraw-Hill.

RHINEHART, R.R., FELDER, R.M. AND FERREL, J.K. (1987). Gasification of coal in a pilot-scale fluidized bed reactor 3: Gasification of a Texas lignite. *Industrial & Engineering Chemistry Research* 26: 2048–2057.

ROBERTS, D.G. AND HARRIS, D.J. (2000). Char gasification with O_2, CO_2 and H_2O: Effects of pressure on intrinsic reaction kinetics. *Energy and Fuels* 14: 483–489.

ROBERTS, D.G. AND HARRIS, D.J. (2007). Char gasification in mixtures of CO_2 and H_2O: Competition and inhibition. *Fuel* 86: 2672–2678.

ROHSENOW, M.W. AND HARNETT, J.P. (1973). *Handbook of Heat Transfer*. New York: McGraw-Hill.

ROSS, D.P., YAN, H.-M., ZHONG, Z. AND ZHANG, D-K. (2005). A non-isothermal model of a bubbling fluidised-bed coal gasifier. *Fuel* 84: 1469–1481.

ROSS, M., HEIDENRICH, C.A. AND ZHANG, D.K. (2000). Devolatilisation times of coal particles in a fluidised bed. *Fuel* 79: 873–883.

SAFFER, M., OCAMPO, A. AND LANGUERIE, C. (1988). Gasification of coal in a fluidised bed in the presence of water vapour and oxygen: An experimental study and a first attempt at modelling the reactor. *International Chemical Engineering* 28: 46–61.

SAITO, M., SATAKATA, M. AND SAKAI, T. (1987). Terminology for Model Credibility. *Simulation* 32: 103–104.

SCHLESINGER, M.E. (1979). Measurement of single coal particles in a laminar flow furnace. *Combustion Science and Technology* 51: 109–128.

SIT, S.P. AND GRACE, J.R., (1981). Effect of bubble interaction on interphase mass transfer in fluidised beds. *Chemical Engineering Science* 36: 327–355.

SNIDER, D.M., CLARK, S.M. AND O'ROURKE, C.J. (2010). Eulerian-Lagrangian method for three-dimensional thermal reacting flows with application to coal gasifiers. *Chemical Engineering Science* 66: 1285–1295.

STEIN, M., DING, Y.L., SEVILLE, J.P.K. AND PARKER, D.J. (2000). Solids motion in bubbling gas fluidised beds. *Chemical Engineering Science* 55: 5291–5300.

SYRED, N., KURNIAWAN, K., GRIFFITHS, T., GRALTON, T. AND RAY, R. (2007). Development of fragmentation models for inclusion in CFD codes. *Fuel* 86: 2221–2231.

VEREENIGING REFRACTORIES TECHNICAL DATA BOOK (2013). http://www.verref.co.za

VILIENSKI, T. AND HEZMALIAN, D.M. (1978). Dynamics of the combustion of pulverized fuel. *Energia, Moscow,* 246.

WEIMER, A AND CLOUGH, D. (1980). Modelling a low-pressure steam-oxygen fluidized bed coal gasification reactor. *Chemical Engineering Science* 36: 549–567.

WEN, C.Y. AND CHEN, L.H. (1982). Fluidized bed freeboard phenomena: Entrainment and elutriation. *American Institute of Chemical Engineering Journal* 28: 117.

WEN, C.Y. AND FAN, L.T. (1975). Heterogeneous models. In: *Models for Flow Systems and Chemical Reactors, Chemical Process Engineering,* Volume 3, Chapter 10, New York: Marcel Dekker.

WEN, C.Y. AND TSENG, H.P. (1979). A model for a fluidized bed coal gasifier simulation. *72nd American Institute of Chemical Engineers Meeting,* San Francisco, USA.

WEN, C.Y., et al. (1982). User's manual for computer simulation and design of the moving bed coal gasifier. DOE/MC/16474-1390, NTIS/DE83009533.

WILKE, C.R. (1950). A viscosity equation for gas mixtures. *The Journal of Chemical Physics* 18: 517–519.

YAN, H.-M., HEIDENREICH, C. AND ZHANG, D.K. (1999). Modelling of bubbling fluidised bed coal gasifiers. *Fuel* 78: 1027-1047.

YAN, H-M. AND ZHANG, D-K. (2000). Modelling of fluidised bed coal gasifiers: Elimination of the combustion product distribution coefficient by considering homogeneous combustion. *Chemical Engineering and Processing* 39: 229–237.

YAN, H-M., HEIDENREICH, C. AND ZHANG, D-K. (1998). Mathematical modelling of a bubbling fluidised bed coal gasifier and the significance of ‘net flow’. *Fuel* 77: 1067–1079.

YATES, J.G. (1995). Review Article Number 49. *Chemical Engineering Science* 51: 167.

YE, D.P., AGNEW, J.B. AND ZHANG, D.K. (1997). Gasification of South Australian low-rank coal with carbon dioxide and steam: Kinetics and reactivity studies. *Fuel* 77: 1209–1219.

YEOBAH, J.D. (1980). Effects of calcined dolomite on the fluidised bed pyrolysis of coal. *Industrial & Engineering Chemistry Process Design and Development* 19: 646.

YOON, H., WEI, J. AND DENN, M.M. (1978). A model for moving bed coal gasification reactors. *American Institute of Chemical Engineers Journal* 24: 885.

YU, Y., LU, J., ZHANG, X. AND ZHANG, S. (2007). Numerical simulation of bubbling fluidized bed coal gasification by the kinetic theory of granular flow (KTGF). *Fuel* 86: 722–734.

ZHANG, H., CEN, K., YAN, J. AND NI, M. (2002). The fragmentation of coal particles during coal combustion in a fluidized bed. *Fuel* 81: 1835–1840.

5.6 Chapter 5 and Appendix E nomenclature

a	decay constant for freeboard solids concentration	-
a_{CH4}	devolatilisation yield coefficient for methane	-
a_{CO}	devolatilisation yield coefficient for carbon monoxide	-
A_{ex}	external surface area of gasifier bed section	m^2
A_{in}	internal surface area of gasifier bed section	m^2
A_i	devolatilisation yield coefficient	-
A_B	gasifier bed area	m^2
A_d	distributor area	m^2
a_i	gas property calculation coefficient of gas component i	-
A_m	logarithmic mean surface area	m^2
a_p	bed char particle size estimation coefficient	-
a_s	solids specific surface area	m^2m^{-3}
b_{CH4}	devolatilisation yield coefficient for methane	C^{-1}
b_{CO}	devolatilisation yield coefficient for carbon monoxide	C^{-1}
B_E	fractional bed expansion	-
B_i	devolatilisation yield coefficient	-
b_i	gas property calculation coefficient of gas component i	-
B_I	bubble phase flow of increment I	$mol.s^{-1}$
B_I^{bnf}	bubble phase flow of increment I before net flow	$mol.s^{-1}$
b_p	bed char particle size estimation coefficient	-
C	gas concentration	$mol.m^{-3}$
C_{ash}	ash in coal	wt.%
C_{char}	carbon in char	wt.%
C_D	drag coefficient	-
C_{fixed}	fixed carbon in coal	wt.%
C_i	concentration of gas component i	$mol.m^{-3}$
C_i^b	concentration of gas component i in the bubble phase	$mol.m^{-3}$
C_i^e	concentration of gas component i in the emulsion phase	$mol.m^{-3}$
c_{pair}	heat capacity of air	$J.mol^{-1}C^{-1}$
c_{pb}	heat capacity of the bubble gas	$J.mol^{-1}C^{-1}$
c_{pBC}	heat capacity of the bed char	$J.kg^{-1}C^{-1}$
c_{pe}	heat capacity of the emulsion gas	$J.mol^{-1}C^{-1}$

c_{pg}	heat capacity of gas mixture	$J.mol^{-1}C^{-1}$
c_{pi}	heat capacity of gas component i	$J.mol^{-1}C^{-1}$
c_{ps}	heat capacity of solids mixture	$J.kg^{-1}C^{-1}$
c_{psteam}	heat capacity of steam	$J.mol^{-1}C^{-1}$
CV_{CC}	calorific value of the carbon in char	$MJ.kg^{-1}$
d_b	bubble diameter	m
D_{BO}	minimum bubble diameter	m
D_{BM}	maximum bubble diameter	m
D_e	equivalent gasifier bed diameter	m
D_g	gas diffusivity	$m^2.s^{-1}$
d_p	char particle diameter/coal particle diameter	m or mm
D_t	gasifier bed diameter	m
E	Arrhenius activation energy	$kJ.mol^{-1}$
e	surface emissivity	-
E_{CO2}	Arrhenius activation energy of the char-CO_2 reaction	$kJ.mol^{-1}$
E_{H2O}	Arrhenius activation energy of the H_2O-char reaction	$kJ.mol^{-1}$
E_I	emulsion phase flow of increment I	$mol.s^{-1}$
E_I^{bnf}	emulsion phase flow of increment I before net flow	$mol.s^{-1}$
e_{Ts}	convergence criteria for solids temperature	°C
e_x	convergence criteria for fixed carbon conversion	-
f^b_g	flowrate of bubble phase gas	$mol.s^{-1}$
f^e_g	flowrate of emulsion phase gas	$mol.s^{-1}$
f^b_{gi}	flowrate of gas component i in the bubble phase	$mol.s^{-1}$
f^e_{gi}	flowrate of gas component i in the emulsion phase	$mol.s^{-1}$
f_L	relative reactivity factor in the Johnson rate equation	-
f_{wgs}	parameter for the catalytic water-gas shift reaction	-
g	gravitational constant	$m.s^{-2}$
H_b	dynamic bed height	m
H_{bc}	bubble to cloud heat transfer coefficient	$J.m^{-3}s^{-1}C^{-1}$
H_{be}	bubble to emulsion heat transfer coefficient	$J.m^{-3}s^{-1}C^{-1}$
H_{ce}	cloud to emulsion heat transfer coefficient	$J.m^{-3}s^{-1}C^{-1}$
H_d	heat transfer through the distributor plate	$W.m^{-2}$
h_d	heat transfer coefficient through the distributor plate	$W.m^{-2}K^{-1}$

H_{mf}	bed height at minimum fluidisation conditions	m
h_p	particle-to-emulsion gas heat transfer coefficient	$J.m^{-2}s^{-1}C^{-1}$
H_w	heat transfer through the furnace wall	$W.m^{-2}$
h_w	furnace wall heat transfer coefficient	$W.m^{-2}K^{-1}$
i	gas component number	-
j	reaction number	-
k_{0CO2}	pre-exponential factor of the char-CO_2 reaction	$atm^{-1}s^{-1}$
k_{0H2}	adsorption constant for hydrogen	$atm^{-1}s^{-1}$
k_1	rate constant of Johnson char-steam rate equation	min^{-1}
k_2	rate constant of Johnson char-hydrogen rate equation	min^{-1}
K_{be}	interchange coefficient between bubble and emulsion gas	$m^3(m^{-3})^b s^{-1}$
k_{CO}	rate constant of carbon monoxide combustion	$mol^{-2}m^6s^{-1}$
K_{CO2i}	LH rate constant for char-CO_2 gasification	$atm^{-1}s^{-1}$
k_d	external diffusion rate of carbon combustion	$mol.m^{-2}s^{-1}atm^{-1}$
K_{eq1}	equilibrium constant in Johnson rate equation 1	-
K_{eq2}	equilibrium constant in Johnson rate equation 2	-
k_{ep}	emulsion-to-particle mass transfer coefficient	$m.s^{-1}$
k_g	thermal conductivity of gas mixture	$J.m^{-1}s^{-1}C^{-1}$
k_{gi}	thermal conductivity of pure gas component i	$J.m^{-1}s^{-1}K^{-1}$
k_{H2}	rate constant of carbon hydrogen combustion	$mol^{-2}m^6s^{-1}$
k_{H2Oi}	LH rate constants of char-steam gasification	$atm^{-1}s^{-1}$
k_I	rate constant of Johnson char-steam rate equation	s^{-1}
k_{II}	rate constant of Johnson char-hydrogen rate equation	s^{-1}
k_o	pre-exponential factor	$Pa^{-1}\ s^{-1}$
k_{O2}	rate constant of carbon combustion	$mol.m^{-2}s^{-1}atm^{-1}$
k_s	external diffusion rate of carbon combustion	$mol.m^{-2}s^{-1}atm^{-1}$
K_{wgs}	equilibrium constant of the water-gas shift reaction	-
k_{0H2O}	pre-exponential factor of the H_2O-char reaction	$atm^{-1}s^{-1}$
k_{wgsb}	rate constant of the water-gas shift reaction (bubble phase)	$mol^{-1}m^3s^{-1}$
k_{wgse}	rate constant of the catalytic water-gas shift reaction	$mol.m^{-3}s^{-1}atm^{-1}$
kw_i	thermal conductivity of thermal insulation	$W.m^{-1}K^{-1}$
m	reaction order	-
M_{daf}	dry ash-free coal feedrate	$kg.h^{-1}$

M_i	devolatilisation yield of gas component i	$kg.h^{-1}$
n	reaction order	-
N	number of experiments	-
n_d	number of orifices in the distributor	-
NF_I	net flow of increment I	$mol.s^{-1}$
n_i	interphase transfer rate of gas component i	$mol.m^{-3}s^{-1}$
nQ	dry molar gas flowrate	mol.h
NQ	dry gas flowrate	Nm^3h^{-1}
O	number of performance variables	-
P_i	partial pressure of gas component i in the gas	Pa
p_i	partial pressure of gas component i in the gas	atm
P_{O2}	partial pressure of oxygen	Pa
Q_d	heat transfer through the gasifier distributor	W
Q_I	gasifier energy input	$MJ.h^{-1}$
Q	gasifier energy losses	$MJ.h^{-1}$
Q_w	heat transfer through the gasifier wall	W
Q_r	heat transfer from bed to freeboard	W
R	universal gas constant	$J.mol^{-1}K^{-1}$
Re_p	particle Reynolds number	-
r_{CH4}	combustion rate of methane	$mol.m^{-3}s^{-1}$
r_{CO}	combustion rate of carbon monoxide	$mol.m^{-3}s^{-1}$
r_{H2}	combustion rate of hydrogen	$mol.m^{-3}s^{-1}$
r_j	rate of reaction j based on gas volume	$mol.m^{-3}s^{-1}$
r_j'	rate of reaction j based on solids surface area	$mol.m^{-2}s^{-1}$
r_j''	rate of reaction j based on solids volume	$mol.m^{-3}s^{-1}$
r_{O2}	char combustion rate	$mol.m^{-2}s^{-1}$
r_{wgs}	rate of the water-gas shift reaction in the bubble phase	$mol.m^{-3}s^{-1}$
r_{wgsc}	rate of the water-gas shift reaction in the emulsion phase	$mol.m^{-3}s^{-1}$
T	gas temperature	K
T_a	ambient temperature	°C
T^b	bubble temperature	°C
T_b	bed temperature	°C
T_d	outside temperature of the distributor plate	K

TDH	transport disengaging height	m
T^e	emulsion temperature	°C
T_{fb}	freeboard temperature	°C
T_g	gas temperature	°C
T_p	pretreatment temperature of char	K
T_r	temperature of reactants	°C
T^s	solids temperature	°C
U	superficial gas velocity	$mol.s^{-1}$
U_b	bubble velocity	$mol.s^{-1}$
U_{mf}	minimum fluidising velocity	$m.s^{-1}$
U_l	overall heat transfer coefficient	$W.m^{-2}.K^{-1}$
U_s	slug velocity	$m.s^{-1}$
u_t	terminal falling velocity of particle	$m.s^{-1}$
V_B	bubble volume	m^3
Vf_{gi}	molar flow of gas component i due to coal devolatilisation	$mol.s^{-1}$
v_g	interstitial gas velocity	ms^{-1}
v_{ij}	stoichiometric coefficient of component i in reaction j	-
WNQ_{gas}	wet gas flowrate	Nm^3h^{-1}
X	fractional conversion of fixed carbon in coal	-
$\left(\frac{dX}{dt}\right)_j$	fractional char conversion rate by reaction j	s^{-1}
X_i	mass fraction of gas component i in the volatiles	-
X_{MV}	mass fraction volatiles in the coal	-
x_{on}^e	measured performance variable o for the n-th experiment	-
x_{on}^p	predicted performance variable o for the n-th experiment	-
xw_i	thickness of thermal insulation	-
X_{tars}	mass fraction tars in volatiles	-
Y_c	mass fraction dry ash-free carbon in coal	-
y_i	mole fraction of gas component i	-
z	height above distributor	m
Z	objective function for model parameter estimation	-
z_0	parameter in Darton equation	m
γ_f	solids concentration of the freeboard	$kg.m^{-3}$

γ_{fo}	solids concentration at the top of the bed	$kg.m^{-3}$
ΔH^{0}_{evap}	latent heat of water evaporation at 25 °C	$MJ.kg^{-1}$
ΔH_{H2}	adsorption enthalpy of hydrogen	$KJ.mol^{-1}$
ΔH^{0}_{rj}	heat of reaction j	$J.mol^{-1}$
ΔH^{b}_{gi}	sensible heat of gas component i in the bubble phase	$J.mol^{-1}$
ΔH^{e}_{gi}	sensible heat of gas component i in the emulsion phase	$J.mol^{-1}$
ΔZ	height of an incremental bed section	m

Greek letters

α	parameter in structural factor of Johnson rate equation	-
β	grain model structural parameter	-
ε_{mf}	bed voidage at minimum fluidisation conditions	-
λ	net flow calculation parameter	-
ρ_{char}	char density	$kg.m^{-3}$
ρ_g	gas density	$kg.m^{-3}$
μ_g	gas viscosity	$kg.m^{-1}s^{-1}$
μ_i	viscosity of gas component i	$kg.m^{-1}s^{-1}$
φ	combustion product distribution coefficient	-
δ	bubble slug fraction of the bed	-
ψ	random pore model structural parameter	-
Θ	mean temperature difference	K
σ	Stefan-Boltzmann constant	$W.m^{-1}T^{-4}$

Acronyms/Abbreviations

CFD	Computational fluid dynamics
CV	Calorific value
CPFD	Computational particle fluid dynamics
CSTR	Continuously stirred tank reactor
FBG	Fluidised bed gasifier
FBC	Fluidised bed combustor
GG	Grootegeluk

KTGF	Kinetic theory of granular flow
LH	Langmuir-Hinshelwood
N/R	Not reported
NV	New Vaal
ODE	Ordinary differential equation
RHS	Right-hand side
TFM	Two fluid model

CHAPTER 6 GENERAL CONCLUSIONS AND RECOMMENDATIONS

This thesis presents results of the characterisation, bench-scale kinetic evaluation and pilot-scale fluidised bed gasification of two high-ash South African coals. The development of a fluidised bed coal gasification model is described, together with the evaluation of the predictive capability of the model by comparing the model outputs with the results from a pilot-scale fluidised bed gasifier at the CSIR.

6.1 Conclusions

The conclusions drawn from this investigation are the following:

6.1.1 Coal characterisation

- Due to the relatively high-ash contents and low calorific values of New Vaal and Grootegeluk coals, they are classified as Grade D coals. Based on the rank classification system using vitrinite reflectance, the rank of New Vaal coal is medium-rank bituminous (D) and the rank of Grootegeluk coal is medium-rank bituminous (C). The grade and rank of New Vaal and Grootegeluk coals are similar to those of other selected high-ash coals utilised by Sasol and Eskom for power generation.

- Comparison of the petrographic analysis of New Vaal and Grootegeluk coals with other South African coals show that New Vaal coal has a notably lower vitrinite reflectance, indicating a higher gasification reactivity. Grootegeluk coal has relatively higher vitrinite and volatile matter contents.

6.1.2 Bench-scale coal gasification and devolatilisation experiments

- Char-steam gasification experiments carried out in a thermogravimetric analyser found that the relative reactivity factor (f_L) in the Johnson char-steam rate equation is 8.65 and 1.91 for New Vaal and Grootegeluk coals respectively. This indicates that New Vaal coal has a significantly higher char-steam gasification reactivity than Grootegeluk coal. Furthermore, the results indicate that thermogravimetric analyser data are required to estimate the value of f_L for high-ash South African coals since the correlation recommended by Johnson, which is based on the dry-ash-free carbon content of the coal (Y_c), results in a significant under-prediction of f_L in the case of New Vaal coal.

- Char-CO_2 gasification TGA data was applied to obtain parameters for a first-order char-CO_2 rate equation. From the results it can be concluded that the char-CO_2 gasification rate is higher (10–15 times) for New Vaal coal compared to Grootegeluk coal and that the char-steam gasification rate is higher (5–10 times) than the char-CO_2 gasification rate for both coals.

- Coal devolatilisation tests carried out in a bench-scale fluidised bed reactor shows that Grootegeluk coal produces higher concentrations of CH_4 and lower concentrations of CO, H_2 and CO_2 than New Vaal coal. This can be attributed to the higher vitrinite and volatile matter content of Grootegeluk coal.

6.1.3 Pilot-scale fluidised bed gasification tests

- Stable gasification of two high-ash, low-grade South African coals with a particle size of 0.5 to 4 mm was achieved in a 140 kW pilot-scale atmospheric pressure bubbling fluidised bed gasifier operating at temperatures between 880 and 980 °C.

- The fixed carbon conversion and gasification efficiency obtained in the gasifier increases with bed temperature, char residence time, coal reactivity and steam concentration in the gasifier. The maximum fixed carbon

conversion achievable using Grootegeluk and New Vaal coals is, however, limited to ± 88% due to thermal fragmentation and attrition of coal in the gasifier. The fines generated in the gasifier are elutriated to the freeboard region where the conversion rate is low due to the absence of oxygen, the presence of high concentrations of CO and H_2 which inhibit the gasification reactions, and the lower temperatures and residence times of char particles compared with the bed.

- Enrichment of the oxygen concentration of the gasification air from 21 vol.% to 36 vol.% by means of oxygen addition produces a significant increase in the calorific value of the gas (3.0 to 5.5 MJ/Nm^3). This can be attributed to the reduced dilution effect of nitrogen and the higher steam concentrations in the gasifier when oxygen-enriched air and steam are used as the gasification agents.

- The high-ash content of the coals tested results in a reduction of the gasification efficiency due to the sensible heat loss in the ash. In terms of gasifier operation, the advantage of high-ash coals is that the the drainage rate of bed ash is higher, which reduces the accumulation of coarse particles on the distributor, and thereby prevents hotspot formation and clinkering of the bed.

6.1.4 Fluidised bed gasifier modelling

- A fluidised bed gasifier model was developed which is based on the two-phase theory of fluidisation, chemical reaction rates, coal devolatilisation, interphase mass transfer and heat transfer. Parameters for the model were obtained by means of thermogravimetric analyser experiments, bench-scale devolatilisation experiments and heat loss calculations. The predictive capability of the model was evaluated by comparing model predictions with the results of the pilot-scale gasification test carried out on Grootegeluk and New Vaal coals. It is concluded that the agreement between experimental and predicted results is satisfactory considering the complexity of the fluidised bed coal gasification process.

- The advantage of models that are based on reaction kinetics is that in addition to being able to predict the fixed carbon conversion, they predict gas component concentrations and chemical reaction rates as a function of bed height in the gasifier and therefore provide useful insights and understanding of coal gasification in a fluidised bed.

- Furthermore, the model is useful for analysing the effect of major operating variables such as reactant temperature, bed height and coal particle size on the performance of the gasifier and can therefore be used for design, optimisation and scale-up of fluidised bed coal gasifiers.

6.2 Contribution to coal science and technology

The following outputs from this research can be seen as contributions to the current knowledge base on the fluidised bed gasification of coal:

- Determination of parameters for the Johnson char-steam rate equation for two high-ash South African coals by means of thermogravimetric analyser tests. The rate equation and associated parameters can be incorporated into fluidised bed coal gasifier models that are based on the two-phase theory of fluidisation and gasifier models that use computational fluid dynamic (CFD) techniques to describe the hydrodynamics in the gasifier.

- Generation of a comprehensive set of experimental data on the pilot-scale atmospheric fluidised bed gasification of two high-ash South African coals using oxygen-enriched air-steam, oxygen-steam and air-steam mixtures as the gasification agents. These data can be used for parameter estimation and validation of fluidised bed coal gasifier models.

- Development of a fluidised bed coal gasifier rate model based on the two-phase theory of fluidisation, accounting for coal devolatilisation, chemical reactions, transfer processes and attrition of char. Proposal for an alternative

sub-model to predict the products of coal devolatilisation and incorporation of the sub-model into the fluidised bed coal gasifier model.

- This study has shown that a fluidised bed coal gasifier model, using parameter values obtained by means of bench-scale experiments on two high-ash South African coals, gives satisfactory agreement between model predictions and pilot-scale fluidised bed gasification test results carried out on these two coals. A reasonable estimation of the performance of coals other than New Vaal and Grootegeluk coals in fluidised bed coal gasifiers can therefore be made by using the model with parameters obtained from bench-scale tests on these other coals and estimating the value of the gasifier heat losses (Q) by means of a heat loss calculation.

6.3 Recommendations for future investigations

The following recommendations are proposed for further investigation, which could contribute to the expansion of knowledge of the utilisation of high-ash South African coal in fluidised bed gasifiers:

- This investigation has shown that the use of a conventional bubbling fluidised bed gasifier design for the gasification of high-ash South African coals results in low fixed carbon conversions, which leads to low gasification efficiencies. To increase the fixed carbon conversion it is recommended that a high-velocity circulating fluidised bed design of the type shown in Figure 1.6 be investigated. Initial investigations could be limited to bench-scale, thermogravimetric analyser and modelling studies using New Vaal coal. If these are promising, a pressurised pilot-scale gasifier could be considered.

- Although agglomeration and defluidisation of the bed was not experienced during the atmospheric pilot-scale bubbling fluidised bed gasification tests carried out on high-ash South African coals, the literature suggests that at higher pressures (> 0.5 MPa), higher temperatures are generated in the lower part of the bed which could increase the tendency of the bed to agglomerate

and defluidise. To address bed agglomeration at higher pressures it is recommended that the suitability of the U-GAS® ash-agglomerating fluidised bed gasifier (Figure 1.5) be evaluated for the gasification of high-ash South African coals.

- The following improvements to the model are recommended to improve its predictive capability and to expand its range of application:

    - Include reactions involving sulphur and nitrogen species to predict the emission of pollutants such as H_2S, COS, SO_2, NO, NO_2, N_2O, HCN and NH_3,
    - include the formation of C_2H_6 in the devolatilisation sub-model,
    - upgrade all sub-models to allow simulation to be carried out at pressures up to 3 MPa
    - and expand the hydrodynamic model to include the high-velocity circulating fluidised bed regime.

- One option for addressing the low fixed carbon conversion problem of fluidised bed coal gasifiers is to utilise the high-carbon char that is produced by the gasifier in a secondary pulverised fuel or fluidised bed combustor for steam generation and pre-heating of reactants to the gasifier. It is therefore recommended that the combustion characteristics of the cyclone and bed char produced by the pilot-scale gasifier at the CSIR be investigated using a thermogravimetric analyser and bench-scale reactors.

APPENDIX A: GENERAL INTRODUCTION

Appendix A.1: Coal utilised by gasification in South Africa to 2036

Table A.1 shows an estimation of the amount of coal that was utilised by gasification between 2006 and 2012 and the amount of coal that will be utilised by gasification between 2012 and 2036.

Table A.1: Domestic primary energy supply and coal utilisation by gasification

Year	Total primary energy supply (EJ/a)	Coal contribution to primary energy mix (%)	Primary energy supplied by coal (EJ/a)	Total coal utilised domestically (Mt/a)	Coal utilised by gasification (Mt/a)[1]
2006	5.64	74.1	4.18	171	30
2007	5.72	73.6	4.21	172	30
2008	5.81	73.1	4.25	174	30
2009	5.90	72.6	4.28	175	31
2010	5.99	72.0	4.31	176	31
2011	6.08	71.5	4.35	178	31
2012	6.17	71.0	4.38	179	31
2013	6.32	70.5	4.46	182	32
2014	6.48	70.1	4.54	186	33
2015	6.64	69.6	4.62	189	33
2016	6.81	69.2	4.71	193	34
2017	6.98	68.7	4.79	196	34
2018	7.15	68.3	4.88	200	35
2019	7.33	67.8	4.97	203	36
2020	7.51	67.3	5.06	207	36
2021	7.70	66.9	5.15	211	37
2022	7.89	66.4	5.24	215	38
2023	8.09	66.0	5.34	218	38
2024	8.29	65.5	5.43	222	39
2025	8.50	65.0	5.53	226	40
2026	8.71	64.6	5.63	230	40
2027	8.93	64.1	5.73	234	41
2028	9.15	63.7	5.83	239	42
2029	9.38	63.2	5.93	243	43
2030	9.62	62.8	6.04	247	43
2031	9.86	62.3	6.14	251	44
2032	10.11	61.8	6.25	256	45
2033	10.36	61.4	6.36	260	46
2034	10.62	60.9	6.47	265	46
2035	10.88	60.5	6.58	269	47
2036	11.15	60.0	6.69	274	48

[1]Figure 1.3 in Chapter 1 shows that Sasol utilised 40 Mt/a coal for synfuel production in 2006. This consisted of 30 Mt/a by means of gasification in Sasol FBDB gasifiers and 10 Mt/a by means of PF combustion.

The estimation given in Table A.1 is based on the following assumptions:

2006 to 2012

- Primary energy supply increased by 1.5% per annum.
- Contribution of coal to primary mix decreased from 74.1% to 71.0%.
- Coal utilised by gasification accounted for 17.5% of all locally utilised coal.

2012 to 2036

- Primary energy supply will increase by 2.5% per annum.
- Contribution of coal to primary mix will decrease from 71% to 60%.
- Coal utilised by gasification will account for 17.5% of all locally utilised coal.

APPENDIX B: COAL CHARACTERISATION

Appendix B.1: Calculation of coal particle density

The bulk density of low-porosity coals ($\varepsilon_{coal} < 5\%$) can be measured using the water displacement method (Engelbrecht, 2007).

Appendix B.2: Calculation of BET coal porosity

For cylindrical pores the porosity of coal can be calculated using equation (2.3). Equation (2.3) was derived using surface area and volume calculations (Engelbrecht, 2007).

$$\varepsilon_{coal} = \frac{d_{pore} S_{BET} \rho_{coal}}{40000} \quad (2.3)$$

Where:

ε_{coal}	porosity of coal	(%)
d_{pore}	average pore diameter by BET analysis	nm
S_{BET}	surface area of coal by BET analysis	$m^2.g^{-1}$
ρ_{coal}	coal particle density	$kg.m^3$

APPENDIX C: BENCH-SCALE GASIFICATION AND DEVOLATILISATION EXPERIMENTS

Appendix C.1: Effect of temperature on char-steam gasification rate

The effect of temperature on the char-steam gasification rate using reacting gas mix one (20 vol.% H_2O, 5 vol.% H_2, 5 vol.% CO, 70 vol.% N_2) is given in Figure C.1a. These are tests NV1, NV4, NV7, GG1, GG4 and GG7 given in Table 3.2 (Chapter 3).

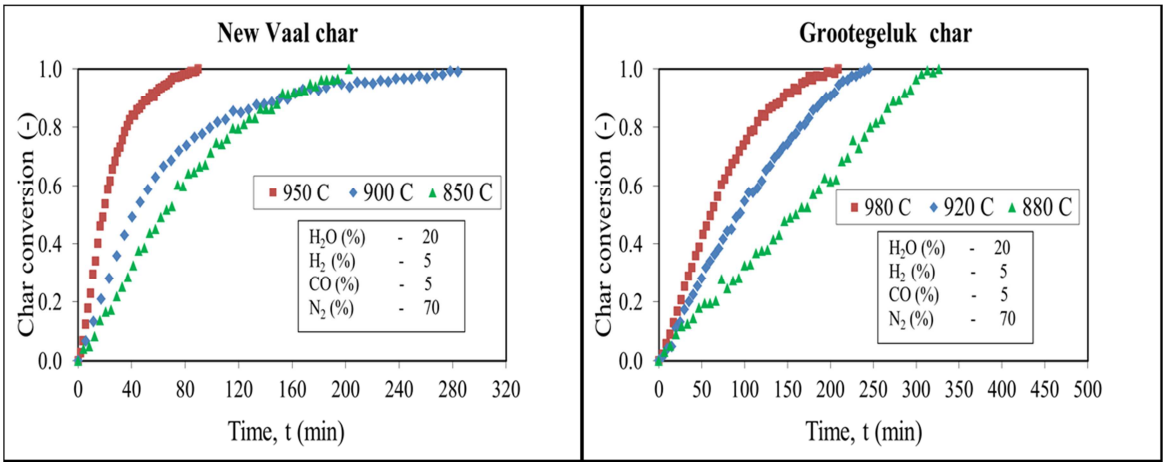

Figure C.1a: Effect of temperature on char gasification rate at 87.5 kPa

The effect of temperature on the char-steam gasification rate using reacting gas mix two (30 vol.% H_2O, 10 vol.% H_2, 10 vol.% CO, 50 vol.% N_2) is given in Figure C.1b. These are tests NV2, NV5, NV8, GG2, GG5 and GG8 given in Table 3.2 (Chapter3).

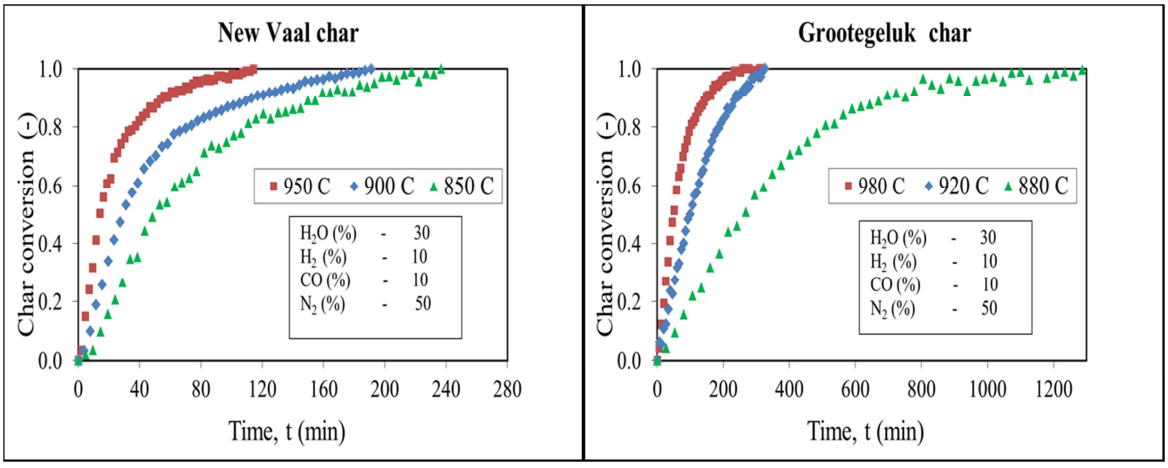

Figure C.1b: Effect of temperature on char gasification rate at 87.5 kPa

Appendix C.2: Effect of steam concentration on the char-steam gasification rate

The effect of steam concentration on the char-steam gasification rate at 850 °C (New Vaal char) and 880 °C (Grootegeluk char) is given in Figure C.2a. These tests are NV1, NV2, NV3, GG1, GG2 and GG3 given in Table 3.2 (Chapter 3).

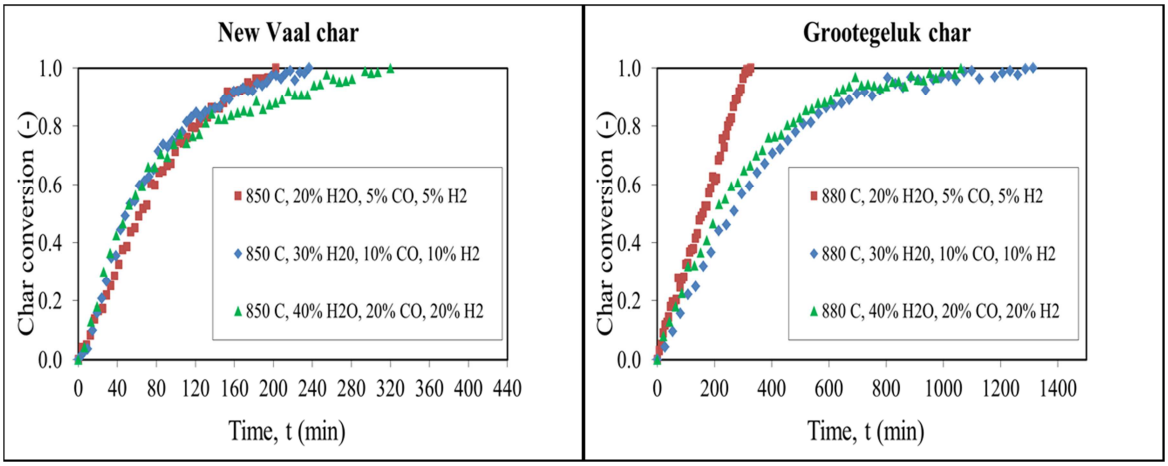

Figure C.2a: Effect of steam concentration on char gasification rate at 87.5 kPa

The effect of steam concentration on the char-steam gasification rate at 900 °C (New Vaal char) and 920 °C (Grootegeluk char) is given in Figure C.2b. These tests are NV4, NV5, NV6, GG4, GG5 and GG6 given in Table 3.2 (Chapter 3).

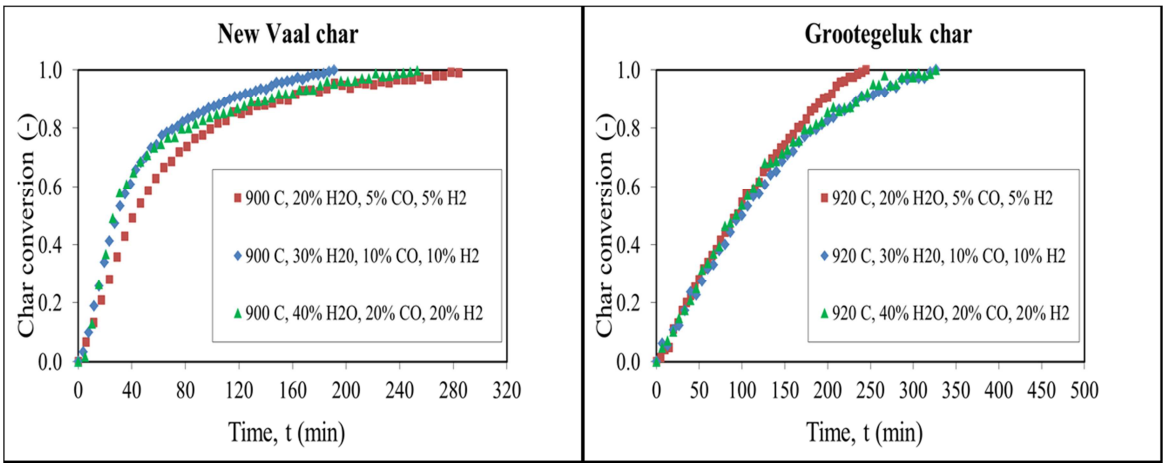

Figure C.2b: Effect of steam concentration on char gasification rate at 87.5 kPa

Appendix C.3: Coal devolatilisation sub-model development

Equations are derived that calculate the rate of evolution of CO, CO_2, H_2, CH_4, H_2O and N_2 as a result of coal devolatilisation. The equations are based on elemental mass balances and are therefore consistent with the proximate and ultimate analysis of the coal and the coal feedrate to the gasifier, thereby providing a basis for an overall gasifier elemental mass balance closure.

The devolatilisation sub-model of the fluidised bed coal gasifier model is based on the following assumptions:

- The volatile yield is equal to volatile matter content of the coal as determined by the SABS ISO 562:1998 method.
- Due to the rapid devolatilisation rate and high devolatilisation temperature (900 – 980° C) the formation of ethylene (C_2H_4), ethane (C_2H_6), light oils and tar are not included in the devolatilisation model.
- The volatiles and inherent moisture in the coal produce CO, CO_2, H_2, CH_4, H_2O and N_2 during the devolatilisation stage.
- The difference between the total and fixed carbon in the coal produces the carbon for the CO, CO_2 and CH_4 in the volatile gases.
- The hydrogen in the H_2, CH_4 and H_2O originates from the hydrogen in the coal (ultimate analysis) and the hydrogen in the inherent moisture (proximate analysis).
- The oxygen in the CO, CO_2 and H_2O in the volatiles originates from the oxygen in the coal (ultimate analysis) and the inherent moisture in the coal.
- The N_2 in the volatiles originates from the nitrogen in the coal (ultimate analysis). The evolution of NH_3, HCN and NO_x has not been included in the model.
- The reactions of CO_2 and H_2O (produced during devolatilisation) with char have not been included in the devolatilisation model.

Appendix C.3.1: Elemental mass balance equations

Based on the above assumptions, elemental mass balances can be carried out for carbon, hydrogen and oxygen.

Carbon balance

{Carbon from coal} = {Carbon in gas}

In symbols and using units of mol/h

$$G_{coal}(C - C_{fixed})\left(\frac{10}{12}\right) = nQ(V_{CO_2} + V_{CO} + V_{CH_4}) \quad \text{(C.3.1)}$$

Hydrogen balance

{Hydrogen from coal} = {Hydrogen in gas}

In symbols and using units of mol/h

$$G_{coal}\left(H + \left(\frac{2}{18}\right)IH_2O\right).10 = nQ(2V_{H_2} + 2V_{H_2O} + 4V_{CH_4}) \quad \text{(C.3.2)}$$

Oxygen balance

{Oxygen from coal} = {Oxygen in gas}

In symbols and using units of mol/h

$$G_{coal}\left(O + \left(\frac{16}{18}\right)IH_2O\right).\left(\frac{10}{16}\right) = nQ(2V_{CO_2} + V_{H_2O} + V_{CO}) \quad \text{(C.3.3)}$$

Where:

$$V_{CO} + V_{H_2} + V_{CH_4} + V_{CO_2} + V_{H_2O} = 100 \quad \text{(C.3.4)}$$

The above mass balance produces four equations (C.3.1 – C.3.4) with six unknowns (V_{CO}, V_{H2}, V_{CH4}, V_{CO2}, V_{H2O} and nQ).

If values of V_{CO} and V_{CH4} are obtained from the bench-scale fluidised bed reactor tests, four equations and four unknowns result after rearrangement of equations (C.3.1) to (C.3.4), which can be represented by a single matrix equation (C.3.5).

$$\begin{bmatrix} 0 & 1 & 0 & av \\ 2 & 0 & 2 & bv \\ 0 & 2 & 1 & cv \\ 1 & 1 & 1 & 0 \end{bmatrix} \cdot \begin{bmatrix} V_{H_2} \\ V_{CO_2} \\ V_{H_2O} \\ (nQ)^{-1} \end{bmatrix} = \begin{bmatrix} dv \\ ev \\ fv \\ gv \end{bmatrix} \qquad \text{(C.3.5)}$$

$$\Rightarrow \quad \begin{bmatrix} V_{H_2} \\ V_{CO_2} \\ V_{H_2O} \\ (nQ)^{-1} \end{bmatrix} = \begin{bmatrix} 0 & 1 & 0 & av \\ 2 & 0 & 2 & bv \\ 0 & 2 & 1 & cv \\ 1 & 1 & 1 & 0 \end{bmatrix}^{-1} \cdot \begin{bmatrix} dv \\ ev \\ fv \\ gv \end{bmatrix} \qquad \text{(C.3.6)}$$

In equation C.3.6:

$$\begin{aligned} av &= -G_{coal}(C - C_{fixed})\left(\frac{1000}{12}\right) \\ bv &= -G_{coal}\left(H + \left(\frac{2}{18}\right)IH_2O\right)1000 \\ cv &= -G_{coal}\left(O + \left(\frac{16}{18}\right)IH_2O\right)\left(\frac{1000}{16}\right) \\ dv &= V_{CO} - V_{CH_4} \\ ev &= -4V_{CH_4} \\ fv &= -V_{CO} \\ gv &= 100 - (V_{CO} + V_{CH_4}) \end{aligned} \qquad \text{(C.3.7)}$$

The solution of equation (C.3.6) gives the values of V_{H2}, V_{CO2}, V_{H2O} and nQ. The values of V_{CH4} and V_{CO} in equation (C.3.7) are on a wet basis. Since the values in Table 3.8 are on a dry basis, the values on a wet basis have to be initially guessed to allow the dry-based values to be calculated. An iteration procedure is used until the calculated dry-based values of V_{CH4} and V_{CO} are equal to the values in Table 3.8,

Figure 3.12 and Figure 3.13. These values are given by linear equations (C.3.8) – (C.3.11).

New Vaal:

$V^{d}_{CH4} = 0.046T - 17.9$ (C.3.8)

$V^{d}_{CO} = -0.033T + 35.8$ (C.3.9)

Grootegeluk:

$V^{d}_{CH4} = -0.116T + 131$ (C.3.10)

$V^{d}_{CO} = 0.053T - 27.5$ (C.3.11)

The molar evolution rates of CO, H_2, CH_4, H_2O, CO_2 and N_2 into the emulsion phase of the fluidised bed coal gasifier as a result of coal devolatilisation are given by equation (C.3.12).

$$
\begin{aligned}
Vf_{gCO} &= (nQ.V_{CO})/3600 \\
Vf_{gH_2} &= (nQ.V_{H_2})/3600 \\
Vf_{gCH_4} &= (nQV_{CH_4})/3600 \\
Vf_{gH_2O} &= (nQV_{H_2O})/3600 \\
Vf_{gCO_2} &= (nQV_{CO_2})/3600 \\
Vf_{gN_2} &= (G_{coal}N\left(\frac{10}{28}\right))/3600
\end{aligned}
\qquad \text{(C.3.12)}
$$

APPENDIX D: PILOT-SCALE FLUIDISED BED COAL GASIFICATION

NOTE: Symbols used in Appendix D are defined in the nomenclature at the end of Chapter 4.

Appendix D.1: Pilot-scale fluidised bed gasifier

Appendix D.1.1: Coal feeding

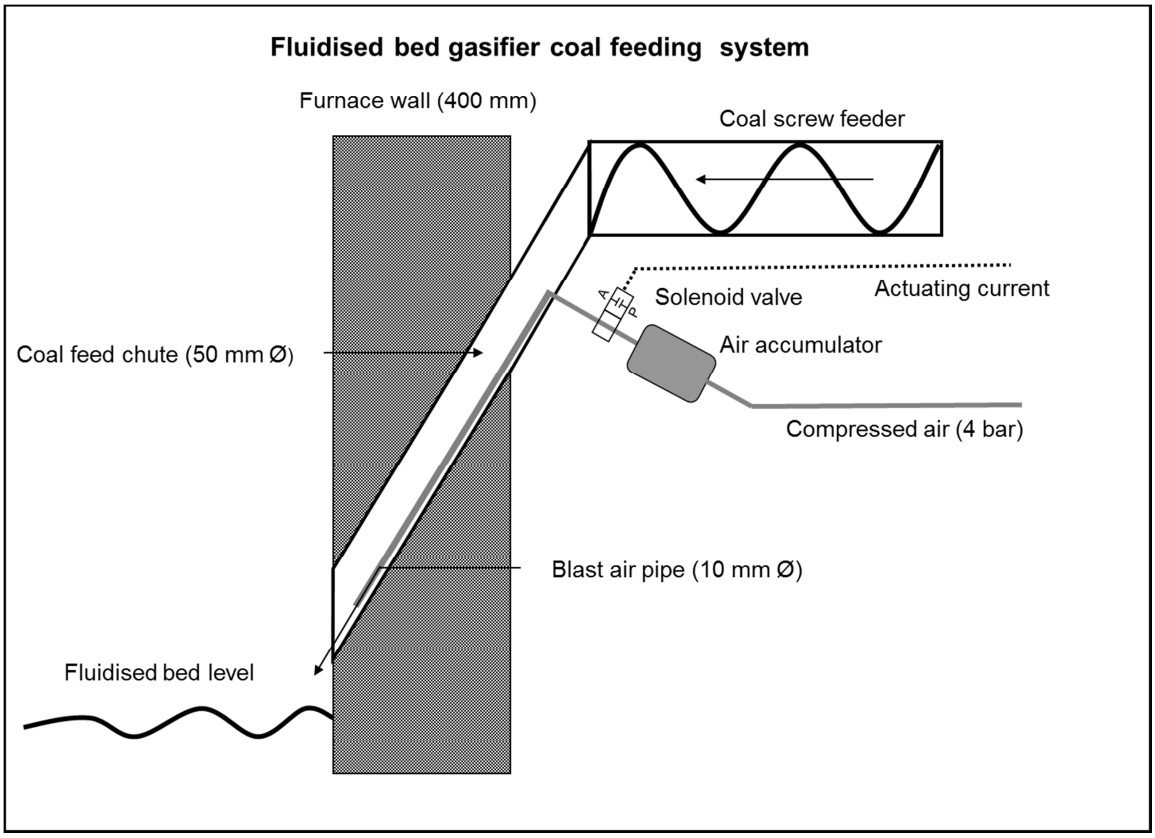

Figure D.1.1: Coal feed screw and coal feed chute

Appendix D.1.2: Steam generation

Figure D.1.2: Electrode boiler rated at 60 kg/h saturated steam at 600 kPa pressure

Appendix D.1.3: Bed char extraction

Figure D.1.3: Water-cooled bed char extraction screw conveyor

Appendix D.1.4: Hot gas cyclone

Cyclone dimensions:
Cyclone inlet: 200 mm x 80 mm
Barrel diameter: 400 mm
Barrel height: 300 mm
Cone height: 650 mm
Bottom outlet diameter: 80 mm
Vortex finder diameter: 150 mm

Figure D.1.4: Hot gas cyclone for capture of elutriated char

Appendix D.1.5: Gas cooling and cleaning

Scrubber dimensions:
Inlet diameter: 400 mm
Scrubber diameter: 1000 mm
Scrubber height: 5000 mm
Outlet diameter: 200 mm

Figure D.1.5: Gas quench scrubber

Appendix D.1.6: Flaring of gas

Figure D.1.6: Flare for low-CV gas

Appendix D.1.7: Calculated values of U_{mf} as a function of char particle size

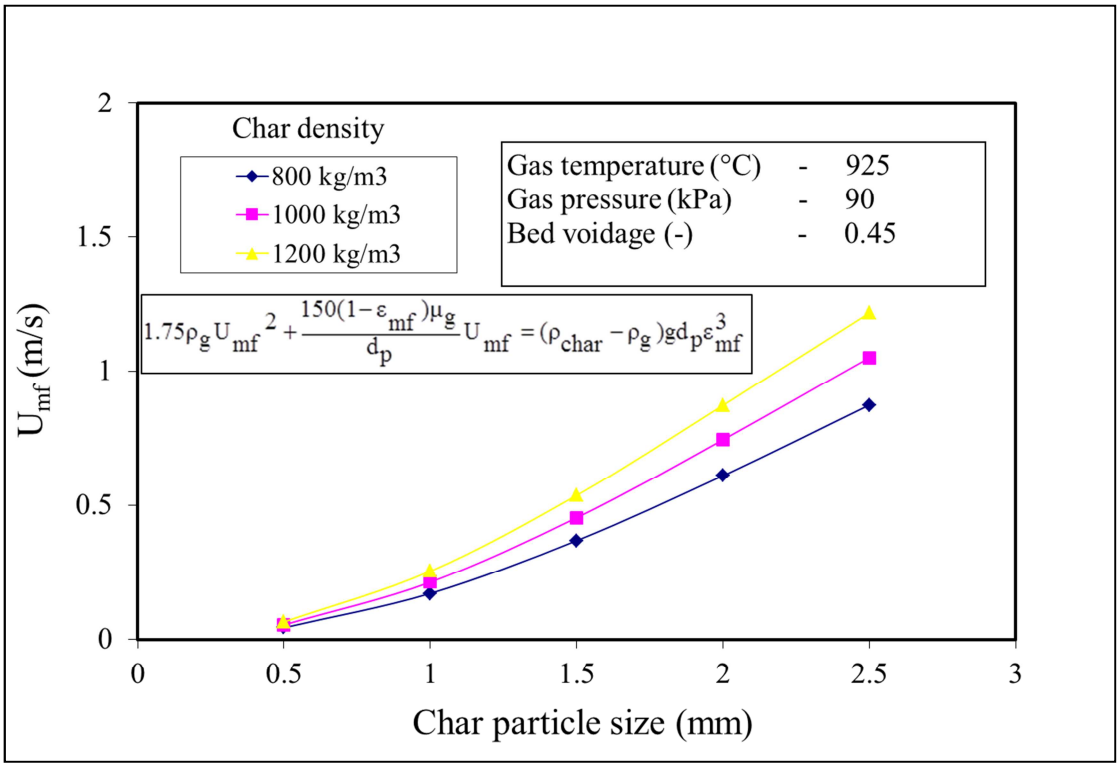

Figure D.1.7: U_{mf} as a function of char particle size for various char densities

Appendix D.1.8: FBG distributor plate

Figure D.1.8: FBG distributor plate removed from the furnace

Appendix D.1.9: Distributor pressure drop

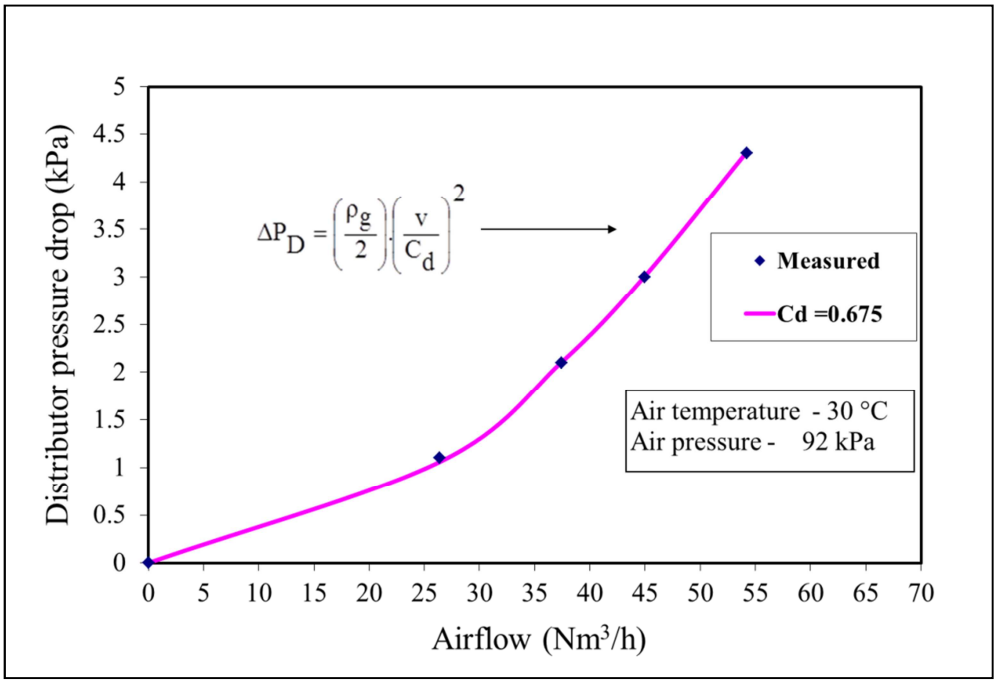

Figure D.1.9: Distributor pressure drop as a function of airflow

Appendix D.1.10: Coal feeder calibration and calculation formulae

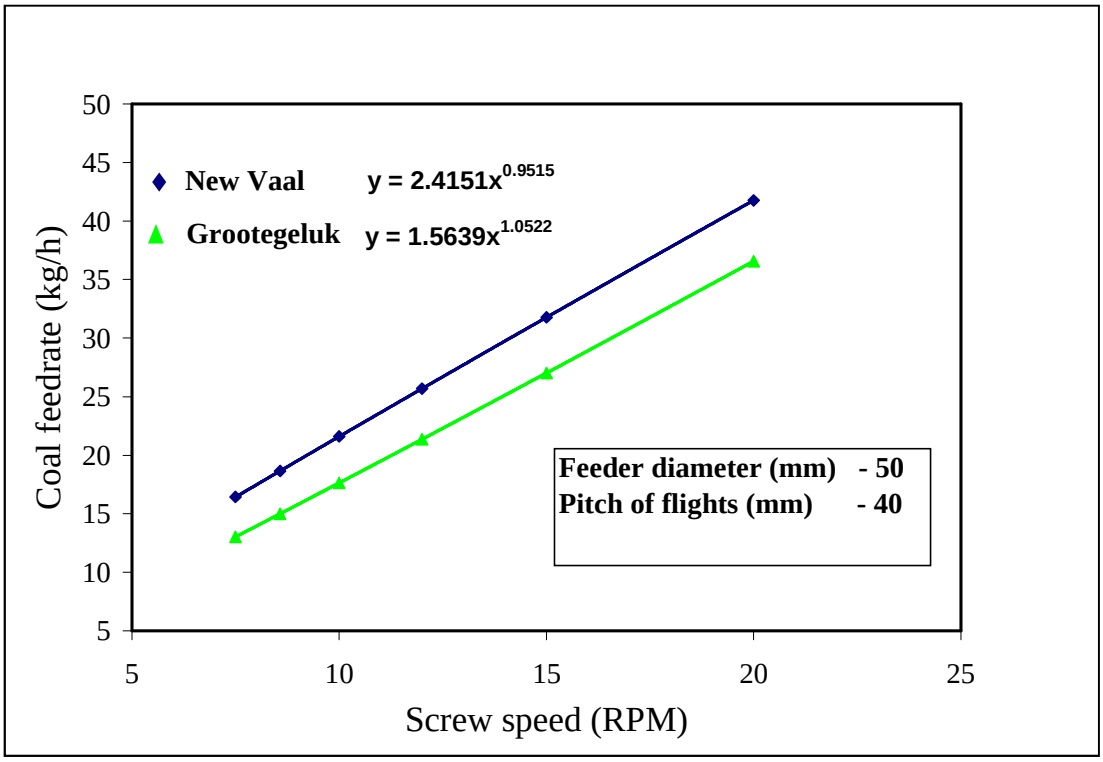

Figure D.1.10: Coal feedrate as a function of screw rotational speed

Appendix D.1.11: Airflow measurement

Figure D.1.11: Airflow orifice plate and manometer

Appendix D.1.12: Airflow calculation

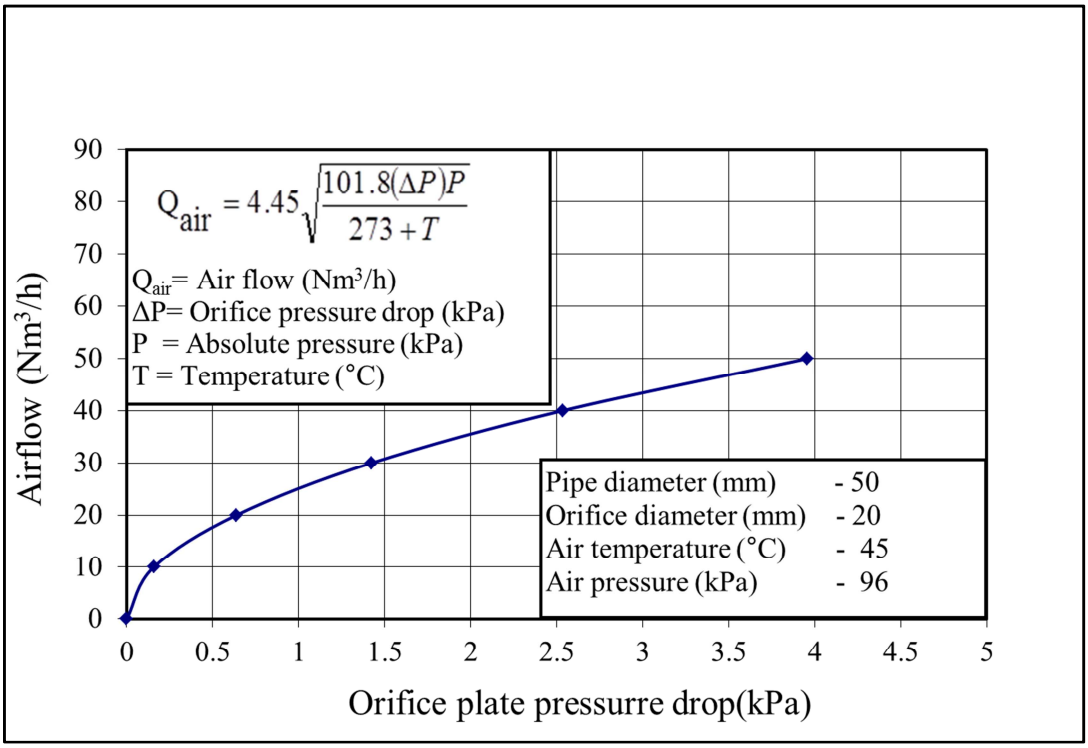

Figure D.1.12: Orifice plate calibration and calculation formulae

Appendix D.1.13: Steam flow measurement

Figure D.1.13: Rotameter for steam flow measurement

Appendix D.1.14: Steam flow calculation

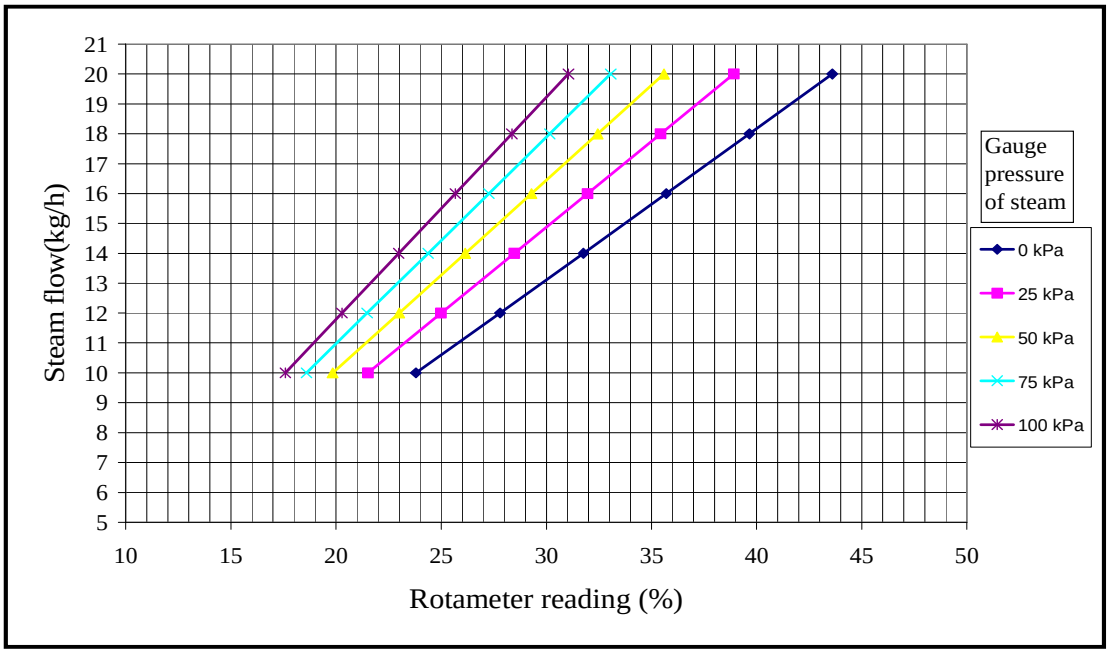

Figure D.1.14: Steam flow calibration graph

Appendix D.1.15: Oxygen flow measurement

Figure D.1.15: Rotameter for oxygen flow measurement

Appendix D.1.16: Oxygen flow calculation

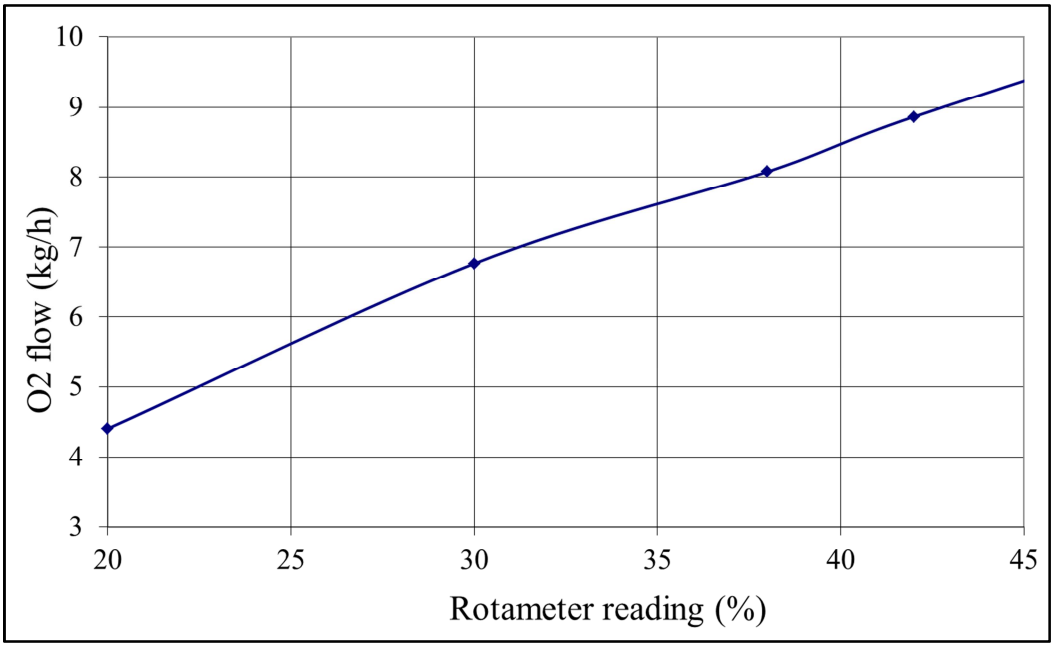

Figure D.1.16: Oxygen flow calibration graph

Appendix D.1.17: Analysis of CO, CH_4 and CO_2

Figure D.1.17: Servomex infrared gas analyser

Appendix D.1.18: Analysis of H_2

Figure D.1.18: Servomex thermal conductivity analyser

Appendix D.1.19: Analysis of O_2

Figure D.1.19: Hartman and Braun paramagnetic analyser

Appendix D.2: Fluidised bed gasification test results and calculations

Appendix D.2.1: Temperature and gas concentration profiles for Grootegeluk coal

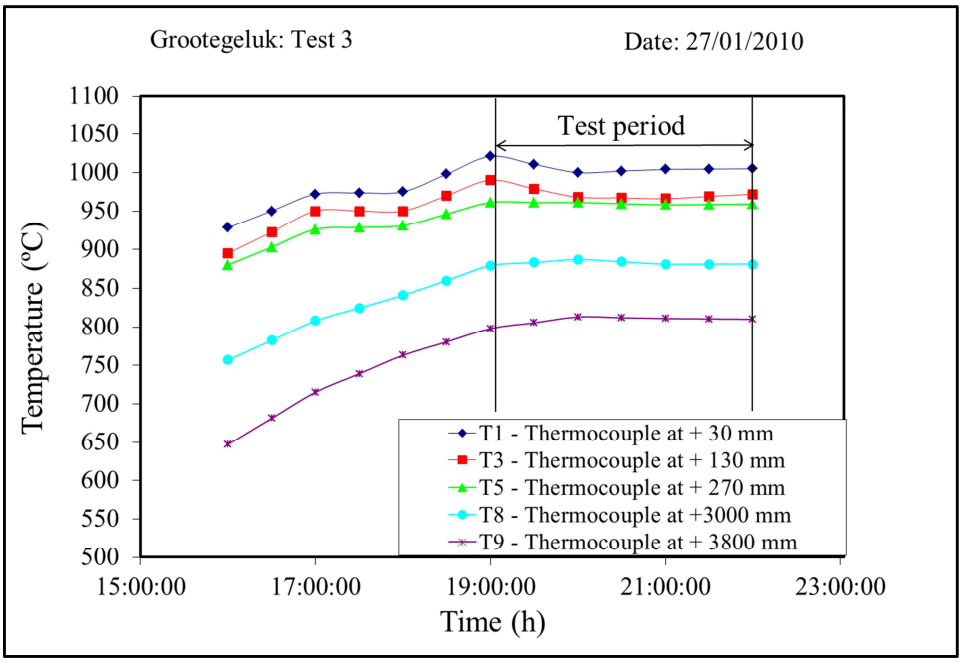

Figure D.2.1a: Gasifier temperature profile for Grootegeluk coal (Test 3)

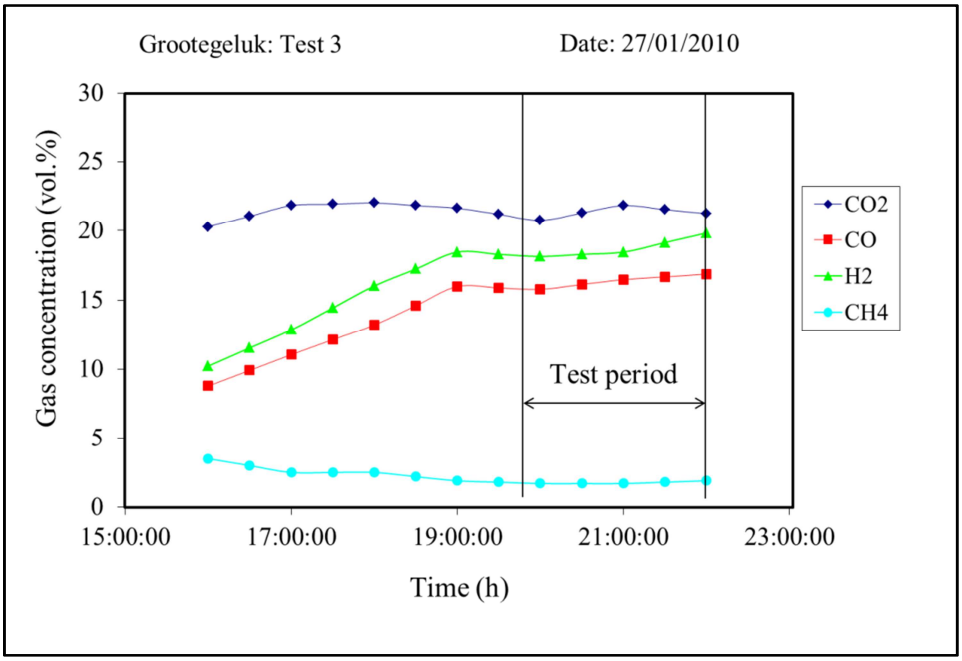

Figure D.2.1b: Gasifier gas concentration profile for Grootegeluk coal (Test 3)

Appendix D.2.2: Calculation of bed char residence time

For the purposes of this study the average residence time of char particles in the gasifier (τ) is defined as:

τ (min) = (mass of char in the bed (kg)/char feedrate (kg/h)).60 (D.2.2a)

Note: Since the volatiles are released from the coal in less than 0.5 min (Ross, 2000) after entering the gasifier, the char feedrate (ash + fixed carbon) is used in the calculation of the char residence time and not the coal feedrate.

In order to calculate the mass of char in the gasifier, the mass of char above the lower pressure probe, which is located 130 mm above the distributor plate, is calculated using the measured pressure drop. The mass of char below the probe is calculated using the height of this section (130 mm), the char density and the bed voidage.

Bed pressure drop (Pa) = ΔP_B = P1-P2 (see Figure 4.5, Tables 4.9 and 4.10)

$$\Delta P_B = \frac{M_1 g}{A_B} \quad \text{(D.2.2b)}$$

Where:

M_1 = bed mass above pressure probe (kg) (above P1)

g = gravitational constant (m/s^2) = 9.81

A_B = bed area (m^2) = 0.04

$$\Rightarrow \quad M_1 = \frac{\Delta P_B A_B}{g} = \frac{\Delta P_B}{245.5} \quad \text{(D.2.2c)}$$

Bed mass below pressure probe = M_2 (below P1)

$$M_2 = A_B(1-\varepsilon)\rho_{char}H_p \qquad \text{(D.2.2d)}$$

Where:

ε = bed voidage at bed velocity ≈ 0.80 (bed velocity > 5 x U_{mf}) (voidage below the probe)

ρ_{char} = char density (kg/m^3) – function of carbon in bed char (Figures 4.18 and 4.19)

H_p = distance from distributor to pressure probe P1 = 0.130 m

$$\text{Total bed mass (kg)} = M_t = M_1 + M_2 = \frac{\Delta P_B}{245.5} + A_B(1-\varepsilon)\rho_{char}H_p \qquad \text{(D.2.2e)}$$

$$\text{Residence time of char (min)} = \tau = \frac{M_t}{G_{char}}.60 \qquad \text{(D.2.2f)}$$

$$G_{char} = \frac{G_{coal}(C_{ash} + C_{fixed})}{100} \qquad \text{(D.2.2g)}$$

Where:

G_{coal} = coal feedrate (kg/h)

C_{ash} = ash in coal (wt.%)

C_{fixed} = fixed carbon in coal (wt.%)

The accuracy of the calculated char residence time (τ) is associated mainly with errors in the measurement of ΔP_B and G_{coal}. Using the tolerances given in Section 4.3.3 and equations (D.2.2a) to (D.2.2f), the accuracy of the calculated residence time (τ) is estimated to be ± 3 min.

Appendix D.2.3: Calculation of the concentration of oxygen in the enriched air and in the total inlet flow

The following measured values are used to calculate the concentration of oxygen in the enriched air ($O_{EAIR)}$) and in the total inlet flow (O_{INLET}):

Airflow (Nm^3/h) = Q_{air}
Oxygen flow (kg/h) = G_{O2}
Steam flow (kg/h) = G_{steam}

Total molar flow of oxygen (mol/h) = $nO_2 = Q_{air}.(44.64).(0.21) + \frac{G_{O2}.(1000)}{32}$

Total molar flow of air and oxygen (mol/h) = nEAIR = $Q_{air}.(44.64). + \frac{G_{O2}.(1000)}{32}$

Total inlet flow (mol/h) = nINLET = $Q_{air}.(44.64). + \frac{G_{O2}.(1000)}{32} + \frac{G_{steam}.(1000)}{18}$

Oxygen concentration of enriched air (vol.%) = $O_{EAIR} = \frac{nO_2}{nEAIR}.100$ (D.2.3a)

Oxygen concentration of total inlet flow (vol.%) = $O_{INLET} = \frac{nO_2}{nINLET}.100$ (D.2.3b)

The accuracy of the calculated concentration of oxygen in the enriched air ($O_{EAIR)}$) and in the total inlet flow (O_{INLET}) is associated mainly with errors in the measurement of $Q_{air,}$ G_{O2} and $G_{steam.}$ Using the tolerances given in Section 3.3.3 and equations (D.2.3a) to (D.2.3b), the accuracy of the calculated values of O_{EAIR} and O_{INLET} is estimated to be ± 1%.

Appendix D.2.4: Calculation of Stoichiometric, and steam:carbon molar ratios

The following measured values are used to calculate the stoichiometric (Φ_{MR}) and steam:carbon ($H_2O:C_{MR}$) molar ratios:

Airflow (Nm^3/h) = Q_{air}	Oxygen flow (kg/h) = G_{O2}
Steam flow (kg/h) = G_{steam}	Coal feedrate (kg/h) = G_{coal}
Carbon in coal (wt.%) = C	Hydrogen in coal (wt.%) = H
Sulphur in coal (wt.%) = S	Oxygen in coal (wt.%) = O

Total molar flow of oxygen (O) (mol/h) = nO = $(Q_{air}.(44.64).(0.21) + \frac{G_{O2}.(1000)}{32}).2$ (D.2.4a)

Total molar flow of steam (mol/h) = nH_2O = $\frac{G_{steam}.(1000)}{18}$ (D.2.4b)

Total molar flow of carbon in the coal (mol/h) = nC = $\frac{G_{coal}.(\frac{C}{100}).(1000)}{12}$ (D.2.4c)

Total molar flow of hydrogen (H) in the coal (mol/h) = nH = $G_{coal}.\left(\frac{H}{100}\right).(1000)$ (D.2.4d)

Total molar flow of sulphur (S) in the coal (mol/h) = nS = $\frac{G_{coal}.(\frac{S}{100}).(1000)}{32}$ (D.2.4e)

Total molar flow of oxygen (O) in the coal (mol/h) = nOC = $\frac{G_{coal}.(\frac{C}{100}).(1000)}{16}$ (D.2.4f)

Stoichiometric molar ratio = $\Phi_{MR} = \frac{nO}{2(nC) + \frac{nH}{2} + 2(nS) - nOC}.$ (D.2.4g)

Steam:carbon molar ratio = $H_2O : C_{MR} = \frac{nH_2O}{nC}.$ (D.2.4h)

The accuracy of the calculated the stoichiometric (Φ_{MR}) and steam:carbon ($H_2O:C_{MR}$) molar ratios is associated mainly with errors in the measurement of Q_{air}, G_{O2}, G_{steam}, G_{coal}, C, H, O, and S. Using the tolerances given in Section 3.3.3 and Equations (D.2.4a) to (D.2.4b), the accuracy of the calculated values of Φ_{MR} and $H_2O:C_{MR}$ is estimated to be ± 1%.

Appendix D.2.5: Calculation of fluidising velocity (U)

The fluidising velocity is calculated based on the gasifier inlet flow of air, oxygen and steam and the bed temperature (T4) and pressure (P_B = 90 kPa) at 200 mm above the distributor plate. The actual velocity at this position in the bed will be slightly higher (± 10%) since the gas volume increases due to the gasification reactions taking place in the gasifier.

Note:

- Normal (N) conditions are 101.325 kPa and 273 °C
- 1 Nm^3 contains 44.64 gmoles of an ideal gas

Q_{air} = air flow (Nm^3/h)
G_{O2} = oxygen flow (kg/h)
G_{Steam} = steam flow (kg/h)
P_B = bed pressure (kPa)
T_B = bed temperature (°C) = T4
A_B = bed area (m^2)

Total gas flow to bed (Nm^3/h) = $NQ_{total} = Q_{Air} + \frac{G_{Steam}.1000}{(18)(44.64)} + \frac{G_{O2}.1000}{(32).(44.64)}$

$$NQ_{total} = Q_{Air} + 1.245G_{steam} + 0.7G_{O2}$$

Total flow to bed at bed conditions (m^3/h) = $Q_{total} = NQ_{total}\left(\frac{101.325}{P_B}\right)\left(\frac{T_B + 273}{273}\right)$

$$U(m/s) = \frac{Q_{total}}{3600.A_B} = \frac{(Q_{Air} + 1.245G_{Steam} + 0.7G_{O2})\left(\frac{101.325}{P_B}\right)\left(\frac{T_B + 273}{273}\right)}{3600.A_B} \quad \textbf{(D.2.5)}$$

The accuracy of the calculated fluidising velocity (U) is associated with errors in the measurement of Q_{air}, G_{steam}, T_B and P_B. Using the tolerances given in Section 3.3.3 and equation (D.2.5), the accuracy of the calculated U is estimated to be ± 0.1 m/s.
The equation to calculate the minimum fluidising velocity (U_{mf}) is given in Appendix E.1.1.1.

Appendix D.2.6: Calculation of dry gas calorific value (CV_{gas})

The gross calorific value of the gas is the gross heat of combustion of:

$CO + ½ O_2 => CO_2$	ΔH_{c298} = -283.1 kJ/mol = -12.639 MJ/Nm^3
$H_2 + ½ O_2 => H_2O$	ΔH_{c298} = -286.0 kJ/mol = -12.766 MJ/Nm^3
$CH_4 + 2O_2 => CO_2 + 2H_2O$	ΔH_{c298} = -890.8 kJ/mol = -39.765 MJ/Nm^3
$H_2S + 1½ O_2 => SO_2 + H_2O$	ΔH_{c298} = -519.0 kJ/mol = -23.179 MJ/Nm^3

$$=> \quad \boxed{CV_{gas}(MJ/Nm^3) = 0.12639 V_{CO} + 0.12766 V_{H_2} + 0.39765 V_{CH_4} + 0.23179 V_{H_2S}} \quad \text{(D.2.6)}$$

Where:

V_{CO} = CO concentration of the gas (vol.%)

V_{H_2} = H_2 concentration of the gas (vol.%)

V_{CH_4} = CH_4 concentration of the gas (vol.%)

V_{H_2S} = H_2S concentration of the gas (vol.%)

V_{H_2S} is calculated based on the assumption that all the sulphur in the coal forms H_2S:

$$V_{H_2S} = \frac{0.7 G_{coal} S}{NQ_{gas}}$$

Where:

G_{coal} = coal feedrate to the gasifier (kg/h)

S = sulphur in the coal (wt.%)

NQ_{gas} = dry gas flow (Nm^3/h) – (Appendix D.2.7)

The accuracy of the calculated calorific value (CV_{gas}) is associated with errors in the measurement of V_{CO}, V_{H2}, V_{CH4}, S and G_{coal}. Using the tolerances given in Section 4.3.3 and equation (D.2.6), the accuracy of the calculated CV is estimated to be ± 0.15 MJ/Nm^3.

Appendix D.2.7: Calculation of dry gas flowrate (NQ_{gas})

Accurate measurement of the dry gas flowrate was not possible since the gas after the scrubber contained an unknown and variable amount of moisture. The dry syngas flowrate (NQ_{gas}) was therefore calculated using a nitrogen balance method.

The following measured values were used to calculate the dry gas flowrate:

Q_{air} = airflow (Nm^3/h)

V_{CO} = CO concentration of the gas (vol.%)

V_{H_2} = H_2 concentration of the gas (vol.%)

V_{CH_4} = CH_4 concentration of the gas (vol.%)

V_{CO_2} = CO_2 concentration of the gas (vol.%)

V_{O_2} = O_2 concentration of the gas (vol.%)

OTH = H_2S, COS, SO_2, NH_3, HCN and C_2^+ = 0.4 vol.%

$$NQ_{gas} = \frac{79Q_{air}}{\left[100 - \left(V_{co} + V_{H_2} + V_{CH_4} + V_{CO_2} + V_{O_2} + OTH\right)\right]} \qquad \text{(D.2.7a)}$$

For the tests using oxygen and steam as the gasification agents, a carbon balance method was used to calculate the dry gas flowrate (NQ_{gas}):

$$NQ_{gas} = \frac{G_{coal} C_{TOTALCON} C}{53.57.(V_{co} + C_{CH_4} + V_{CO_2})} \qquad \text{(D.2.7b)}$$

Where:

G_{coal} = coal feedrate (kg/h)

$C_{TOTALCON}$ = total fixed carbon conversion (%)

C = total carbon in coal (wt.%)

Appendix D.2.8: Calculation of dynamic bed height

The dynamic bed height (H_b) is defined as the expanded height of the fluidised bed when it is fluidised at the operating fluidising velocity.

$$=> H_b = \frac{M_t}{A_B(1-\varepsilon_e)\rho_{char}} \qquad \text{(D.2.8)}$$

where:

H_b = dynamic bed height (m)

M_t = total bed mass (kg) (Appendix D.2.2, equation (D.2.2d))

A_B = area of bed = 0.04 m^2

ε_e = voidage of the expanded bed (0.83 - 0.87 – calculated using model)

ρ_{char} = char density (kg/m^3) – function of carbon in bed char (Figures 4.18 and 4.19)

Appendix D.2.9: Calculation of char elutriated to the cyclone, fixed carbon conversion and total carbon conversion

Calculation of the total and fixed carbon conversion is based on the assumption that the char produced by the gasifier does not contain any volatile matter. The char would contain small amounts of volatile matter since the char produced by the gasifier has a relatively wide residence time distribution. The volatile matter content would be less than ± 1% due to the high average residence time of particles in the gasifier (16 – 49 min).

The following measured values are used to calculate the fixed carbon conversion ($C_{FIXEDCON}$), total carbon conversion ($C_{TOTALCON}$) and percentage char elutriated (A_E):

Coal feedrate (kg/h) = G_{coal} = a (measured)

Fixed carbon in coal (wt.%) = C_{fixed} = b_1 (measured)

Total carbon in coal (wt.%) = C = b_2 (measured)

Ash in coal (wt.%) = C_{ash} = c (measured)

Bed char flowrate (kg/h) = G_{BC} = d (measured)

Carbon in bed char (wt.%) = C_{BC} = e (measured)
Carbon in elutriated char (wt.%) = C_{EC} = f (measured)

The elutriated char flowrate could not be accurately measured since a certain percentage by-passes the cyclone and cannot be collected. The elutriated char flowrate is therefore determined by means of an ash balance.

Elutriated char flowrate (kg/h) = G_{EC} = g (calculated)

$ac = d(100-e) + g.(100-f)$ (ash balance) (D.2.9.a)

$$\Rightarrow g = \frac{ac - d(100 - e)}{100 - f} \quad \text{(D.2.9.b)}$$

The percentage elutriated char is calculated from the bed and elutriated char flowrates.

Percentage elutriated char (%) = A_E = h (calculated)

$$h = \frac{g.100}{d + g} \quad \text{(D.2.9.c)}$$

The fixed carbon conversion is calculated by means of a carbon balance:

Fixed carbon conversion (%) = $C_{FIXEDCON}$ = i (calculated)

$$i = \frac{(ab_1 - (ed + fg)).100}{ab_1} \quad \text{(D.2.9.d)}$$

The total carbon conversion is calculated by means of a carbon balance:

Total carbon conversion (%) = $C_{TOTALCON}$ = j (calculated)

$$j = \frac{(ab_2 - (ed + fg)).100}{ab_2} \qquad \text{(D.2.9.e)}$$

The accuracies of the calculated fixed carbon conversion ($C_{FIXEDCON}$) and total carbon conversion ($C_{TOTALCON}$) are associated mainly with errors in the measurement of G_{coal}, G_{BC}, C_{BC} and C_{EC}. Using the tolerances given in Section 3.3.3 and equations (D.2.9a) to (D.2.9e), the accuracy of the calculated fixed carbon conversion is estimated to be ± 2.5%.

Appendix D.2.10: Calculation of the cold gas efficiency(η_{CG})

The cold gas efficiency (η_{CG}) is defined as the energy in the cold clean gas (cooled to 25 °C) as a percentage of the energy in the coal.

Energy in cold gas (MJ/h) = NQ_{gas}. CV_{gas}

Energy in coal (MJ/h) = G_{coal}. CV_{coal}

$$\Rightarrow \quad \eta_{CG} = \frac{NQ_{gas}.CV_{gas}}{G_{coal}CV_{coal}}.100 \qquad \text{(D.2.10)}$$

Appendix D.2.11: Particle size distributions (New Vaal coal tests)

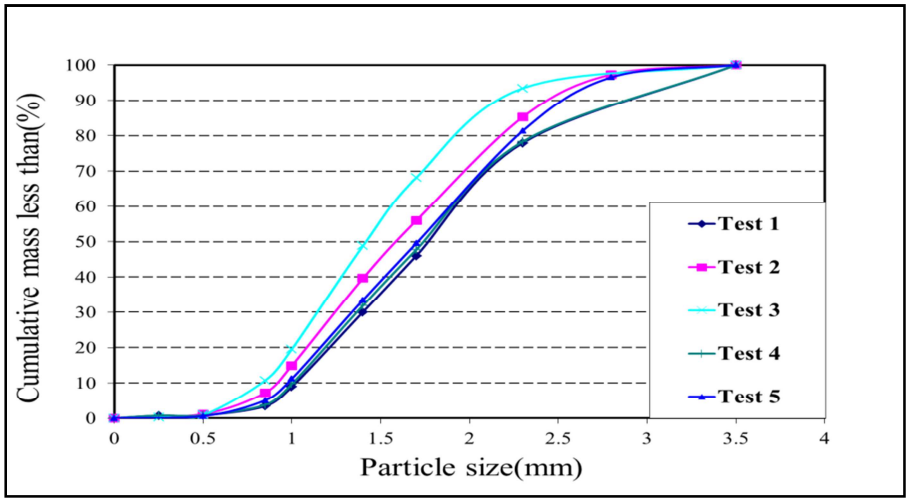

Figure D.2.11a: Particle size distribution of New Vaal coal

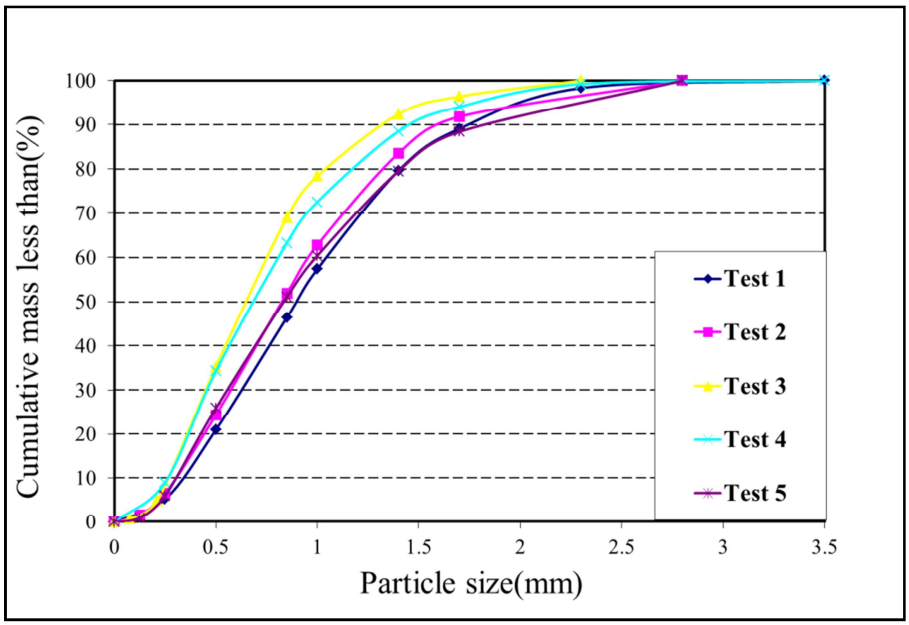

Figure D.2.11b: Particle size distribution of bed char

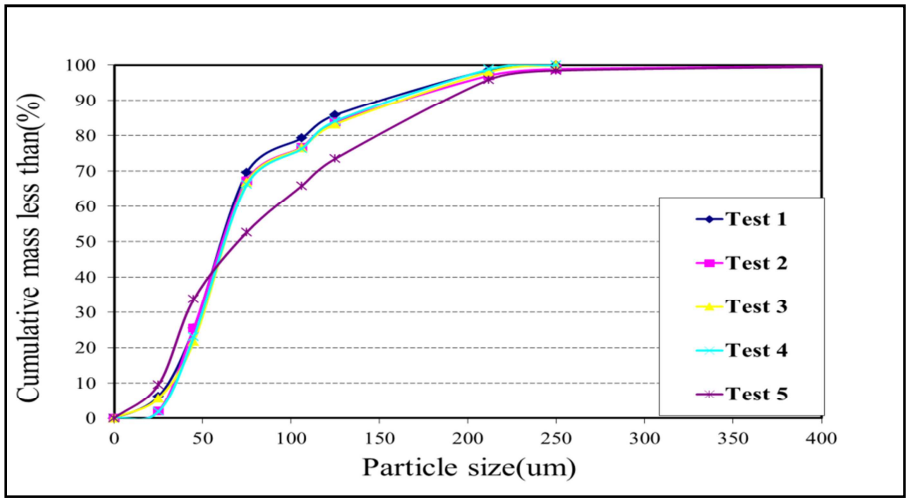

Figure D.2.11c: Particle size distribution of cyclone char

Appendix D.2.12: Particle size distributions (Grootegeluk coal tests)

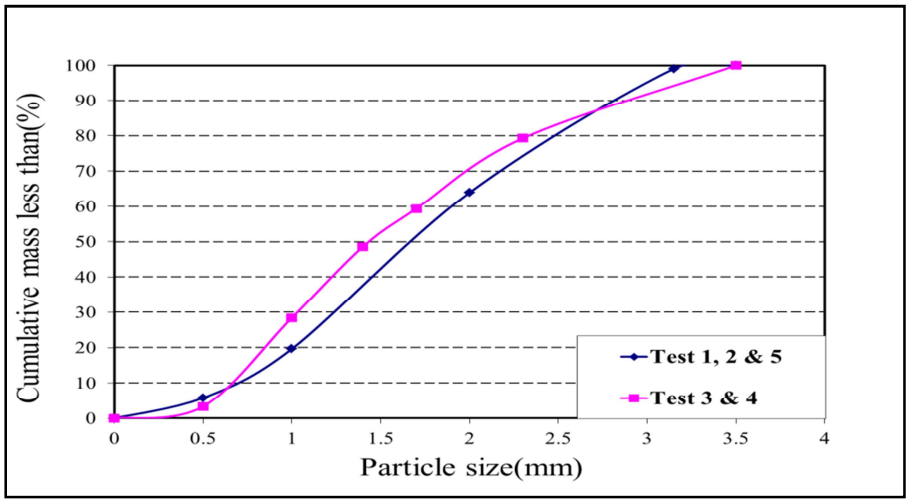

Figure D.2.12a: Particle size distribution of Grootegeluk coal

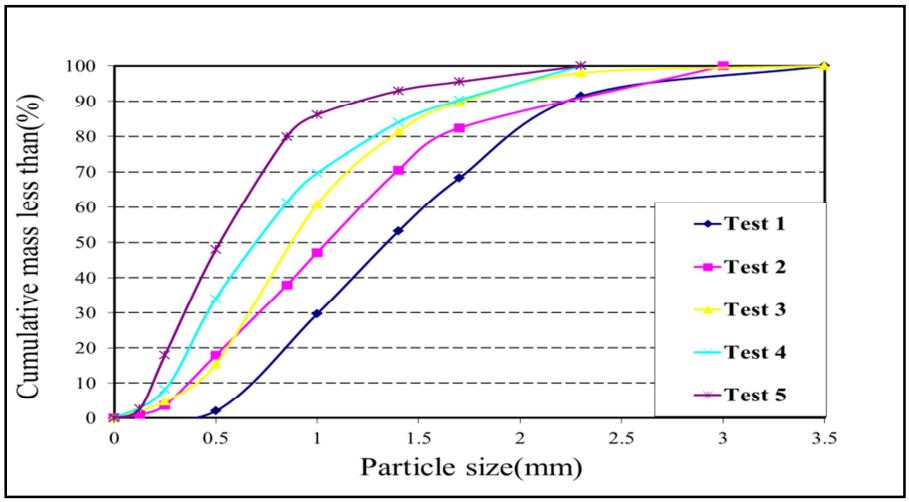

Figure D.2.12b: Particle size distribution of bed char

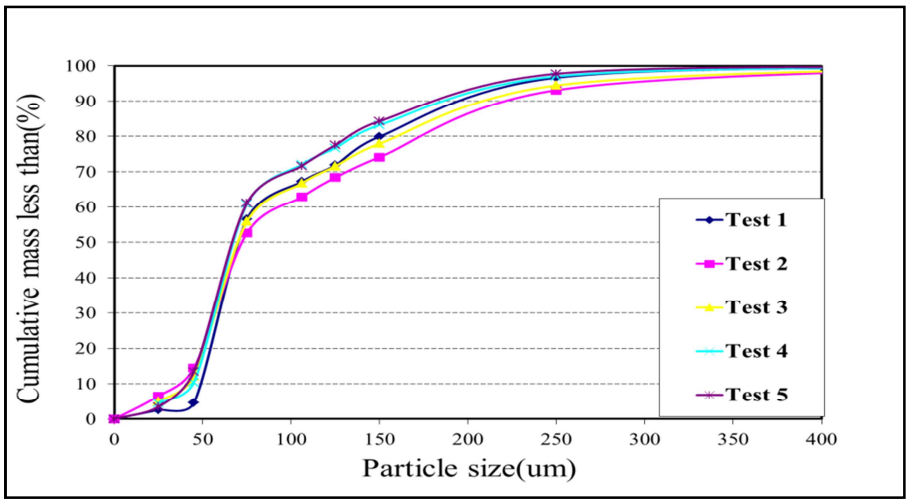

Figure D.2.12c: Particle size distribution of cyclone char

Appendix D.2.13: Particle size distributions (oxygen and steam tests)

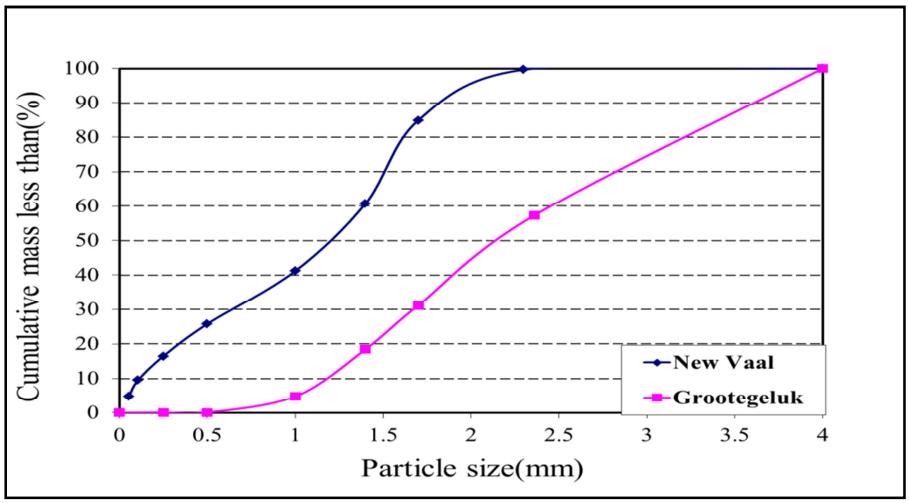

Figure D.2.13a: Particle size distribution of coal

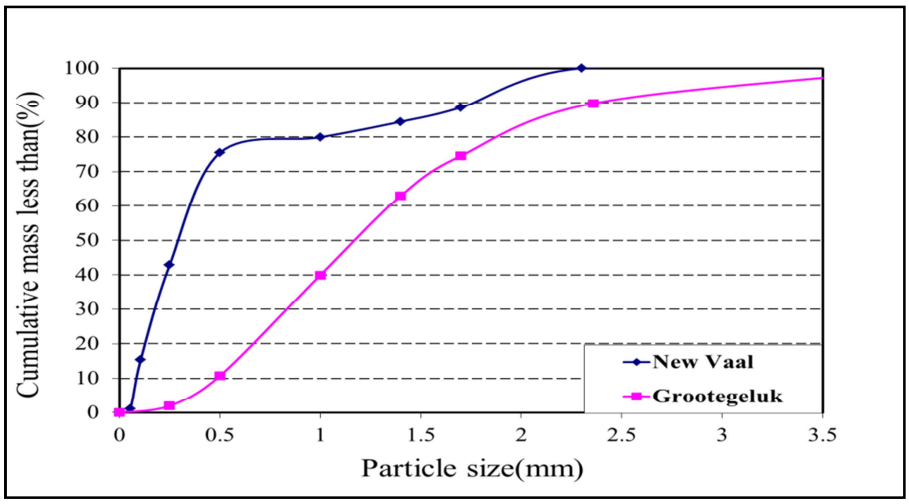

Figure D.2.13b: Particle size distribution of bed char

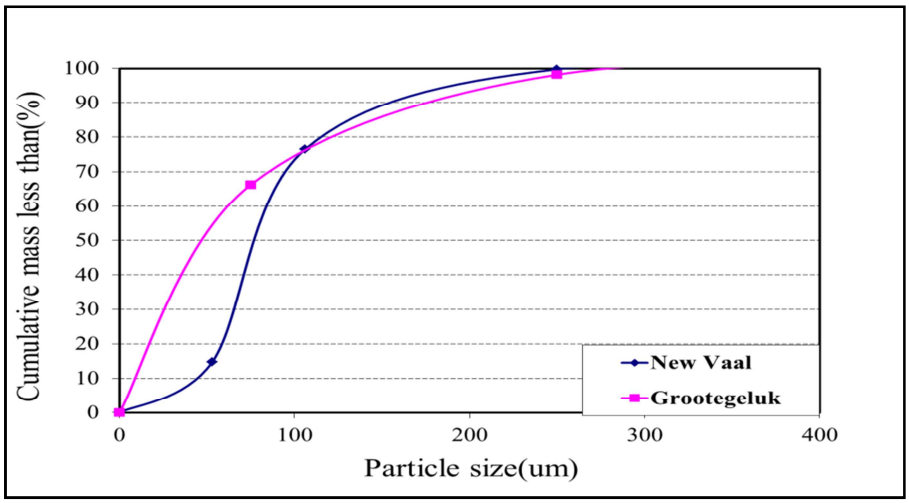

Figure D.2.13c: Particle size distribution of cyclone char

Appendix D.2.14: Gasifier temperature variation for Grootegeluk coal

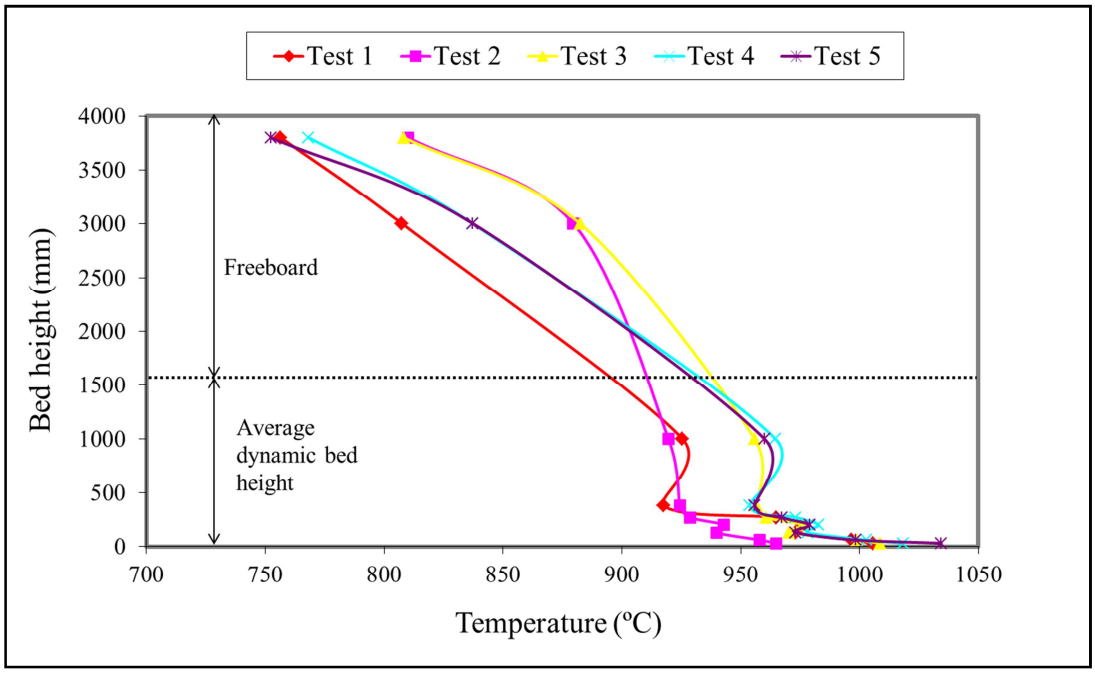

Figure D.2.14: FBG temperature as a function of height for Grootegeluk coal

Appendix D.2.15: Proximate and ultimate analyses of New Vaal and Grootegeluk coal

Table D.2.1: Proximate and ultimate analysis of NV and GG coal

Test condition	Standard	New Vaal			Grootegeluk
		Oxygen, air and steam (Tests 1 - 4)	Oxygen, air and steam (Test 5)	Oxygen and steam	Oxygen and steam
Proximate analysis					
Ash content (%)	ISO 1171	37.50	40.70	40.40	32.60
Inherent moisture (%)	SABS 925	5.91	5.70	5.80	1.90
Volatile matter (%)	ISO 562	20.74	20.50	19.20	29.40
Fixed carbon (%)	By diff.	35.85	33.10	34.60	35.70
Ultimate analysis					
Carbon (%)	ISO 12902	44.07	39.26	42.58	52.60
Hydrogen (%)	ISO 12902	3.54	3.45	2.19	3.96
Nitrogen (%)	ISO 12902	0.98	0.90	0.89	0.86
Sulphur (%)	ISO 19759	0.66	0.84	0.69	1.48
Oxygen (%)	By diff.	7.34	9.16	7.46	6.60
Calorific value					
Calorific value (MJ/kg)	ISO 1928	17.71	15.76	15.56	21.20

(All percentages are given as wt.%)

APPENDIX E: FLUIDISED BED COAL GASIFIER MODELLING

NOTE: Symbols used in Appendix E are defined in the nomenclature at the end of Chapter 5.

Appendix E.1: Fluidised bed gasifier modelling literature survey

Appendix E.1.1: Hydrodynamics

Appendix E.1.1 1: Minimum fluidising velocity

The correlation of Geldart (1986) is given by equation (E.1.1.1a).

$$1.75\rho_g U_{mf}^{\ 2} + \frac{150(1-\varepsilon_{mf})\mu_g}{d_p} U_{mf} = (\rho_{char} - \rho_g) g d_p \varepsilon_{mf}^3 \qquad \text{(E.1.1.1a)}$$

The correlation of Sit and Grace (1981) is given by equation (E.1.1.1b).

$$U_{mf} = \left(\frac{U}{d_p \rho_g}\right)\left\{\left[638 + \frac{0.0651 d_p^{\ 3} \rho_g (\rho_{char} - \rho_g) g}{\mu_g}\right]^{0.5} - 25.25\right\} \qquad \text{(E.1.1.1b)}$$

Appendix E.1.1.2: Bubble diameter

The correlation of Darton et al. (1977) is given by equation (E.1.1.2).

$$d_b = 0.54(U - U_{mf})^{0.4}(z + z_0)^{0.8} g^{-0.2} \qquad \text{(E.1.1.2)}$$

Where z_0 is found by making z = 0, replacing d_b with D_{B0}, which is calculated by the equation of Mori and Wen (1975) (equation (4.1) in Chapter 4) and solving for z_0.

Appendix E.1.2: Devolatilisation

Appendix E.1.2 1: Correlation of Lee *et al.* (1998)

Coefficients obtained for an Australian sub-bituminous coal are given in Table E.1.2.1.

$$\frac{M_i}{M_{daf}} = A_i + B_i T \qquad \text{(E.1.2.1)}$$

Table E.1.2.1: Coefficients for an Australian sub-bituminous coal

Species	Parameters	
	A_i	B_i
CO	-0.102	2.168E-04
H_2	-0.073	8.233E-04
CH_4	0.011	2.561E-04
CO_2	0.039	2.999E-06

Appendix E.1.2 2: Correlation of Ma *et al.* (1988)

$$\frac{M_i}{M_{daf}} = A_i + B_i T \qquad \text{(E.1.2 2)}$$

Table E.1.2.2: Coefficients for New Mexico sub-bituminous coal

Species	Parameters	
	A_i	B_i
CO	-0.625	6.52E-04
H_2	-4.93E-02	5.02E-05
CH_4	-0.325	3.43E-04
CO_2	-9.95E-02	1.43E-04
H_2S	-2.28E-02	2.29E-05
COS	-2.79E-02	3.16E-06
Tar	0.1175	0

Appendix E.1.2.3: Data of Yeboah *et al.* (1980)

Table E.1.2.3: Data for Illinois No. 6 coal

Gas composition (vol.%)	Temperature (K)				
	873	**923**	**973**	**1033**	**1073**
CO	12.5	14.1	15.5	17.0	17.9
CO_2	15.0	13.7	13.0	12.0	17.9
H_2	37.1	39.8	41.6	42.8	43.6
CH_4	21.8	20.5	19.1	17.5	16.8
C_2H_6	4.1	3.8	3.3	2.9	2.6
C_3H_6	3.6	3.5	3.0	2.8	2.3

Appendix E.1.3: Heterogeneous reactions

Appendix E.1.3.1: Char-steam gasification reaction

The structural factor is F(X) in equation (4.25), which is given by equations (E.1.3.1a) and (E.1.3.1b).

$$F(X) = (1-X)^{2/3}\exp(-\alpha X^2) \qquad \text{(E.1.3.1a)}$$

$$\alpha = \frac{52.5p_{H_2}}{1+54.3p_{H_2}} + \frac{0.521p_{H_2}^{0.5}\,p_{H_2O}}{1+0.707p_{H_2}+0.5p_{H_2}^{0.5}p_{H_2O}} \qquad \text{(E.1.3.1b)}$$

The term k_I in equation (4.25) is given by equations (E.1.3.1c), (E.1.3.1d) and (E.1.3.1e).

$$k_I = \frac{k_1}{60} \qquad \text{(E.1.3.1c)}$$

$$k_1 = \frac{\exp\left(9.0201 - \frac{12910}{T}\right)\left(1 - \frac{p_{CO}p_{H_2}}{p_{H_2O}K_{eq1}}\right)}{\left[1 + \exp\left(-22.216 + \frac{24881}{T}\right)\left(\frac{1}{p_{H_2O}} + 16.35\frac{p_{H_2}}{P_{H_2O}} + 43.5\frac{p_{CO}}{p_{H_2O}}\right)\right]^2} \quad \text{(E.1.3.1d)}$$

$$\log_{10}K_{eq1} = 7.49 - \frac{7070}{T} \quad \text{(E.1.3.1e)}$$

Appendix E.1.3.2: Hydrogen-char gasification

The structural factor is F(X) in equation (4.30), which is given by equations (E.1.3.1a) and (E.1.3.1b).

The term $G(T, p_i)_{H2}$ in equation (4.30) is given by equations (E.1.3.2a), (E.1.3.2b) and (E.1.3.2c).

$$k_{II} = \frac{k_1}{60} \quad \text{(E.1.3.2a)}$$

$$k_2 = \frac{p_{H_2}^2 \exp\left(2.6741 - \frac{13672}{T}\right)\left(1 - \frac{p_{CH_4}}{p_{H_2}^2 K_{eq2}}\right)}{\left[1 + p_{H_2}\exp\left(-10.452 + \frac{11097}{T}\right)\right]} \quad \text{(E.1.3.2b)}$$

$$\log_{10}K_{eq2} = -5.373 + \frac{4723}{T} \quad \text{(E.1.3.2c)}$$

Appendix E.1.4: Homogeneous reactions

Appendix E.1.4.1: Water gas-shift reaction

The rate expression of Chen *et al*. (1987) is given by equation (E.1.4.1).

$$r_{wgs} = \frac{k_{wgsb}}{(RT)^2}\left[P_{CO}P_{H2O} - \frac{P_{CO2}P_{H2}}{K_{wgs}}\right] \quad \text{(E.1.4.1)}$$

$$k_{wgsb} = 2.780E06\exp\left(\frac{-1510.7}{RT}\right)$$

$$K_{wgs} = 0.0265\exp\left(\frac{3985.5}{T}\right)$$

Appendix E.1.5: Interphase heat and mass transfer

Appendix E.1.5.1: Interphase mass transfer

The mass interchange coefficient derived by Kunii and Levenspiel (1969) is given by equations (E.1.5.1a), (E.1.5.1b) and (E.1.5.1c).

$$K_{bc} = 4.5\left(\frac{U_{mf}}{d_b}\right) + 5.85\left(\frac{D_g^{0.5} g^{0.25}}{d_b^{1.25}}\right) \quad \text{(E.1.5.1a)}$$

$$K_{ce} = 6.78\left(\frac{\varepsilon_{mf} D_g u_b}{d_b^{3}}\right)^{0.5} \quad \text{(E.1.5.1b)}$$

$$\frac{1}{K_{be}} = \frac{1}{K_{bc}} + \frac{1}{K_{ce}} \quad \text{(E.1.5.1c)}$$

The mass interchange coefficient derived by Wen and Fan (1975) is given by equation (E.1.5.1d).

$$K_{be} = \frac{0.11}{d_b} \quad \text{(E.1.5.1d)}$$

Appendix E.1.6: Fines generation and elutriation

The terminal falling velocity of char particles can be calculated using the correlation of Geldart (1986) given in equations (E.1.6a) and (E1.6b).

$$u_t = \left(\frac{4d_p(\rho_{char} - \rho_g)g}{3\rho_g C_D} \right)^{0.5} \qquad \text{(E.1.6a)}$$

For $0 < Re_p < 0.4$ $\qquad C_D = \frac{24}{Re_p}$

For $0.4 < Re_p < 500$ $\qquad C_D = \frac{10}{(Re_p)^{0.5}}$

For $0 < Re_p < 0.4$ $\qquad C_D = 0.43$

$$Re_p = \frac{\rho_{char} u_t d_p}{\mu_g} \qquad \text{(E.1.6b)}$$

Appendix E.2: Fluidised bed coal gasifier modelling

Appendix E.2.1: Conversion of reaction rate units

To convert $(\frac{dX}{dt})_j$ in (s^{-1}) to r''_j in ($mol.m^{-3}s^{-1}$)

$(\frac{dX}{dt})_j$ in (s^{-1}) is multiplied by $\left(\frac{C_{char}.\rho_{char}}{72} \right)$ (E.2.1)

C_{char} – carbon in char (wt.%) $= \left(\frac{C_{fixed}}{C_{fixed} + C_{ash}} \right) 100$

C_{fixed} – fixed carbon in coal (wt.%)

C_{ash} – ash in coal (wt.%)

ρ_{char} – char density ($kg.m^{-3}$)

Appendix E.2.2: Net flow calculation

Figure E.2.2 shows a schematic diagram which illustrates the origin of net flow gas. Due to char combustion, char gasification, gas combustion and coal devolatilisation, the molar gas flow in the emulsion phase increases. Based on the two-phase theory of fluidisation, all gas in excess of that required to maintain incipient fluidisation condition passes through the bed in the bubble phase. Therefore the output emulsion and bubble phase molar flow rates of an incremental bed section must be adjusted in order to maintain incipient fluidisation conditions in the emulsion phase as required by the two-phase model of fluidisation.

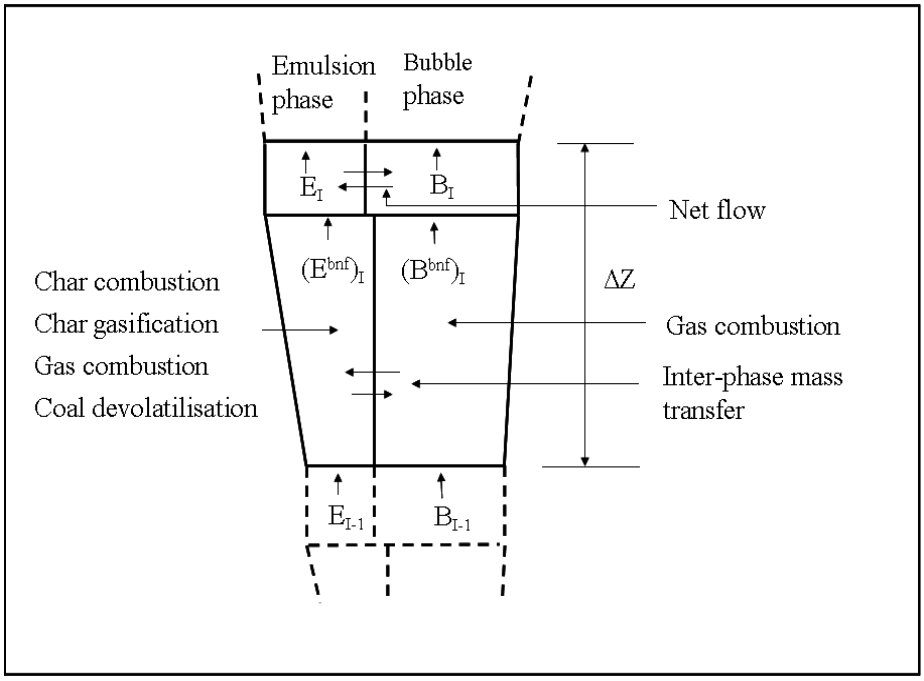

Figure E.2.2: Schematic representation of the two-phase model of fluidisation

According to the two-phase theory of fluidisation, the outlet gases therefore have to satisfy equation (E.2.2a).

$$\frac{E_I}{E_I + B_I} = \frac{U_{mf}}{U} = \lambda \qquad \text{(E.2.2a)}$$

Conservation of mass requires:

$$E_I + B_I = E_I^{bnf} + B_I^{bnf} \qquad \text{(E.2.2b)}$$

Substituting equation (E.2.2b) into (E.2.2a) gives:

$$E_I = \lambda(E_I^{bnf} + B_I^{bnf}) \quad \text{(E.2.2c)}$$

Since the net flow is the gas which flows from the emulsion to the bubble phase, it can be represented by equation (E.2.2d):

$$NF_I = E_I^{bnf} - E_I \quad \text{(E.2.2d)}$$

Substituting equation (E.2.2c) into equation (E.2.2d) gives the final equation to calculate the net flow of an incremental bed section.

$$NF_I = (1-\lambda)E_I^{bnf} - \lambda B_I^{bnf} \quad \text{(E.2.2e)}$$

In differential form equation (E.2.2e) becomes:

$$NF_R = \frac{dNF}{dz} = \frac{df_g^e}{dz} - [\frac{d\lambda}{dz}] f_g^e - [\frac{df_g^e}{dz}]\lambda - [\frac{d\lambda}{dz}].f_g^b - [\frac{df_g^b}{dz}]\lambda \quad \text{(E.2.2f)}$$

Appendix E.2.3: Gasifier overall carbon balance

The calculation of the overall gasifier carbon balance and selection of a new value of fixed carbon conversion (X) for the next iteration loop is shown below.

Input data

The guessed value of fixed carbon conversion (X(k)) = 0.800

Coal flow ($G_{coal)}$ = 19.6 kg/h

Total carbon in coal (C) = 52.93 wt.%

Fixed carbon in coal (C_{fixed}) = 38.1 wt.%

Based on the above: Total carbon input = 0.240 mol/s; fixed carbon input = 0.173 mol/s.

Molar gasifier output flows of the gas components are calculated by the model using a fixed carbon conversion of 0.800.

f_{gCO2} = 0.100 mol/s

f_{gCO} = 0.086 mol/s

f_{gCH4} = 0.013 mol/s

f_{gH2} = 0.107 mol/s

f_{gN2} = 0.207 mol/s

The output carbon flow is therefore:

(0.100 + 0.086 + 0.013) = 0.198 mol/s

The calculated fixed carbon conversion is therefore:

X(calc) = 0.756

The new guessed value of the fixed carbon conversion is calculated by taking the average between the previous guessed value and the calculated value.

$$X(k+1) = \frac{(X(k) + X(calc))}{2} = 0.779 \qquad \text{(E.2.3a)}$$

The above procedure is repeated until:

$$X(k+1) - X(k) < e_x \qquad \text{(E.2.3b)}$$

Where e_x is the convergence criteria for fixed carbon conversion.

Appendix E.2.4: Gasifier overall energy balance

In order to calculate the rates of heterogeneous chemical reactions and the yield of volatiles, it is required initially to guess a value for the solids temperature (T_s). Once the fixed carbon conversion has been obtained by solving the inner loop calculations as given above, an overall energy balance is carried out over the bed to obtain a new solids temperature. The energy balance for Test 4 on Grootegeluk coal is given in Table E.2.2 as an example.

Input flows are:

Coal flow: 19.6 kg/h

Steam flow: 15 kg/h

Oxygen flow: 7.6 kg/h

Air flow: 26.9 Nm^3/h

Reactant temperature (steam + oxygen + air): 274 °C

Table E.2.1: Gasifier heat inputs

Energy input (MJ/h)	Calculation (MJ/h)	Calculated value (MJ/h)
Potential energy in coal	$G_{coal}.\ CV_{coal}$	420.2
Sensible energy in oxygen	$G_{O2}\,(1\ 000/32)c_{pO2}(T_r\text{-}25)/1E\text{-}06$	1.8
Sensible energy in air	$G_{air}(1\ 000/28.84)c_{pair}(T_r\text{-}25)/1E\text{-}06$	7.0
Sensible energy in steam	$G_{steam}(1\ 000/18)c_{psteam}\ (T_r\text{-}25)/1E\text{-}06$	7.3
Latent energy in steam	$G_{steam}.\Delta H^0_{evap}$	36.7
Total		472.9

The gasifier heat outputs are based on the following output values:

Dry gas calorific value : 5.80 MJ/Nm^3

Dry gas flow : 41.3 Nm^3/h

Wet gas flow : 58.9 Nm^3/h

Char flow : 8.02 kg/h

Carbon in char : 22.5 wt.%

Calorific value of carbon in char : 30 MJ/kg

Heat losses : 44.2 MJ/h

Heat capacity of bed char : 1.19 kJ/(kg.°C)

Heat capacity of wet gas : 1.618 kJ/(Nm^3.°C)

Table E.2.2: Gasifier energy outputs

Energy input (MJ/h)	Calculation (MJ/h)	Calculated value (MJ/h)
Potential energy in gas	$NQ_{gas}.CV_{gas}$	239.6
Potential energy in bed char	$G_{BC}.(C_{char}/100).CV_{CC}$	54.3
Sensible energy in bed char	$G_{BC}.c_{pBC}(T_s\text{-}25)\ /1\ 000$	9.1
Sensible energy in gas	$WNQ_{gas}\ .c_{pg}(T_s\text{-}25)/1\ 000$	91.1
Latent energy in water in gas	$(WNQ_{gas}\text{-}\ NQ_{gas}\ )(44.64)(0.018)\Delta H^0_{evap}$	34.6
Energy losses	Q	44.2
Total		472.9

Since the solids temperature and the gas temperature are equal at the top of the bed the solids temperature can be obtained by solving equation (E.2.4a).

$$T_S(\text{calc}) = \frac{Q_I - \left(NQ_{gas}.CV_{gas} + G_{BC}\left(\frac{C_{char}}{100}\right)CV_{CC} + \left(WNQ_{gas} - NQ_{gas}\right).(44.64)(0.018)\Delta H^0_{evap} + Q \right)}{\frac{G_{BC}c_{pBC}}{1000} + \frac{WNQ_{gas}.c_{pg}}{1000}} + 25$$

(E.2.4a)

Using the above values gives T_s(calc) = 980 °C. The guessed value of T_s is: T_s(l) = 970. The new guessed value of T_s is given by equation (E.2.4b):

$$T_s(l+1) = \frac{\left(2T_s(l) + Ts(\text{calc})\right)}{3} = 973.3 \qquad \text{(E.2.4b)}$$

Equation (E.2.4b) shows that the new guessed value (T_s(l+1)) is weighted towards the previous guessed value (T_s(l)) in order to prevent the new guessed value from being too high or too low and thus being outside the validity of the kinetic equations and resulting in numeric overflows or underflows.

The above procedure is repeated until:

$$T_s(l+1) - T_s(k) < e_{Ts} \qquad \text{(E.2.4c)}$$

Where e_{Ts} is the convergence criteria for the solids temperature.

Appendix E.2.5: Transport and thermodynamic properties

Appendix E.2.5.1: Gas viscosity

The correlation of Rohsenow and Hartnett (1973) was used to estimate the pure gas component viscosities and is given by equation (E.2.5a).

$$\mu_i = a_i + b_i F_i(T_g) \qquad \text{(E.2.5a)}$$

The viscosity of a gas mixture is estimated from the pure gas component viscosities using equation (E.2.5b). Equation (E.2.5b) is a simplified version of the rigorous estimation method of Wilke (1950). The difference in the estimated gas mixture viscosities using the simplified and rigorous methods is less than 2%.

$$\mu = \sum_{i}^{7} u_i y_i \qquad \text{(E.2.5b)}$$

y_i - mole fraction of gas component i in the gas mixture.

The coefficients a_i, b_i, and $F_i(T_g)$ in equation (E.2.5a) are given in Table E.2.3.

Table E.2.3: Coefficients used in estimating pure component viscosities[1]

Components	a_i	b_i	$F_i(T_g)$	Range of validity (°C)
O_2	150.3	0.3265	(T_g+273)	500 – 1 350
N_2	0.0	5.950	$(T_g+273)^{0.6085}$	500 – 1 350
CO_2	131.5	0.2611	(T_g+273)	500 – 1 350
H_2O	0.0	0.4465	$(T_g+273)^{0.9657}$	500 – 1 350
H_2	60.6	0.1415	(T_g+273)	500 – 1 000
CO	0.0	6.868	$(T_g+273)^{0.5894}$	500 – 1 350
CH_4	-613.2	127.8	$Ln(T_g+273)$	500 – 1 000

[1]Viscocity ($kg.m^{-1}s^{-1}$)

Appendix E.2.5.2: Gas thermal conductivity

The data of Rohsenow and Hartnett (1973) were used to estimate the pure gas component viscosities and are given by equation (E.2.5c).

$$k_{g_i} = a_i + b_i F_i(T_g) \qquad \text{(E.2.5c)}$$

The viscosity of a gas mixture is given by:

$$k_{gi} = \sum_{i}^{7} k_{gi} y_i \qquad \text{(E.2.5d)}$$

y_i is the mole fraction of gas component i in the gas mixture.

The coefficients a_i, b_i, and $F_i(T_g)$ in equation (E.2.5c) are given in Table E.2.4.

Table E.2.4: Coefficients used in estimating gas component thermal conductivities[1]

Components	$a_i \times 10^2$	$b_i \times 10^5$	$F_i(T_g)$	Range of validity (°C)
O_2	1.77	5.346	(T_g+273)	427 – 1 227
N_2	2.028	4.254	(T_g+273)	427 – 1 227
CO_2	1.814	4.873	(T_g+273)	827 – 1 350
H_2O	-1.949	10.84	(T_g+273)	427 – 1 027
H_2	8.588	34.24	(T_g+273)	427 - 923
CO	1.640	4.814	(T_g+273)	427 – 1 227
CH_4	-5.531	22.40	(T_g+273)	< 773

[1]Thermal conductivity ($J.m^{-1}s^{-1}K^{-1}$)

Appendix E.2.5.3 Gas heat capacity

The mean gas heat capacities were obtained from correlations given by Reid *et al*. (1977) and are expressed by equation (E.2.5e).

$$c_{pgi} = a_i + b_i F_i(T_g) \qquad \text{(E.2.5e)}$$

The mean gas heat capacity of a gas mixture is given by:

$$c_{pgi} = \sum_{i}^{7} c_{pgi} y_i \qquad \text{(E.2.5f)}$$

y_i - mole fraction of gas component i in the gas mixture.

The coefficients a_i, b_i and $F_i(T_g)$ in equation (E.2.5e) are given in Table E.2.5.

Table E.2.5: Coefficients used in estimating gas component heat capacities[1]

Components	a_i	$b_i \times 10^3$	$F_i(T_g)$	Range of validity (°C)
O_2	31.34	1.360	(T_g+273)	900 – 1 100
N_2	28.83	1.920	(T_g+273)	900 – 1 100
CO_2	39.64	8.102	(T_g+273)	900 – 1 250
H_2O	31.33	5.746	(T_g+273)	900 – 1 250
H_2	26.83	2.440	(T_g+273)	900 – 1 100
CO	29.30	1.820	(T_g+273)	900 – 1 100
CH_4	35.40	19.99	(T_g+273)	900 – 1 250

[1] Mean gas heat capacity ($J.mol^{-1}K^{-1}$)

The mean specific heat capacity is an integrated average of specific heat between any given temperature and the base temperature (25 °C). Multiplying the mean specific heat capacity by the temperature difference between any given temperature and the base temperature gives the amount of heat required to raise the temperature of one mole of gas from the base temperature to the specified temperature.

Appendix E.2.5.4 Solids heat capacity

The mean solids heat capacities were obtained from Liley and Gambill (1980).

$$c_{psk} = a_k + b_k F_k(T_s) \qquad \text{(E.2.5g)}$$

The mean gas heat capacity of a solids mixture is given by:

$$c_{ps} = \sum_{k}^{2} c_{psk} m_k \qquad \text{(E.2.5h)}$$

m_k - mass fraction of solid component k in the solids mixture.

The coefficients a_k, b_k and $F_k(T_s)$ in equation (E.2.5g) are given in Table E.2.6.

Table E.2.6: Coefficients used in estimating solid component heat capacities[1]

Components	$a_k \times 10^{-3}$	b_k	$F_k(T_s)$	Range of validity (°C)
Fixed carbon	-0.844	343.7	$Ln(T_s)$	200 – 1 093
Ash	0.915	0.294	T_s	200 – 1 093

[1]Mean solid heat capacity ($J.kg^{-1}K^{-1}$)

The mean solids heat capacity is an integrated average of specific heat between any given temperature and the base temperature (25 °C). Multiplying the mean specific heat capacity by the temperature difference between any given temperature and the base temperature gives the amount of heat required to raise the temperature of 1 kg of solid from the base temperature to the specified temperature.

Appendix E.2.5.5 Heats of reaction

Heats of reaction were obtained from Liley and Gambill (1980) and are given in Table E.2.7.

Table E.2.7: Heats of reaction

Reaction number (j)	Equation number	Reaction equation	ΔH^0_{rj} (J/mol)
1	(4.13)	$C + \varphi O_2 \rightarrow 2(1-\varphi)CO + (2\varphi - 1)CO_2$	$-2(1-\varphi)(111500)$ $-(2\varphi - 1)(393500)$
2	(4.14)	$C + H_2O \rightarrow CO + H_2$	131 300
3	(4.15)	$C + CO_2 \rightarrow 2\,CO$	172 000
4	(4.16)	$C + 2H_2 \rightarrow CH_4$	-74 800
5	(4.31)	$CO + H_2O \rightarrow CO_2 + H_2$	-41 200
6	(4.32)	$CO + ½\,O_2 \rightarrow CO_2$	-283 000
7	(4.33)	$H_2 + ½\,O_2 \rightarrow H_2O$	-241 800
8	(4.34)	$CH_4 + 2O_2 \rightarrow 2H_2O + CO_2$	-802 000

φ Combustion product distribution coefficient ($0.5 < \varphi < 1$)

Appendix E.2.6: Reactions for the formation of sulphur and nitrogen-containing species in the gas

$S + H_2$	→	H_2S	(E.2.6a)
$S + O_2$	→	SO_2	(E.2.6b)
$H_2S + CO_2$	→	$COS + H_2O$	(E.2.6c)
$H_2S + 3O_2$	→	$2SO_2 + 2H_2O$	(E.2.6d)
$N_2 + O_2$	→	$2NO$	(E.2.6e)
$NO + 3/2H_2O$	→	$NH_3 + 5/4O_2$	(E.2.6f)
$N_2 + 3/2H_2$	→	NH_3	(E.2.6g)

Pinto *et. al*, (2012).

Appendix E.2.7: Deviations between predicted and measured gasifier performance variables

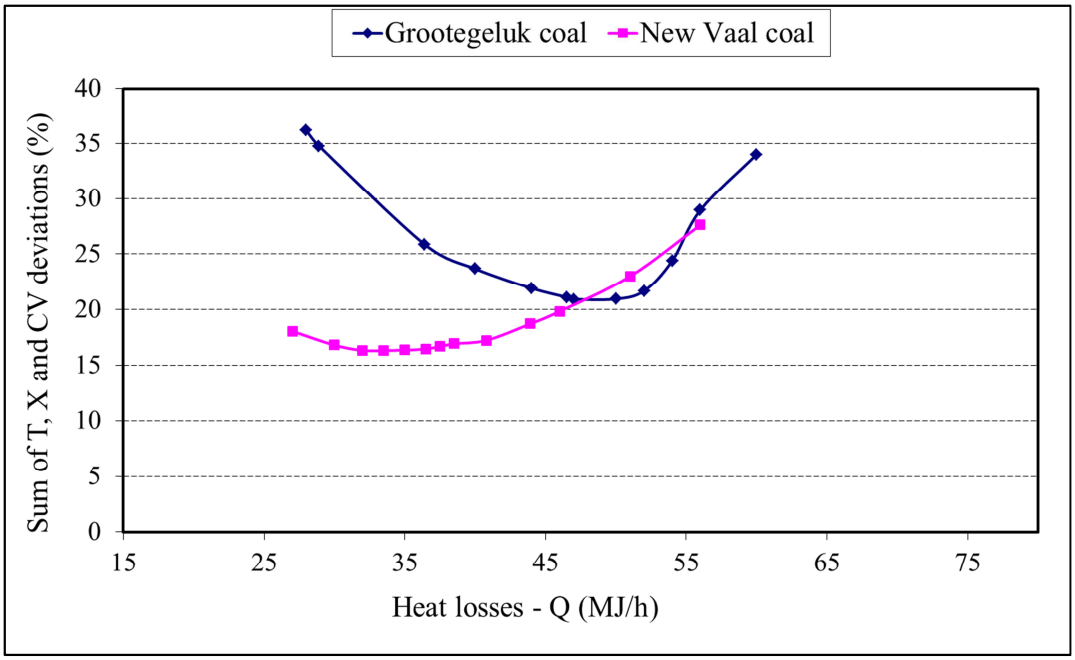

Figure E.2.7: Effect of Q on sum of performance variables deviation

Appendix E.2.8: Estimation of fluidised bed heat losses

As shown in Figure E.2.8 heat losses from the fluidised bed consist of:

- Heat transfer through the furnace wall
- Heat transfer through the distributor plate
- Heat transfer from the bed to the freeboard

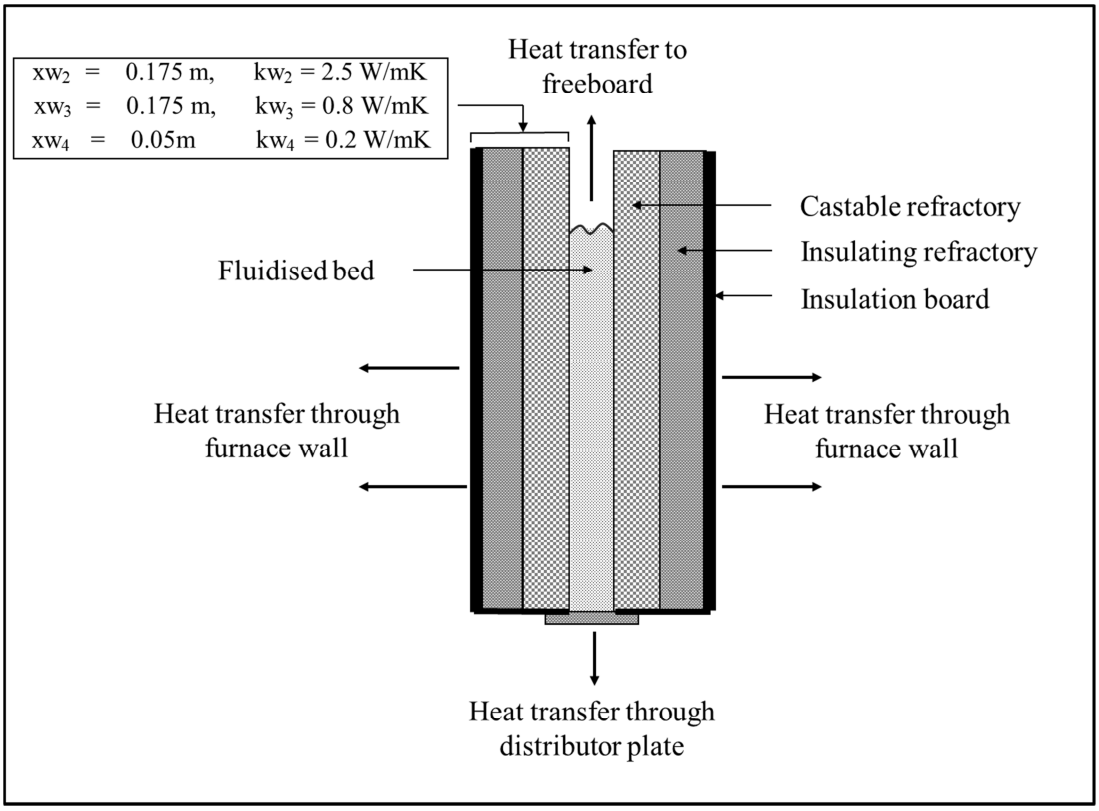

Figure E.2.8: Diagrammatic representation of fluidised bed heat losses

Heat transfer through the furnace wall

Heat transfer through the refractory furnace wall encounters five thermal resistances:

1. Forced convection from the fluidised bed to the inside wall of the gasifier.
2. Conduction through the castable refractory layer.
3. Conduction through the insulating refractory layer.
4. Conduction through the insulation board.

5. Radiation from the outside wall of the gasifier to the surrounding air.

The heat transfer coefficient for each thermal resistance, the temperature at the interface of the resistances and the heat transferred through each resistance is given in Table E.2.8.

Table E.2.8: Heat transfer through the wall of the gasifier

Heat transfer resistance	**Thermal conductivity ($W.m^{-1}K^{-1)}$**	**Heat transfer coefficient ($W.m^{-2}K^{-1}$)**	**Inside temperature (°C)**	**Outside temperature (°C)**	**Heat transferred ($W.m^{-2}$)**
1	-	90.0	945	930	1 425
2	2.5	14.3	930	831	1 425
3	0.8	4.6	831	519	1 425
4	0.2	4.0	519	163	1 425
5	-	10.7	163	30	1 425

The forced convection heat transfer coefficient between the fluidised bed and the furnace wall (90.0 $Wm^{-2}K^{-1}$) is given in Geldart (1986).

The heat transfer coefficient of the refractory and insulating board layers (resistances 2 to 4) were calculated using equation (E.2.8a) given in Coulson and Richardson (1977).

$$h_{wi} = \frac{k_{wi}}{x_{wi}} \qquad \text{(E.2.8a)}$$

For i = 2, 3 and 4.

The thermal conductivity and thickness of the refractory and board layers are given in Figure E.2.8 above. The thermal conductivities were estimated using the Vereeniging Refractories Technical Data Book (2013) for typical castable, insulation and board products. The Vereeniging Refractories Technical Data Book was used since records of the products used by the contractor in 1995 when the furnace was constructed

could not be found. The radiative heat transfer coefficient (resistance 5) was calculated using the Stefan-Boltzmann equation (E.2.8b) given in Coulson and Richardson (1977).

$$h_{w5} = \sigma e(T_w^4 - T_a^4) \quad \text{(E.2.8b)}$$

σ - Stefan-Boltzmann constant (5.67E-08)

e - Furnace wall emissivity (0.9)

T_w - Temperature of the furnace wall (436 K)

T_a - Ambient temperature (303 K)

In order to calculate the heat transferred through the gasifier wall as given in Table E.2.8 (1 425 Wm^{-2}), an energy balance is carried out by equating the heat transferred through each of the five thermal resistances. The heat balance produces five linear equations with the unknowns in the equations being the temperatures between the thermal resistances. Solution of the equations gives the interface temperatures which allow calculation of the heat transferred using equation (E.2.8c).

$$H_w = h_{wi}(T_i - T_{(i-1)}) = 1425 \text{ W.m}^{-2} \quad \text{(E.2.8c)}$$

The total heat transfer through the wall of the gasifier is calculated using equation (E.2.8d).

$$Q_w = H_w A_m = 4700 \text{ W} \quad \text{(E.2.8d)}$$

A_m - logarithmic mean surface area

$$A_m = \frac{A_{ex} - A_{in}}{ln\left(\frac{A_{ex}}{A_{in}}\right)} \quad \text{(E.2.8e)}$$

A_{in} = internal surface area of gasifier bed section

A_{ex} = external surface area of gasifier bed section

$$A_{in} = 4\sqrt{A_B}H_b \quad \text{(E.2.8f)}$$

A_B = gasifier area in the bed section = 0.04 m^2

$$A_{ex} = 8(xw_2 + xw_3 + xw_4)\sqrt{A_B}H_b \quad \text{(E.2.8g)}$$

H_b = average dynamic bed height = 1.46 m

$x_{w2, 3, 4}$ = thickness of refractory and board layers (see Figure E.2.8)

Heat transfer through the distributor plate

Heat transfer through the distributor plate of the furnace encounters three thermal resistances.

1. Forced convection from the fluidised bed to the inside wall of the distributor plate.
2. Conduction through the stainless steel distributor plate (10 mm thickness).
3. Radiation from the outside walls of the distributor plate to the surrounding air.

The heat transfer coefficient for each thermal resistance, the temperature at the interface of the resistances and the heat transferred through each resistance is given in Table E.2.9.

Table E.2.9: Heat transfer through the distributor plate of the gasifier

Heat transfer resistance	**Thermal conductivity ($W.m^{-1}K^{-1}$)**	**Heat transfer coefficient ($W.m^{-2}K^{-1}$)**	**Inside temperature (°C)**	**Outside temperature (°C)**	**Heat transferred ($W.m^{-2}$)**
1	-	90.0	945	614	30 200
2	45	4500	624	607	30 200
3	-	10.63	607	30	30 200

The convective heat transfer coefficient between the fluidised bed and the distributor plate (90.0 $W.m^{-2}K$) is given in Geldart (1986).

The heat transfer coefficient of the distributor plate was calculated using equation (E.2.8h), (Coulson and Richardson, 1977).

$$h_{d2} = \frac{k_{d2}}{x_{d2}} = \frac{45\ Wm^{-1}K^{-1}}{0.01m} = 4500\ \text{W.m}^{-2}\text{K}^{-1} \quad \text{(E.2.8h)}$$

k_{d2} = Thermal conductivity of the distributor plate (45 $W.m^{-1}K^{-1}$)

x_{d2} = Thickness of the distributor plate (0.01 m)

The radiative heat transfer coefficient (resistance 3) was calculated using equation (E.2.8i).

$$h_{d3} = \sigma e(T_d^4 - T_a^4) \quad \text{(E.2.8i)}$$

T_d = Outside temperature of the distributor plate (880 K)

T_a = Ambient temperature (303 K)

The heat transferred through the distributor plate is given by equations (E.2.8j) and (E.2.36).

$$H_d = H_{di}(T_i - T_{(i-1)}) = 30200\ \text{W.m}^{-2} \quad \text{(E.2.8j)}$$

$$Q_d = H_d A_d = 3800\ \text{W} \quad \text{(E.2.8k)}$$

Heat transfer from the bed to the freeboard

Heat transfer from the bed to the freeboard of the gasifier consists of thermal radiation from the bed to the freeboard and was calculated using equation (E.2.8l). It is assumed that the bed and the freeboard are parallel surfaces separated by a distance of two metres and that the area factor (F_A) is equal to 0.8 (Hsu, 1962).

$$Q_{fb} = A_B F_A \sigma e\left(T_b^4 - T_{fb}^4\right) = 1700\ \text{W} \quad \text{(E.2.8l)}$$

T_b = average bed temperature (1218 K)

T_{fb} = average freeboard temperature (1033 K)

A_B = bed area at the top of the bed (0.04 m^2)

F_A = area factor for radiative heat transfer between parallel surfaces (0.8)

Using equations (E.2.8a) – (E.2.8l), the heat loss components and the total heat losses can be calculated and are given in Table E.2.10.

Table E.2.10: Fluidised bed gasifier heat losses

Heat loss component	Heat transfer coefficient ($W.m^{-2}$)	Effective area (m^2)	Heat transferred	
			kW	$MJ.h^{-1}$
Heat transfer through the furnace wall	1 400	3.24	4.7	17.0
Heat transfer through distributor plate	30 200	0.1	3.8	13.8
Heat transfer from the bed to the freeboard	54 000	0.032	1.7	6.2
Total fluidised bed heat losses			**10.3**	**37.0**

Due to the uncertainties associated with the values of the thermal conductivities of the refractories used in the furnace and the area factor for the calculation of the bed to freeboard radiation heat losses, the estimated error in the heat loss calculation is ±25%.The estimated total heat loss from the fluidised bed is therefore:

$$Q = \frac{(Q_w + Q_d + Q_{fb}).36}{10000} \quad = \quad 37.0 \pm 9.0 \text{ MJ/h}$$